A STRUCTURAL STUDY BY TRANSMISSION ELECTRON MICROSCOPY OF THE REACTIONS OF SOME GRAPHITE INTERCALATION COMPOUNDS

- by -

Katherine Gardner Saunders B.Sc., C. Chem., M.R.I.C.

Department of Chemistry, University of Glasgow

Thesis submitted for the degree of Doctor of Philosophy in the University of Glasgow.

September 1978.

CONTENTS

Tables

Figures

Acknowledgements

The work described in this thesis was carried out in the Chemistry Department of the University of Glasgow between October 1969 and December 1972.

I would like to express my gratitude to my supervisors, Dr J.R. Fryer and Dr K.C. Campbell for their encouragement and guidance throughout this work in particular to Dr J.R. Fryer for his patience during the writing of this thesis. Thanks are also due to Mrs H. Douglas, Dr T. Baird and Dr A.T. Cocks for much invaluable help, discussion and advice. I would also like to thank Dr B.L. Saunders for his interest and help during the early stages of this work and Miss C. Ritchie and Mrs Y. Bradbury for their excellent typing.

Summary

The intercalation compounds potassium graphite, graphite ferric chloride, graphite copper sulphide and graphite iron have been prepared. The structures of these compounds, examined by transmission electron microscopy and electron diffraction exhibit similar features, the most common being dark areas with bright discs and ring moiré patterns. Electron diffraction patterns from areas of ring moiré patterns are distorted indicating uneven intercalation.

Potassium graphite, prepared and examined in situ at 573K, appears to contain a mixture of Stage I and higher compounds. Graphite ferric chloride is evenly intercalated and is a stage I compound while graphite copper sulphide appears to be a stage II or higher compound. Graphite iron contains iron in three forms, namely, a graphite iron intercalation complex, iron crystallites and some finely dispersed iron. The areas of iron crystallites also contain THF which causes exfoliation of the graphite as a result of the heating effect of the electron beam. Graphite ferrous chloride formed by reduction of graphite ferric chloride exhibits aggregations of $FeCl_2$ within the graphite layers. Some expulsion of $FeCl_3$ also occurs on heating graphite ferric chloride.

The catalytic activity of potassium graphite, graphite ferric chloride, graphite copper sulphide and graphite ferrous chloride for ammonia synthesis from N_2/H_2 was studied in the range 483-723K and the structures of the intercalation compounds examined after reaction by transmission electron microscopy and electron diffraction. Gaseous products were analysed by mass spectrometry, infra-red analysis, and wet chemical methods and in no case was free ammonia observed.

Reaction was observed above 483K after 1 hour in a flow system over potassium graphite. Reaction occurs within the graphite layers and decomposition of the potassium graphite to KNH_2 at 573K

was observed possibly via a ternary intermediate. Reduction of graphite ferric chloride and graphite copper sulphide takes place on reaction with nitrogen and hydrogen in the range 523-723K. The graphite ferrous chloride formed, exhibited some activity for ammonia synthesis with formation of aggregates within the layers which were provisionally identified as NH_4Cl.

The catalytic activity of graphite ferrous chloride and graphite iron for the hydrogenation of butadiene was also studied. At 573K graphite ferrous chloride catalysed the polymerisation of butadiene in a similar manner to free ferrous chloride. Electron diffraction indicated that a small amount of iron was formed which could be responsible for the minor hydrogenation reaction observed. Graphite iron exhibited low catalytic activity for the hydrogenation of butadiene compared to iron. Heating graphite iron causes the decomposition of the compound with agglomeration and expulsion of iron particles from the lattice. These iron particles exhibited high catalytic activity for carbon deposition in the butadiene, hydrogen system.

INTRODUCTION

1.1 Graphite Structure

1.1.1 Ideal Lattice

The crystal structure of graphite has been extensively studied since the early work of Ewald (1914), Debye and Scherrer (1917) and Bernal (1924). Graphite is described as a layered structure composed of infinitely large planar layers of carbon hexagons. The carbon is sp^2 hybridised and has a C-C distance of 0.1421 nm. The planes of carbon are arranged in parallel and are bonded together by Van der Waals forces. The distance between planes is 0.33538 nm (Franklin 1951) for well oriented graphite. According to Franklin, in less well oriented graphite the experimentally measured interplanar distance is an average value depending on the proportion of oriented layers with 0.335 nm spacing and disoriented layers with 0.344 nm spacing. There are two main types of stacking sequence for the carbon planes; hexagonal (Bernal 1924) and rhombohedral (Laidler and Taylor 1940 and Lipson and Stokes 1942 a and b). In the hexagonal form, the carbon atoms of one layer are displaced relative to the next layer in ABAB stacking, while in rhombohedral graphite, the stacking is ABCABC where the third layer has the same relative position to the second layer as the second layer has to the first. Finch and Wilman (1936) and Boehm and Hofmann (1955) showed that both these stacking sequences occur in natural graphite and the hexagonal form can be converted to the rhombohedral form by mechanical treatment (Bacon 1950 and 1952), heat (Boehm and Hofmann 1955) and chemical treatment (Laidler and Taylor 1940 and Lukesh

1951a and b).

1.1.2 Non-ideal Crystal Characteristics

There are two common defects in the graphite crystal. One is stacking disorder which may arise from defects in the relative positions of the carbon layers. The other type of defect is in the structure of the carbon plane.

(a) Stacking Disorder

When the stacking sequence for the planes of carbon hexagons is no longer ABAB or ABCABC, then it constitutes stacking or "turbostratic" disorder. As mentioned previously, the interlayer spacing depends on the extent of stacking disorder in the crystal (Franklin 1951 and Bacon 1950, 1951, 1952 and 1958). Stacking disorder can be produced in several ways. Bollmann (1960, 1961 a,b and c) showed that stacking faults may be caused by the presence of interstitial atoms which have been displaced by irradiation. Intercalated atoms may also produce this effect (Heerschap, Delavignette, and Amelinckx 1964). The dissociation of perfect dislocations into partials with fractional Burgers vectors also cause stacking fault disorder in the region between the partials (Read 1953 and Friedel 1964).

(b) Layer Defects

The structure of the layers of carbon hexagons in graphite may be disrupted from its planar aromatic state by formation of new bonds with, for example, impurity atoms such as oxygen, by formation of a hole defect (Ubbelohde 1957, Ubbelohde and Lewis 1960) as a result of irradiation of the graphite or by the presence of twin planes produced by tilting of the layer planes. Since 1950 (Lukesh 1950) many workers have studied this last defect in graphite by X-ray and electron microscopy (Baker et al 1965).

1.1.3 Electronic Structure of Graphite

In graphite, three of the four valence electrons of carbon are used to form covalent sp^2 hybridised bonds with three neighbouring carbon atoms in the layer plane. The remaining electron enters the π orbital and is delocalised. Since the carbon planes are fairly far apart compared to carbon-carbon distances the interactions between the layers are commonly neglected and the band model for graphite is then treated as a two dimensional problem. Early work by Coulson (1947) and Wallace (1947) suggested that the π band could be regarded as being split into a filled valence band and an empty conduction band. Later work by Coulson and Taylor (1952) and McLure (1959) indicated that the conduction and valence bands were either just touching or slightly overlapping at the corners of the Brillouin zone.

As a result of the work by Slonczewski and Weiss (1958) who included the perturbation of the interlayer interactions in their calculations for a three dimensional band structure, graphite is now regarded as a semimetal consisting of sets of small isolated pockets of holes in the valence band and small isolated pockets of electrons in the conduction band, the total number of holes being equal to the number of electrons. Unlike a semiconductor a semimetal has a small but finite overlap of the valence and conduction bands. This accounts for the high electrical conductivity of graphite.

The electronic structure and Fermi surface of graphite have been studied extensively and reviewed by Haering and Mrozowski (1960) and later by Cracknell (1969).

1.1.4 Crystal Structure of Graphite

Graphite has the well known hexagonal structure shown in Fig 1. Four reference axes are used to define the lattice planes; three are in the plane of the layers at 120° to each other and are denoted by

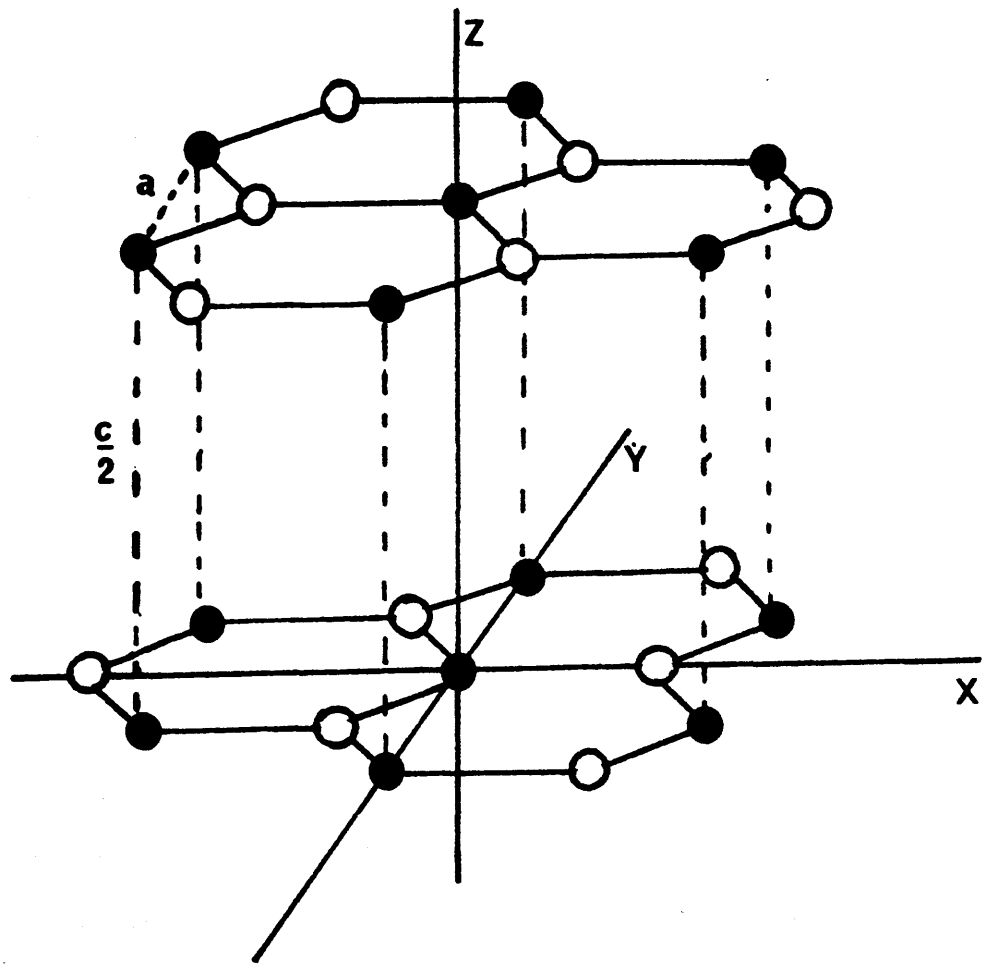

Figure 1. Graphite Structure.

a_1, a_2, and a_3 and the fourth axis is perpendicular to the layer plane and is denoted by c. The Miller indices are (h, k, h+k, ℓ). The third index is used to clarify some of the symmetry relations in graphite. The unit length along an a axis is regarded as equivalent to one side of the carbon hexagon and the ℓ direction unit distance is twice the distance between layers for ABAB stacking. The projection of the unit cell on the basal plane is shown in Fig 2. In this case the side AB of the cell giving the crystallographic 'a' distance is 0.246 nm.

1.1.5 Graphite Diffraction Pattern

The diffraction pattern produced by a beam of electrons normal to the graphite layer planes consists of a series of reflections derived from the carbon planes parallel to the c axis, the reflections $10\bar{1}0$ and $11\bar{2}0$ being most prominent. Finch and Wilman (1936) using conventional electron diffraction and Dawson and Follett (1959) using electron diffraction in the electron microscope, describe this pattern.

Powder X-ray work has been reviewed by Bacon (1958). One main difference in the patterns obtained using the X-ray technique compared to electron diffraction is that both the (h, k, h+k, 0) planes and the (0001) planes in the plane of the layers diffract to give a pattern of about twenty lines.

1.1.6 Moiré Patterns and Double Diffraction

The first reported moiré patterns were of graphite (Mitsuishi et al 1951) and these patterns were subsequently observed by others on a range of materials. At first, two separate explanations were propounded for the occurrence of moiré patterns. The first by Hillier (1954), suggested that they arose from the match and mismatch of two overlapping lattices, while Dowell, Farrant and Rees (1954, 1958), sought to explain the phenomenon by postulating that the moiré

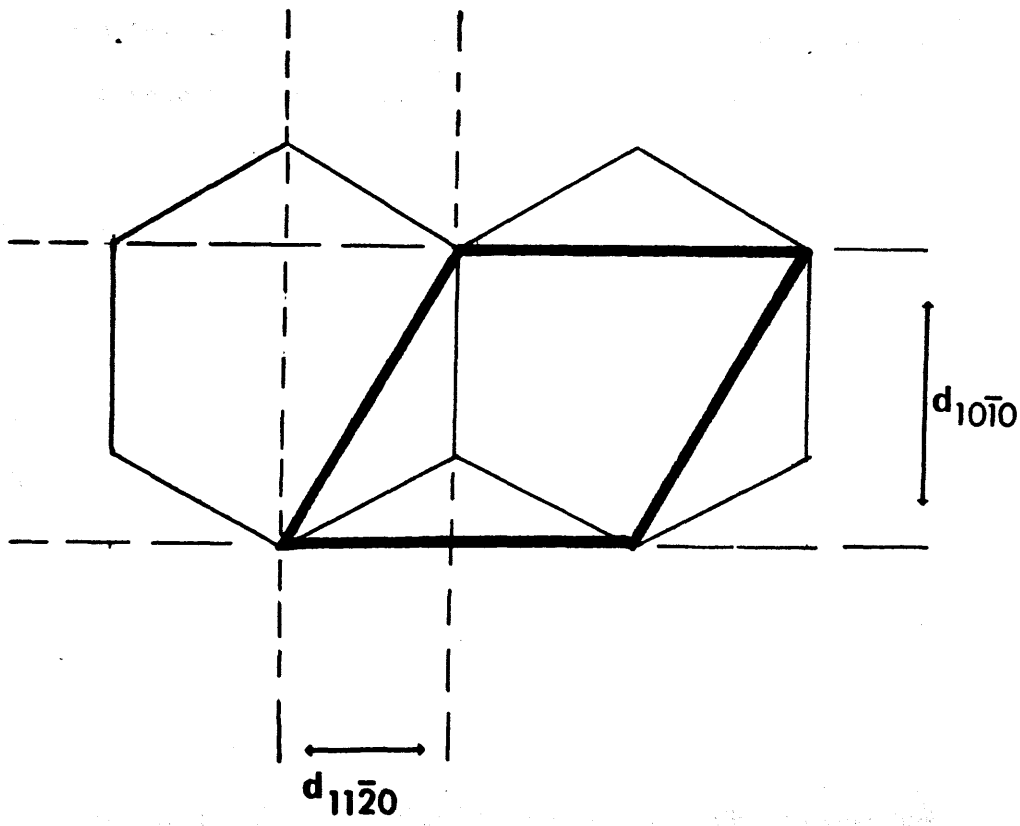

Fig. 2 Projection of Graphite Unit Cell on Basal Plane

patterns were fringes arising from interference within the zero order beam. A comprehensive theory incorporating these two ideas was given by Bassett, Menter and Pashley (1958) who distinguished two types of moiré pattern. The first type is the rotation moiré pattern arising from the overlap of two crystallites of the same material in such a way that there is a rotation angle α about an axis normal to the specimen plane between the crystallites, where α is usually very small. If the lattice spacing is d, the moiré pattern gives a magnified image of the planes with a spacing d/α. The second type, called the "parallel" moiré pattern, is the result of superposition of two lattices in parallel orientation with different lattice spacings d_1 and d_2. In this case the moiré spacing is given by $d_1 d_2 / |d_1 - d_2|$. This was initially described by Bassett, Menter and Pashley (1957) for gold on copper, nickel on lead, and cobalt on palladium.

In order to understand the mechanism of the image formation of the moiré pattern, the electron diffraction pattern from the overlapping crystals is considered. The crystal nearest the electron beam produces, as well as the undeviated central beam, a series of diffracted beams which all act as primary beams for the second crystal. Thus a complex double diffraction pattern will be formed along with the normal diffraction patterns for the two crystals. Some of these doubly diffracted beams will be closely parallel to the central beam and interference of these beams in the image plane will produce a moiré pattern. Figure 3a shows the diffraction pattern from two superimposed lattices with two sets of spots (P and Q) corresponding to the two crystal lattices and spot S which has been produced by diffraction at each of the lattices in turn.

A third type of pattern is possible and is known as a spot moiré. This pattern is produced in the same way from the cry-

stal lattices but the final pattern consists of rows of dots. This was shown by Dowell Farrant and Rees (1954, 1958) to be related to the positions of the atoms in the lattice (Patterson distribution).

1.1.7 Transmission Electron Microscopy

Transmission electron microscopy provides a powerful method for the detailed examination of materials. Structural information may be obtained from the contrast in the final image which can be of two types, absorption and diffraction contrast.

Absorption contrast occurs when there are thickness or atomic number differences across a specimen resulting in different degrees of absorption of electrons.

Diffraction contrast occurs when part of the incident electron beam is transmitted and part diffracted by particular crystal planes. Diffraction occurs according to Braggs Law when $n\lambda=2d\ \mathrm{Sin}\theta$ where λ is the wavelength of the electrons, d is the crystal spacing and θ is the angle of incidence of the beam. The diffracted beams come to point foci at the back focal plane of the objective lens and each spot represents reflection from a definite set of crystallographic planes within the lattice. The normal diffraction pattern for graphite lying on its basal plane is shown in fig 3b. Thus if an aperture is inserted in the focal plane of the objective lens only the transmitted beam and some of the diffracted beams contribute to the final image according to the diameter of the aperture. Therefore, areas giving rise to diffracted beams have a net loss in intensity. Structural information can be obtained by this technique since it will distinguish between perfect and imperfect regions in a crystal.

Diffraction contrast analysis can be used for the observation of dislocations in a crystal lattice and is based on work by Hirsch et al (1956) and Whelan and Hirsch (1957, 1960). It has been reviewed by Howie (1961), Howie and Whelan (1961) and Gevers

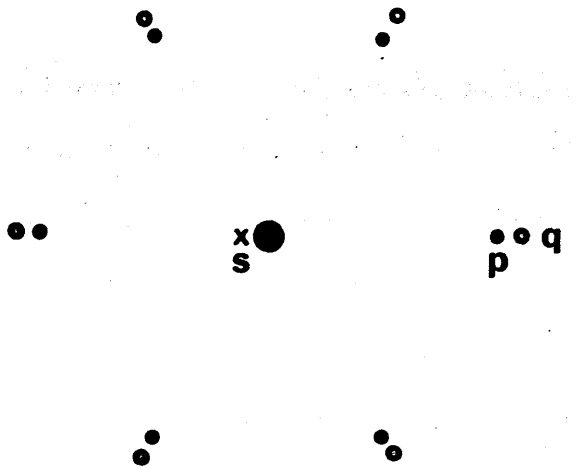

Figure 3(a). Diffraction Pattern from Two Superimposed Crystals.

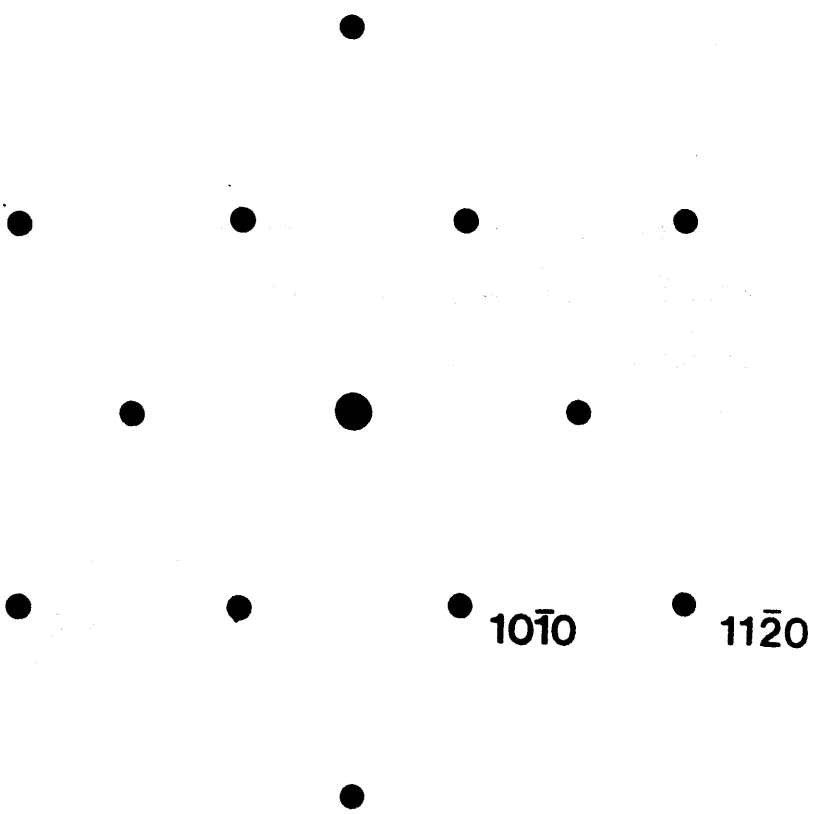

Figure 3(b). Typical Graphite Diffraction Pattern.

(1963). The study of dislocations in graphite has been dealt with by Williamson and Baker (1958, 1960, 1961), Amelinckx and Delavignette (1960 a, b, c), Delavignette and Amelinckx (1960, 1961) and Bollmann (1962). The subject has been reviewed by Amelinckx (1963) Amelinckx and Delavignette (1961, 1963) and Gevers (1963).

In the theory, perfect dislocations may be split into partials. The region between the two partials is a stacking fault corresponding to an area where the stacking sequence has been altered. The partial dislocations can interact with each other to produce a triangular region of stacking fault which has different contrast characteristics.

In the review paper by Amelinckx (1963) contrast analysis is used to determine the Burgers Vector of a dislocation. Dislocations are visible by virtue of their effect on the intensity of the Bragg reflections, so that if their displacements around the defect are parallel to the strongly reflecting plane used for dark field illumination, (i.e. when one of the diffracted beams is used to form an image), the dislocation will lose its effect on the illuminating beam and disappear. By finding the diffraction vector of the spot used for illumination when a dislocation becomes invisible, the Burgers Vector can be calculated since it is perpendicular to the vector of the diffraction spot, i.e. $g.b = 0$, where g is the reciprocal lattice vector for the diffraction spot, and b is the Burgers vector of the dislocation.

The diffraction contrast theory also predicts that when $g.b$ is an integral there is no stacking fault contrast within a dislocation loop but the dislocation is visible. When $g.b$ is non integral the defect appears as a disc of stacking fault contrast.

The Burgers Vector of basal plane dislocations in graphite

were determined by Delavignette and Amelinckx (1960) and Williamson (1961) who found that a dislocation in the basal plane has a Burgers Vector of $b = {}^1/_3a\,[11\bar{2}0]$. However it is usually split into two partials with Burgers Vector ${}^1/_3a\,[10\bar{1}0]$ with stacking fault contrast between them.

1.2 Intercalation of Graphite

1.2.1 General

Intercalation compounds of graphite are compounds in which an electron donor or acceptor is inserted between the carbon layer planes. The formation of intercalation compounds of graphite has been known since the reaction of graphite with bisulphate by Schafhaeutl in 1841 and the first alkali metal graphite compounds were prepared in 1926 by Fredenhagen and Cadenbach. Since these studies, graphite intercalation compounds have been extensively investigated and the subject has been reviewed by Riley (1945 a,b) Hennig (1959), Croft (1960), Ubbelohde and Lewis (1960), Novikov et al (1971) and Ebert (1976). Three main classes have been distinguished; non-conducting, lamellar and residue compounds.

1.2.2 Non-conducting Compounds

In this type of intercalation compound, the carbon is sp^3 hybridised and forms a covalent bond with the intercalate. This means that the aromatic character of the graphite planes is destroyed and the planes become puckered. This leads to the loss of the conducting properties of the original graphite. Ruff and Brettschneider (1934) reacted graphite with fluorine to form $(CF)_n$, one of the chief examples of this type of compound. According to Rudorff and Rudorff (1947 a and b) the c spacing increases from 0.335 to 0.8 nm.

1.2.3 Lamellar Compounds

In these compounds the intercalate takes up an ordered

arrangement within the graphite lattice, occupying, in the case of the most concentrated compounds, every interplanar spacing. With less concentrated compounds, the intercalate may occupy every second, third or more space with consequent expansion of the graphite planes in the c direction in all cases. Typical electron donors are the alkali metals and common electron acceptors are bromine and bisulphate. These reagents interact with the conduction band of graphite by donating or accepting electrons thus altering the electrical and magnetic properties of the graphite,(McDonnell, Pink & Ubbelohde, 1951, Hennig and McClelland, 1955, Hennig 1956, 1960 , and Ubbelohde, 1961). The resulting intercalation compounds have been described by Dzurus and Hennig (1957) using the nomenclature of semiconductors, as P and N type lamellar compounds.

The formation of an intercalation compound is usually accompanied by a change of colour. Examples of donor complexes are the graphite alkali metal compounds and typical acceptor complexes are graphite, bromine and graphite, transition metal halide compounds.

1.2.4 Residue Compounds

When a lamellar intercalation compound decomposes on exposure to a vacuum, water, heat or air, it loses most of its intercalated material. However, a definite proportion of the intercalate remains within the graphite giving what is known as the residue compound. The residue is thought by Hennig (1952) and Ubbelohde (1957) to be trapped at crystal imperfections, while Maire and Mering (1959) having observed X-ray lines of bromine in a bromine residue compound,suggested that single layers of intercalate are present at the interfaces between perfect and imperfect layer planes. The amount of intercalate retained depends upon the parent lamellar compound, but given a fully intercalated compound, this amount is reproducibly constant. Hérold (1971)

in the light of his bent layer model, suggested that the residue compound is a mixture of graphite and very dilute intercalation compounds. However, the electron microscopy study of the graphite ferric chloride residue compound (Heerschap and Delavignette 1967), indicated that the residual intercalate is in the form of small isolated loops of intercalation compound which are pinned at crystal imperfections.

1.2.5 Lamellar Compounds Studied

The particular compounds investigated in this thesis are potassium graphite, graphite $FeCl_3$, graphite $FeCl_2$ and graphite iron. It is not yet certain whether the graphite iron compounds can be classified as an intercalation compound. This point will be discussed in a later section. Potassium graphite is a donor complex and its properties are typical of these compounds.

1.3 Potassium Graphite Donor Complex

The alkali metal intercalation compounds have been comprehensively reviewed by Novikov and Vol'pin (1971). A brief summary will be given here with particular reference to the potassium graphite compound.

1.3.1 Preparation of Potassium Graphite

The main methods of preparation are as follows:

1. By heating graphite with potassium in a sealed ampoule to 573-673K. This method was adopted by Fredenhagen and Cadenbach (1926) who were the first to prepare this compound. They produced a C_8K and $C_{16}K$ compound.

2. Fredenhagen and Suck (1929) prepared the compounds C_9K and $C_{18}K$ by maintaining the graphite at a fixed temperature (673-723K) while varying the temperature of the potassium from 473 to 673 or 723K.

3. Hérold and co-workers (1951 and 1955) reversed this method

and maintained the potassium constant at about 523K while changing the graphite temperature from 523 to 873K. The products of this reaction were C_8K, $C_{24}K$ and $C_{40}K$.

4. Rudorff et al (1954, 1955 and 1959) prepared a large number of compounds by reaction of graphite with solutions of alkali metals in ammonia, methylamine and pyridine at temperatures between 173 and 223K. Using liquid ammonia these workers found that a ternary graphite lamellar compound was formed. In the case of C_8K some of the potassium goes into solution with the ammonia to form $C_{12.5}K(NH_3)_2$ whereas in the case of $C_{24}K$ there is hardly any potassium removed from the graphite. The compound formed is $C_{28}K(NH_3)_{2.8}$.

5. Stein et al (1965 and 1967) prepared alkali metal lamellar compounds by exchange between graphite and aromatic radical-ions such as sodium naphthalene in tetrahydrofuran. In this reaction the equilibrium quantity of potassium intercalated is independent of the radical anion but the rate of reaction does depend upon the radical anion. These workers also found that 80% of the penetration of the potassium into the graphite takes place during the first five hours. Reaction is completed after a further 35-45 hours. This is based on the work of Scott et al (1934), Paul (1956) and Haijitink (1956) on the reaction of alkali metals with aromatic hydrocarbons.

Nominé and Bonnetain (1967) studied the thermal decomposition of these compounds and showed that although lithium and sodium formed various phases with the solvent depending on the degree of solvation, potassium graphite has only one phase and at room temperature will eventually lose its intercalated solvent.

1.3.2 Structure

Information on the structure of the potassium graphite compound

has been obtained mainly by using X-ray methods. Vol'pin and Novikov (1971) in their review consider this aspect of the alkali metal lamellar compounds of graphite in great detail. The studies carried out by Schleede and Wellmann (1932) and later by Rudorff and Schulz (1954b) and Hérold (1955) enabled a model for the structure of potassium graphite to be proposed. The compound can be formed in various stages (Fig 4a). For example in the C_8K compound every interplanar space of the graphite is filled with a layer of potassium. This is the stage I compound. In a stage II compound, $C_{24}K$, every second interplanar space is occupied by potassium. Several stages of these compounds may be prepared. In 1962 Matuyuma obtained a range of compounds up to stage XI. Recently, Salzano and Aronson (1967) showed the presence of a $C_{10}K$ compound and Hérold and Carton in 1972 demonstrated the presence of a non stochiometric phase present between KC_8 and KC_{24}. The latter is thought to be a first stage compound in which the metal atoms are disordered. It is evident from identity period measurements on various stages of intercalation compounds that the filled layer has a constant thickness for a given intercalate and that the interplanar distance for the unfilled layer is identical to that of the original graphite. X-ray techniques have also shown that within the potassium layer there is order, and that the potassium atoms are arranged in a triangular pattern in the most concentrated compound (Fig 4b). In higher stage compounds, the potassium rearranges to form an hexagonal pattern which, in Fig 4c, would result from movement of atom A out of the lattice. Another characteristic of intercalation compound formation discovered by the X-ray technique is the superposition of the graphite layers adjacent to the intercalate. The graphite stacking sequence becomes AA or BB.

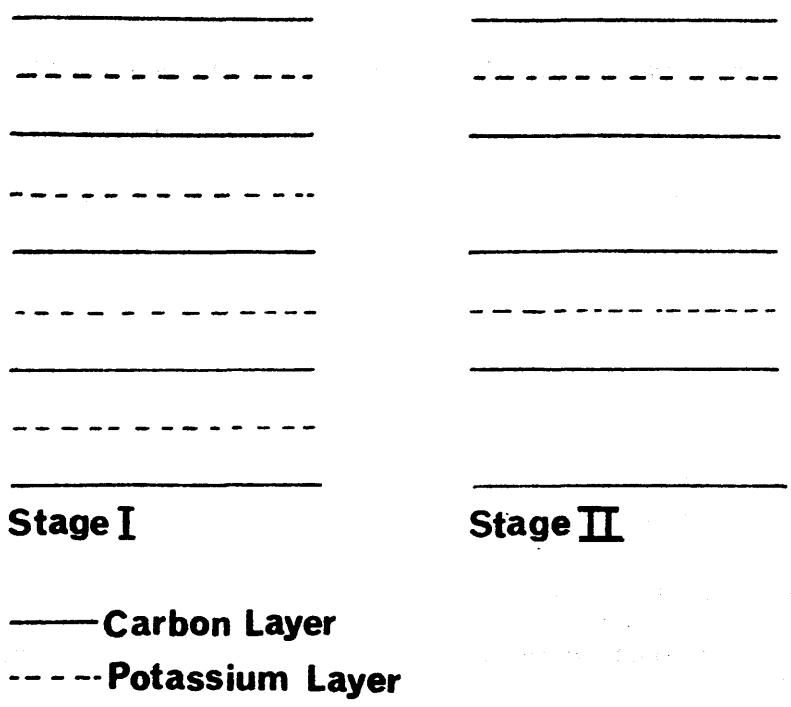

Figure 4(a). Stage Model for Potassium Graphite.

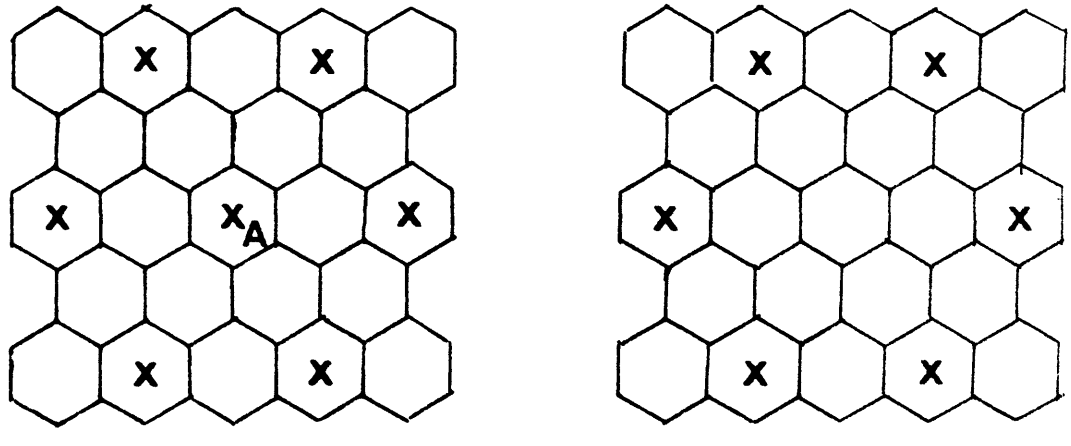

(b) (c)

X Potassium

Figure 4(b). Arrangement of Potassium in Graphite c-plane for KC_8.

Figure 4(c). Arrangement of Potassium in Graphite c-plane for KC_{24}.

The potassium intercalate not only possesses long range order within the layer, but also long range order down through the graphite planes, and in fact forms a superlattice. The central layers are displaced relative to each other by $\frac{1}{2}0$, $\frac{1}{2}\frac{1}{2}$, $0\frac{1}{2}$. This means that the identity period for the first stage compound should be four times that found with the 00ℓ reflections. Stages II and IV should have twice the identity period calculated from 00ℓ reflections and stages III and V have the same value for the identity period as calculated from 00ℓ and from 10ℓ reflections. The position of the intercalated metal atom is below the centre of the carbon hexagon which means that for C_8K the distance between the metal atom and carbon atom is 0.414 nm.

It was shown from work by Parry and Nixon (1968) that the carbon networks remote from the potassium layer may undergo partial displacement, unlike those layers directly adjacent to the metal intercalate which undergo complete displacement. These workers therefore suggested that for stages II - IV the arrangement would be

Stage II AB K BC K CA KA

Stage III ABA KA CA KA

Stage IV AB ABK BC BC K CACA K A

1.3.3 Hérold's Model

Another model for the structure of lamellar compounds, not included in Vol'pin's review, has been proposed by Daumas and Hérold (1971) to explain the results of their studies of the chemical reactions between oxygen and other volatile oxides, and potassium graphite intercalation compounds. They found that the lamellar compounds transformed rapidly from one stage to another as reaction proceeded. As this is difficult to reconcile with

the Rudorff and Schulz, stage model, they formulated a "bent layer" model. This model, while differing in structural detail, would in no way alter the characteristics of the compound with respect to its other physical and chemical properties. In the model, they agree with the first stage structure generally accepted as alternating layers of carbon and metal with a $^{C}/_{K}$ ratio of $^{1}/_{8}$. However, in the second and subsequent stage compounds the picture changes. (Fig 5). Under the stage model, a change from stage I to a stage II compound not only involves redistribution of the alkali metal to a dodecahedral structure but also involves the complete loss of every second layer of potassium. With the new model, all the interlayer spaces are occupied by equal quantities of material no matter what the stage of the compound and each interplaner space is portioned into domains occupied by one layer of metal which expands the c-spacing and empty domains where the original spacing is conserved. The superposition of the full and empty zones preserves the characteristic stacking sequence; thus, changing from a stage I to a stage II compound or a higher stage involves just an increase in the areas unoccupied within a layer. This means that, for example, during the reaction of KC_8 with carbon monoxide, at any instant the metal atoms between the layers are displaced to give the most stable structure in the form of one compound or a mixture of stages of lamellar compounds.

1.3.4 Structure of Ternary Graphite Metal Solvent Compounds

Rudorff et al (1954a, 1955, and 1959) studied the structure of the ternary alkali metal graphite ammonia compounds. It was shown that, in general, they are similar to the ordinary ternary intercalation compounds. The solvent molecules are situated in the same layer as the metal ions and solvate them. The number of

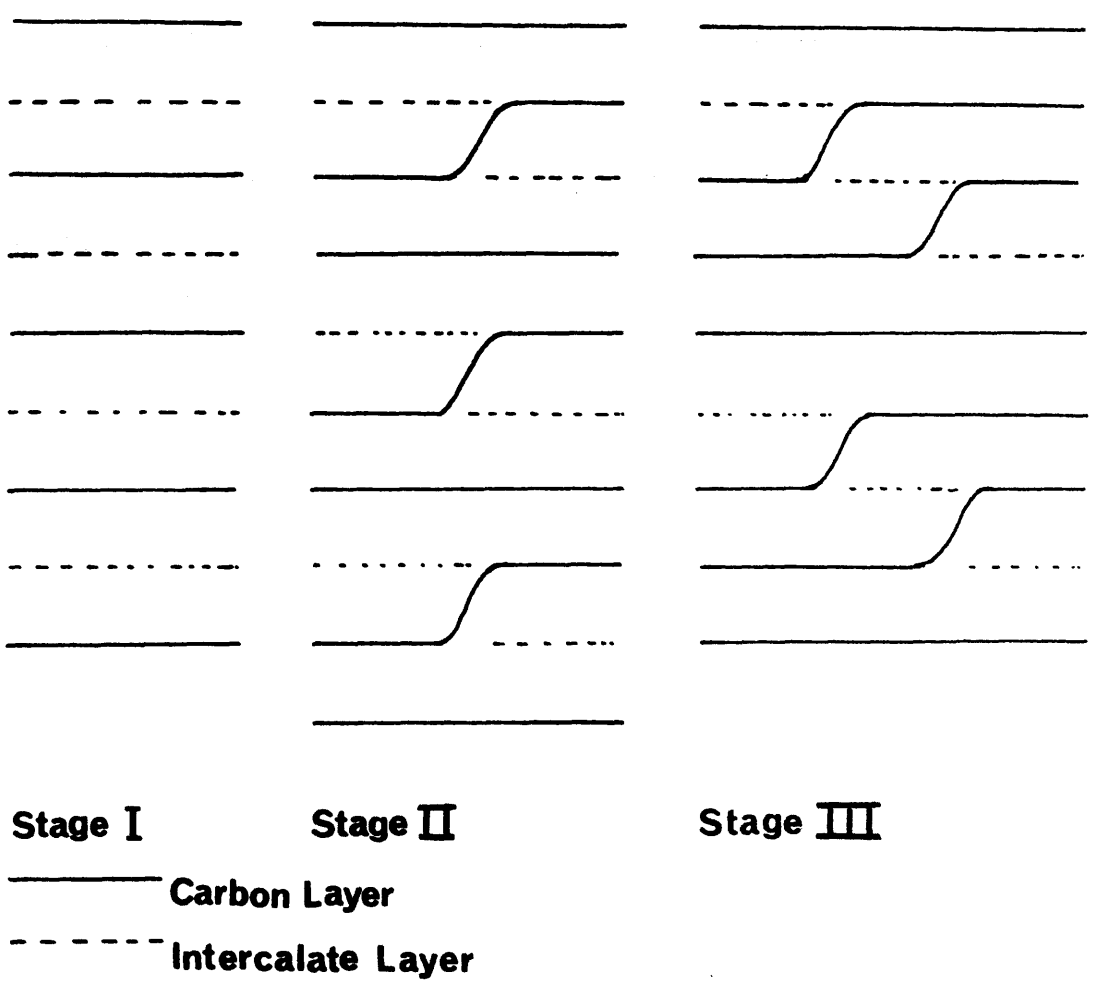

Figure 5. Hérold's Bent Layer Model.

solvent molecules per ion decreases with increasing molecular size. In the ternary compounds the thickness of the filled layer is no longer determined by the size of the metal or the stage of the compound, but is determined by the size of the solvated ion. For the graphite alkali metal ammonia compound the interlayer spacing is 0.66 nm. In the stage I compound the potassium is now associated with 12 carbon atoms as in stage II - V as a result of the presence of the solvent molecules between the layers. Again there is superposition of the graphite layers adjacent to the filled layers, and the identity period for even stage compounds is doubled.

Ginderow and Setton (1968) investigated the lithium and sodium hexamethyl phosphoramide compounds and in general found that the main points above also applied to these compounds. Other solvent systems have been studied e.g. tetrahydrofuran, by Stein et al (1965, 1967) and later by Nominé and Bonnetain (1967, 1968). The work by the latter authors led to the proposal that different phases were present in the stage I compounds, characterised by the degree of solvation of the metal, and the partial arrangement of the solvent molecules.

1.3.5 Physical Properties of Potassium Graphite Lamellar Compounds

The physical properties of graphite, including its electrical conductivity, magnetic susceptibility and bonding are markedly altered during the intercalation process. These properties have been the subject of intensive study and reviewed by Salzano (1967) Ubbelohde (1959, 1960, 1971a) and Hennig (1951, 1952, 1957).

Novikov and Vol'pin summarise the main features of these investigations and their main points are listed below.

a) Electrical Conductivity

1. Intercalation of an alkali metal into graphite results in an increase in conductance of ten times in the a direction and two hundred times in the c direction.

2. Intercalation compounds exhibit a positive temperature coefficient of resistance.

3. An increase in the potassium content leads to a continuous decrease in resistance along the c axis but resistance reaches a limit along the a axis.

Ubbelohde (1971b) investigated the anisotropy of well parallelised graphite on intercalation with potassium. He found that the conductivity increased considerably in the c direction and that the anisotropy ratio of the conductivity in the a direction and c direction decreased compared to the parent graphite.

Novikov and Vol'pin point out that similar generalisations also apply to the solid alkali metal aromatic hydrocarbon complexes.

b) Magnetic Susceptibility and E.S.R.

Natural graphite is diamagnetic, but, on intercalation weak paramagnetism is observed. Contradictory evidence concerning the relation between this paramagnetism and temperature has been obtained by Juza et al (1949,1957) and Rudorff et al (1954 a, 1954 b 1955). According to Juza it is independent of temperature but Rudorff found that it decreases with decreasing temperature. E.S.R. investigations of the alkali metal intercalation compounds prepared from solutions of metals in liquid NH_3 confirmed the metallic nature of these compounds and ionic character of the bond in the compounds. E.S.R. work by Ginderow and Setton (1968) on the compounds prepared using a hydrocarbon solvent for the metal led to the calculation of the percentage of unionised material. In

the potassium benzophenone compound potassium is 6% unionised. However, doubt has been cast on this work by Rose et al (1968) who pointed out that the spectra can result from complexes of the intercalated material with solvent hydrocarbon.

1.3.6 Nature of Bond

In his review, Vol'pin considers the current theories about the nature of the bond involved in the alkali metal intercalation compounds. The model which explains most of the phenomena discussed above, was suggested by Salzano and Aronson (1965 a, b 1966 a, b, 1967). They proposed that the alkali metal donates an electron to the conduction band of the adjacent carbon layer of the graphite. Therefore the metal atoms are considered to be completely ionised and an electrostatic type of bond is formed between the positive metal ions and electrons in the conduction band of the graphite.

In addition to the well known increase in conductivity on formation of an intercalation compound, and its positive temperature coefficient, two other important facts are explained by this simple model. One is that the sum of the radii of metal ions and Van der Waals thickness of the carbon layer is equal to the interplanar spacing, and the second is that the thickness of the filled layer is the same for compounds of different stages. Further evidence in favour of this model is given by data which showed that electrons are transferred to the graphite (Hennig 1965), and also by the moessbauer spectra of Caesium compounds (Montet et al, 1968), which showed that the metal is completely ionised.

However, for compounds above $C_{24}M$, that is C_8M, and $C_{10}M$, where M in the metal atom, some predictions of the theory are not accurate. Specifically the theory predicts that C_8M should have the smallest

heat of formation since the repulsion between layers will be strongest for these compounds, but these compounds are the most stable. In addition the heats of formation calculated on this model do not agree with those found experimentally.

Recent work by Bach (1971) using the E.S.C.A. technique to provide more information on the electronic structure of the potassium graphite series of compounds from C_8K to $C_{84}K$ has shown that there is a charge transfer from potassium to the graphite, and by examination of the carbon 1s peak he postulated that there are two stages of ionisation of the compound in addition to the initial state.

1.3.7 Chemical Reactions of Graphite Alkali Metal Intercalation Compounds

Vol'pin has only briefly reviewed this aspect of graphite alkali metal intercalation compounds. The following summary includes recent work not covered by Vol'pin with particular emphasis given to the potassium graphite compound.

a) Reaction with Water

The reaction of potassium graphite with water was studied by Rudorff in 1954 who discovered that hydrogen was evolved. This was confirmed by Daumas and Herold (1971) who found that the products of the reaction were potassium hydroxide, hydrogen and graphite. A similar reaction, reported by Stein et al. (1965, 1966) takes place in the ternary insertion compounds with tetrahydrofuran as the solvent molecule.

b) Reaction With Hydrogen

According to Saehr and Hérold (1960a, b, 1965) the C_8K compound absorbs hydrogen slowly at room temperature, and the rate of reaction increases with temperature. The reaction scheme may be represented as follows,

$$C_8K + X/2\ H_2 \rightleftarrows C_8KH_X$$

where X varies from 0.15 to a limiting value of 0.67. Further studies by Colin and Hérold (1967, 1971) showed that in the case of $C_{24}K$, the rate of reaction was much slower and the compound formed was $C_{24}KHy$, where y varied from 0.3 to 0.5.

An X-ray study of the $C_8KH_{0.67}$ compound, prepared with very pure hydrogen, indicated that a ternary compound with a hexagonal structure was produced. Traces of oxygen or water vapour in the reacting gas resulted in the formation of potassium hydride and graphite exclusively.

c) Reaction With the Halogens

Diebold and Hérold (1961, 1963) reported the reaction of gaseous chlorine, bromine and iodine in C_8K and C_8Cs. It was found that complete reaction took place to form a metal halide and graphite. The structure of the lamellar compounds is destroyed leaving the salt in the form of well dispersed small crystallites within the graphite lattice. In this form, the compound is capable of further intercalation by an alkali metal and subsequent reaction with halogen in the same way.

d) Reaction With Oxygen and Volatile Oxides

Daumas and Hérold have studied the reaction of C_8K with oxygen and carbon monoxide (1969), nitrous oxide, nitric oxide, nitrogen dioxide, sulphur dioxide and carbon dioxide (1971).

It was found that in the case of oxygen, if a large quantity of gas was allowed to react with the intercalation compound, reaction was very fast and resulted in the formation of potassium carbonate. However if the rate of oxidation was controlled, a relatively stable two phase system was produced

consisting of graphite and αKO_2. Using powder X-ray lines to monitor the course of the reaction, it was found that as oxidation proceeded, the C_8K had undergone a gradual transformation to the $C_{24}K$ compound, and further oxidation resulted in the regeneration of graphite. Reaction of the gases nitrous oxide, nitric oxide, nitrogen dioxide, sulphur dioxide and carbon dioxide with the C_8K compound produced the next stage intercalation compound as intermediate before eventual production of graphite and the corresponding nitrate, sulphate or carbonate. Reaction of CO followed the same pattern, but in this case the full range of compounds was developed, starting with the stage II compound through to the stage IX compound. The final products were graphite and potassium carbonate. The residue compounds formed appear to be a mixture of stage X and higher intercalation compounds.

In order to account for the transitions from one stage compound to another during the reaction of C_8K with carbon monoxide, the authors have postulated a new model for the structure of intercalation compounds which has been summarised in section 1.3.3.

e) Reaction With Organic Compounds

The reaction of benzene, toluene, naphthalene and α methylstyrene in cyclohexane at ambient temperature with a third stage potassium graphite compound $C_{37}K$ was studied by Rashkov et al (1976). They found that a ternary compound was formed $KC_{37}Ar_x$ with only partial reaction of the potassium in the layers. X-ray studies indicated that the organic molecule is in the lattice between the potassium and the graphite layer planes. In addition, solvents THF, dimethoxyethane and dioxane gave a solvated intercalated cation.

1.3.8 Catalytic Properties of Potassium Graphite Intercalation Compounds.

Until 1970, intercalation compounds had not been widely used or investigated as catalysts, and Vol'pin in his review covered only the early work involving their application in organic polymerisation reactions and alkylation reactions. Since that time, interest in these compounds as catalysts has increased and a comprehensive review of their catalytic properties has been presented recently by Boersma (1974).

Early workers used the alkali metal intercalation compounds for a variety of reactions. Examples of these reactions ranged from polymerisation of alkenes (Podall et al., 1958, Parrod and Beinert, 1961, Hambling and Anderson, 1963), the isomerisation of alkenes (Ottmers and Rase, 1966), and the alkylation of alkenes, and benzene derivatives both on the ring, and on the side chain (Podall and Foster 1958). C_8K was also used as a reducing agent by Jensen et al. (1965) who reacted C_8K with bis(trialkyl phosphite) nickel II dichlorides and excess trialkyl phosphite to give a zerovalent nickel complex, trialkyl phosphite nickel.

a) Hydrogenation, and Condensation Reactions

The first workers to investigate the potassium graphite compound as a catalyst for hydrogenation were Ichikawa et al. (1967). They discovered that potassium graphite, in common with other electron donor/acceptor complexes of sodium and potassium with polycondensed aromatic hydrocarbons, selectively hydrogenated ethylene, propylene, methylacetylene, but-1-ene and butadiene at 298K. They found that methylacetylene was selectively hydrogenated first to propylene and then to propane. Similarly, butadiene gave a mixture of cis and trans but-2-ene which was converted to butane at 298K. More recent detailed work by

Boersma (1974) showed that the hydrogenation of ethylene, studied over the range 343 - 388K followed first order kinetics with the order of decreasing catalytic activity being $C_{36}K$ > $C_{24}K$ > $C_8KH_{0.67}$. The hydrogenation of benzene, toluene and propyl-benzene over C_8K and $C_{24}K$ was studied by Ichikawa et al. (1972a). Using hydrogen at 100 to 150 bar, high yields were obtained. Below 10 bar almost no reaction occurred.

The condensation of benzene to biphenyl has been investigated using the C_8K compound (Beguin and Setton 1976) and the $C_{24}K$ compound (Lalancette at al 1976a) as catalysts. In the presence of $C_{24}K$, benzene in cyclohexane reacts to give biphenyl at reflux temperatures.

b) Polymerisation Reactions

Since the initial work on polymerisation reactions, several workers have used the alkali metal graphite compounds as initiators. Golé and Stein (1968) tested the $C_{32}K$ compound for the polymerisation of styrene. Very high molecular weight products were formed and the reaction rate was proportional to initiator concentration. The anionic polymerisation and copolymerisation of vinyl monomers initiated by potassium graphite was investigated by Panenotov and Rashkov (1972). Golé et al (1973), used the ternary alkali metal solvent graphite compounds for the polymerisation of isoprene. In addition, the C_8K and $C_{24}K$ compounds, in the presence of alkyl amines, catalyse the stereospecific formation of 1,4 trans-polybutadiene (Ichikawa et al 1972b). The stereospecificity is the result of complex formation with the butadiene and alkyl amine, and electron donation from the amine to the potassium cation in the intercalation compound.

c) Fischer-Tropsch Synthesis

Ichikawa et al. (1969a) investigated the catalytic formation of hydrocarbons (C_1 - C_4) from hydrogen and carbon monoxide over sodium and potassium graphite. They found that carbon monoxide and hydrogen were adsorbed to a considerable extent by the intercalation compounds, the main products of the reaction being C_2 and C_3 hydrocarbons at 573K. No information on reaction rates was given.

d) Exchange and Isomerisation Reactions

The hydrogen-deuterium exchange reaction has been studied by Watanabe et al. (1971, 1972). They used a series of potassium graphite compounds at 323-333K and discovered that the order of reactivity was $C_{24}K > C_{36}K >> C_8KHx > C_8K$. The C_8K had zero activity. At the same time Ichikawa and Kawase (1972c) reported the methane-deuterium exchange reaction on C_8K and $C_{24}K$. At 573K, methane and deuterium react to give CH_3D and CH_2D_2, with a rate of reaction over $C_{24}K$ twice that for C_8K. This is similar to the reactivity order found by Watanabe (1971, 1972) and by Ottmers and Rase (1966) for isomerisation reactions. The deuterium exchange with hydrogen atoms on hydrocarbons with acidity greater than benzene was investigated by Lalancette et al (1976a) using the $C_{24}K$ compound. They concluded, in agreement with Watanabe et al (1973) and Colin and Hérold (1971) that the deuterium is physically adsorbed either on the surface or within the lattice and is partly dissociated. The isomerisation of cis to trans stilbene and 2-alkynes to 1-alkynes was also found to occur on $C_{24}K$ under mild conditions (Lalancette et al 1976a).

e) Reduction of Carbonyls

The C_8K compound is also active for the reduction of ketones. Lalancette et al (1972) reduced saturated and conjugated

ketones by C_8K in THF. They suggested that the mechanism of the reaction was similar to electrochemical reduction and required adsorption of the ketone on the surface of the intercalation compound crystallite.

f) Sorption of Gases

Recently, Watanabe et al. (1973) investigated the molecular sieve type sorption on alkali metal graphite intercalation compounds. They used hydrogen, deuterium, nitrogen, methane and rare gases for studies on C_8M and $C_{24}M$ at 196 to 63 K where M is potassium, rubidium or caesium. Their results showed that C_8M compounds were non sorptive while the $C_{24}M$ compounds adsorbed gases to varying degrees. A mechanism was suggested to explain this behaviour based on the size of the gas molecules and the size of the intercalated metal. They proposed that the adsorption was slit-type adsorption between the intercalated carbon layer planes and that in the C_8M compound the alkali metal atoms were closely packed compared to the $C_{24}M$ compounds resulting in steric hindrance to the entering gas molecules. In addition, although the interplanar spacing was large enough for small molecules to enter the graphite lattice without expansion, larger molecules were accommodated between the layers with consequent increase in the interplanar spacing. This means that these compounds are not as selective as the zeolites. From the heats of sorption for the $C_{24}M$ compounds the adsorption was found to be physical adsorption. The selective chemisorption of hydrogen and deuterium by C_8K has been examined (Lagrange et al 1976). The equilibrium $H_2 + D_2 \rightleftarrows 2HD$ formed on contact with C_8K was studied, it was shown that the chemisorbed deuterium/hydrogen layer showed maximum enrichment in hydrogen at low concentrations of deuterium.

g) Synthesis of Ammonia

The synthesis of ammonia from nitrogen and hydrogen was also attempted by Ichikawa et al (1969b, 1970) using various electron donor-acceptor (EDA) complexes of transition metal phthalocyanins and potassium graphite. They found that for potassium graphite, nitrogen was adsorbed as the temperature was raised. Conversely ammonia was adsorbed at room temperature with the evolution of hydrogen; nitrogen only appearing at 573K. According to the authors, the conversion of nitrogen and hydrogen to ammonia was low and occurred in the temperature range 323 to 673K. At this time, Tamaru (1970) reviewed the field of EDA complexes of alkali metals as catalysts, and suggested that electron donation from the alkali metal to acceptor films produced strong local electrostatic fields which gave rise to hydrogen activation. Further studies of the catalytic synthesis of ammonia were carried out by Ichikawa et al (1972d) using a graphite potassium transition metal chloride system. Greatly enhanced conversion rates were obtained for this compound. However, it has been suggested subsequently that the alkali metal intercalation compound has reduced the transition metal chloride to the metal and that it was the metal which was the catalyst for the reaction. The presence of reduced metal has been confirmed by a Moessbauer study of the ternary compound by Tricker, et al (1974).

1.4 Acceptor Complexes of Graphite

Graphite reacts with a variety of electron acceptors to form intercalation compounds. Well known members of this group are the graphite-bromine, ferric chloride, and bisulphate compounds. In general, in the case of acceptor compounds, there is transfer of electrons from the conduction band of the graphite to the empty or singly filled orbitals of the intercalated group. This means

that the charge carriers will be positive holes and the resulting complexes will be P-type conductors.

The discovery and investigation of these compounds began with Schafhaeutl in 1841 when he prepared the graphite bisulphate compound. Later work by Thiele in 1932 on graphite ferric chloride and by Frenzel in 1933 on graphite bromine, prepared the way for a comprehensive study of acceptor complexes by such workers as Rudorff (1938), Ubbelohde (1951) and Hennig (1952). Graphite acceptor intercalation compounds have been the subject of several reviews (Riley, 1945, Croft 1960, Ubbelohde and Lewis 1960, Ebert 1976). The formation of intercalation compounds of graphite with a range of electron acceptors was first achieved by Croft in 1956(a). He worked on the principle that most materials will be intercalated provided they are able to undergo an electron transfer process, and provided there is sufficient electron affinity in the cation. As general principles for intercalation these hold true, not just for graphite, but also for analagous systems such as boron nitride (Croft 1956b), where the nitride acts as an acceptor. Other examples of this phenomenon include the intercalation of polar molecules.

1.4.1 Preparation of Graphite Ferric Chloride

First prepared by Thiele in 1932, graphite ferric chloride was studied extensively by Rudorff and Schulz (1940). They prepared the compound by heating a mixture of excess anhydrous ferric chloride and graphite at various temperatures. Excess ferric chloride was removed by sublimation. They found that in the range 453 to 573K the compound formed contained 56 - 72% of ferric chloride (C_{5-9} Fe Cl_3) and from 598 to 673K, the ferric chloride content was 30 - 37% (C_{30} Fe Cl_3). Above 773K all the ferric chloride content was expelled. A third compound was produced by heating the 56-72% ferric chloride graphite in a sealed tube

at 673K and quenching before ferric chloride could sublime. This compound contained, after washing, 42.8% $FeCl_3$ (C_{18} $FeCl_3$). Heating or washing the 56-72% compound with water, ether, or alcohol removed part of the ferric chloride to give a C_{10} $FeCl_3$ compound. In 1952, Croft repeated this work, and found that in the range 453 to 673K, the compound formed contained 60-72% ferric chloride. If excess ferric chloride was removed by sublimation above 582K, the compound decomposed to give a 31-37% ferric chloride complex. He also found that an acid wash of dilute hydrochloric acid to remove excess ferric chloride decomposed the compound to give a 56-57% ferric chloride complex ($C_{10}FeCl_3$). The intercalation isotherm of ferric chloride on graphite in the temperature range 573 to 623K was studied by Hooley and Bartlett in 1967, to establish the equilibrium compositions of the products of the reaction. They found a low threshold pressure for intercalation and two independent compound compositions of $C_{6.7-7.2}FeCl_3$ and $C_{12}Fe\ Cl_3$. At 623K both compounds were formed but at 573K only the C_7 compound was detected. They also found that C_7 Fe Cl_3 thermally decomposes above 548K in vacuum to give C_7 $FeCl_2$ and Cl_2.

A different method of preparation of the metal halide compounds was developed by Knappwost (1966) who heated graphite with the powdered metal to 323-473K and exposed the mixture to chlorine or bromine in a nitrogen carrier gas. This work was repeated by Novikov et al (1970) who chlorinated a graphite iron mixture at temperatures from 473 to 673K. The amount of intercalated ferric chloride decreased with increasing temperature, and decreased with increasing reaction time. The maximum amount of ferric chloride incorporated was 68% at 473K after six hours.

In 1969 Knappwost et al. claimed to have made second and third stage ferric chloride compounds. Preparation of the second

stage compound, 48-51% by weight ferric chloride, involved maintaining graphite at 623K and exposing it to ferric chloride vapour produced by heating the solid to 573K. For the third stage compound, 34-40% ferric chloride, the graphite was held at 683K and the ferric chloride at 573K.

An investigation into the formation of metal halide intercalation compounds of graphite was conducted by Bach and Ubbelohde (1971). By measuring the resistance of specially prepared well aligned graphite samples and monitoring weight uptake, the reaction characteristics for the intercalation of $GaCl_3$, $InCl_3$, $FeCl_3$, WO_2Cl_2, $Ga\ Br_3$ and WCl_6 were investigated. In the case of the ferric chloride graphite compound, the graphite was held at 483K and the halide at 423K and under these conditions, a $C_{18}FeCl_{3.5}$ compound, claimed to be a second stage compound was produced. However, no X-ray study was carried out by these workers to determine independently the stage of the compound. The introduction of a partial pressure of 350 mm of chlorine gas accelerated the reaction in all cases. The rate of intercalation of ferric chloride was reduced by five times when no chlorine was added. However it was pointed out that with no added chlorine, under reaction conditions, a small partial pressure of chlorine would be developed. The later work by Hooley (1973a, b) and Lalancette (1976b) confirmed that chlorine is required for the intercalation of the transition metal halides.

In 1970 Hooley and Soniassy outlined a method for preparing the first stage ferric chloride graphite with 97% the theoretical composition of $C_{6.1}FeCl_3$. They achieved this by heating graphite and ferric chloride to 588K and 583K respectively thus producing a pressure of ferric chloride of 650 torr.

Another method of preparation was reported by Novikov,

et al in 1970. A graphite ferric chloride mixture was heated in a sealed ampoule filled with chlorine. After an acid wash, the amount of ferric chloride incorporated into the graphite was 40% at 473K and 50% at 523K. Above 573K the graphite was unchanged.

A stable graphite ferric chloride compound for use as a catalyst was prepared by heating graphite and $FeCl_3 6H_2O$ in chlorine saturated with dichloroethane at 0.15 atm and 573K (Derleth and Fischer 1972).

The preparation of metal chloride graphite compounds from $SOCl_2$ solutions, analagous to the alkali metal solvent preparation technique, was carried out by Boeck and Rudorff (1973). Ferric chloride was not specifically prepared but intercalation of UCl_5, $AlCl_3$, $NbCl_5$, $TaCl_5$, and $MoOCl_4$ to varying stages was achieved.

A similar method was used by Lalancette et al (1976b) for the intercalation of a range of transition metal chlorides including ferric chloride from CCl_4 solutions at reflux temperatures. They found that rapid intercalation occurred only if an atmosphere of chlorine was also present. Intercalation also depended on the solubility of the salt in CCl_4.

1.4.2 Effect of Graphite Particle Size on Graphite Ferric Chloride Formation

The early work of Rudorff and Schulz (1940) showed that the composition of the product i.e. $C_{10}FeCl_3$ below 582K and $C_{30}FeCl_3$ between 583 and 683K was independent of graphite flake size in the range 250 to 550μm. diameter. In 1953, Barker and Croft, using 60μm. and 250μm. flakes, noted that the smaller the particles the more rapid was the reaction, and found that $C_{10.4}Fe\ Cl_3$ was always formed after washing. Rudorff and Landel (1958) found that with 330 to 1400μm. diameter flakes $C_{10.3}FeCl_3$ was the main

reaction product while for smaller flakes $C_{12.3}FeCl_3$ was formed. It should be noted that Knappwost and Grigutsch (1969) came to the conclusion that the amount of Fe^{3+} eluted was not a good method for the characterisation of the intercalation compounds since it was a function of particle size. A comprehensive investigation into the effect of flake size on the composition of graphite ferric chloride was carried out by Hooley and Soniassy (1970). They found that the composition was independent of flake cross section in the range 25 to 650μm. and independent of thickness from one to 60μm., $C_{6.3}FeCl_3$ being produced. The time taken to reach equilibrium concentration was in the order, 500μm. < 650μm< 2600μm. Novikov and Vol'pin (1970) also studied the effect of particle size on the preparation of graphite ferric chloride for flakes of diameters 50 to 100μm., 250 to 500μm. and colloidal graphite. They found that in the range 50 to 100μm., and with colloidal graphite the amount of ferric chloride intercalated reached a maximum at 523K and remained constant to 673K, whereas in the range 250 to 500μm. the amount of ferric chloride increased with increasing temperature up to 623K. They showed that the maximum amount of material intercalated and the temperature of maximum intercalation increased with increasing particle size.

1.4.3 Effect of Solvents on Graphite Ferric Chloride

From the work by Rudorff and Schulz (1940), the graphite $FeCl_3$ compound was thought to be very stable, since after extraction with several different solvents and mineral acids, the amount of $FeCl_3$ in the complex was only reduced from 72 to 56% and from 37% to 31%. As a result, graphite ferric chloride in common with other salt-type compounds was believed to be more stable to heat, solvents and acids than other simple atomic or molecular inter-

calation compounds. However, it should be noted that in a personal communication, Bach has indicated that from resistance measurements these compounds start to decompose immediately after exposure to air. Various workers have subsequently investigated the effects of solvents. Gross (1962) studied the effect of ethanol on graphite $FeCl_3$. He found that after the first washing, the dried compound would lose a further amount of $FeCl_3$ on its second washing. This process could be repeated until all the $FeCl_3$ was removed from the graphite. Brusset et al (1967) studied the effect of various solvents and number of washings. X-ray diffraction of powders were used to follow changes in composition using a $C_{14}FeCl_3$ compound with a flake size of less than 120μm. They found that after 27 cycles of agitation and successive washing and drying for 150 days the compound composition was $C_{26}FeCl_3$. From their X-ray work they found that water, HCl, acetone, methylethyl acetone, diethyl acetone, and acetyl acetone, randomly removed layers of ferric chloride leaving a structure less ordered in the c direction. Further investigation into the effect of acetone on these compounds was carried out by Hooley and Soniassy (1970), who correlated the solvent action with the thickness of the original flake. In agreement with Brusset et al., they found that the solvent removes complete layers of $FeCl_3$, but they suggest, contrary to Brusset, that the spaces are regular. Hooley and Soniassy found the fraction of spaces formed by the acetone was a negative exponential function of the thickness of the original flake. Various explanations related to a general intercalation mechanism were postulated to explain their observations. Hooley (1972) pursued the study of the effect of flake thickness on intercalation of graphite using solutions of metal chlorides in nitromethane. Measurement of the peripheral expansion of flakes of graphite of diameter 0.5 to 3mm., as an indication of intercalation, showed that intercalation decreases

as the concentration of the metal chloride decreases and as the thickness increases. Curious behaviour was observed in the expansion of graphite in a solution of $FeCl_3$ in nitromethane which consisted of the cessation of expansion, for flakes greater than 10 to 30μm thick, at a value which increased with increasing $FeCl_3$ concentration, and with flake diameter. It was possible to shrink the flake in nitromethane then reintercalate with a solution of ferric chloride in nitromethane. This increased the total amount of ferric chloride intercalated until a maximum composition of C_7FeCl_3 was realized. The time taken to reach the zero expansion stage increased with flake thickness and diameter. One mole of nitromethane was intercalated for each mole of $FeCl_3$.

1.4.4 Preparation of Graphite Ferrous Chloride

This compound was first prepared by Gross (1962) by reduction of ferric chloride compounds in hydrogen at 648K. Investigation of this reaction has also been carried out by Vol'pin et al (1970) at 648K to 673K. They found that a 54% ferrous chloride compound was formed from a 60% ferric chloride compound.

1.4.5 Structural Studies on Graphite Ferric Chloride

a) X-Ray Studies

The first X-ray investigation of graphite ferric chloride was carried out by Rudorff and Schulz (1940). They found three types of ferric chloride compounds which they designated stage I, II and III corresponding to 56%, 44% and 30 to 37% ferric chloride in the graphite. However Cowley and Ibers (1956) examined the material from the same preparative route using high resolution electron diffraction and X-ray diffraction and found no stage II and III compounds. Instead they found that the product previously described

as 56% ferric chloride graphite had 17% free graphite and 83% graphite ferric chloride (C_7FeCl_3). In this latter compound, the ferric chloride layers, consisting of an hexagonal arrangement of iron atoms with a triangular net of chlorine atoms above and below the iron, were found to be parallel and situated within the graphite interplanar spaces. The graphite interplanar spacing expanded from .335nm to .941nm. From the diagram (Fig 6), it can be seen, that the structure is a compromise by the chlorine atoms between occupying preferred positions relative to the carbon lattice and to maintaining the normal Cl - Cl distances found in ferric chloride. As a result, about half of the chlorine atoms occupied preferred positions, distorting the Cl - Cl distances to a value in the range 0.315 to 0.42nm compared to the normal 0.34, 0.349, and 0.375nm. The iron chlorine distances were approximately equal as a result of slight relative rotation of the chlorine triangles above and below the iron. The angle between the a-axis of the ferric chloride, and that of the graphite, was 30°. The free graphite, found in this compound, had only a trace of rhombohedral form, indicating that its presence did not result from lack of intercalation, but from decomposition of the intercalated compound when it was cooled from reaction temperature (Boehm and Hofmann 1955). The graphite ferric chloride compounds with less than 56% ferric chloride, produced by thermal decomposition, have less ferric chloride in each layer and more free graphite. When the percentage of ferric chloride had fallen below 40, the layer stacking sequence was random in the c direction. An X-ray study carried out later by Novikov et al (1970) agreed with the work of Cowley and Ibers (1956), in that the compounds formed by heating a graphite ferric chloride mixture in a sealed ampoule at all tempera-

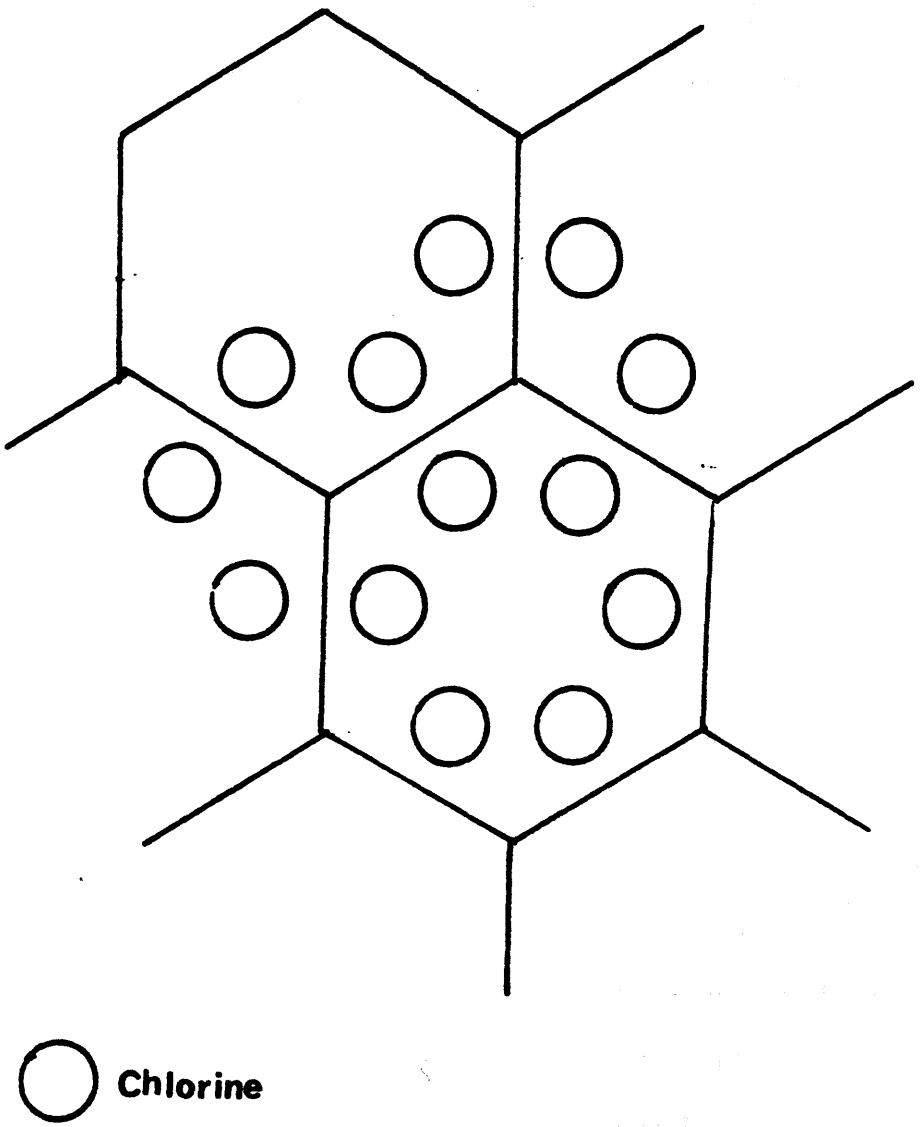

Figure 6. Graphite Ferric Chloride: The preferred chlorine positions relative to carbon layer. (Cowley and Ibers 1956)

tures above 473K in argon or chlorine resulted in stage I compounds, the different percentage of ferric chloride incorporated, resulting mainly from the amount of free graphite. At 473K, a disordered compound was formed. When the method of preparation was the chlorination of a graphite iron mixture at 623K, a mixture of stage I and stage II compounds was obtained. At 673K, a predominantly stage II compound was present, while above this temperature the compound was disordered. A mixed stage I and II compound was also obtained when a graphite ferric chloride mixture was heated in a stream of chlorine.

A different description of the graphite 52 - 57% ferric chloride compounds was proposed by Hohlwein and Metz (1974). According to these workers, the X-ray diffraction patterns of these compounds showed line shifts and line broadenings which were incompatible with the "stage" model used for describing most of the intercalation compounds. They ascribed their results to a disturbance in the sequence of the layers of graphite and ferric chloride. This model was further refined in 1975 when the authors proposed that the stacking of the layers in these compounds was, in general, disordered but that there was a tendency for the formation of periodic structures. They found that from the diffraction data the degree of order could be ascertained. Its dependence on the preparation conditions was also investigated. They found that the saturated 69% ferric chloride first stage compound always had an ordered stacking sequence (order=1). However, in the range down to 40% ferric chloride, the degree of order was about 0.5. For lower ferric chloride contents, the degree of order decreased. Above 54% ferric chloride, phase separation into domains of pure graphite, pure first stage compound,

and disordered intercalation compound was also observed.

b) Electron Microscopy Study of Graphite Ferric Chloride

Heerschap and Delavignette (1964, 1967) found that intercalation had not altered the ABAB stacking of the graphite layer planes. Dissociation of the ferric chloride residue compound into free graphite and a ferric chloride inclusion was demonstrated. Section 1.6 deals with the electron microscopy of intercalation compounds in more detail.

c) Moessbauer Spectroscopy Study of Graphite Ferric Chloride and Graphite Ferrous Chloride

Hooley et al (1967, 1968) studied the moessbauer spectra of the C_7FeCl_3, $C_{12}FeCl_3$, C_7FeCl_2 and $C_{12}FeCl_2$ stage I and II compounds. The ferric chloride compounds were prepared at 573K and 623K respectively according to the method reported by Hooley (1967). The ferrous chloride compounds were prepared according to the method of Gross (1962), by reduction of the ferric chloride compounds in hydrogen at 648K. It was found that there was electron charge transfer to the Fe III in the ferric chloride compounds at room temperature. This was consistent with Crofts' hypothesis that there was transfer of the π electrons in the graphite conduction band to the d shell of the cations. At room temperature the amount of electron transfer was equal in both stage I and II compounds, but at 80K there was no apparent electron transfer. This was explained by a decrease in the population of the conduction band with decreased temperature. The iron was found to be in virtually only one oxidation state, the Fe^{II}/Fe^{III} ratio being $^1/_{20}$. Thus the formula proposed by Dzurus and Hennig (1957) of $C_n^+Cl^-FeCl_2 3FeCl_3$ where n = 30 to infinity was not substantiated by the experimental results. The graphite ferrous

chloride compounds showed no charge transfer to the iron and had two different sites for the ferrous iron. One of the sites was the normal ferrous chloride lattice site and the other remained unexplained.

Moessbauer studies on the graphite ferric chloride compounds prepared by a variety of methods were also performed by Freeman (1968) Hohlwein et al (1969) and Vol'pin et al (1970). Their results agree well with those of Hooley et al. However, Vol'pin et al (1970) also found that for the graphite ferric chloride prepared in an argon atmosphere using synthetic colloidal graphite the Fe^{3+} high spin ion had two different sites. The small amount of Fe^{2+} found in the spectrum for graphite ferric chloride could arise from the decomposition of $FeCl_3$, the complete transfer of an electron to $FeCl_3$, from trace impurity in the original $FeCl_3$, or from a combination of these mechanisms.

Recent work by Tominaga et al (1974) on graphite ferric chloride was in agreement with previous work. However, for graphite $FeCl_3/AlCl_3$ compounds, these workers found that the spectra changed for different $FeCl_3/AlCl_3$ ratios and high spin Fe II appeared in the spectra for ratios of one or less.

Hohlwein et al (1974) reinvestigated the magnetic properties and Moessbauer spectra of stage I graphite ferric chloride compounds. They did not find any Fe^{2+} at room temperature but it was present at 4.2K. The room temperature isomer shift was close to the value found by Hooley, (1967, 1968), Vol'pin (1970) and Tominaga (1974) but they interpreted this as a relaxation phenomenon. It was suggested that, at room temperature, there is electron hopping of the extra electron in Fe^{2+} among all the iron sites,

and this electron is trapped only at low temperatures. They also postulated that Henning's formula (1957) is correct.

The moessbauer spectra of graphite ferric chloride compounds have been compared with those of ferric chloride naphthalene, anthracene, phenanthrene and perylene (Jadhao et al 1974). It was found that the hydrocarbons are better π electron donors than graphite.

An X-ray and moessbauer study of the first and second stage ferrous chloride graphite compounds has been carried out by Ohhashi and Tsujikawa (1974). They found that the Fe^{2+} ions were in a triangular lattice in the middle of the graphite layers with the nearest six Cl^- ions octahedrally coordinated to the Fe^{2+} ion. In order to explain the two kinds of Fe^{2+} ion sites in the ratio 1:2 found by moessbauer spectra, they proposed that the chloride octahedra around the Fe^{2+} were distorted, one being compressed and two elongated.

1.4.6 Electronic Behaviour of Graphite Ferric Chloride

In 1940 Rudorff and Schulz measured the electrical conductivity of graphite ferric chloride and found that it was greater than that for graphite. The sign of the Hall coefficient measured by Hennig (1956) indicated that electrons were transferred from the graphite to the chloride.

The intercalation of a range of metal halides was studied by simultaneous measurement of electrical resistance and weight gain (Bach and Ubbelohde 1971a,). The results were in agreement with previous workers but threshold conditions for intercalation were lower. From these results a structure for the intercalated metal halides was proposed which involved charge transfer from the

graphite to form a "bond resonance network" in the metal halide anion layers.

$$MX_3 \ldots . (MX_4)^- \ldots . MX_3 \ldots . (MX_4)^-$$

Assuming similar mobilities for charge carriers an attempt was made to correlate the resistivity with the extent of charge transfer and hence with the electron affinity of the ions. However there was insufficient evidence for this comparison. It is of note that the use of well aligned graphite allows a greater degree of reproducibility in intercalation studies. Its use has been pioneered by Ubbelohde who has also investigated its preparation and properties (1969 a,b,c.) Dresselhaus et al (1977) have modelled the electronic effect of intercalation in the dilute limit of stage IV or V. From their studies, experiments designed to detect the number of carriers per intercalated species were suggested.

1.4.7 Catalytic Properties of Graphite Iron Chlorides

a) Graphite $FeCl_3$

Very little interest had been shown in graphite metal chloride intercalation compounds as catalysts, when the present work was initiated. One reaction studied since that time is the further chlorination of chlorinated hydrocarbons using a graphite $FeCl_3$ or $CuCl_2$ compound as catalyst (Schmidhammer and Gabler 1972). The silica supported compound was reacted at 503 - 563K.

Recently, Freeman (1974) made use of graphite metal halide compounds as Friedel Crafts catalysts for acylation and alkylation. The graphite $AlCl_3$ compound was found to be just as effective as free $AlCl_3$, the main difference being that the intercalation compound tended to produce a higher ratio of more substituted derivatives. The author concluded that the intercalation

compound acts as a reservoir for metal chloride, the removal of chloride being temperature and solvent dependent, and that the metal chloride acted as a normal Friedel-Crafts catalyst. He postulated that adsorption of the reactant on the graphite could result in preferential reaction paths. The low catalytic activity of graphite $FeCl_3$, was rationalised in terms of the slow release of $FeCl_3$. Slinkin et al (1975) found that graphite ferric chloride catalysed the alkylation and benzoylation of benzene.

b) Graphite $FeCl_2$

The graphite ferrous chloride compounds have not been widely used as catalysts. Korshak et al (1973) reported that they acted as hardening catalysts in polymeric systems and the products were usable as self lubricating plastics.

1.5 Graphite Metal Compounds

1.5.1 Introduction

Although transition metals cannot be directly intercalated with graphite it is possible to reduce intercalated salts of the metal within the graphite and retain the layer structure of the original compound. The first metal compound prepared was graphite iron (Klotz et al 1962) and recently Vol'pin et al (1970b, 1975a) prepared a range of transition metal graphite compounds. Initially, these materials provided a two dimensional ferromagnetic layer for magnetic studies (Knappwost 1966, 1969) and were not widely studied. At the time the work described in this thesis was undertaken, simple preparation methods for graphite metal compounds were still being developed and their use as catalysts was unknown.

1.5.2 Preparation of Graphite Iron

Klotz and Schneider (1962) formed a graphite iron compound

containing 22% iron by the reduction of graphite ferric chloride with sodium in liquid ammonia. The reduction of metal chlorides in graphite by various reducing agents was later studied by Vol'pin et al (1970b, 1971, 1975a). According to these authors (1975a), whose work in 1970 and 1971, tended to be contradictory, when the metal chloride intercalation compound is reduced by hydrogen at 573K for 4 hours, the intercalation compound decomposes and the layer structure is destroyed. Reduction by aromatic anion radicals such as lithium biphenyl, sodium in liquid ammonia or lithium aluminium hydride, at room temperature, results in retention of the layer structure of the iron within the graphite. The reduction of stage I and II ferric or ferrous chloride graphite compounds produced the corresponding stage I and II iron graphite compounds. Other metal graphite compounds were also prepared in this way. These included chromium, molybdenum, tungsten, iron, cobalt, nickel, manganese and copper. An electrochemical reduction of TiF_4, CrO_3, $CrCl_3$ $FeCl_3$, $CuCl_2$ $TaCl_5$ and $AuCl_3$ graphite complexes has been carried out by Touzain et al (1976) and the mechanism of the reduction has been investigated. The reduction of the intercalated transition metal chloride by intercalated alkali metal has also been shown to occur in the ternary potassium ferric chloride graphite (Ichikawa et al 1972d, Tricker et al 1974, Vol'pin et al 1975b). The reduction is carried out by heating a mixture of the chloride and potassium at 373-425K in an inert atmosphere.

1.5.3 Structural Studies of Graphite Iron

Almost all of the investigations into the structure of these compounds have been performed by Vol'pin et al (1971, 1975a).

These authors, in common with Ubbelohde and Tamaru et al consider graphite as an extension of a large organic molecule and liken intercalation compounds to organometallic complexes. From this model Cr, Mo, W, MnI, FeII and Co III should form compounds with graphite analagous to bis (arene) complexes and Fe, Co, Ni, Mn and Cu should form π complexes of allylic and olefinic types.

a) X-ray Studies

Vol'pin et al (1971,1975a) examined the structure of the stage I and II iron compounds by X-ray methods. In both cases the filled layer thickness was 0.58 to 0.60nm which corresponded to the sum of the thickness of a graphite layer and a monatomic iron layer with Van der Waals bonding.

In some stage I compounds, X-ray lines were found which could be assigned to a spacing of 0.466 nm. However these were not clear and were badly reproduced. This spacing could be explained by a π complex of the allylic or olefinic type where typical Fe - C distances are 0.4 - 0.44nm. Knappwost and Metz (1969) also found an identity period of 0.599nm for the graphite iron compound reduced by sodium in liquid ammonia and explained this spacing as the sum of a monatomic layer of iron and a graphite layer.

1.5.4 Magnetic Studies of Graphite Iron

Knappwost and Metz (1966, 1969) studied the magnetisation of thin layers of iron in a stage I graphite ferric chloride compound reduced by sodium in liquid ammonia. They found that the layers of iron had a saturation magnetisation much lower than in bulk iron. In 1969, they found that the magnetic moment of the graphite iron at saturation did not correspond to the iron content of the sample, and suggested that the iron layers formed large islands separated

by graphite and were coupled antiferromagnetically in the c direction while having a ferromagnetic interaction along the c plane. The spontaneous magnetism exhibited by the compound, which showed the same magnetism and temperature dependence as compact iron, was attributed to non-overlap of some of the layers of iron.

Vol'pin et al (1971) considered the antiferromagnetic coupling unlikely as the sign of the interaction of the intercalated iron was the same as pure iron (Karimov et al 1971). They proposed that there was a ferromagnetic interaction between the layers. As evidence of this the saturation field for the magnetic moment was typical of ferromagnetic materials. In addition, their magnetic and chemical analysis indicated that 30 - 80% of the iron was transformed into an ordered form, and 20 - 70% was in a form which was not magnetically ordered. This latter form could correspond to the proposed Fe(0) complexes with graphite, thus accounting for all the iron content of the sample. It was suggested that the differences in the magnetic data of Vol'pin et al (1971) and the work of Knappwost and Metz, could be the result of the different methods of reduction employed. The formation of amides and of non magnetic γ iron was thought to be the explanation for the lower iron contents measured by magnetic methods. A further attempt to elucidate the nature of the bond between the iron and the graphite in the reduced ferric chloride compounds was made using moessbauer spectroscopy.

1.5.5 Moessbauer Studies on Graphite Iron

A moessbauer study was carried out by Novikov et al (1971) on reduced stage I and II graphite $FeCl_3$ and reduced stage I graphite $FeCl_2$ using lithium biphenyl as reducing agent. Later studies (Novikov et al 1975a) were carried out on iron and ^{57}Co

graphite compounds. The spectrum of the iron compound reduced by lithium biphenyl is complicated but was interpreted as resulting from three types of structures: superparamagnetic particles of α iron, iron clusters which could result from monolayers of iron in the graphite, and a paramagnetic form arising from an iron graphite π complex. This complex comprised at the most 45% of the system. This low percentage was explained as the result of instability of the complex even under mild reducing conditions, leading to decomposition, with aggregation of Fe atoms into ferromagnetic and superparamagnetic clusters. Washing the samples with alchohol and HCl produced an increase in the ferromagnetic structures but did not destroy the π complex. High temperature reduction in hydrogen reduced all the iron to Fe(0) which aggregated to form α Fe particles or alternating layers of graphite and ferromagnetically ordered iron atoms. It was suggested from the magnetic and moessbauer data that there was a 4S electron density transfer from Fe(0) to graphite in the complex, the iron atom structure becoming $3d^{6}4S^{0.35}$.

1.5.6 Catalytic Properties of Graphite Metal Compounds

No catalytic studies had been carried out using these compounds when the work described in this thesis was performed. Subsequently Novikov et al (1973) have utilised graphite nickel, reduced by lithium biphenyl, and further reduced with hydrogen as a selective catalyst for the hydrogenation of isopropanol to acetone and dehydrogenation of cyclohexanol to cyclohexanone.

Using excess alkali metal as a reducing agent, Ichikawa et al (1972e) investigated the activity of the groups 1VB

VB, V1B, V11B, and V111, transition metal graphite compounds for the reduction of carbon oxides. Ethane, ethylene, Me_2O and ammonia were produced from reaction of the complexes with CO/H_2, CO_2/H_2 or $air/CO/H_2$ mixtures at 573K and low pressures. Mashinskii et al (1976) also studied the synthesis of hydrocarbons from carbon monoxide and hydrogen at 573K using graphite metal compounds prepared by reduction of the graphite transition metal chloride by potassium. They found that when the potassium/metal ratio was 1 the compounds were not catalytically active. However, if this ratio is increased there is a corresponding increase in the activity of Co,Mn,and Fe compounds. Other active metal compounds treated with excess potassium were Cu,Os,Cr,Ni,Cu,Pt,and Pd. The catalytic activity appears to be related to an electron transfer from the potassium to the metal.

The synthesis of ammonia was investigated by Ichikawa et al (1972d) using a potassium ferric chloride graphite compound. They found enhanced catalytic activity using this compound compared to either potassium or ferric chloride graphite. A comprehensive study of ammonia synthesis at 523, 573 and 673K and the nitrogen isotope exchange reaction using a transition metal, potassium graphite compound was carried out by Vol'pin et al (1975c, 1977). They found that the graphite metal compounds with excess potassium were more active than the metal chloride potassium complexes. The maximum ammonia conversion at 673K and maximum nitrogen exchange at 623K occurred at a K:Fe ratio of 7:1 indicating that the potassium promotion effect is the activation of nitrogen. Moessbauer studies indicated that the catalytic activity is related to the presence of a negatively charged form of iron produced by electron

donation from potassium. Rodewald (1976) used graphite intercalated with SbF_5 & H_2PtCl_6 and $AlCl_3$ & H_2PtCl_6 reduced with hydrogen for the isomerisation of cyclohexane to methylcyclopentane and of hexane to C_6 isomers. The reduced intercalation compounds were more effective for these reactions than $HSbF_5SO_3F$.

1.6 Electron Microscopy of Graphite Intercalation Compounds

Eeles and Turnbull (1963, 1965) studied the interlamellar compounds of bromine and iodine, using electron diffraction, X-ray diffraction and electron microscopy. They reported that the bromine compound was highly ordered, and discovered a residue compound $C_{28}Br$ with a 2 dimensional bromine structure, consisting of chains of bromine molecules oriented with respect to the graphite layers. This structure was independent of the type of graphite used. Transmission electron microscopy showed the presence of loop and line defects which moved rapidly due to the heating effect of the beam. These defects were very similar to those studied by Heerschap and Delavignette (1964) in the residue compounds of graphite bromine and graphite iodine monochloride and were interpreted as dislocations with stacking fault contrast on one side which formed boundaries of intercalated areas. Contrast analysis revealed that the carbon networks on either side of the intercalate had shifted to AA stacking. A mechanism for the production of residue compounds was proposed which involved movement of these boundary dislocations which would leave behind loops of occluded reactant on their way through the crystal.

In the graphite ferric chloride case, Heerschap and Delavignette (1964, 1967) found that the direction of the burgers vector for the boundary dislocations was perpendicular to the c

planes and, therefore, the graphite had not altered the ABAB stacking on intercalation. Dislocation loops of ferric chloride were found. The formation of the residue compound of ferric chloride graphite was studied and shown to proceed by dissociation of the intercalate into free graphite and a ferric chloride inclusion.

Bacon and Sprague (1961a) describe the intercalation of ferric chloride, bromine and caesium chloride. The compounds examined did not have an ordered structure but had material trapped in cracks and grain boundaries, in conflict with the results of Eeles and Turnbull and Heerschap and Delavignette.

The concentrated potassium graphite and the residue compounds of sodium and potassium have recently been studied by Halpin and Jenkins, (1971). They found that both sodium and potassium remained in the graphite lattice in the form of intercalated rafts, even after heating to 1273K. From contrast analysis, it was confirmed that there was AA stacking at these intercalated areas, and they retained their C_8K or $C_{24}K$ structure. Some heavily doped material gave a diffraction pattern which was ascribed to a thin epitaxial layer of potassium on the surface of the graphite such that the [111] direction of the potassium was parallel to the c direction of the graphite. Halpin and Jenkins (1971) also found a diffraction pattern which they attributed to a potassium superlattice with a spacing of 0.426nm and which they claimed corresponded to a $C_{10}K$ structure. Characteristic features in heavily doped material including ring defects, line and dot moirés, and bright discs. They proposed that the ring defects or contoured areas were moiré patterns caused by tilted lenticular defects. The bright discs were shown to arise from electron absorption

and probably indicate a gap in the intercalated potassium layer.

Carr (1965, 1970) studied the intercalation and oxidation of graphite with a mixture of sulphuric and nitric acids at room temperature. The main structural changes observed on intercalation were the appearance of diffraction phenomena in the form of electron transparent discs and distorted line, dot and spot moiré patterns similar to those found for the concentrated potassium graphite (Halpin and Jenkins 1971). In addition, dense particles were found which could have been a direct image of retained material in the residue compound. The dense particles were mobile and moved along pores in the graphite suggesting that they were composed of sulphuric acid. Dense discs similar to a spot moiré pattern were also observed and attributed to trapped bisulphate material. The residue compound was found to be generally disordered with spot moiré patterns resulting from small areas of original lamellar compound. The origin of the electron transparent discs was thought to be the collapse of the graphite layers on formation of the residue compound, leading to crumpling of the graphite sheets. It was these crumpled areas which were thought to be associated with the discs. Rearrangement of these badly fitting parts of the crystal could explain the observed movement of the discs. This mechanism was also used to explain the formation of vacuum blisters which could give rise to the distorted moiré patterns.

Recently, Evans and Thomas (1975) made a high resolution study of potassium graphite, graphite bromine, graphite ferric chloride and the ternary compounds graphite potassium ferric chloride, and potassium graphite bromine. Although the authors appear to agree with the work of Cowley and Ibers on graphite $FeCl_3$ their

published diffraction pattern was of the graphite ferrous chloride compound. Using the (100) reflections they showed the lattice image of the intercalate and suggested possible configurations which could give rise tothe observed image. Ahigh resolution investigation of the graphite bromine compound confirmed the earlier work of Eeles and Turnbull for the chain structure of the bromine molecules within the graphite. The electron diffraction pattern for the potassium graphite compound corresponded to the pattern obtained by Halpin& Jenkins (1971) for the surface epitaxial potassium film on the heavily doped complex. In agreement with Halpin and Jenkins (1971) they also found potassium in hexagonal islands with oriented edges. When powdered SP1 graphite was used for intercalation, it was shown from the interplanar spacings that the potassium was intercalated at random in the residue compound. Investigation of the "ternary compounds" showed that in the case of potassium bromine graphite, the bromine had decomposed the potassium graphite to form graphite with epitaxial K Br crystals on the graphite surface. Similarly, electron diffraction showed that potassium reduced the $FeCl_3$ to α iron and potassium chloride.

1.7 Aim of the Present Work

Graphite intercalation compounds have potential catalytic activity for a range of reactions with the possibility of selectivity in the reaction product. This selectivity would arise if reaction occurred within the layer planes of the graphite where steric constraints are likely to be important. Interest in intercalation compounds as catalysts results, not only from their structural properties, but also their electronic properties. It is possible to prepare an intercalation compound with any number and type of charge carrier and it may be possible to

design an intercalation compound with the required electronic characteristics for a specific reaction.

Reaction within the graphite planes could result in structural modifications in the intercalation compound, providing information on reaction sites and the formation of intermediates. In addition, changes in catalytic activity may result from modification of the original compound structure under reaction conditions. The most suitable technique for studying these structural changes in detail is transmission electron microscopy.

The present work was therefore undertaken to examine the structure of concentrated intercalation compounds and the structural changes occurring after use as potential catalysts for the synthesis of ammonia from nitrogen and hydrogen, and the hydrogenation of butadiene. The compounds chosen were potassium graphite, a typical donor complex, graphite ferric chloride and graphite copper sulphide, typical acceptor complexes and graphite iron, a new type of compound with the possibility of activity at different iron sites. When this work was undertaken, no transmission electron microscopy study had been carried out on these concentrated intercalation compounds.

2. EXPERIMENTAL

2.1 Materials

2.1.1 Graphite

Spectroscopically pure (SPI) graphite was used in the preparation of the potassium graphite used in atmospheric pressure studies. This material is a very pure, almost single crystal natural graphite, and its impurity content is shown in Table 1. (Carr 1965).

Pile grade A (PGA) polycrystalline graphite was used as a starting material for potassium graphite in the elevated pressure ammonia synthesis runs. Typical analysis figures are given in Table 2 (Carr 1965).

Madagascar natural graphite, supplied by Rocol Ltd, was used to prepare graphite ferric chloride, and graphite iron. The stated impurity content is listed in Table 3. This graphite is less pure than SPI or PGA graphite, the main impurities being aluminium, silicon, iron and molybdenum.

2.1.2 Chemical Reagents and Solvents

All solid and liquid chemicals used in this study were BDH analar grade except potassium, lithium and anhydrous ferric chloride.

Potassium, for the preparation of potassium graphite, and 99.9% lithium for the preparation of lithium biphenyl, were obtained from BDH. They were stored under liquid paraffin and cleaned (with analar benzene) before use. Further purification of the potassium was carried out by distillation into breakseal tubes (Sections 2.2.1 and 2.3.1). 96% Anhydrous ferric chloride supplied by BDH was sublimed under vacuum before use in the preparation of graphite ferric chloride. Iron powder was reduced with hydrogen at atmospheric pressure at 673K for 10 hours before use.

TABLE 1

SPI Graphite

Typical Analysis (ppm)

Boron	< 0.02
Iron	0.05
Copper	0.04
Aluminium	< 0.015
Barium	< 0.015
Beryllium	< 0.015
Bismuth	< 0.06
Calcium	< 0.15
Chromium	< 0.015
Cobalt	< 0.015
Indium	< 0.04
Lead	< 0.025
Magnesium	< 0.025
Manganese	< 0.015
Molybdenum	< 0.015
Nickel	< 0.025
Silicon	< 0.015
Strontium	< 0.02
Tin	< 0.02
Titanium	< 0.02
Tungsten	< 0.08
Vanadium	< 0.02
Zinc	< 0.08
Sodium	< 0.10
Lithium	< 0.005

TABLE 2

PGA Graphite

Typical Analysis (ppm)

Ash %	0.005 - 0.025
Boron	0.03 - 0.16
Iron	<2 - 16
Copper	<0.01 - 0.5
Phosphorus	<0.1 - 0.2
Hydrogen	15 - 40
Aluminium	0.25 - 2.5
Barium	0.3 - 15
Beryllium	<0.02 - <0.03
Bismuth	<0.06 - <0.15
Calcium	7 - 60
Chromium	0.1 - 0.7
Cobalt	<0.01 - <0.03
Indium	<0.04 - 0.08
Lead	0.04 - 2.5
Lithium	<0.04 - 0.15
Magnesium	0.03 - 1.5
Manganese	0.01 - 0.06
Molybdenum	<0.02 - 1.5
Nickel	0.03 - 8
Silicon	15 - 60
Sodium	<1 - 2
Strontium	0.011 - 1
Tin	<0.02 - 0.08
Titanium	1 - 15
Tungsten	<0.08 - <0.2
Vanadium	0.4 - 30
Zinc	<0.08 - <0.2
Dysprosium	<0.008 - 0.015
Europium	<0.0011 - 0.008
Gadolinium	<0.005 - 0.015
Samarium	<0.04 - 0.04

TABLE 3

Purified Madagascar Graphite

Typical Analysis (ppm)

Aluminium	160
Barium	<0.02
Beryllium	<0.02
Bismuth	<0.04
Boron	<0.1
Calcium	1
Cadmium	<0.2
Chromium	1
Cobalt	2
Copper	1.4
Iron	160
Lead	4
Lithium	0.2
Magnesium	10
Manganese	14
Molybdenum	40
Nickel	2
Potassium	6
Silicon	540
Silver	0.04
Sodium	4
Tin	<0.04
Titanium	10
Vanadium	2
Zinc	<0.2
Zirconium	1

Analar tetrahydrofuran was dried by distillation from sodium hydroxide pellets before use in the preparation of lithium biphenyl.

2.1.3 Gases

Hydrogen gas (99% Purity), was obtained from Air Products and in the reduction experiments was further purified by an Engelhard Catalytic Purifier which, according to specifications, reduced the oxygen content to <1 ppm. Nitrogen gas was obtained from Air Products. In the ammonia synthesis heated copper turnings or freshly made potassium films were used to purify the gases. A mixture of 33% nitrogen/hydrogen was supplied by BOC and further purified over a fresh potassium film. 99.9% pure butadiene was supplied by B.O.C. and used without further purification.

2.2 Apparatus

2.2.1 Vacuum Systems

System I

The apparatus used for the preparation and reaction of potassium graphite, graphite ferric chloride, graphite ferrous chloride and graphite copper sulphide with a nitrogen/hydrogen gas mixture is shown in Figure 7. It consisted of a vacuum system of Pyrex glass supported on a framework of Aluminium Alloy rods. The main system was constructed from 12 mm ID tubing with the pumping system manifold and gas purification vessels A and B of 25 mm ID tubing. Springhams high vacuum greased stopcocks were used in the system. KEL-F high temperature grease was used for stopcocks 17 and 18 near the reaction zone and Apiezon L was used for all other stopcocks. The pumping system consisted of an Edwards E04 Oil diffusion pump backed by an Edwards rotary pump. A cold finger trap for acetone/solid CO_2 separated the diffusion and rotary pump and a similar trap separated the diffusion pump from the vacuum system. The rotary pump was isolated from the glass system by a

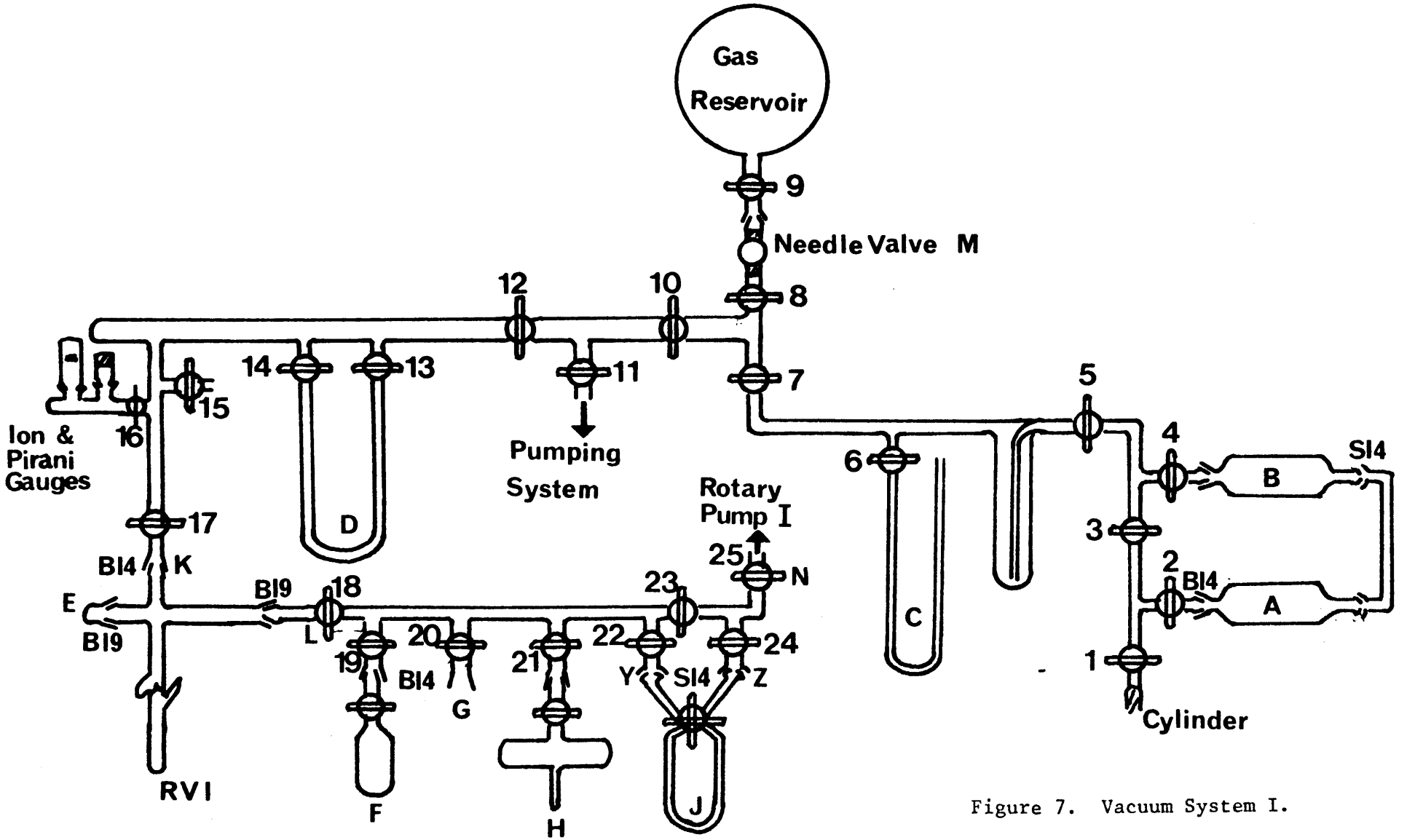

Figure 7. Vacuum System I.

length of flexible rubber tubing. An Edwards Pirani gauge and a Metrovac VC-9 ion gauge were used to measure pressures <1 torr. The gas pressures > 1 torr for the reaction vessel were measured on mercury manometer D with the reference arm under vacuum.

The system can be divided into 4 main parts; the gas inlet system, stopcocks 1-9, the reaction zone, stopcocks 17-18, the gas product collection system, stopcocks 18-25 and the potassium distillation system from stopcock 15.

Gases were admitted to the system I via the gas inlet system. This consisted of 3 mm OD copper tubing attached to the cylinder head and connected to the vacuum system via a copper to glass seal. The gas was purified by passing through vessels A + B which contained either heated copper turnings, or had a freshly deposited potassium film. These vessels were attached to the system by ball and socket joints sealed with black wax. A solid carbon dioxide/acetone slush trap was also included after the vessel A + B and the purified gas was stored in a 5 litre bulb fitted with a tap and an Edwards needle valve. Gas pressures above 1 torr were measured by a mercury manometer C with the reference arm at atmospheric pressure.

The potassium distillation system, figure 8, consisted of a distillation vessel P and a bank of four breakseal receiver tubes attached by thick walled side arms to a manifold. The distillation vessel P, made of 18 mm ID Pyrex tubing, contained the cleaned potassium. This was introduced into the vessel via a thick walled side arm which was subsequently sealed. The manifold was connected to the glass vacuum system via valve 15.

The reaction vessel varied with the particular intercalation compound and preparation method employed. For the synthesis of potassium graphite by Hérold or Rudorff's method using distilled potas-

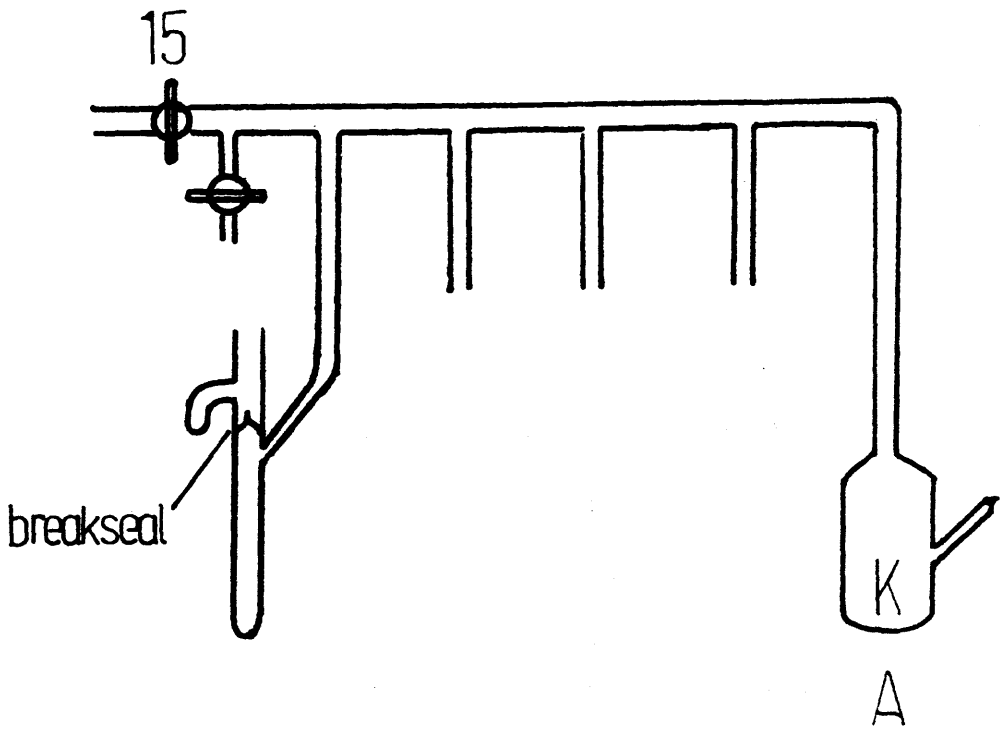

Figure 8. Apparatus for Potassium Distillation.

sium, the Pyrex reaction vessel RV1, 15 cm long with the main body 15 mm ID, (figure 9) was used. This was attached to the vacuum system at cones K and L which were sealed with black wax. The breakseal tube containing distilled potassium was glassblown to the reaction vessel at the beginning of each run. The graphite was contained in a silica boat inserted through the B19 cone E and held in place by a glass rod. For the Rudorff synthesis using potassium pieces cleaned in benzene, reaction vessel RV2 was employed. The graphite ferric chloride compound was prepared in an 18 cm long tube RV3 attached at cone E of RV2.

The gaseous product collection system was designed for removal of Mass Spectrometric samples at F and G and Gas Infra Red samples at H. U-tube, J, for flow experiment product collection was fitted at ball and socket joints Y and Z.

System II

The vacuum system for the reaction of graphite ferric chloride, graphite ferrous chloride and graphite iron with butadiene/hydrogen gas mixtures, is shown in figure 10. This was constructed as in the Vacuum System I from 15 mm ID tubing. The system was pumped via stopcocks 8 and 22. System II can be divided into three main areas; the gas inlet system from stopcocks 1-7, the reaction zone, stopcocks 11-12, and the gas product collection system from stopcocks12 - 23.

Gas was admitted to the system through the gas inlet system which consisted of a purification vessel H, a liquid nitrogen cooled trap J, mercury manometer A and a 5 litre bulb G which acted as a butadiene reservoir. The purification vessel H was used for hydrogen only and contained a film of freshly deposited potassium. The reaction vessel for reaction of graphite iron was RV4 (Figure 11), volume 61 mls, constructed from 25 mm ID silica with a cold finger

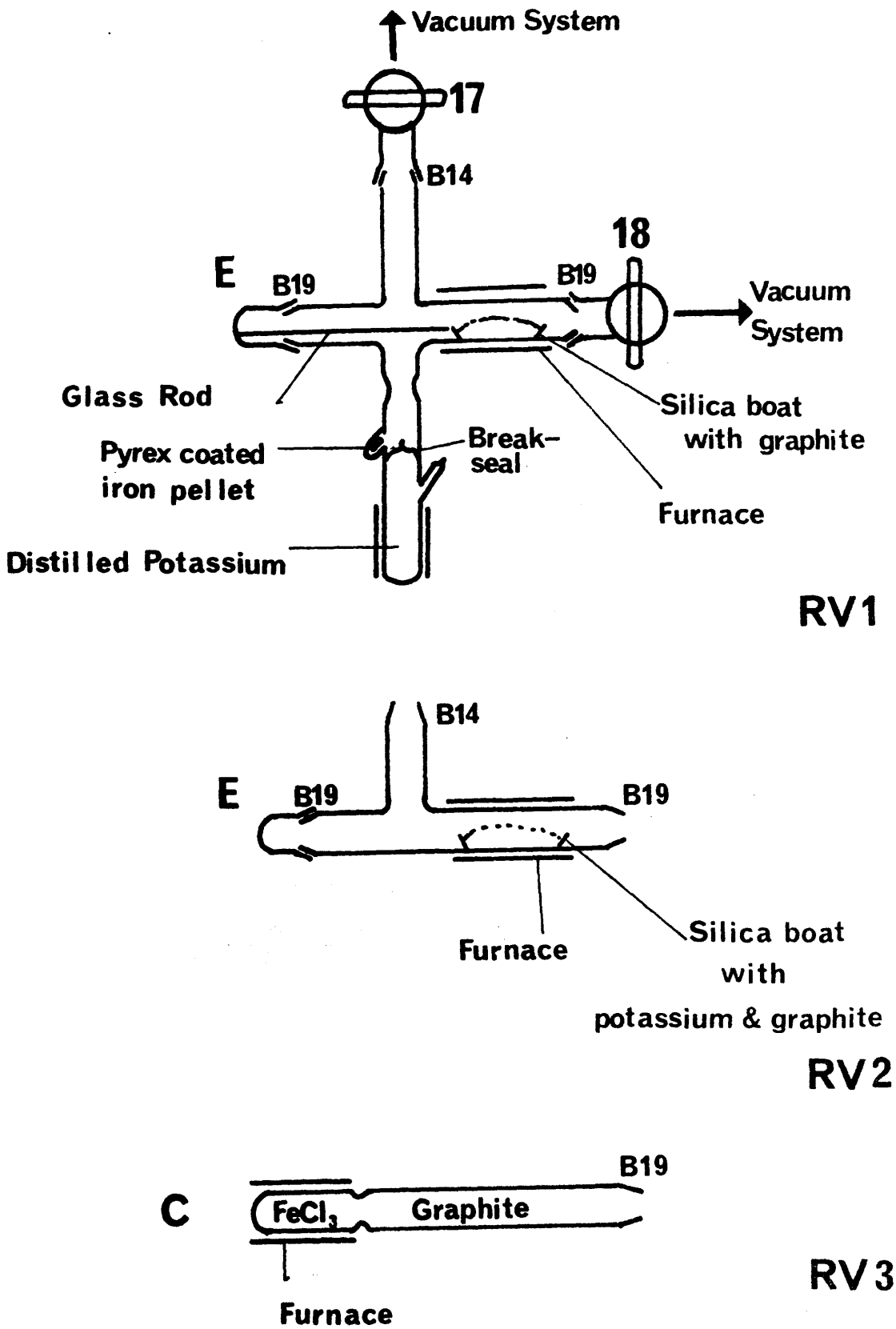

Figure 9. Reaction Vessels 1-3.

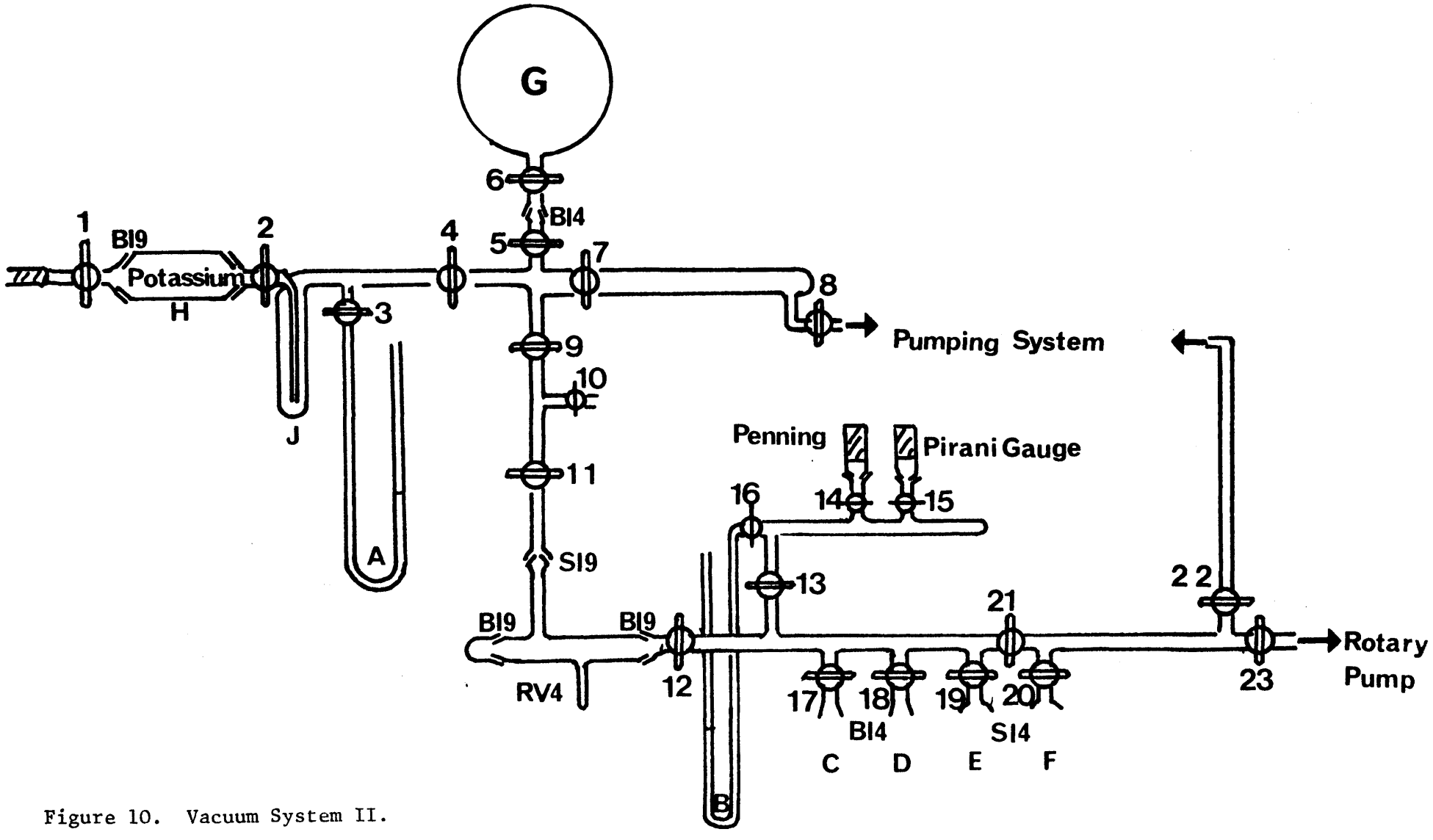

Figure 10. Vacuum System II.

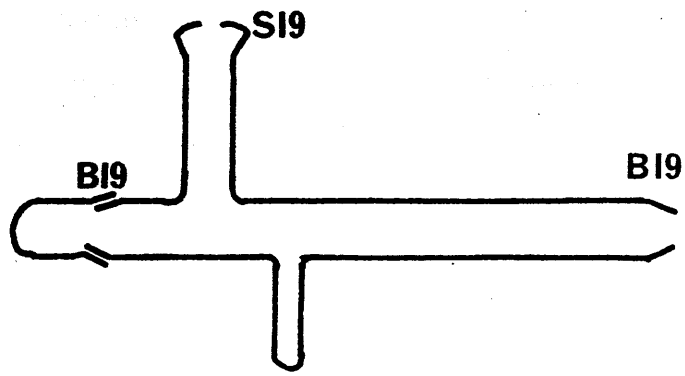

RV4

Figure 11. Silica Reaction Vessel 4.

for butadiene condensation. The reaction vessel for graphite ferric chloride and ferrous chloride preparation and reaction was RV3 fitted with a B24 socket and attached to RV4. Pressures <1 torr in the reaction zone were measured at K using an Edwards Pirani Gauge model 9A with total range 760-0.001 torr with automatic range switching. For pressures > 1 torr a mercury manometer B with the reference arm open to the atmosphere was used. Gas samples for Mass Spectrometric and Gas Infra Red Analysis were removed as in System I using tubes at C,D,E and F.

2.2.2 Furnace Construction

The reaction vessels and gas purification systems were heated using furnaces made to fit tightly round the reaction zone of the vessels. The furnaces were constructed by forming a piece of mica to the correct size and shape. The former was covered with a thin layer of high temperature cement and allowed to harden in a warm oven. Nichrome wire (11Ω/yd resistance) was wound round the furnace. The windings were coated with cement and allowed to harden. The heating voltage was applied across the Nichrome wire by means of a "Variac" controller. The furnace temperature was measured using Platinum/13% Rhodium/Platinum thermocouple cemented in the centre of the furnace. A similar thermocouple immersed in a dewar flask containing ice water was used as a reference and all connections were made using compensating leads. The potential difference between the two thermocouple junctions was measured using a potentiometer and temperatures obtained from JMC standard calibration tables.

2.2.3 Elevated Pressure Reaction System

The apparatus for the reaction of a high pressure (2 atm) nitrogen/hydrogen gas mixture with potassium graphite is shown in figure 12.

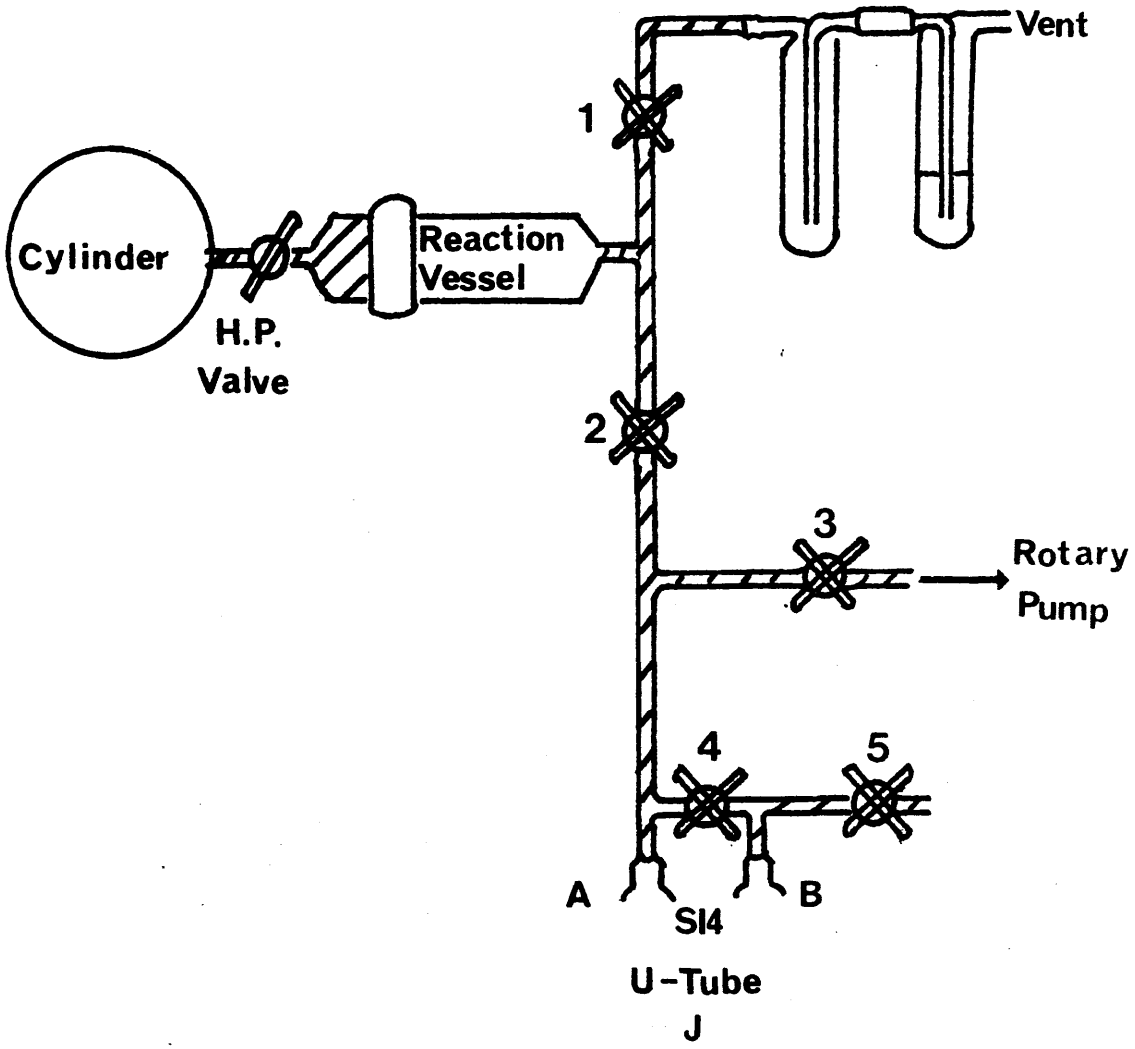

Figure 12. Elevated Pressure Apparatus.

A cylinder of nitrogen/hydrogen 1/3 gas mixture was connected via a high pressure regulator to ¼" ID copper tubing. The reaction vessel, which was a cylinder of ½" ID copper tubing 8 cm long was attached to the gas inlet line via a Swagelok connection. The reaction vessel was braised to a ¼" ID copper tubing system fitted with Edwards needle valves 1-5. The system was evacuated using an Edwards rotary pump. Gas samples for analysis were collected in U-tube J attached at sockets A + B which were connected to the system by copper to glass seals.

2.2.4 In Situ Reaction System

The experimental system for in situ reaction in the electron microscope has been described previously (Fryer 1968). Figure 13 shows the gas inlet system for the microscope. This was constructed from ¼" ID Cu tubing fitted with an Edwards valve and a fine control needle valve for the gas connection to the microscope via the objective aperture. The system was evacuated using an Edwards oil diffusion pump E02 backed by a rotary pump. A reservoir was used to allow the pumps to be switched off during observation, to reduce vibration in the microscope. The specimen heating was effected by a Siemens Pt resistance heater. The temperature was calculated from the calibration curve of input power against temperature. The pressure in the inlet system was measured using a Pirani gauge.

The gas was sprayed onto the surface of the specimen from a small orifice in a specially adapted objective aperture centring rod.

2.3 Preparation of Intercalation Compounds

2.3.1 Potassium Graphite

The concentrated potassium graphite compound, C_8K, was prepared by Hérold's method (1955) using distilled potassium and by the method of Rudorff and Schulz (1954) using either distilled potassium or potassium

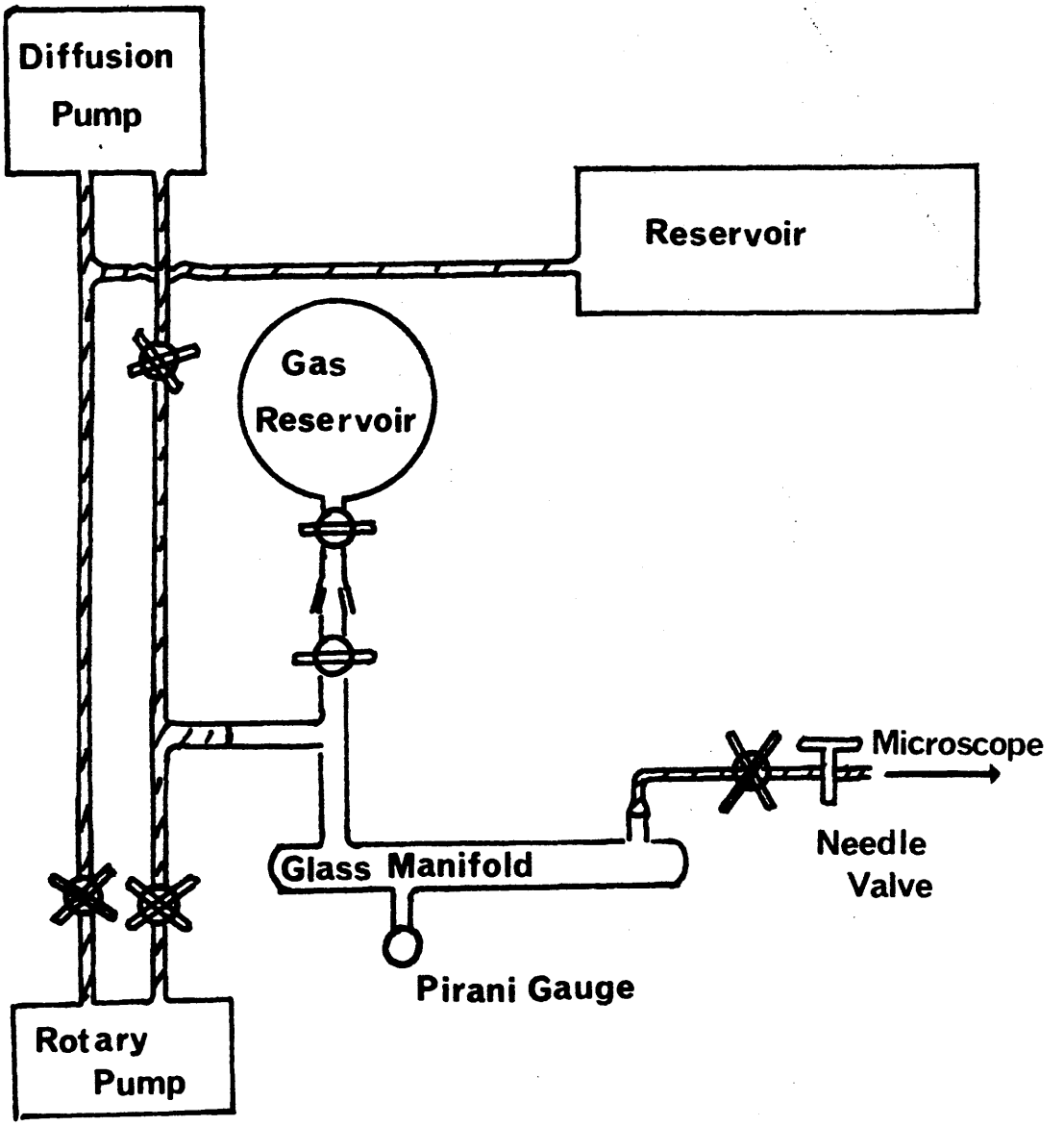

Figure 13. Schematic Diagram of Gas Inlet System for In Situ Studies

pieces cleaned in benzene.

The potassium distillation was carried out using the apparatus described in Section 2.2.1. Approximately 2 g of potassium pieces, cleaned in benzene, were introduced into the distillation vessel A (Figure 8) via the side arm which was sealed off. The system was evacuated and the potassium was distilled using a bunsen flame and condensed in the receiver tubes cooled in solid CO_2/ acetone slush. The glass between A and the receiver tubes was also heated to avoid premature condensation of the potassium. After distillation was completed the receiver tubes were removed from the system by sealing off the side arms under vacuum.

a) Hérolds method

In this method the graphite and potassium are heated separately, the potassium being maintained at a constant temperature T, (523K), while the temperature of the graphite, T_2, ($T_2 > T_1$), is varied depending on the stage of compound required. This method ensures that excess potassium is distilled back to the potassium melt and is not adsorbed on the graphite intercalation compound.

The C_8K compound was prepared using the glass vacuum system I described in section 2.2.1 and reaction vessel RV1 (Figure 9). A silica boat containing 1.0 g SP1 graphite was inserted into RV1 and held in place by means of a glass rod. The vessel was evacuated to 10^{-4} torr and isolated. The breakseal on the distilled potassium was ruptured using the glass coated iron slug held in the small side arm and controlled by an external magnet. The potassium and the graphite were then heated to the temperatures 523 and 573K respectively and allowed to react for 12 hours. A colour change to golden yellow was observed within a few minutes.

b) The method of Rudorff and Schulz (1954) involves heating

together a mixture of graphite and clean potassium under vacuum. The reaction temperature is determined by the particular stage of compound required and for the Stage I compound is 573K. The vacuum system I (section 2.2.1) and reaction vessels RV1 and RV2 (Figure 9) were used for this preparation.

RV1 was used for the preparation involving distilled potassium. 1.0g SP1 graphite was placed in a silica boat and inserted into the reaction vessel. The system was evacuated and RV1 isolated. The breakseal was ruptured and the potassium was distilled from the receiver tube and condensed on the walls of RV1 around the graphite. The receiver tube was sealed off and the potassium and graphite were then heated together at 573K for 12 hours. Reaction vessel RV2 was used for the preparation involving freshly cut potassium pieces cleaned in benzene. Approximately 0.45 g of clean potassium pieces were placed in the silica boat with 1.0 g of SP1 graphite and inserted into RV2. The system was evacuated and RV2 isolated as before. The mixture of graphite and potassium was heated to 573K for 12 hours to produce the C_8K compound.

In Situ Preparation

In order to examine the potassium graphite compound in the TEM, without decomposition in air, the compound was prepared within the microscope. A Pt/Ir 7-holed mount coated with a SiO film was dipped into some SP1 graphite and examined in the Transmission Electron Microscope to ensure that suitable thin flakes of graphite were available for intercalation. A small piece of clean freshly cut potassium was placed on the mount which was quickly fitted to the Siemens hot stage and inserted into the microscope. The heater power was adjusted to give a specimen temperature of 573K and maintained for four hours. This treatment tended to cause disintegration of the SiO film and only

a few areas of graphite were available for examination at the end of each run.

2.3.2 Graphite Ferric Chloride

The preparation method employed was based on the work of Rudorff and Schulz (1940) and Croft (1956a) and gives the first stage compound (C_7FeCl_3). Reagent grade anhydrous ferric chloride (ca. 4g) was inserted into the end A of reaction vessel RV3 (Figure 9) on systems I or II and 1.5 g graphite, PGA or Rocol was placed near the mouth of the reaction vessel at B. Triton kaowool, outside the reaction zone, was used to prevent movement of the graphite on evacuation.
The reaction vessel was attached to the vacuum system I or II described in section 2.2.1, and evacuated to ca.10^{-4} torr. A furnace was placed over the part of the reaction vessel containing the ferric chloride which was sublimed under vacuum at 573K for 6 hours. At the end of this time the furnace was removed and the portion of the reaction vessel containing the residual material was removed by melting the glass and drawing it off under vacuum. The remaining part of the reaction vessel containing the graphite and sublimed $FeCl_3$ was then heated under vacuum at 573K for 12 hours. Excess ferric chloride was sublimed from the graphite ferric chloride at the end of the preparation by adjusting the furnace position to cool one end of the reaction vessel.

2.3.3 Graphite Copper Sulphide

This compound was prepared according to Croft's method (1956c). Analar copper powder, sulphur and SP1 graphite were mixed in the ratio 1:2:1 and inserted into a reaction vessel RV3 (Figure 9). A Triton kaowool plug was used to retain the mixture in the reaction tube which was attached to the glass vacuum system I. The reaction tube was evacuated carefully and the mixture was heated to 793K for 17 hours. The compound was washed with CS_2 before use.

2.3.4 Graphite Ferrous Chloride

Graphite ferric chloride was prepared as described in section 2.3.2 and reduced according to the method of Gross (1962). Without cooling the intercalation compound, 600 torr of purified hydrogen from a cylinder was admitted to the previously evacuated vessel via the gas inlet system. The reduction was allowed to proceed for 6 hours at 663 K. The system was again evacuated and the process repeated.

2.3.5 Graphite Iron

The graphite iron compound was prepared by reduction of graphite ferric chloride using lithium biphenyl in THF (Vol'pin et al 1970).

Lithium biphenyl was prepared according to the method of Eisch (1963). The reaction vessel consisted of a 100 ml 3-necked flask fitted with a condenser, nitrogen inlet and nitrogen outlet. THF was dried by refluxing for 24 hours over fresh sodium and 25 mls were distilled under nitrogen into the reaction vessel. 2.31g biphenyl and 0.23 g lithium, freshly cleaned in benzene, were added to the THF. The mixture was stirred with a magnetic stirrer for 2 hours until a deep blue colour was obtained. The condenser inlet was replaced by a sleeved thermometer dipping into the solution and $\sim$3 g of freshly prepared graphite ferric chloride were transferred under nitrogen from the vacuum system to the lithium biphenyl solution. The solution was allowed to react with continuous stirring for 12 hours with the temperature maintained below 323K using a water bath. The compound after reduction was heavily contaminated and was washed repeatedly in dry THF, ethanol and methanol before use. It was observed that a bar magnet caused the graphite iron flakes to align themselves with the basal plane parallel to the magnetic field.

2.3.6 Analysis of Graphite Iron

Solution Method

The iron estimation was carried out by the Thiocyanate method (Vogel). A weighed portion of graphite iron was boiled in a 4N HCl solution for 4-5 hours to dissolve the iron. The solution was evaporated nearly to dryness to remove excess acid, and diluted with water. The iron was oxidised to Fe^{3+} with dilute $KMnO_4$ and made up to 500 mls with demineralised water. 5 ml of ∿ 4N thiocyanate solution and 2-4 ml 4N HCl were added to 50 mls of the iron solution. The transmittance at 480mμ of the resulting solution was determined using a Uvispek spectrometer relative to acidified thiocyanate solution. A calibration curve, constructed using standard iron solutions, was used to convert transmittance values to concentration.

Gravimetric method

Weighed quantities of graphite iron were placed in a platinum crucible fitted with a lid and heated in a muffle furnace to 1273K for several hours. The crucible was allowed to cool in a dessicator and weighed. This procedure was repeated until reproducible results were obtained. It was assumed for the calculation of results that all the iron had been converted to magnetite.

2.4 Catalytic Action of Intercalation Compounds

2.4.1 Reaction of Potassium Graphite with Nitrogen/Hydrogen Gas Mixture

The apparatus used has been described in section 2.2.1. The gas mixtures used were 25% nitrogen/hydrogen or 33% nitrogen/hydrogen mixtures and were either premixed from a cylinder or were made up in the 5ℓ reservoir in vacuum system I. The gases were purified via vessels A + B and the gas trap was cooled to 77K. The potassium graphite concentrated compound was prepared as described in Section 2.3.1. In practice, although the conditions were correct for

the formation of C_8K and the characteristic golden colour was present, not all of the graphite in the centre of the silica boat had free gas access and it is possible that lower stage compounds were also present. Both static and flow experiments were carried out.

For the flow experiments, tap 25 (Figure 7) was replaced by a needle valve. The 5 litre bulb was used to provide a reservoir of gas which was gradually pumped through the reaction vessel containing potassium graphite at reaction temperature, and through the gas collection system by the rotary pump I. The flow rate was adjusted using the two needle valves M & N, to give a flow rate of 10 mls/min at a pressure of 30 torr for the required time, usually 1 hour. The flow rate had been previously calibrated for the needle valve settings.

The products were trapped out at the U-tube, cooled to liquid nitrogen temperature for the duration of the experiment. In addition, attempts were made to condense products at various time intervals, typically after 15 and 30 mins reaction time by cooling the MS or IR cell to 77K. At the end of the reaction time the product in J was analysed for ammonia using Nesslers reagent or, the product was vacuum distilled into the appropriate receivers for MS or IR analysis. In a few cases, after reaction, the intercalation compound was heated to 673K and any decomposition products collected in the MS or IR gas sampling vessels. For static experiments the gas mixture and intercalation compound were prepared in the same way. The system was evacuated and reaction temperature adjusted to the required value. A total gas pressure of 750 torr was admitted to the reaction vessel. The reaction vessel was isolated and the reaction allowed to proceed for the required time. Gas samples were removed by condensing the products into the tubes F, G and H at 77K. Removal of the cooled catalyst was carried out after pressurising the system with nitrogen.

Each experiment was repeated at least twice for a given set of experimental conditions. Reaction conditions are summarised in Table 4. Blank runs on SPI and PGA graphite were also carried out.

2.4.2 Product Analysis

The mass spectra were obtained using an AEI MS 12 and were interpreted by comparison with the breakdown patterns of possible products. The gas infra-red spectra were obtained using a Perkin Elmer grating spectrometer. The path length for the gas cell was 10 cm and usually had a gas pressure > 2 torr. The spectra were calibrated against polystyrene bands at 1029, 1603 and 2851 cm^{-1}.

Nessler's reagent, K_2HgI_4, was also used to detect the presence of ammonia. This reagent reacts with ammonia to produce a yellow colouration and was used for a qualitative analysis and also for quantitative assessment of ammonia using a Hilger Uvispek spectrometer. Nessler's reagent was prepared according to the method of Snell and Snell. 10g of analar potassium iodide were mixed with 7 mls of demineralised water. A saturated solution of analar mercuric iodide was added to the KI solution until a red precipitate persisted. 80 mls of 9N NaOH solution was added and the mixture left to settle for 1 day. The supernatant liquid was decanted into a brown bottle. This reagent will detect 0.02mg NH_3/litre H_2O. The product contained in the U-tube J was dissolved in demineralised water and the solution made up to 25 mls. 2½ mls of this solution was placed in a UV cell and 1 drop (0.05 mls) Nessler's reagent added. This solution was allowed to stand for 5 mins before measuring the transmittance at 410 mμ relative to a demineralised water blank. The conversion to ammonia concentration was made using a calibration curve set up using standard NH_4Cl solutions. The limit of detectability of this technique under static conditions was >1% conversion to ammonia.

TABLE 4

Reaction Conditions for Ammonia Synthesis from Nitrogen/Hydrogen

Catalyst	Temperature	Time (Hrs)	Press. (torr)	Type	N_2/H_2 Ratio
Concentrated Potassium Graphite	483-573K	1	30	FLOW	1/3
	573K	0.25,1.25,20	760	STATIC	"
	533K	2.5,10	2 ATS	FLOW	"
	573K				
	723K	21	2 ATS	STATIC	
SPI Graphite	563K	15	600	STATIC	1/3
	523K	1	30	FLOW	"
PGA Graphite	523K	0.5	50	FLOW	"
	513K	1	400	STATIC	"
Gr $FeCl_3$	558K	1.5	40	MIXED	1/2
		24	640	STATIC	"
	523K	15	600	STATIC	"
GrCuS	723K	54	500	STATIC	1/2
	673K	36	"	STATIC	"
Reduced Graphite $FeCl_3$	563K	22	700	STATIC	1/2

2.4.3 Elevated Pressure Reaction of Nitrogen/Hydrogen Mixture with Potassium Graphite

The apparatus has been described in Section 2.2.3, Figure 12. The potassium graphite was prepared in situ by Rudorff's method using cleaned potassium pieces and PGA graphite. The temperature of the potassium graphite was then adjusted to the required reaction temperature. For the flow experiments, the gas mixture at 2 atmospheres was passed through the reaction vessel into the atmosphere via a Dreschel bottle containing silicone oil. For gas sampling, part of the flow was diverted through the U-tube immersed in liquid nitrogen. At the end of the reaction the collected product was redistilled into the MS + IR collection vessels using the gas product collection system of the vacuum system I (section 2.2.1). For static experiments, the gas mixture at two atmospheres pressure was admitted to the prepared potassium graphite in the reaction vessel. The vessel was isolated and the reaction allowed to proceed for the required time. The products were collected in the liquid nitrogen cooled U-tube at the end of each run.

Reaction conditions are summarised in table 4.

2.4.4 In Situ Reaction of Potassium Graphite

The apparatus and modifications to the electron microscope and the in situ preparation of the potassium graphite have been described in sections 2.2.4 and 2.3.1. After preparation of the complex in the microscope the temperature was adjusted to the reaction temperature and the gas inlet system was evacuated for 1 hour before opening to the microscope. The gas flow through valve A was adjusted to give $\sim 10^{-3}$ torr on the microscope penning gauge. This pressure is low enough for the high voltage supply to function but because of the design of the gas inlet this corresponds to a much higher

pressure (c.a. 1 torr) at the specimen. The potassium graphite was reacted at various temperatures by adjusting the power input to the heater and micrographs taken at suitable time intervals.

2.4.5 Reaction of Acceptor Complexes with Nitrogen/Hydrogen Mixture

The synthesis of ammonia from nitrogen and hydrogen was investigated using graphite ferric chloride, graphite copper sulphide and reduced graphite ferric chloride. The vacuum system I (section 2.2.1) and the reaction vessel RV3 (Figure 9), were used in this series of experiments. The procedure adopted was that described in section 2.4.1. The reaction conditions are summarised in table 4. In some cases the catalyst was heated to >673K at the end of the experiment to exfoliate the graphite and release any trapped product.

2.4.6 Reaction of Graphite Iron with Butadiene/Hydrogen

The apparatus, System II, has been described in section 2.2.1. The butadiene was stored in the 5 litre bulb G fitted with a cold finger. 0.5 g of graphite iron, prepared as in section 2.3.5 was placed in the reaction vessel RV4 (Figure 11). Triton kaowool plugs, outside the heating zone, were used to prevent movement of the graphite iron.

For experiments above 393K, the graphite iron was heated gently under continuous evacuation to 393K before reaction to remove trapped THF. The catalyst was cooled and 200 torr butadiene, measured on manometer B, was admitted to the reaction vessel. The excess butadiene in the line was condensed back into bulb G using the liquid nitrogen cooled cold finger. The butadiene in the reaction vessel was condensed into the liquid nitrogen cooled cold finger and the reaction vessel re-evacuated. The gas inlet system was evacuated and 460 torr hydrogen was admitted to the reaction vessel via vessel H which contained a freshly deposited potassium film and through gas

trap J cooled to 77K. The reaction vessel was isolated and the butadiene allowed to warm up. The graphite iron was reheated to the reaction temperature and allowed to react for the required time. After reaction the total product pressure was measured at manometer B. The condensable products were collected in the MS tube C and I R tube E cooled to 77K. The final pressure was noted. The experimental conditions summarised in Table 5 were designed to study the effect of reaction temperature on the product distribution. In addition, a more detailed study of the product variation with reaction time was made in the temperature range 573-673K.

2.4.7 Reaction of Reduced Graphite Ferric Chloride, Reduced Ferric Chloride, Graphite Iron acid washed, Graphite Bisulphate, Iron Powder and Madagascar Flake Graphite with Butadiene/Hydrogen

Comparative experiments were carried out using the same apparatus and procedure as for graphite iron (section 2.2.4, 2.4.6) using graphite iron washed with nitric acid to remove surface iron, graphite bisulphate, and iron powder. Similar runs were also performed using reduced graphite ferric chloride, reduced ferric chloride and madagascar flake graphite. Comparison of the iron powder with the graphite iron was difficult because the particle size of the iron powder was much larger than the iron particles in graphite iron. In the latter case, the effective particle size and surface area of the iron were difficult to estimate as they varied with temperature. In order to highlight any activity by iron the quantity used was four times that for graphite iron.

2.5 Transmission Electron Microscopy

All the graphite intercalation compounds were examined before and after reaction using Transmission Electron Microscopy

The use of electron microscopes to obtain enlarged images of specimens dates from Knoll and Ruska (1932). The theories of electron optics (Heidenreich 1964, Hirsch et al 1965) and the practical techniques used in microscopy (Kay 1965) have been described. More recent reviews of the state of development have been given by Fisher et al (1970) and Cosslett 1970.

The microscope used for most of this work, the Siemens Elmiskop I, has been described in detail by Hirsch et al (1965). The main operational modes used were bright field, dark field and selected area diffraction.

2.5.1 Bright Field

The beam of electrons, accelerated from a tungsten filament by a potential of 40, 60, 80 or 100 kV, is focussed on a specimen, using a single or double condenser system, as a spot whose diameter can be varied between 60μ to 2μ according to the degree of demagnification produced by the first condenser lens. The image of the specimen is magnified by three magnetic lenses, the objective, the intermediate and the projector lens and a final magnification of up to x160,000 can be attained.

The contrast in the image obtained arises from interactions between the electron beam and the atoms of the specimen and may produce diffraction, atomic number, or thickness contrast.

2.5.2 Diffraction

The electron beam incident on a crystalline specimen will be diffracted at angles determined by the lattice parameters. The beams are focussed at the second focal plane of the objective lens and an image of the pattern at this plane is obtained by suitable use of the intermediate and projector lenses. In selected area electron diffraction, which was introduced by

TABLE 5

Reaction Conditions for Butadiene/Hydrogen Mixture

Catalyst	Temperature	Time (Hours)	Press. atm	Gas Mixture But/H_2
Reduced $GrFeCl_3$	570K	18	1	1/2
Reduced $FeCl_3$	573K	24	"	
Graphite	573K	18	"	
Graphite Fe	313, 358 388, 413	20	1	1/2
a)	448,473,543 583, 618, 703	"	"	"
b)	588,608,623 633,643,655 665	18	0.8	"
c)	623 643 663	1,2,4	0.8	1/2
Graphite Fe	620	18	0.8	Butadiene
Fe Powder	as in (a) and (b)	24	1	1/2
Graphite Fe washed with HNO_3	as in (a)	24	1	1/2
Graphite Bisulphate	as in (a)	20	1	1/2
Graphite	573K 473K	18 "	1 "	1/2 "

Le Poole (1947) and employed frequently during this work, a diffraction aperture is placed in the path of the beam at the first intermediate image plane. The strength of the intermediate lens is reduced until an image of the second focal plane of the objective lens is projected on the final screen. From the diffraction pattern the particular lattice spacing d corresponding to a reflection of radius R can be calculated from the equation

$$dR = K$$

where K is the camera constant given by the product of the electron wavelength and the effective camera length L. The camera constant is experimentally determined and its value found by measuring R from a known specimen, usually polycrystalline thallous chloride. Inaccuracies in the SAD technique have been discussed by Phillips (1960) Agar (1960) Recke (1961) Alderson and Halliday (1965) Hirsch et al (1965) and Andrews et al (1967) and are due mainly to spherical aberration and variations in the value of K.

2.5.3 Dark Field

With a crystal specimen, a selected area diffraction pattern is obtained as described. To obtain a dark field image the objective aperture is placed over a particular Bragg reflection and the diffraction aperture and specimen image are focussed at the first intermediate image plane. Areas on the specimen giving rise to the particular reflection used will appear bright against a dark background.

To remove spherical aberration errors introduced by the use of electrons remote from the optical axis, the illuminating system can be tilted about the object until the desired

reflection lies along the new optical axis. Dark field microscopy is important in specimen orientation and contrast analysis.

2.5.4 High Voltage Electron Microscopy

Conventional microscopy using 30-200 kV accelerating voltage can only be used to examine thin specimens (e.g. <0.1μm for metals). With 1MeV accelerating voltage there is greater transmission of electrons at small scattering angles through thick specimens enabling materials up to ten times the conventional TEM thickness to be examined. Such specimens, (>1μm thick) are considered to be more representative of bulk material. Other advantages of this technique are the possibility of using an enclosed reaction cell for in situ reaction under controlled conditions and the smaller absorption of energy from the electron beam.

2.6 Specimen Preparation for Electron Microscopy

2.6.1 Mounting

Normal TEM copper grids of diameter 3.05 mm coated with an evaporated carbon film were used for most examinations of compounds after reaction. For the in situ preparation of potassium graphite and in situ reaction work, platinum/iridium mounts 2.30 mm in diameter with seven 70 μm diameter holes were used. These mounts required a silicon monoxide film which was evaporated from a molybdenum boat onto a Formvar film already on the mounts. The Formvar film was then removed by firing the mounts in a porcelain basin.

2.6.2 Preparation

The production of small thin specimens by ultrasonic disintegration was avoided in this work as the compounds were

sensitive to decomposition in common liquids used to obtain suspensions for this technique. The samples were obtained, therefore, by dipping a copper grid into the intercalation compound which allowed retention of some small flakes.

2.7 Other Structural Analysis Techniques

2.7.1 Optical Microscopy

A Wild optical microscope fitted with a 35 mm camera was used to examine the intercalated graphite iron flakes in the reflected light mode.

2.7.2 X-Ray Powder Analysis

A Philips X-ray powder diffraction camera was used for the examination of graphite iron before and after reaction. The specimen was prepared by mixing approximately 1 mg of material with an equal amount of Durafix and rolling into a thin whisker. This was allowed to dry for 4 hours, positioned in the camera, and exposed to CoKα radiation (protected for CoKβ by an Fe filter) for ∿6 hours.

2.7.3 E.S.R.

An E.S.R. spectrum of potassium graphite was obtained using an AEI ESR instrument with the specimen at room temperature and at 77K. The potassium graphite was prepared by Rudorff's method (1954), transferred to a spectrosil E.S.R. tube and sealed under vacuum.

3. POTASSIUM GRAPHITE DONOR COMPLEX: RESULTS

3.1 Electron Microscopy of Standard Graphite

Plate 1 shows an electron micrograph of a typical area of polycrystalline SP1 natural graphite. A selected area diffraction pattern obtained from a single crystal area (plate 2) reveals the hexagonal symmetry of the graphite when lying on its basal (0001) plane. The selected area diffraction technique gives a projection of the (h, k, o) planes. The pattern consists of two sets of spots, the inner set having been diffracted by the $\{10\bar{1}0\}$ planes with a spacing of 0.213 nm and the outer set by the $\{11\bar{2}0\}$ planes with a lattice spacing of 0.123 nm. The second type of pattern commonly obtained from random arrays of crystals lying on their basal planes is a typical Debye-Scherrer ring pattern. It consists of two rings corresponding to the $\{10\bar{1}0\}$ and $\{11\bar{2}0\}$ planes of graphite.

3.2 Electron Microscopy of the Potassium Graphite Compound

Potassium graphite had not been examined in the electron microscope before the present work was carried out because of its extreme reactivity to air. In order to study the compound it was prepared and examined in situ at 573K in the electron microscope. The features observed after intercalation were line moiré patterns, ring or distorted moiré patterns, small concentric rings or dots, dark areas and bright discs. Only a few areas exhibited dislocation networks.

3.2.1 Interference Effects

Two types of interference patterns were observed in potassium graphite (plate 3). The first consisted of small dots or concentric rings (X) with either a dark or light centre. Typical diameter dimensions were 13.5 - 40 nm. These small dots appeared after

Plate 1

SPI Graphite

x 244150

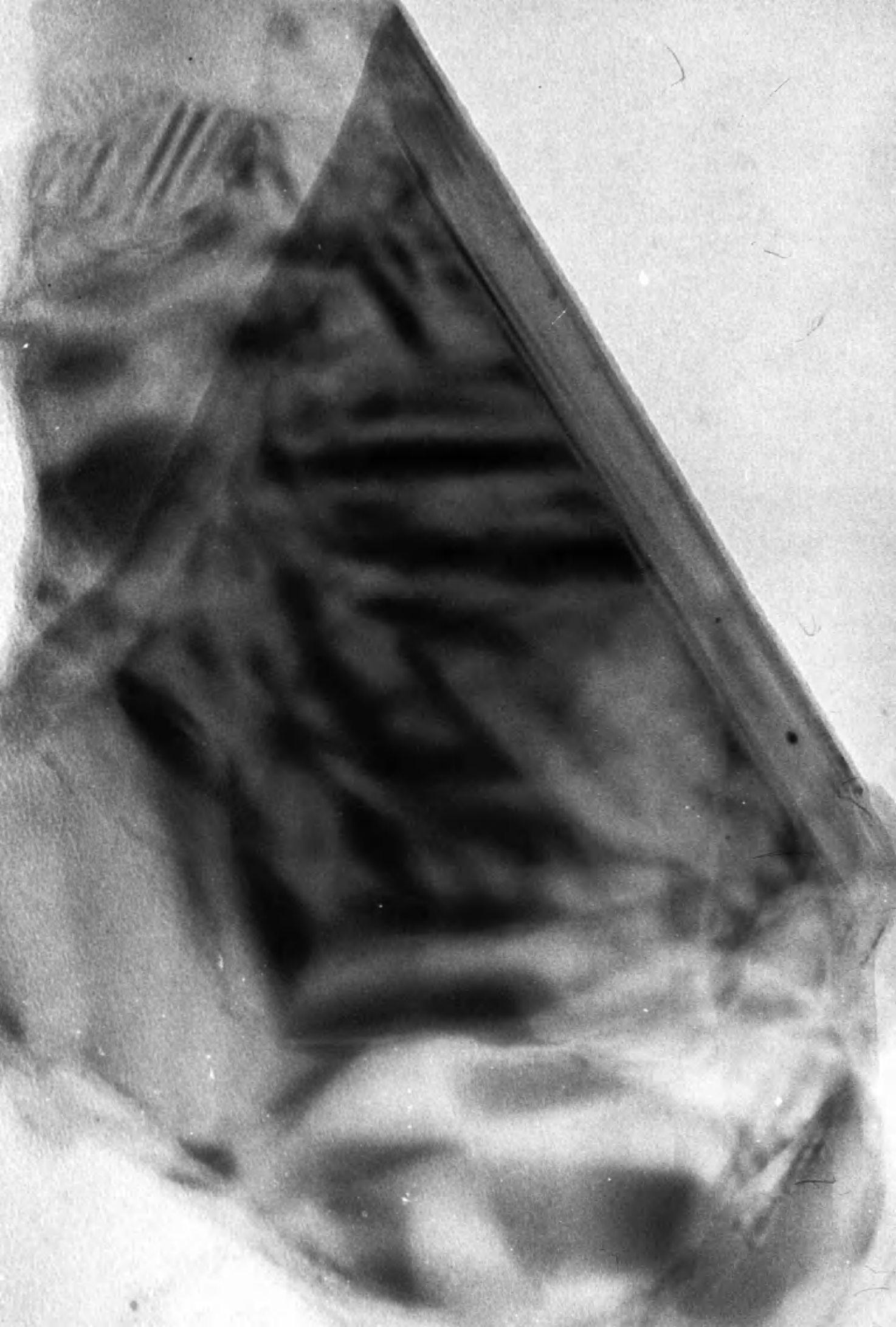

Plate 2

SPI Graphite Diffraction Pattern

Plate 3

Concentrated Potassium Graphite

prepared in situ at 573K

x 130200


Y
Z
Y
P
X

Plate 4

Selected Area Diffraction Pattern

from Concentrated Potassium Graphite

reaction with potassium and appear to be associated with intercalation.

The second type of pattern was a distorted moiré pattern (Y) with an interference fringe spacing in the order 10 to 100 nm. The patterns, the most common phenomena of concentrated intercalation compounds, were also observed by others (Halpin and Jenkins 1971). The size of these ring patterns and the number of the rings varied across the specimen.

In addition, line moiré patterns were a common feature in intercalation compounds. In plate 3 the line moiré patterns were at an angle of 60^{o} with a spacing of ca. 6.6 nm. From the selected area diffraction pattern (Plate 4) it can be seen that the line moiré is a rotation moiré. From the moiré spacing, the line moirés must arise from two graphite crystals with a small rotation of ca 1.8^{o}. There is also another crystal with a relative rotation of 18^{o} giving rise to double diffraction spots. However, in this case the moiré magnification of ca. 3 gives a moiré spacing too small to be visible.

3.2.2 Bright Discs

A bright disc is the term used to describe a region in the graphite which appears more transparent to the electron beam than the surrounding region. Similar features have been reported as bubbles (Bacon and Sprague 1961b), as "transparent discs" in graphite bisulphate (Carr 1965) and as bright discs in the potassium graphite compound (Halpin and Jenkins 1971). The discs, e.g. plate 3 at P, were 50-500nm in diameter with sharp well-defined edges which display Fresnel fringes. They appeared to overlap and were dispersed throughout the graphite lattice. Very little movement of the discs in the heat of the beam was observed. In general the bright discs were not common in the concentrated potassium

graphite intercalation compound.

3.2.3 Dark Areas

Dark areas were observed in the specimens of potassium graphite. They had sharp edges which displayed Fresnel fringes and one area could overlap another in a similar manner to the bright discs. An indication that these areas were within the graphite lattice was given in area Z where a channel runs through the centre of two overlapping areas. These areas have two main forms, a circle extending from 10 to 100 nm in diameter and an irregular form which could have a maximum Feret's diameter of several hundred nanometres.

3.2.4 Dislocations

Throughout the area in plate 3 there was a network of defects 5 to 15 nm wide. The contrast of these defects was similar to that associated with basal dislocations and they were similar to those reported for the bromine graphite compound (Eeles and Turnbull 1965) and to those observed in graphite ferric chloride (Amelinckx and Delavignette 1967). No tilting facilities were available for contrast analysis of these dislocations.

3.3 Electron Microscopy of Potassium Graphite After Reaction

3.3.1 Electron Microscopy of Potassium Graphite After Reaction In-situ in the Transmission Electron Microscope

In order to monitor any changes in structure which could be occurring in the catalyst as the reaction with nitrogen and hydrogen proceeds, an attempt was made to observe the reaction in the electron microscope. The potassium graphite was prepared in the microscope as previously described and exposed to a jet of N_2/H_2 from a modified objective aperture alignment control (Fryer 1968). A series of micrographs were taken showing the effect of the gas mixture on bright discs and distorted moiré patterns at 473K.

Bright Discs

Plates 5 and 6 are micrographs of an area of potassium graphite at 473K which was monitored before and during reaction at 5 minute intervals. Plate 7 is the same area after 4 days exposure to air. Before reaction, (Plate 5), some of the bright discs had taken up a regular shape with straight sides and sharp angles. A few minutes after exposure to N_2/H_2 (Plate 6) some of the bright discs disappeared or moved. The discs also decreased in size and tended to assume a more angular shape.

After the initial changes in morphology, on contact with the gas, there was some further movement of the discs relative to each other and further changes in shape with increasing exposure time. The bright discs therefore were mobile under reaction conditions. The movement of the discs appeared to be restricted to one direction and their velocity was low.

After 4 days exposure to air (Plate 7), some of the discs were unchanged while others had disappeared or decreased in size. A distorted moiré pattern was visible and the whole area was covered with small dark circular areas in the size range 5-50nm.

Distorted Moiré Patterns

A typical area containing distorted moiré patterns, small dots and concentric rings is shown in Plate 8. This micrograph was taken shortly after exposure to reaction gas. During reaction the moiré patterns did not change (Plate 9). After 4 days exposure to air, most of the moiré patterns had disappeared (Plate 10). In their place some bright discs of varying shapes and sizes were present in the bulk of the graphite. Small electron dense circular areas were again present.

Plate 5

Concentrated Potassium Graphite Containing Bright Discs,

prepared in situ: Before Reaction

and Selected Area Diffraction Pattern

x 89000

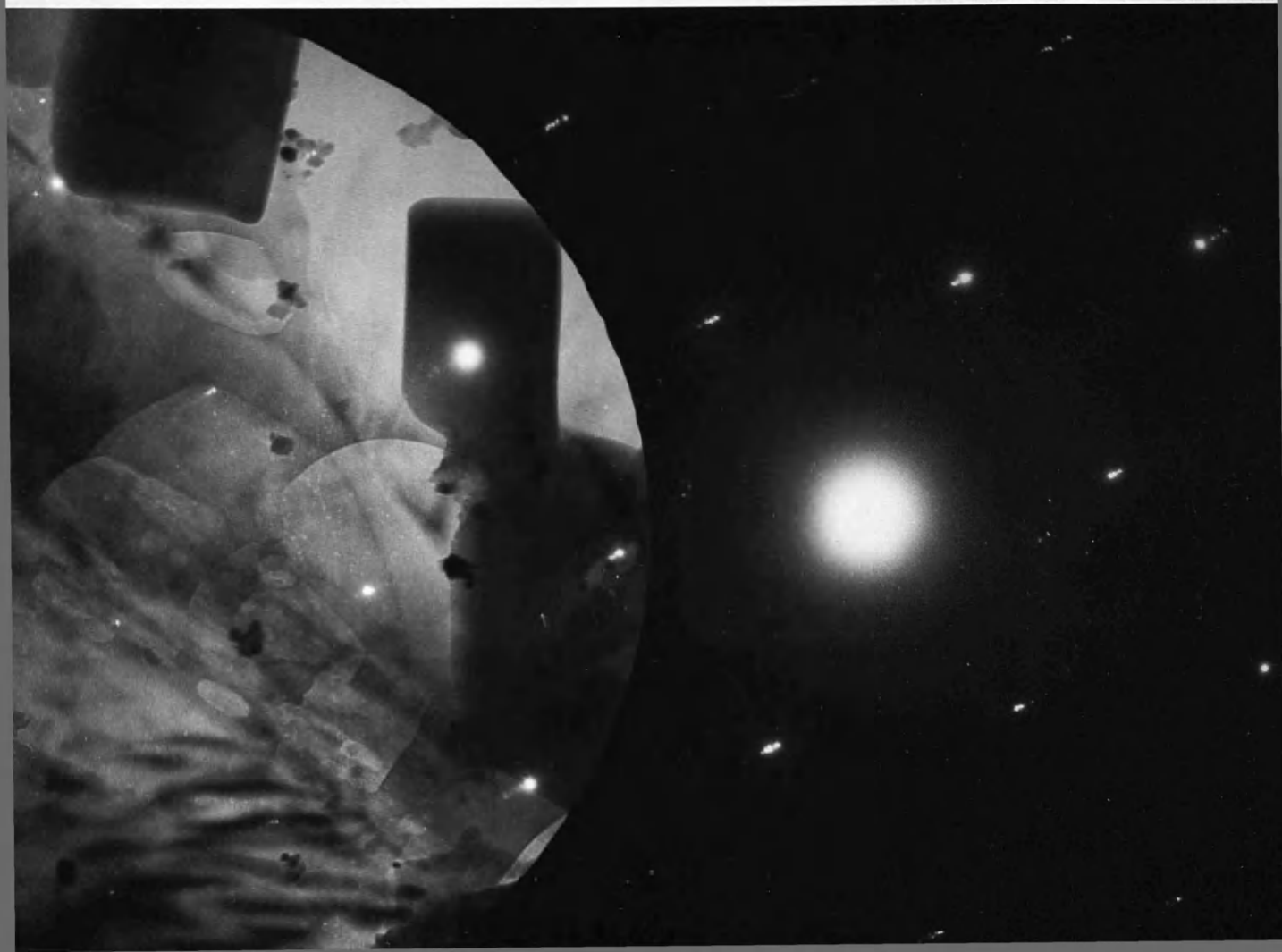

Plate 6

Concentrated Potassium Graphite After Reaction

at 473K for 5 minutes (upper micrograph)

and 10 minutes (lower micrograph) with N_2/H_2

x 102000

Plate 7

Concentrated Potassium Graphite

After Reaction and 4 days exposure to Air

x 115,500

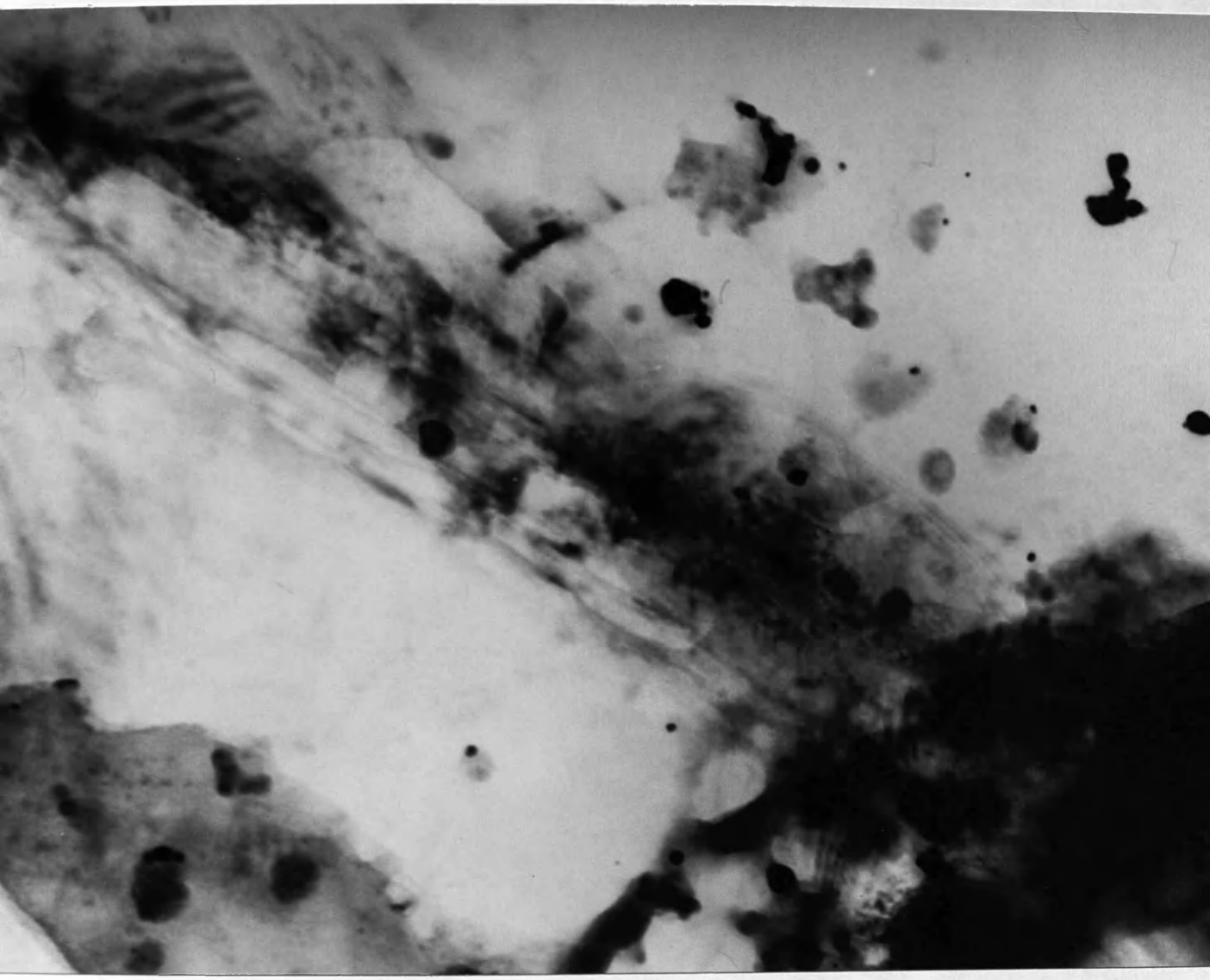

Plate 8

Concentrated Potassium Graphite Exhibiting Distorted Moiré Patterns

Prepared in situ: after initial exposure to N_2/H_2

x 102000

Plate 9

Concentrated Potassium Graphite

After Reaction in situ with N_2/H_2 for 10 minutes at 473K

x 102000

Plate 10

Concentrated Potassium Graphite

After Reaction and 4 days Exposure to Air

x 100800

3.3.2 Effect of Air on Potassium Graphite

Attempts were made to transfer potassium graphite prepared as described in Section 2.3.1 to the electron microscope under Argon to avoid decomposition of the compound. Despite all precautions, oxidation always occurred during transfer to form K_2CO_3, αKO_2, trace KOH and graphite. Bright field examination confirmed that only a few areas retained any intercalation features.

3.3.3 Electron Microscopy of Potassium Graphite after Reaction with N_2/H_2

The reaction temperature and gas environment for the in-situ reactions was not well defined and hence studies were carried out on the potassium graphite, prepared and reacted with a N_2/H_2 mixture outside the electron microscope, as described in Section 2.4.1 - 2.4.3. After reaction, nitrogen was admitted to the system and the compound was transferred immediately to the electron microscope. It was found that although the decomposition of pure potassium graphite is normally rapid in air (Section 3.3.2) the compound, after reaction and short exposure to air during transfer, retained many of the features associated with intercalation. However, some of these features, especially the moiré patterns, could not be observed on the electron microscope screen and were visible only on inspection of the photographic plates.

a) Effect of Reaction Temperature on the Morphology of the Potassium Graphite

The catalyst was examined after a reaction time of one hour in a 1/3 N_2/H_2 mixture at a total pressure of 30 torr under flow conditions (Table 4). The temperature range investigated was 483-573K. In all cases, after reaction, the compound was black and the particles tended to adhere to each other. An electron microscope

examination demonstrated that the compound was not homogeneous. Areas of unreacted graphite were present together with a graphite compound which still retained some of the characteristics of the concentrated intercalation compound. Typical areas with their accompanying diffraction patterns, after reaction at temperatures of 483K, 533, 553 and 573K are shown in plates 11-17. The main features observed at 483K were networks of line defects and line moiré patterns with only a few areas (Plate 11) containing the characteristic intercalation features of line and distorted moirés. At higher temperatures, 533-573K, intercalation features were increasingly more common (Plates 12-17). Two new features were observed after reaction. At 553K an almost circular dark area as in (x) (Plate 14) was observed, while at 573K thick dark outlines on the distorted moiré patterns were present (Plate 16). The distorted moiré patterns characteristic of an intercalation compound suggested that after reaction above 550K, the stability of the compound in air was increased.

b) Effect of Reaction Time on Morphology of Potassium Graphite

Potassium graphite was prepared and allowed to react with the N_2/H_2 mixture at 573K for periods of 0.25 hours, 1.25 hours and 20 hours at 750 torr under static conditions (Table 4). Examination indicated that again the catalyst was not homogeneous. In addition to the common electron dense material distributed over the surface, which could be attributed to oxidised residual potassium, only a few areas containing intercalation features were observed in each case. However, there was an increase in intercalated areas with increasing reaction time. This is illustrated in plates 18-25. Plate 18 shows an area typical of the compound after 15 minutes reaction. No intercalation features were present. After 1.25 hours (Plate 20) some intercalated areas were observed with evidence of some

Plate 11

Potassium Graphite After Reaction at 483K with N_2/H_2

in System I and transfer to Electron Microscope

Selected Area Diffraction Pattern

Plate 12

Potassium Graphite After Reaction at 533K with N_2/H_2

x 89400

Plate 13

Selected Area Diffraction Pattern

of Potassium Graphite After Reaction at 533K

Plate 14

Potassium Graphite After Reaction at

553K with N_2/H_2 in System I

x 104200

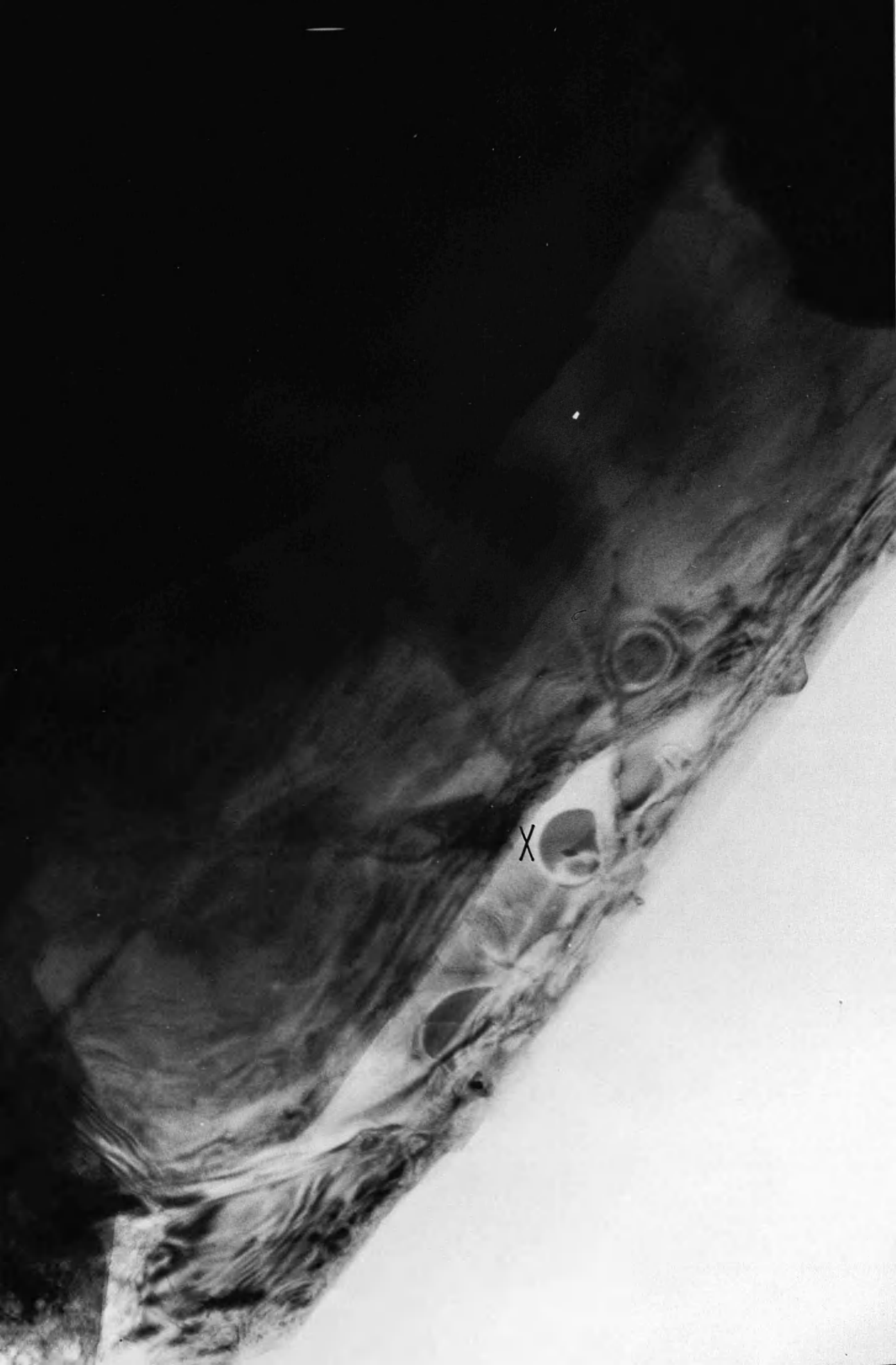

Plate 15

Selected Area Diffraction Pattern

of Potassium Graphite After Reaction at 553K

Plate 16

Potassium Graphite After Reaction at

573K with N_2/H_2 in System I

x 11300

Plate 17

Selected Area Diffraction Pattern

of Potassium Graphite After Reaction at 573K

Plate 18

Potassium Graphite After Reaction

at 573K in N_2/H_2 for 15 mins. and transfer to electron microscope

x 95000

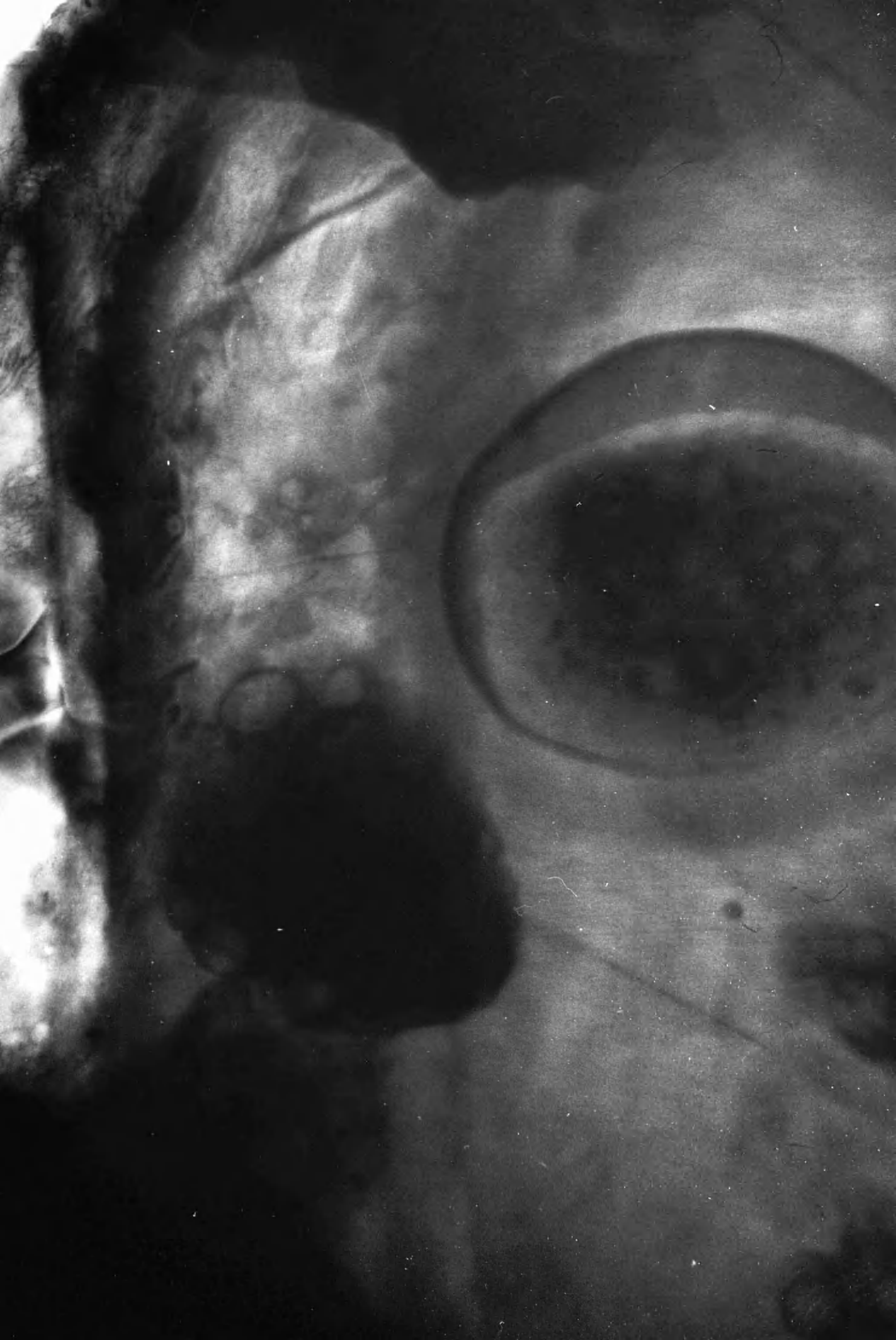

Plate 19

Selected Area Diffraction Pattern of

Potassium Graphite After Reaction with N_2/H_2 for 15 mins. at 573K

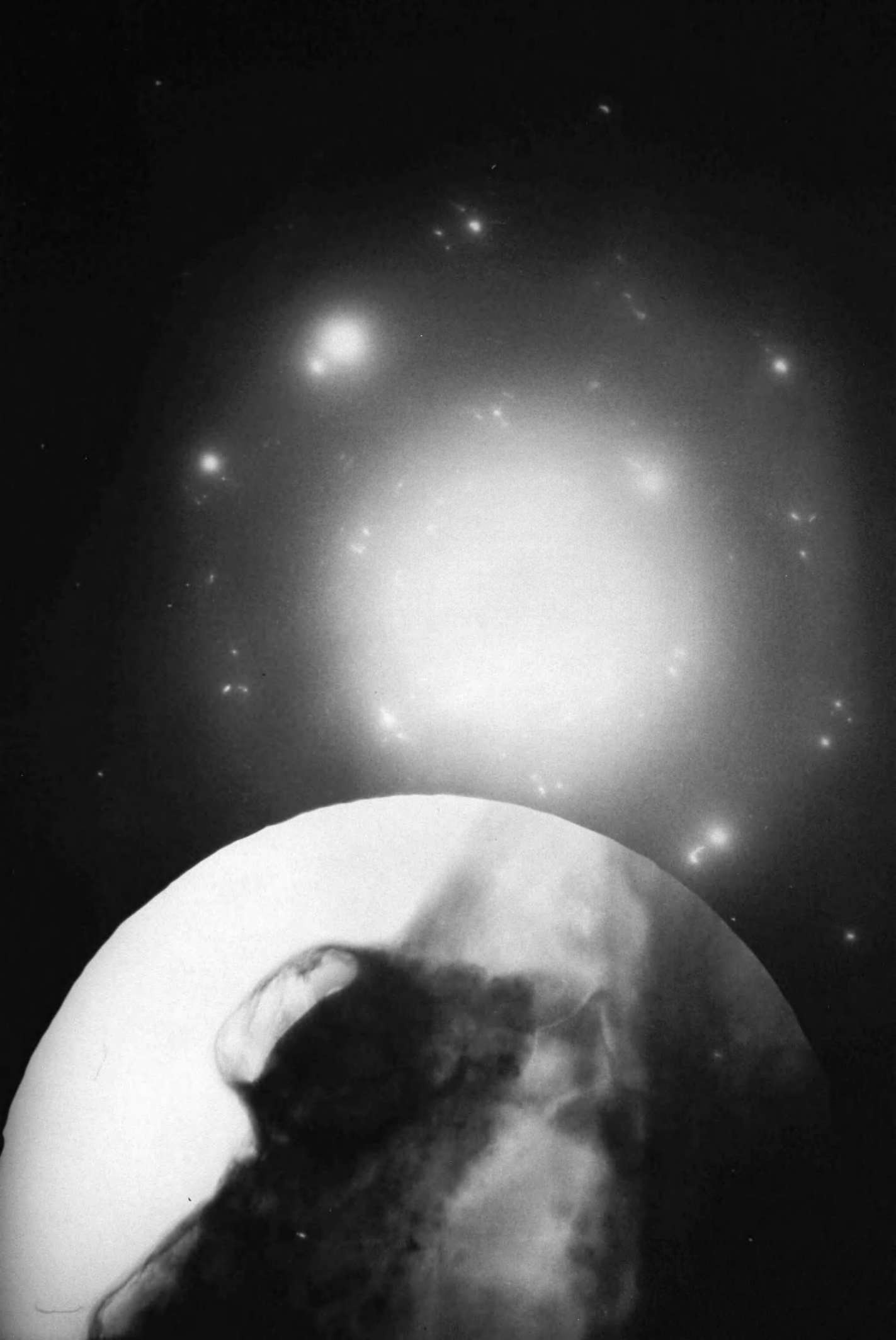

Plate 20

Potassium Graphite After Reaction

with N_2/H_2 for 1 hour at 573K

x 104500

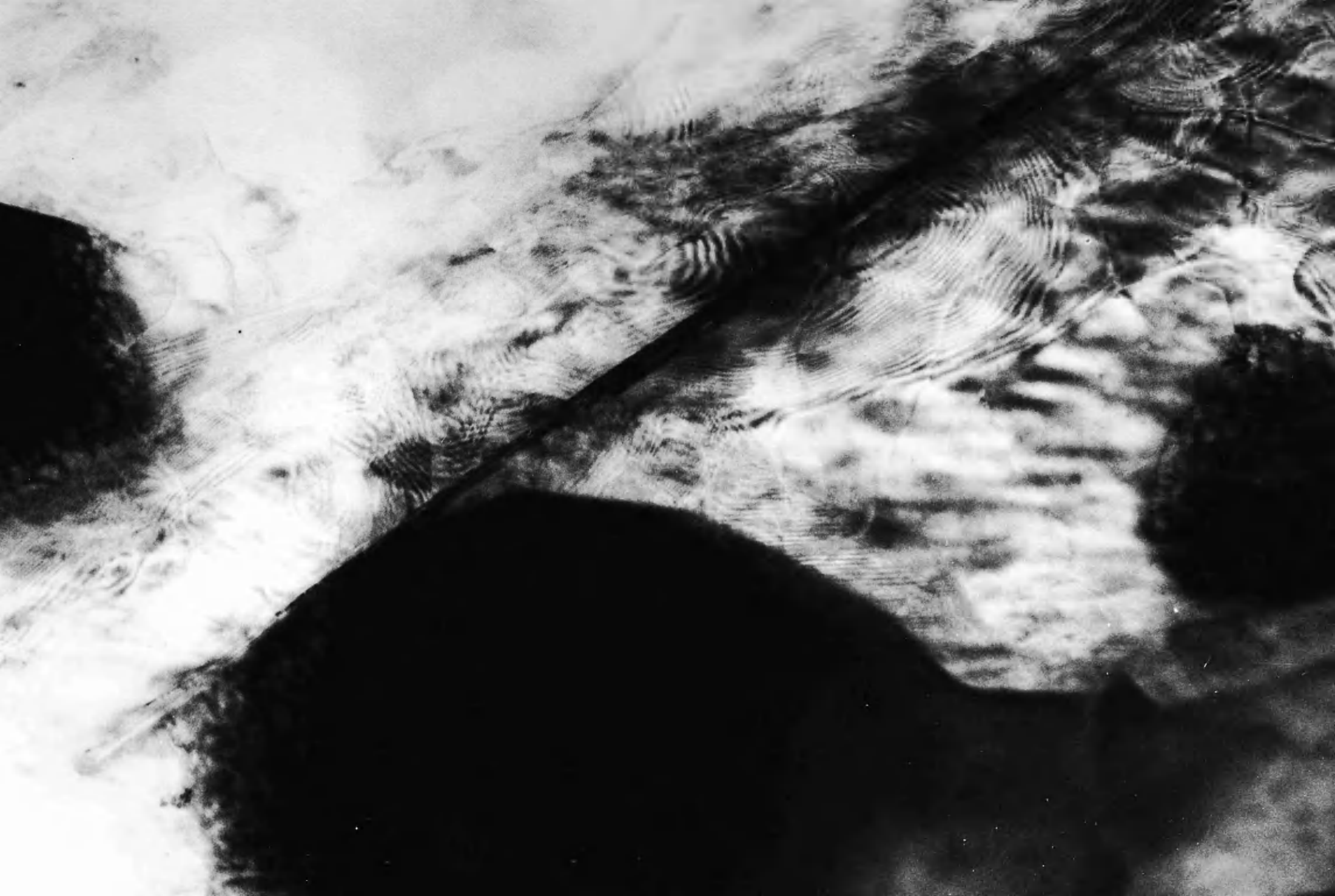

Plate 21

Selected Area Diffraction Pattern of

Potassium Graphite After Reaction with N_2/H_2 at 573K for 1 hr

Plate 22

Potassium Graphite After Reaction

with N_2/H_2 for 20 hours at 573K

x 98800

Plate 23

Selected Area Diffraction Pattern of

Potassium Graphite After Reaction

with N_2/H_2 for 20 hours at 573K

Plate 24

Potassium Graphite After Reaction

with N_2/H_2 for 20 hours at 573K

x 95000

Plate 25

Selected Area Diffraction Pattern of

Potassium Graphite After Reaction

with N_2/H_2 for 20 hours at 573K

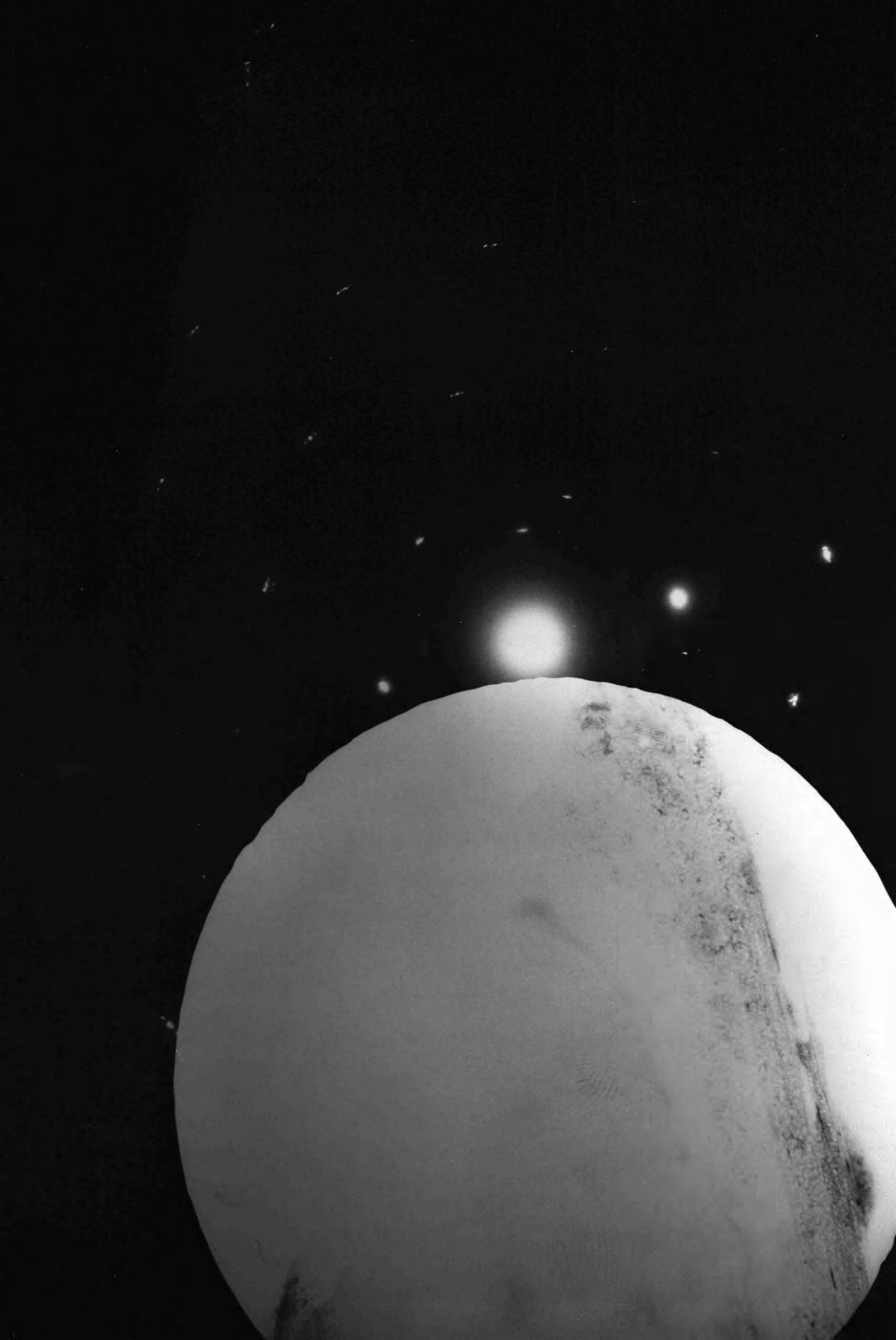

decomposition adjacent to these areas. Plates 22 and 24 show the variety of morphologies observed after 20 hours reaction. The small bright discs (Plate 24) were 10-20 nm in diameter and may indicate some reaction along the edge of the flake.

c) Effect of Elevated Pressure Reaction on Potassium Graphite Morphology

Plate 26 shows an area typical of the potassium graphite after 2.5 hours reaction at 573K and two atmospheres pressure. PGA graphite was used in this experiment. No extensive line or distorted moiré patterns were present suggesting that almost all the intercalation compound had decomposed. However, a large number of very small (20 nm diameter) bright discs were present. After reaction for longer times at all reaction temperatures, a new feature was observed. This was a high contrast irregularly shaped interference effect shown at x in Plate 28. A summary of the effect of reaction conditions on morphology is given in Table 6.

3.4 Electron Diffraction of Potassium Graphite

3.4.1 Potassium Graphite before Reaction

In this investigation, electron diffraction patterns from the potassium graphite intercalation compound had the following characteristics.

Many of the patterns examined were distorted from the normal completely symmetrical hexagonal arrangement (Section 3.1). The reciprocal lattice spots for the graphite $\{10\bar{1}0\}$ and $\{11\bar{2}0\}$ planes corresponded to varying d-spacings which were smaller than the standard value and the angle between the sets of planes was altered from the normal values in some cases. These changes were accompanied by large variations in intensity for some of the diffraction reflections. Double diffraction spots from rotated graphite crystallites were also

TABLE 6

Potassium Graphite : Morphology after Reaction

Time (Hours)	Temp K	Press. N_2/H_2 atm	Flow	Results
1	573K	.04	FLOW	Many intercalation features; plus modified distorted moiré and circular features.
	553			
	533			"
	483			Fewer intercalation features; mainly line moiré and line defects.
0.25	573	1	STATIC	A number of areas retaining intercalation features with a tendency to increase with reaction time.
1.25				
20				Evidence of decomposed K-graphite present in all cases
2.5	573	2	FLOW	Almost all K-graphite decomposed
10	533	"	FLOW	Modified, high contrast, distorted moiré present in discrete regions.
21	723	"	STATIC	

Plate 26

Potassium Graphite After Reaction

with flowing N_2/H_2 at 2 atmospheres for $2\frac{1}{2}$ hours at 573K

x 107200

Plate 27

Selected Area Diffraction Pattern of

Potassium Graphite After Reaction

with flowing N_2/H_2 at 2 atmospheres for $2\frac{1}{2}$ hours at 573K

Plate 28

Potassium Graphite after Reaction

with flowing N_2/H_2 at 2 atmospheres for 21 hours at 723K

x 95000

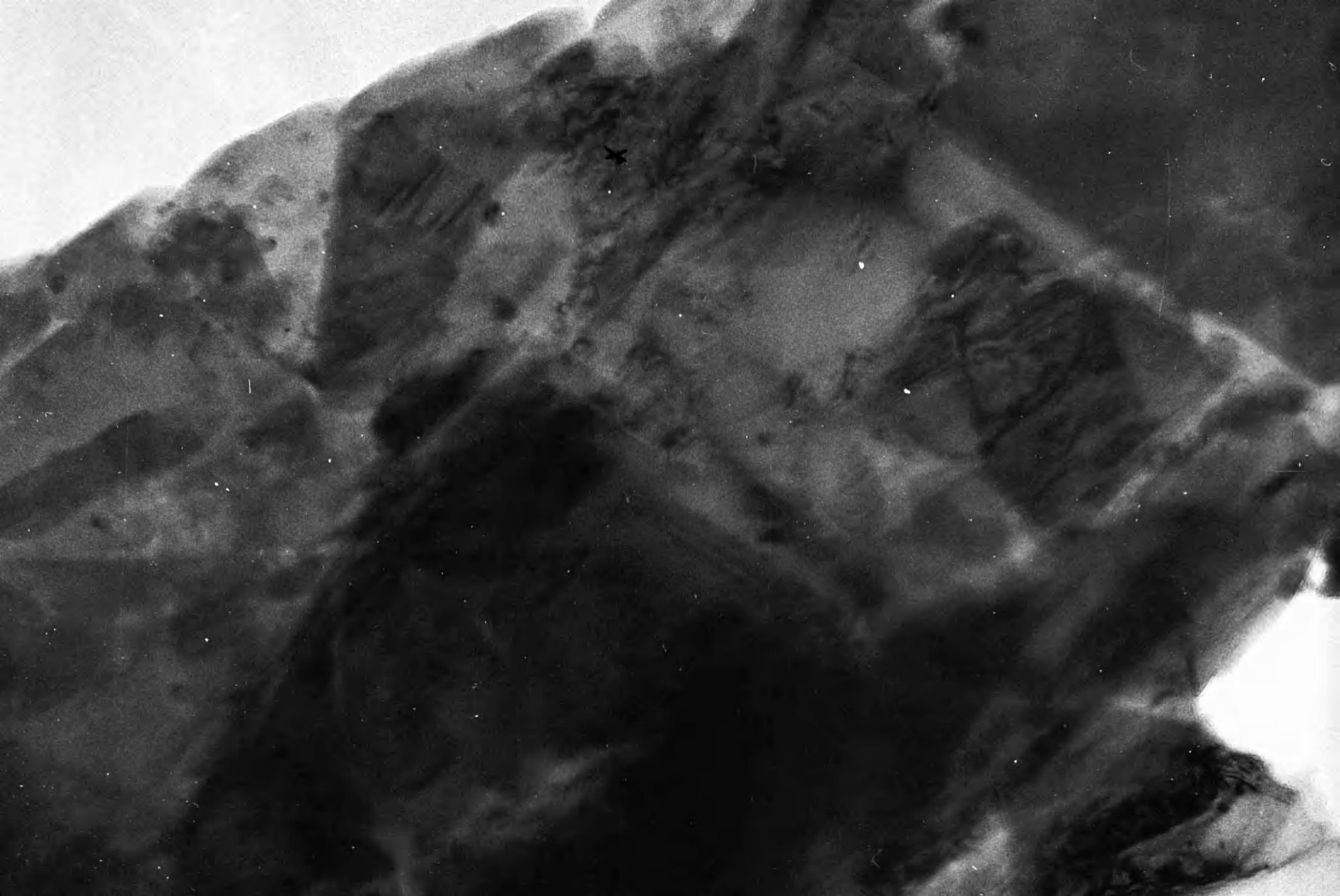

Plate 29

Selected Area Diffraction Pattern for

Potassium Graphite After Reaction

with flowing N_2/H_2 at 2 atmospheres for 21 hours at 723K

present. A typical pattern is shown in Plate 4.

In order to investigate further the origin of these features, the diffraction patterns from SP1 graphite on its basal plane, tilted to 5, 10, 15, 25 and 30°, were obtained using a Jeol 100 C transmission electron microscope with goniometer stage. This instrument was not available when the original experimental work was carried out. The changes in the diffraction patterns are shown in Plate 30. The main features were as expected from consideration of the Ewald sphere construction (Hirsch 1965, Andrews et al 1967).

i) The d-spacing decreased as the angle of tilt increased. For 30° and 15° tilt, the spacings are listed in Table 7(a) using the 0° tilt $(10\bar{1}0)$ and $(1\bar{2}10)$ spacings to calculate the camera constant.

ii) There was a change in intensity in some reciprocal lattice points.

iii) The angles between the sets of planes varied and at 30° tilt changed in the manner shown in Table 7(b).

3.4.2 Electron Diffraction of Potassium Graphite after Reaction

The potassium graphite after reaction was not homogeneous. Several areas had therefore to be chosen for diffraction and most of the data indicated that more than one compound was present in each area. In most cases the characteristics of the patterns examined for the regions which displayed intercalation features were the same as those for the potassium graphite before reaction. However, the distortion of the diffraction pattern was more pronounced after reaction.

Plate 29 is a selected area diffraction pattern from potassium graphite after reaction and shows the large distortion from hexagonal symmetry. A micrograph of the whole flake resting on the support film (Plate 28) showed white fringes on one edge and black

TABLE 7

a) Variation in Graphite d Spacing with Tilt Angle

ANGLE	d Spacing $(10\bar{1}0)$ planes nm	$(11\bar{2}0)$ planes nm
30^{o}	0. 198 0. 186 0. 184	0. 114 0. 110 0. 1055
15^{o}	0. 206 0. 202 0. 198	0. 12 0. 119 0. 115

b) Variation in angle between $\{10\bar{1}0\}$ planes at 30^{o} tilt

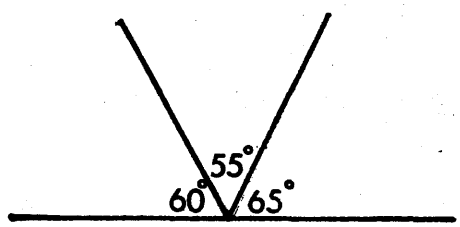

Plate 30

Effect of Tilt on Graphite Diffraction Pattern


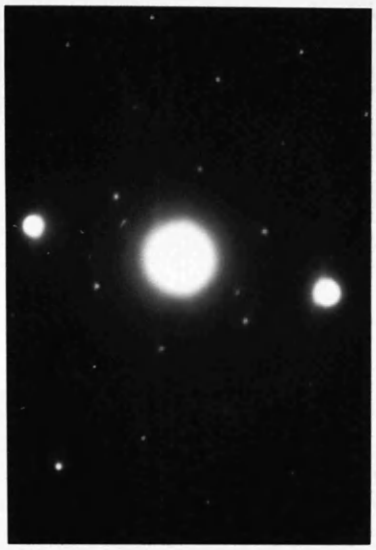
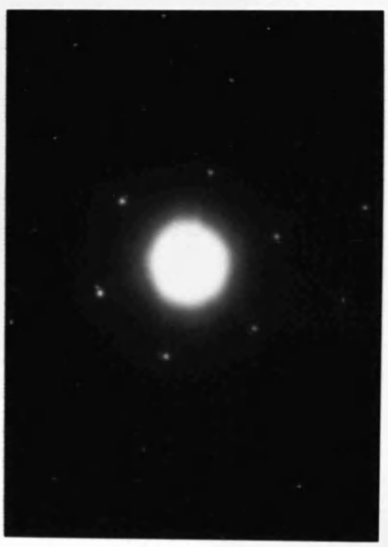

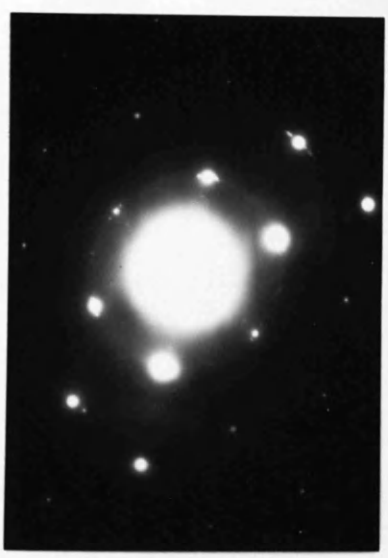


fringes on the opposite edge. The measured overfocussed fringe width was 3.5 nm and the underfocussed fringe width was estimated to be 1.75 nm. Using the equation relating fringe width to off-focal distance (Haine et al 1954) for 100kV electrons the calculated specimen tilt was ca. 62^{o}.

In several cases the pattern was complicated by extra spots which appeared to be the result of double diffraction. These could arise from a potassium superlattice within the graphite or from rotation of two graphite crystals. Plate 11 shows two crystals at an angle of 15^{o} to each other showing a variation on the intensities of the reflections and their d spacings indicating that both crystals are tilted or distorted. The inner spots in the diffraction pattern could be accounted for in terms of double diffraction from the two rotated crystals although the angle of rotation is large. The relative tilt of the two crystals may enhance the conditions for double diffraction. The line moiré spacing of 21.6 nm in the selected area of the diffraction pattern was equivalent to a rotation of ca. $\frac{1}{2}^{o}$ for the $\{10\bar{1}0\}$ planes and must have been produced by a third crystal with this small relative rotation. The diffraction patterns after reaction also contained extra spacings which could be assigned to KOH, αKO_2, KNH_2 or K_2CO_3. There was some difficulty in the interpretation of the data since, for example, K_2CO_3 and αKO_2 have overlapping spacings and can only be distinguished by the 0.297nm spacing for K_2CO_3 if they are in a randomly oriented polycrystalline state. However, this is not possible in the presence of KNH_2. The extra spacings arise from a polycrystalline region but not all the diffraction patterns were in the form of rings. Some of the polycrystalline patterns were observed as ellipses (Plate 21) and arcs (Plate 23). Arcs could be formed by tilting the crystallites from their zone axis

or by partial alignment of the crystallites relative to the graphite. The elliptical pattern may indicate a tilting or distortion of the crystallites within the graphite lattice.

It was also noted that the central zone of spots in the graphite diffraction patterns was extensive and this could be attributed to lattice strains (Kay 1965).

An estimate of the proportion of a particular compound was obtained from the relative number of areas containing that compound.

The accumulated data from 20 diffraction patterns is given in Table 8 for each set of reaction conditions. Table 9 is a list of spacings for the possible products of reaction for comparison with the spacings obtained.

a) Effect of temperature on reaction products

Electron diffractions of areas after reaction at 483-573K (Plates 11, 13, 15, 17) gave graphite diffraction patterns of varying degree of distortion. Some extra spacings were present in the form of faint rings indicating compound formation within or without the graphite (Table 8). The diffraction pattern from Plate 16, containing the new feature of broad distorted moiré fringes, is distorted with a faint ring at 0.297nm which could be attributed to KNH_2. KNH_2 is sensitive to hydrolysis and oxidation and its presence may indicate that it is within the graphite lattice. At lower temperatures, $KH_{0.67}C_8$, identified by comparison with $\{10\bar{1}0\}\{20\bar{2}0\}$ and $\{11\bar{2}0\}$ spacings, and KOH were present.

b) Effect of Reaction Time on Reaction Products

The accumulated diffraction data for the potassium graphite compound after 0.25, 1.25 and 20 hrs reaction at 573K are given in Table 8. The main compounds present, in addition to the graphite and intercalated

TABLE 8

A: TEMPERATURE DEPENDENCE				ELECTRON DIFFRACTION RESULTS FOR POTASSIUM GRAPHITE AFTER REACTION	
Time (Hrs)	Temp (K)	Press/(Ats) N_2/H_2	Flow	Average diffraction spacings nm	Products
1	573	0.04	Flow	0.329 0.297 (Ring) 0.212-0.196(G) 0.14 0.125-0.114(G)	KNH_2
	553			0.426 0.312 0.28 0.265(r) 0.216-0.195(G) 0.121-0.105(G) 0.305 0.25 0.245	KOH $KH_{0.67}C_8$ K_2CO_3
	533			0.356 0.318 0.273(r) 0.268-5(r) 0.212-0.192(G) 0.119-0.103(G) 0.19 0.167	KOH
	483			0.312 0.269(r) 0.212-0.20(G) 0.122-0.105(G)	KOH
B: TIME DEPENDENCE					
0.25	573	1	Static	0.346 0.336 0.310 0.299(r) 0.282(r) 0.21-0.196(G) 0.123-0.115(G) 0.272(r) 0.267(r) 0.24(r) 0.226(r)	αKO_2 K_2CO_3 KOH
1.25				0.45 0.353 0.278 (distorted ring) 0.213(G) 0.20 0.123(G)	Decomp.Prod. αKOH/K_2CO_3
				0.39 0.36 0.33 0.297-0.278 0.198-0.178(G) 0.121-0.107(G)	Intercal αKOH/K_2CO_3/ KNH_2
20				0.362 0.297(r) 0.212-0.203(G) 0.12-0.114(G)	Bubbles KNH_2
				0.376 0.329 0.285 0.277(r) 0.206-0.195(G) 0.121-0.113(G)	Intercal αKOH/K_2CO_3/ KNH_2
C: PRESSURE DEPENDENCE					
2.5	573	2	Flow	0.35 0.319 0.30 0.287 0.27(r) 0.236-0.227(sp) 0.216-0.212(G) 0.20-0.19(r) 0.124(r)	Decomp KOH K_2CO_3
10	533		Flow	0.334(G) 0.226(r) 0.209 0.13(r) 0.123(r)	Intercal KNH_2
				0.334(G) 0.28(r) 0.265(r) 0.21-0.193 0.121-0.114	αKOH K_2CO_3
21	723		Static	0.355 0.293 0.28(r) 0.218-0.205(G)	Intercal KNH_2
				0.158 0.121-0.114(G)	K_2CO_3 KOH

(G) = Graphite
(r) = ring pattern

TABLE 9

X-ray Diffraction Spacings of Possible Reaction Products

αKO_2			αKOH			KOH			K_2CO_3			αKNH_2			$KH_{0.67}C_8$			KH			KNO_2		
d_{nm}	I/I_0	hkl	d_{nm}	I/I_0	hkl	d_{nm}	I/I_0	hkl	d_{nm}	I/I_0	hkl	d_{nm}	I/I_0	hkl	d_{nm}	I/I_0	hkl	d_{nm}	I/I_0	hkl	d_{nm}	I/I_0	hkl
			0.555	10	001	0.400	17		0.559	4	011	0.616	10	001	1.180	F	001						
			0.367	10	101	0.371	13		0.492	2	020	0.386	10	101	0.590	TF	002						
0.335	100	002	0.324	15	011	0.313	23		0.485	2	110	0.350	10	101	0.431	F	100				0.3980	4	101
0.286	100	110	0.285	5	101	0.293	67		0.422	2	111	0.330	30	011	0.398	F	003	0.330	100		0.3420	<1	003
0.217	100	112	0.278	100	002	0.269	100		0.340	14	002	0.309	60	002	0.354	F	102	0.286	80		0.3300	100	012
0.202	80	200	0.276	75	110	0.258	13		0.312	2	121	0.296	100	110	0.339	M		0.202	80		0.2490	12	110
0.195	80	103	0.266	20	111	0.244	17		0.297	20	112	0.274	10	111	0.297	F	004	0.172	80		0.2205	25	104
0.173	80	211	0.255	10	102	0.230	23		0.295	8	031	0.269	10	102	0.268	TTF		0.168	50		0.2117	5	021
0.143	50	220	0.228	10	012	0.198	83		0.283	100	130	0.245	10	102	0.252	TTF	110	0.143	40		0.2016	6	113
0.140	70	213	0.215	10	112	0.183	17		0.2796	18	022	0.242	20	012	0.215	TF	200	0.131	60		0.1992	4	202
0.132	50	222	0.199	10	020	0.177	3		0.279	85	200	0.2285	20	200	0.208	TF	201	0.128	60		0.1850	2	015
		301	0.196	-	201	0.173	3		0.273	4	201	0.2211	30	112	0.201	M		0.117	50		0.1709	2	006
0.119	50	312	0.181	10	112	0.164	10		0.268	<1	210	0.207	30	112	0.188	TTF		0.110	60		0.1653	1	024
0.115	40	303	0.168	5	013	0.155	7		0.263	20	112	0.195	10	020	0.184	TTF	106	0.101	20		0.1615	2	211
0.109	60	224	0.162	10	022	0.146	7		0.254	2	131	0.193	10	202	0.170	TTF		0.965	60		0.1557	<1	122
			0.143	40	113	0.140	7		0.238	25	221	0.183	2	211	0.149	F	008				0.1488	<1	205
						0.137	10		0.236	6	032	0.178	4	202	0.146	TTF	108				0.1441	<1	300
						0.134	7		0.231	18	041	0.175	10	113	0.124	TTF					0.1410	1	116
						0.131	7		0.219	8	221	0.170	4	121	0.117	F					0.1387	<1	107
						0.129	3		0.211	20	222	0.151	2	104	0.114	TTF					0.1378	1	214
						0.124	3		0.199	12	042	0.148	10	220	0.113	TTF					0.1328	1	303
						0.114	7		0.190	2	232	0.144	4	014							0.1279	<1	125
									0.189	2	051										0.1229	<1	018
									0.187	2	213										0.1213	<1	027
									0.186	2	222												

graphite were αKO_2 K_2CO_3 and KNH_2. Some αKOH was also found. All the spacings were taken from polycrystalline ring patterns. Most of the potassium graphite had decomposed after 15 minutes reaction and transfer to the microscope.

After 1 hour reaction, there was a mixture of decomposed material and intercalated regions. The decomposed material appeared to be αKOH but could also be oriented K_2CO_3. Since αKOH only exists when sealed against moisture and CO_2, any αKOH present must be within the graphite. Extra spacings from the intercalated regions as in Plate 21 were difficult to interpret because the pattern was faint, irregular and complicated by double diffraction, but could be assigned to KNH_2. For the same reasons, the diffraction data after 20 hours reaction were difficult to interpret and it was not possible to distinguish in some cases between αKOH, K_2CO_3 or KNH_2. However, Plates 23 and 25 show a 0.297 nm spacing from a few crystals which could only be attributed to KNH_2. It was not possible to decide unambiguously whether the material giving rise to these spacings was located within or on the surface of the graphite layers.

In all cases, the intercalated regions exhibited a distorted pattern complicated by double diffraction spots.

c) Effect of Elevated Pressure Reaction with Nitrogen and Hydrogen

In order to maximise the conditions for ammonia production, the gas pressure was increased to two atmospheres in this set of experiments (Table 4). Examination of the catalyst after reaction did not yield conclusive results since, in general, oxidation of the potassium graphite to KOH and K_2CO_3 had occurred during transfer to the electron microscope. Plate 27 shows a typical diffraction pattern from an area after 2 hours reaction where decomposition has taken

place. The diffraction pattern spacings in Table 8, show that KOH and some K_2CO_3 were the main products. At longer reaction times at both 533 and 723K, the high contrast interference effect (Plate 28) was associated with a diffraction pattern (Plate 29) which in addition to the gross distortion of the graphite lattice exhibited extra polycrystalline spacing attributable to KOH and KNH_2.

3.5. Gaseous Products from Reaction of Potassium Graphite with Nitrogen and Hydrogen

Mass spectrometric and gas phase infra red analyses were carried out on the gaseous products sampled at intervals and at the end of reaction from static and flow experiments (Table 4). Nitrogen was the major observable constituent of the product gas. No direct mass spectrometric data is available on the hydrogen content of the gas as the mass spectrometer was unable to resolve in this region. The water level (in the gas mixture) was reduced from 0.7% before purification, to 0.1% after reaction. Some of the water may have been due to reaction with oxidised surfaces in the spectrometer. After correction for background, and the contribution due to water, the mass spectrometric data showed no peaks attributable to ammonia. The absence of ammonia was confirmed by gas infra red analysis of the products.

Nesslers reagent was also used to test a solution of the product gases in water (Section 2.4.2) no ammonia was detected under any reaction conditions.

Experiments were also carried out using unintercalated PGA and SP1 graphite at 543K. No ammonia was produced.

4. POTASSIUM GRAPHITE DONOR COMPLEX: DISCUSSION

4.1 Structure of Potassium Graphite at 573K

The distorted or ring moiré patterns observed in the concentrated potassium graphite prepared in situ are formed as a result of the intercalation of potassium. Most areas of the compound exhibited these features which disappeared when the compound was allowed to decompose. As the area of the distorted moirés was large it is unlikely that these regions are lenticular cavities containing a gas or impurity as proposed by Halpin and Jenkins (1971).

The moiré patterns are similar to the moiré fringe contrast observed for second phase particles in a matrix, and could arise from double diffraction between two superimposed crystal lattices of different lattice spacing or orientation. Moiré patterns similar to those observed for potassium graphite have been reported for $M_{23}C_6$ precipitates in a Ni/Cr/Ti/Al alloy (Merrick 1963). The distorted moiré patterns could therefore be interpreted as discrete potassium intercalate regions in the graphite. However, in the C_8K or $C_{12}K$ system, it is unlikely that the lattice parameters for the potassium superlattice would give rise to a visible moiré pattern. The moiré patterns can be explained, however, if the potassium is in the form of islands and the moiré pattern arises from interface contrast (Hashimoto 1962), as a result of the curvature at the interface between unintercalated and intercalated graphite. It is therefore proposed that the distorted moiré patterns arise from localised potassium intercalate regions. Ring or distorted moiré patterns have also been reported for other intercalation systems, such as graphite bisulphate (Carr 1965), and in the 4th stage graphite $MoCl_5$ compound (Syme-Johnson 1967).

From the distribution and apparent overlap of the distorted moiré patterns, the intercalation of potassium within the graphite layer

planes is uneven within an interlayer space and possibly disordered in the c-direction. It is likely, therefore, that the intercalation compound has formed according to the "bent layer model" (Hérold 1971) outlined in section 1.3.3. This model, for all compounds except stage I, requires uneven filling of the layer planes (Figure 5) and would result in numerous discrete regions of intercalated potassium of $C_{12}K$ structure. The distorted moiré patterns therefore represent areas of stage II and higher potassium graphite.

The electron diffraction study showed that these regions give rise to an unsymmetrical pattern. This could be explained by a large tilt of the specimen giving rise to a maximum calculated angular displacement ($\Delta\phi$) and maximum apparent change in interplanar spacing of 8.3^{o} and 13.3% for a 30^{o} tilt (Andrews, Dyson and Keown 1967). This agrees well with the experimentally observed results (Section 3.4.1). In addition, for potassium graphite after reaction, the tilt of an intercalated graphite flake, calculated from Fresnel fringe width, was ca 62^{o}. However, it is unlikely that a flake tilted to this extent would be mechanically stable and also that every area containing intercalation features was tilted. It is therefore concluded that the uneven intercalation with the graphite layers has produced internal distortion of the graphite lattice.

No superlattice reflections were observed in the potassium graphite. This is probably the result of liquefaction of the potassium at the preparation temperature. In addition, it has been reported (Nixon and Parry 1967, 1968) that the formation of the $C_{12}K$ structure is accompanied by loss of long range order within the intercalate layer. Islands of $C_{12}K$ would therefore not give rise to extra superlattic reflections. The electron diffraction patterns corresponded to that of graphite in agreement with Halpin and Jenkins (1971).

Halpin and Jenkins (1971) and Halpin (1972) obtained two types of diffraction pattern which were not observed in this study. The first corresponded to an epitaxial film of potassium visible in the bright field on the surface of the graphite. The formation of this film was probably the result of the preparative technique employed. This pattern was also observed by Evans and Thomas (1975) although it was not attributed to a surface film of potassium. The second type of pattern found by Halpin was ascribed to a $C_{10}K$ structure.

The small dot moiré patterns in the potassium graphite could also be attributed to interface contrast (Hashimoto 1962) due to a very small intercalated area. Bonifiglioni and Majoni (1964) however, have found these defects in natural graphite and attributed them to small lenticular cavities in the graphite lattice while Izui and Fujita (1963) observed similar defects in irradiated molybdenite and ascribed them to radiation damage.

The line moiré patterns associated with intercalated areas are mainly rotation moiré patterns and are probably produced by relative movement of the graphite basal plane as a result of unpinning of the lattice by the intercalation process.

Irregular dark areas in the concentrated potassium graphite compound were found to overlap indicating that they are not a surface feature. Halpin (1972) who studied the compound at ambient temperature also observed these dark areas and attributed them to liquid potassium although at normal temperatures the potassium would not be in liquid form. However, this interpretation agrees with the observations in the present study at 573K. The relative contrast of these areas is high and can be explained in two ways. The contrast could arise by absorption of the electron beam by many overlapping layers of fully

intercalated potassium as in a Stage I compound. It is also possible that this potassium is a thicker layer of potassium not within the graphite layer planes, but within the regions separating packets of layer planes, 20-30 layers thick, reported to exist even in single crystal graphite (Fryer 1974).

Within these dark areas, irregularly shaped, overlapping bright discs were observed within the graphite lattice. The contrast of these bright discs arises from an absorption effect. This has been demonstrated by Halpin (1972) by contrast analysis and explains the observation in this study that the region of overlap of the discs appears less opaque to the electron beam than the original discs. Similar bright discs have been observed in residue compounds of graphite ferric chloride (Heerschaap and Delavignette 1967) and of graphite bisulphate (Carr 1965). In the graphite ferric chloride residue compound, it was suggested that the bright discs were areas free of ferric chloride, formed by the dissociation of ferric chloride as a result of the heating effect of the beam. In the graphite bisulphate compound it was suggested that the bright discs were crumpled areas of otherwise regular graphite formed by collapse of the graphite sheets on formation of the residue compound.

In the present study, no collapse of the graphite sheets was observed in the concentrated potassium graphite compound. As no diffraction pattern could be obtained from the bright discs, and as they are associated with the dark areas of potassium, it is probable that they are bubbles of trapped potassium vapour formed on intercalation of the potassium Stage I compound, within the layer planes, or between the crystal "packets". It is unlikely that they are formed by a beam heating effect, as the potassium graphite in this study was examined in the TEM at 573K, at which temperature beam heating effects

would be a minor perturbation. The potassium at 573K would have a partial pressure of almost one torr. These bubbles of potassium vapour would remain as unintercalated regions within the graphite on cooling the specimen.

The bright discs in the potassium graphite prepared in situ had very low mobility compared to that reported for the bright discs observed in graphite bisulphate (Carr 1965) graphite ferric chloride (Heerschap and Delavignette 1967) and the potassium graphite prepared by Halpin (1972). This could be the result of the different types of intercalates studied. In the graphite ferric chloride, boiling of the ferric chloride was proposed to explain the rapid movement observed, while in the bisulphate compound, it was suggested that rearrangement of the crumpled graphite sheets would result in the mobility of the discs. The slow movement observed in this study is consistent with a bubble in a viscous liquid with small fluctuations in temperature causing movement. Shrinkage of the discs was also observed which could be the result of cooling of the specimen.

The bright discs, reported by Halpin and Jenkins (1971), were the predominant intercalation feature and were very mobile. They displayed a secondary fast bubbling action within the discs in a few cases. In addition, exfoliation of the potassium graphite was observed in the heat of the beam. In order to explain these phenomena, which were not observed in the present study, it is suggested that they are the result of the preparative method used by Halpin. In his technique, to avoid oxidation, the potassium graphite was transferred under chloroform to the electron microscope. It is possible that some of the chloroform was intercalated in the graphite. This would explain the abundance of bright discs, their increased mobility in the heat of the beam and the exfoliation of the compound at low temperatures and

normal viewing conditions. In support of this view, the exfoliation observed by Halpin is very similar to that observed in graphite iron containing intercalated THF (Section 7.1.2).

4.2 Reaction Products of Potassium Graphite with Nitrogen/Hydrogen Mixture

From the work of Saehr and Hérold (1960, 1965) Colin and Hérold (1967, 1971) and Ichikawa et al (1969b) it is possible to suggest a range of reaction products for the reaction of potassium graphite with nitrogen and hydrogen and subsequent exposure to air.

First and second stage potassium graphite will behave as an intercalation compound in its reaction with hydrogen to form a hexagonal ternary product KH_xC_8 or KH_yC_{24} where x has a limiting value of 2/3 and y of $\frac{1}{2}$. Hydrogen absorption increases with temperature but the $KH_{0.67}C_8$ compound dissociates at 573K. When oxygen or water vapour is an impurity, the phases formed are graphite and potassium hydride which will further decompose in air at ambient temperatures to give KO_2 and KOH with evolution of hydrogen.

The product of the reaction of potassium graphite with nitrogen is unknown but according to Ichikawa et al (1969b) nitrogen is absorbed by potassium graphite as the temperature is raised.

The formation of ammonia from nitrogen and hydrogen was reported by Ichikawa et al (1969b) using potassium graphite as a catalyst. However, no ammonia was liberated in the present study and later work by Ichikawa et al (1972d) also reported that potassium graphite had no catalytic activity with respect to ammonia synthesis. However it is possible that any ammonia formed would react with the potassium graphite to form a ternary compound (Rudorff 1954) which at reaction temperature would decompose with the formation of KNH_2, graphite and hydrogen. Potassium amide is sensitive to hydrolysis and

oxidation and reacts according to equations 4.2(a) and 4.2(b)

$$KNH_2 + H_2O \rightleftarrows KOH + NH_3 \qquad 4.2(a)$$

$$4KNH_2 + 3O_2 \rightleftarrows 2KOH + 2KNO_2 + 2NH_3 \qquad 4.2(b)$$

Thus the possible solid reaction products are KNH_2, KH_xC_8, KH_yC_{24}, and KH.

Decomposition of the potassium graphite in air gives αKO_2 or K_2CO_3 with traces of KOH and decomposition of the amide and hydrides in air would give KO_2, KNO_2 and KOH.

In the present study, although no ammonia was detected in the effluent gas, KNH_2, $KH_{0.67}C_8$, KOH, αKO_2 and K_2CO_3 were observed in the graphite compound after reaction. As the amide and hydride are sensitive to air, this suggests that they are trapped within the graphite. No KNO_2 was observed in the reaction products indicating that the KOH is not the product of amide decomposition but is probably formed by hydride decomposition.

4.3 Structural Changes during Reaction with Nitrogen and Hydrogen

It has been shown that potassium graphite loses most of its intercalation characteristics and decomposes to αKO_2 K_2CO_3 and trace KOH and graphite on exposure to minute traces of air during transfer to the electron microscope under argon. Halpin (1972) also observed decomposition of the compound in air to form αKO_2. Therefore, as the number of areas retaining intercalation features after reaction increased with increasing reaction temperature and reaction time, stabilisation of the intercalated graphite must have occurred during reaction with nitrogen and hydrogen.

The main morphological features at reaction temperatures <573K under flow conditions were typical of residue compounds,

exhibiting "rafts" or isolated islands of intercalated potassium similar to those described by Halpin (1972), and dislocation networks. The diffraction patterns indicated that the decomposition product was KOH. This is not the normal main decomposition product of potassium graphite and may indicate hydride decomposition.

At 553K, the diffraction pattern indicated some ternary hydride formation and at 573K a polycrystalline KNH_2 pattern was observed. KNH_2 formation was associated with a high contrast moiré pattern with broad fringes. These fringes are similar to those observed for a plate shaped inclusion lying perpendicular to the direction of the electron beam and are due to the curvature of the interface (Hashimoto 1962). The irregular outline of the fringes indicates that the particle is irregular. The appearance of these broad fringes therefore suggests that there is a precipitate within the graphite layer planes which is producing an expansion of the graphite c-spacing greater than the original potassium graphite compound. It was not possible however to unambiguously correlate the polycrystalline KNH_2 with the broad fringed moiré contrast as surface contamination could not be eliminated.

This interface contrast could also arise from the formation of a ternary intercalation compound. This ternary compound could be the ternary hydride compound containing the double layers of potassium within one interplanar space as described by Lagrange (1974). Alternatively a graphite potassium ammonia complex may be formed which may not decompose immediately at 573K giving rise to the broad fringed high contrast moiré patterns (Rudorff 1959). Decomposition of this ammonia complex would give KNH_2.

At all reaction times under static conditions, K_2CO_3 was present indicating that some regions of the original potassium graphite had remained unreacted during exposure to nitrogen and hydrogen, and

were completely oxidised on subsequent exposure to air. It is probable that under static conditions, gas circulation around the potassium graphite flakes is less efficient than under flow conditions. Although there was an increase in the number of retained intercalated areas with increasing reaction time no high contrast broad moiré fringes were observed. Polycrystalline KNH_2 was formed after 1.25 and 20 hours reaction associated with distorted moiré patterns typical of potassium graphite. However, in some areas, (Plate 24), KNH_2 was associated with a network of complex moiré fringes and very small bright discs of 10-20 nm diameter. The complex moiré fringes could be interface fringes resulting from misfit at the intercalate/graphite interface. They would be expected to vary in spacing and orientation as the orientation of the interface varied, in agreement with observations. The bright discs at the edge of the flake could represent bubbles of gas trapped in the graphite, produced by decomposition or reaction of the intercalated material.

Evidence of reaction within the layer planes may also be inferred from the presence of αKOH after 1.25 and 20 hrs reaction. This compound is sensitive to air and water vapour and can therefore only be present sealed within the graphite layer planes.

The morphology of potassium graphite after two hours reaction at two atmospheres pressure was comparable to that after 15 minutes reaction at one atmosphere, indicating that increasing the gas pressure has decreased the rate of reaction within the graphite. After 10 and 20 hours reaction time, under flow and static conditions, modified high contrast moiré patterns were observed in several areas. These features are similar to displacement fringes expected from a thin plate shaped precipitate inclined at an angle to the graphite surface. The wavy nature of the fringes indicates that either the precipitate

is not flat or the graphite surface is uneven. These fringes could be produced by intercalated material arranged in laterally displaced layers which would also give an irregular edge (figure 14). Alternatively, the flake is tilted as indicated by the Fresnel fringes (Plate 29), to give intercalated layers inclined to the incident electron beam.

4.4 In-Situ Reaction at Low Pressure

The reactant gas had only a minor effect on the two main morphological features of potassium graphite. The bright discs showed some movement and shrinkage which could be explained by the cooling effect of the gas. The ring moiré patterns did not alter their positions but contrast changes were observed which may be the result of buckling of the graphite or reaction within the lattice. However, it is possible that the gas pressure at the potassium graphite was too low for significant reaction to occur. The compound after decomposition in air displayed small thin globules of αKO_2 throughout the graphite. The bright discs retained their position, size, and shape in the residue compound while the majority of the ring moiré patterns disappeared. A few bright discs replaced the moiré patterns suggesting that some gas had been formed and remained trapped within the lattice during decomposition of the intercalation compound.

4.5 Mechanism of Reaction

The results of this study can be explained by a mechanism which considers the geometry of the system, and the chemical reaction scheme of the potassium graphite in contact with nitrogen and hydrogen.

In this study, no free ammonia was formed by the reaction of nitrogen and hydrogen with potassium graphite. However,

the morphological changes in the substrate and electron diffraction data indicate that some reaction does occur.

Ammonia or amide formation occurred only at the higher reaction temperatures. This can be explained if the mechanism of ammonia formation is similar to that of the iron catalysed process and involves the production of NH_{ads} or NH_{2ads} by dissociative adsorption of nitrogen and hydrogen on the surface. It is known (Ichikawa et al 1969, Hérold and Saehr 1965) that the dissociative adsorption of hydrogen on potassium graphite takes place at a much lower temperature than for nitrogen and therefore ammonia production, by this route, is likely to be favoured by high temperatures.

The geometry of the graphite intercalation compounds as catalysts is completely different to that of metals or supported catalysts. In the intercalation compounds, every layer of the compound is accessible to reacting gases (Watanabe et al 1973) and hence it would be expected that there would be no particular surface properties associated with intercalation compounds. Reaction, therefore, would take place within the bulk of the graphite and would not be confined to the surface layers as in normal catalytic systems. Watanabe et al (1973) also showed that gas access is mainly affected by geometric limitations and the most concentrated compounds is least active for reaction. In this study the potassium graphite has been found to be a mixture of stage I and higher stage compounds and this restriction would not be important. It is likely that reaction with potassium graphite occurs initially by the slit-type adsorption of hydrogen and nitrogen described by Watanabe.

Any parameter which would increase the energy required to expand the graphite in the c-direction to accommodate the adsorption of gases would be expected to adversely effect reaction within the

layer planes. In this study the decrease in the extent of reaction with increased pressure is probably related to this mode of adsorption. The extent of reaction also decreased with static conditions. It is possible that flow conditions may prevent the build up of equilibrium gas mixtures within the catalyst bed and continually renew the reactant gas.

From studies of the intercalation process (Hooley 1970), intercalation proceeds from the edges of the graphite flake to the centre. The extent of intercalation decreases with increasing thickness and therefore small thin flakes are easily intercalated. Thus, if it is assumed that reaction of the intercalation within the layer planes is subject to the same diffusion mechanism and constraints as the original intercalation, then the edges of thin crystals have the highest probability of showing reaction effects. In order to explain the morphological effects and reaction products identified by electron diffraction, found in these areas, two reaction schemes are proposed for the reaction of nitrogen and hydrogen with potassium graphite.

Both reaction schemes involve initially the reaction of hydrogen with potassium graphite to form KH or the ternary hydride compound. It is likely that the KOH present after reaction at low temperatures is the decomposition product of the hydride in air. As the formation of C_8KH_x is rapid (Hérold 1965) it is probable that the role of nitrogen in the reaction assumes more importance with increasing temperature and there is a changeover to amide formation by two possible routes.

The structural evidence indicates that amide formation is associated with a ternary hydride or ternary ammonia compound. The hydride could therefore act as an ammonia catalyst or as an inter-

mediate in the reaction. Subsequent reaction of the ternary hydride, potassium hydride, or unreacted intercalate with the ammonia would form the amide. This is summarised in equations 4.5 (a)-(d) where for simplicity, the ternary hydride is taken to be $C_8KH_{\frac{1}{2}}$

$$6C_8KH_{\frac{1}{2}} + N_{ads} \rightleftharpoons 6C_8K + NH_3 \qquad 4.5(a)$$

$$4C_8KH_{\frac{1}{2}} + 4NH_3 \rightleftharpoons 4KNH_2 + \text{graphite} + 3H_2 \qquad 4.5(b)$$

$$2C_8K + 2NH_3 \rightleftharpoons 2KNH_2 + H_2 + \text{graphite} \qquad 4.5(c)$$

$$KH + NH_3 \rightleftharpoons KNH_2 + H_2 \qquad 4.5(d)$$

An alternative scheme may be derived from the work of Rudorff (1959) who found that alkali metal amides were formed and hydrogen evolved from ternary alkali metal graphite ammonia complexes at room temperature. It is therefore possible that the potassium graphite does catalyse the formation of ammonia but at the high reaction temperature the ammonia reacts to form the ternary potassium graphite ammonia compound. This ternary compound would in turn decompose at 573K to the amide, graphite, and hydrogen. This is summarised in equations 4.5 (e)-(g).

$$C_8K + N_{ads} + 3H_{ads} \rightleftharpoons C_8K + NH_3 \qquad 4.5(e)$$

$$C_8K + XNH_3 \rightleftharpoons C_8K(NH_3)_x \qquad 4.5(f)$$

if x = 1

$$2C_8K(NH_3) \rightleftharpoons 2KNH_2 + \text{graphite} + H_2 \qquad 4.5(g)$$

Either or both mechanisms may be operative in the reaction and they explain the failure of the potassium graphite to catalyse the production of gaseous ammonia.

5. ACCEPTOR COMPLEXES OF GRAPHITE: RESULTS

5.1 Introduction

Acceptor complexes, graphite ferric chloride and graphite copper sulphide, and the reduced graphite ferric chloride were tested for catalytic activity for ammonia synthesis from nitrogen and hydrogen. Reduced graphite ferric chloride was also used in the reaction of butadiene with hydrogen.

5.2 Graphite Ferric Chloride

5.2.1 Morphology of Graphite Ferric Chloride

The compound, as prepared in Section 2.3.2., had a layer of debris on the surface. This was removed either by a dilute HCl wash or a dilute HCl wash followed by a water wash.

The material consisted of a mixture of graphite and graphitic areas exhibiting bright discs in a dark background. Areas of extensive line moirés were also observed and the distorted moiré patterns, commonly associated with the potassium graphite, were present in a few areas. In addition, some areas of graphite contained small, electron dense, crystallites.

Plate 31, is a micrograph of a typical area which exhibited bright discs (160 nm diameter) surrounded by dark areas similar to those observed in potassium graphite. The dark areas have a mottled appearance which indicates either that these areas do not have a uniform thickness or exhibit some diffraction contrast. This plate also shows one of the few areas of ring moiré patterns observed in this material.

Extensive two dimensional line moirés can be seen in Plate 33. The origin of these patterns is not unambiguous but it is probably a rotation moiré. For the pattern spacing of 35 nm, arising from graphite $10\bar{1}0$ reflections the relative rotation of two graphite

Plate 31

Bright Discs and Distorted Moiré Patterns in

Graphite Ferric Chloride washed with dilute HCl

x 115140

Plate 32

Selected Area Diffraction Pattern for

Graphite Ferric Chloride

Plate 33

Extensive Line Moiré Patterns

in Graphite Ferric Chloride

x 209000

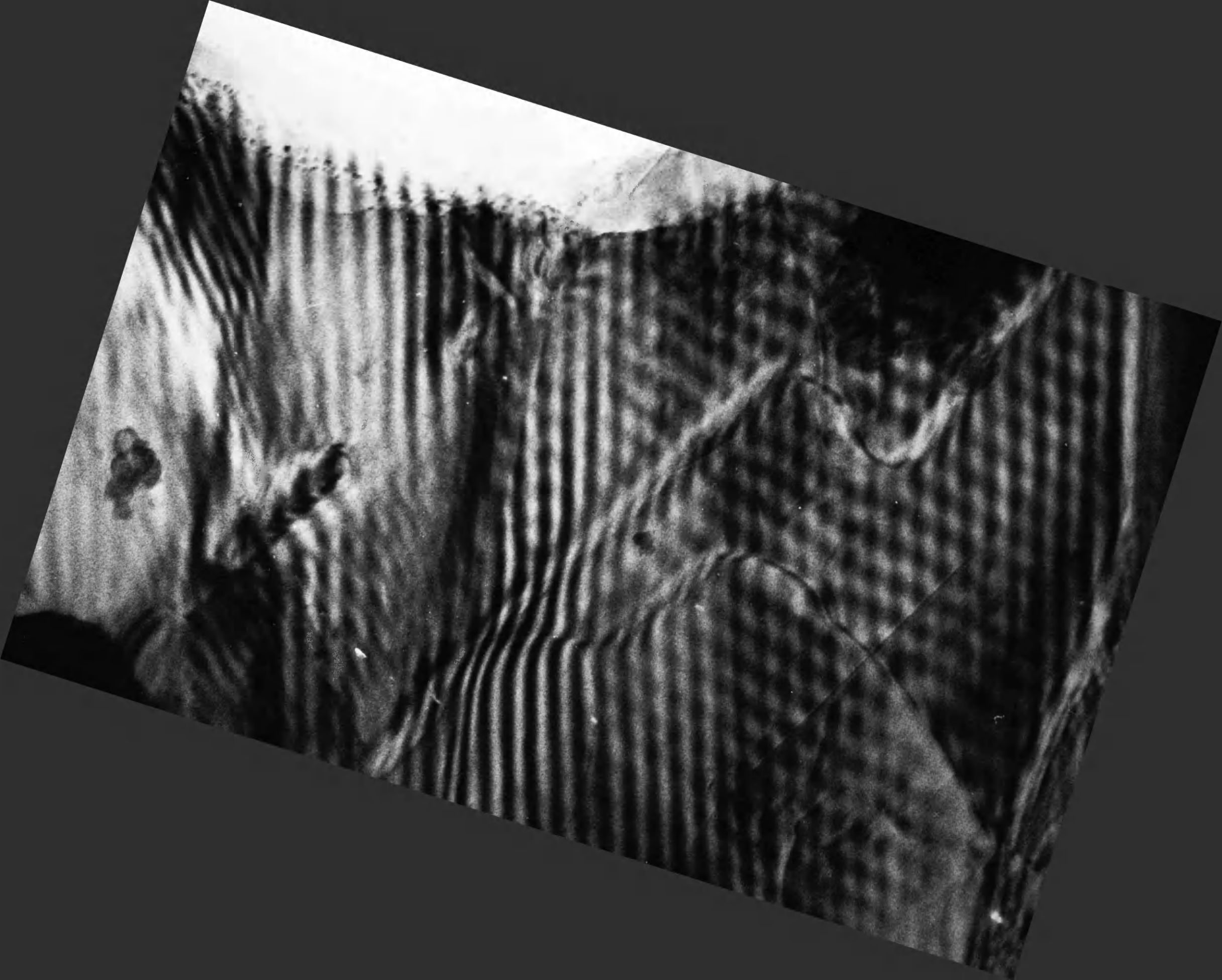

Plate 34

Selected Area Defraction Pattern from

Graphite Ferric Chloride area exhibiting moiré patterns

crystallites would be only 0.35^{o}. The ripples in the pattern indicate that the graphite lattice contains some distortion which could arise at the boundaries of intercalated layers.

The crystallites, which were observed in a few areas, were rectangular with an average side length of 35 nm (Plate 35). Folds in the graphite were revealed after the compound was washed in dilute HCl or dilute HCl and water.

5.2.2 Electron Diffraction of Graphite Ferric Chloride

Table 10 compares the spacings found after the HCl wash from areas containing crystallites, areas exhibiting intercalation features and average results from general areas of the compound. The average diffraction spacings observed after a subsequent water wash are also listed. The electron diffraction data measured from the published diffraction pattern for graphite ferric chloride is also given (Cowley and Ibers 1956). Each set of results is the average of a minimum of six diffraction patterns. The x-ray diffraction spacings for possible compounds present are also given for comparison in Table 11.

The areas containing small crystallites had a polycrystalline ring pattern superimposed on a graphite single crystal pattern. The spacings from the ring pattern correspond to $FeCl_2$.

Areas which displayed extensive line moiré patterns had a very distorted graphite diffraction pattern and in Plate 34 it can be seen that additional reflections from $FeCl_2$ or $FeCl_3$ are also distorted in a similar manner. In addition to a large variation in the spacings observed, there were also large changes in intensity and angles between the planes, comparable to the distortion found in the concentrated potassium graphite.

TABLE 10

Electron Diffraction Results

Graphite Ferric Chloride

Crystallites		Intercalated Areas HCl treatment		Other Areas		After HCl/H_2O treatment		Measured E.D. data Cowley + Ibers (1956)	
d_{nm}	Assignment	d_{nm}	Assignment	d_{nm}	Assignment	d_{nm}	Assignment	d_{nm}	Assignment
0.540 Px	$FeCl_2$	0.525 Px	$FeCl_3$ 100	0.336	G 0002	0.336	G 0002	0.528	$FeCl_3$ 100
						0.270	$FeCl_3$		
0.308 Px	$FeCl_2$			0.214	G $10\bar{1}0$	0.213	G $10\bar{1}0$	0.307	$FeCl_3$ 110
		0.306 Px	$FeCl_3$ 110	0.208	$FeCl_3$	0.206	$FeCl_3$		
0.213	G $10\bar{1}0$	0.212-0.188	G $10\bar{1}0$	0.200	$FeCl_3$	0.200	$FeCl_3$	0.213	G $10\bar{1}0$
0.198 Px	$FeCl_2/FeCl_3$	0.177 Px	$FeCl_3$ 300	0.180	$FeCl_2/FeCl_3$				
0.179 Px	$FeCl_2/FeCl_3$			0.177	$FeCl_3$			0.180	$FeCl_3$ 300
		0.123	G $11\bar{2}0$	0.162	$FeCl_3$				
0.154 Px	$FeCl_2$			0.155	$FeCl_2$			0.124	G $11\bar{2}0$
0.146 Px	$FeCl_2$								
0.124	G $11\bar{2}0$			0.122	G $11\bar{2}0$	0.123	G $11\bar{2}0$	a_G 30° to a_{FeCl_3}	
				0.115	G $11\bar{2}2$	0.115	G $11\bar{2}2$		
				0.106	G $20\bar{2}1$				

Px polycrystalline.

G graphite

TABLE 11

X-ray Diffraction Data (ASTM Index)

$FeCl_2$		$FeCl_3$		$2FeCl_3 7H_2O$	Graphite $FeCl_3$ Cowley + Ibers (1956)		
d_{nm}	Index	d_{nm}	Index	d_{nm}	d_{nm}	Assignment	Index
0.590	003	0.590	003	0.645	0.941	F-C	001
0.307	101,100	0.510	101	0.550	0.525	F	100
0.254	104	0.479		0.515	0.471	F-C	002
0.232	015	0.450	012	0.471	0.335	G	002
0.209	009,107	0.303	110	0.436	0.314	F-C	003
0.195	018,110	0.290	006,015	0.385	0.303	F	110
0.180	112	0.268	113	0.359	0.262	F	200
0.172		0.252	202	0.344	0.213	G	100
0.163	021	0.240		0.331	0.209	G	102/3
0.155		0.223	024	0.316	0.203	G	101
0.147	024	0.208	116,205	0.303	0.198	F	210
0.142	205	0.202	018	0.288	0.175	F	300
0.127	208	0.196	009,211	0.276	0.172	F-C	301
0.117	211	0.175	300	0.261	0.168	G	004
0.114	214	0.167	208	0.253	0.164	F-C	302
		0.163		0.243	0.157	F-C	002
		0.146		0.232	0.152	F	220
		0.134		0.224	0.146	F	310
		0.130		0.214	0.123	G	110
		0.119		0.203	0.118	F-C	008
		0.112		0.199	0.116	G	112
				0.193	0.115	F	410
				0.190	0.112	G	006
				0.186			
				0.174			
				0.170			
				0.165			
				0.160			
				0.154			
				0.151			
				0.142			
				0.139			

F = $FeCl_3$

F-C = Graphite ferric chloride

G = Graphite

Plate 35

Graphite Ferric Chloride

Area Containing Small Crystallites

x 83600

In the diffraction pattern from an area of bright discs and distorted moiré patterns (Plate 32) polycrystalline rings corresponding to the $FeCl_3$ (100) 0.5 25nm, (110) 0.3 06 nm and (300) 0.177 nm spacings were observed indicating that the [001] direction of the $FeCl_3$ is parallel to the graphite c-direction. These spacings are almost identical to those measured from the published electron diffraction pattern for graphite ferric chloride (Cowley and Ibers 1956, Table 10). However, there was no orientation relationship in any of the areas examined, in contrast to reports by the above workers. The streaks in the pattern, (Plate 32), probably arise from a stacking fault which is perpendicular to the direction of elongation of the spots. In some areas of bright discs, only the graphite diffraction pattern was found.

The spacings observed from general areas of the compound could be attributed to randomly oriented ferric chloride. The water wash appeared to remove some of this material. The graphite 0001 reflection probably arises from folds observed in the bright field. The presence of folds may indicate some decomposition of the compound as a result of treatment with acid and water.

5.2.3 Analysis of Graphite Ferric Chloride

The average iron content of these compounds was determined after reduction to graphite iron. The analytical results are reported in Section 7.10. The iron results indicated an average iron chloride content of 40-56% in the graphite. This agrees well with the concentrations observed for the ordered first stage compound plus graphite mixture studied by Cowley and Ibers (1956).

5.2.4 Morphology of Graphite Ferric Chloride after Reaction with Nitrogen and Hydrogen

The graphite ferric chloride exhibited three types of area

after reaction with N_2/H_2 at 523 and 558K. The first type, represented in Plate 36 had a graphite appearance with small crystallites apparently interspersed through the graphite. These areas were similar to those observed before reaction but were more numerous. Contrast at the particle edges suggests some interaction between the particles and the graphite which would not be present if the particles were on the surface. The crystallites had a regular shape and varied in length from 20-50 nm. There was no preferred orientation of the crystallites but some decoration at the graphite crystal edges had occurred.

The second type of area, (Plate 38) had several interesting features. Very dark areas with an elliptical shape and high contrast at one side were observed. The high contrast edge also exhibited fresnel fringes. In some cases, the dark areas were associated with bright discs. Small irregular bright discs were also present on a dark background matrix on or within the graphite. In addition to these features, small rods ca 15 nm long and 5 nm wide were present throughout the graphite lattice.

Plate 40 is typical of the third type of area found. This appeared to contain irregular aggregates on or within the lattice. A few bright discs were also present.

5.2.5 Electron Diffraction Results of Graphite Ferric Chloride after Reaction with Nitrogen and Hydrogen

The spacings observed after reaction are listed in table 12 and represent the overall effect of preparation and reaction. The regions of graphite containing crystallites had a diffraction pattern consisting of polycrystalline rings superimposed on a polycrystalline graphite pattern (Plate 37). The spacings for the polycrystalline rings correspond to ferrous chloride suggesting that reduction of the ferric chloride accompanied by agglommeration had occurred. At 558K

TABLE 12

Electron Diffraction Results

Graphite Ferric Chloride after Reaction with N_2/H_2

Crystals Type 1		Type 2		Type 3		Average 523K		558K		673K heated after reaction		G $FeCl_2$ (Ohhashi Tsujikawa)	
d_{nm}	Assignment	d_{nm}	Assign.	d_{nm}	Assign.	d_{nm}	Assignment	d_{nm}	Assignment	d_{nm}	Assignment	d_{nm}	Assignment
						0.342	G0001	0.650	H	0.664	H		
		0.56_{sp}		0.557_{sp}				0.540	$FeCl_3/FeCl_2$	0.344	H		
0.310	$FeCl_2$	0.310	$FeCl_2$ arcs 100	0.310	Px $FeCl_2$	0.312	$FeCl_2$	0.413	H				
		0.21				0.300	$FeCl_3$	0.310				0.312	$FeCl_2$ 100
0.213	G$10\bar{1}0$	0.213	G$10\bar{1}0$	0.213	G$10\bar{1}0$			0.307	$FeCl_2$	0.30	H		
		0.217											
				0.188	Px $FeCl_2$	0.262		0.292	$FeCl_3$				
0.180	$FeCl_2$	0.183	$FeCl_2$ arcs 110			0.256	$FeCl_2$	0.287	H				
		0.157	$FeCl_2$ arcs 200	0.154	Px $FeCl_2$	0.213	G	0.232	H	0.242	H		
0.124	G$11\bar{2}0$	0.124	G$11\bar{2}0$	0.126	G	0.207	$FeCl_3$	0.212	G	0.231	H	0.213	G$10\bar{1}0$
		0.106	$FeCl_2$ arcs 300	0.117	G $FeCl_2$	0.200	$FeCl_3$	0.208	$FeCl_3$				
						0.180	$FeCl_2$	0.198	$FeCl_3$	0.202	H	0.180	$FeCl_2$ 110
						0.175	$FeCl_3$	0.188				0.156	$FeCl_2$ 200
						0.147	$FeCl_2$	0.180	$FeCl_2$			0.123	G $11\bar{2}0$
						0.123	G	0.175	$FeCl_3$			0.104	$FeCl_3$ 300
						0.115	G	0.170	H			0.090	$FeCl_3$ 220
								0.162					
								0.153	$FeCl_2$	0.14	H		
								0.124	G	0.128	H		

G = Graphite
H = Hydrate 2 $FeCl_3 7H_2O$
Px = Polycrystalline
Sp = spot

Plate 36

Graphite Ferric Chloride after Reaction

with N_2/H_2 at 558K: Area containing small crystallites

Type 1

x 94300

Plate 37

Selected Area Diffraction Pattern from

Graphite Ferric Chloride containing small crystallites

after reaction

Plate 38

Graphite Ferric Chloride after reaction

with N_2/H_2 at 558K

Type 2

x 111930

Plate 39

Selected Area Diffraction Pattern from

Graphite Ferric Chloride after reaction

Type 2

Plate 40

Graphite Ferric Chloride after reaction

with N_2/H_2 at 558K containing aggregates

Type 3

x 126000

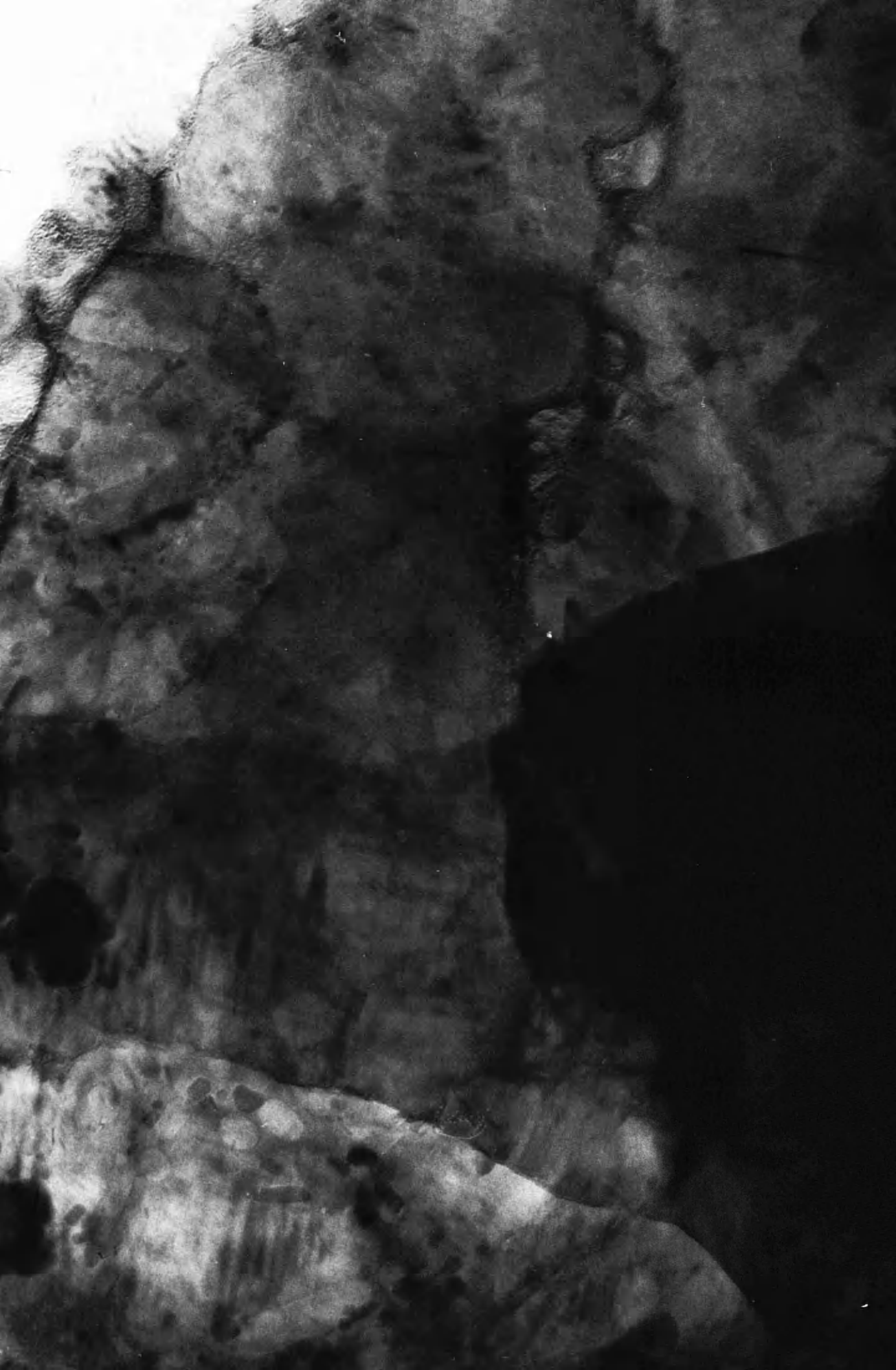

some spacings which could be attributed to 2 $FeCl_3 7H_2O$ were found. The hydrate was also detected on the compound heated to 673K.

In the second type of area (described in Section 5.2.4) the pattern consisted of a graphite single crystal pattern with a superimposed array of small arcs (Plate 39). The pattern could be attributed to $FeCl_2$ but was distorted giving errors in the measured spacings. The $[100]$ $FeCl_2$ direction was parallel to the graphite $10\bar{1}0$ direction and the pattern corresponds closely to the second stage graphite ferrous chloride pattern reported by Ohhashi and Tsujikawa (1974). It should be noted that this pattern is also similar to that reported by Evans and Thomas (1975) which they claimed was that of a graphite ferric chloride compound. However, these authors appear to have incorrectly compared their pattern with that of Cowley and Ibers (1956).

In some cases, (Plate 39) there was a set of spot reflections from planes with a spacing of 0.56 nm parallel to the graphite $\{10\bar{1}0\}$ planes. As the $FeCl_2$ is oriented with its $[001]$ direction parallel to the graphite c-direction and as the 0.56 nm spacing corresponds to the (003) $FeCl_2$ planes, this extra spacing cannot be attributed to $FeCl_2$. The extra spacing was also a sharp "spot" reflection and not a small arc from several crystallites as found for the $FeCl_2$ reflections. This set of reflections was therefore ascribed to double diffraction by the graphite $10\bar{1}0$ reflection.

The third type of area (Section 5.2.4) had a polycrystalline $FeCl_2$ ring pattern superimposed on the graphite single crystal pattern (Plate 41) indicating a more random array of $FeCl_2$. The spot pattern at 0.557 nm was again present in some areas.

5.2.6 Catalytic Results

The reaction with graphite ferric chloride was carried out

Plate 41

Selected Area Diffraction Pattern from

Graphite Ferric Chloride after reaction

Type 3

using a 1:2 ratio of nitrogen and hydrogen at temperatures of 558, and 523K for times up to 24 hours under static and flow conditions (Table 4). In order to drive off any product which may have become trapped in the graphite layer planes the graphite $FeCl_3$ was heated to 673K after reaction in a few instances and the products collected for analysis. The only reaction product found was HCl, probably formed as a result of reduction of $FeCl_3$ to $FeCl_2$.

5.3 Graphite Copper Sulphide

Graphite copper sulphide was prepared as described in Section 2.3.3 and reacted with N_2/H_2 at 673K and 723K (Table 4). In all cases, gas infra red analysis showed that the reaction product was H_2S, indicating that decomposition had occurred. Plate 42 shows the graphite copper sulphide compound after reaction. Intercalation features in the form of ring moirés and extensive line moirés were present. Irregular dark globules exhibiting fresnel fringes were found associated with folds in the graphite. No bright discs were observed. A typical diffraction pattern is shown in Plate 43. The polycrystalline graphite pattern has a few polycrystalline reflections which can be attributed to sulphur and Cu_2S. The diffraction data accumulated from several samples after reaction, listed in Table 13, indicates that copper, sulphur and Cu_2S are present. The copper may be formed by reduction of the sulphide on reaction or some residual copper and sulphur may have remained from the preparation of the compound.

5.4 Graphite Ferric Chloride Reduced with Hydrogen: Reaction with Nitrogen and Hydrogen

As the main product of reaction of graphite ferric chloride with hydrogen was HCl, an attempt was made to eliminate that reaction from the catalytic synthesis of ammonia by prior reduction of the

TABLE 13

Graphite Copper Sulphide after Reaction with N_2/H_2
Electron Diffraction results

Graphite Copper Sulphide after Reaction	
d_{nm}	Assignment
0.657	S 111
0.345 0.339	G 0002/Cu_2S
0.328	S 222
0.254	-
0.23	S 333
0.213	G $10\bar{1}0$
0.209	Cu
0.204	G $10\bar{1}1/Cu_2S$
0.194	Cu_2S
0.185	Cu_2S
0.170	Cu_2S
0.165	G 0004/S444
0.123	G $11\bar{2}0$
0.117	
0.115	G $11\bar{2}2$

G = Graphite

S = Sulphur

Plate 42

Graphite Copper Sulphide

after reaction with N_2/H_2 at 673K

exhibiting distorted moiré patterns

x 107100

Plate 43

Selected Area Diffraction Pattern from

Graphite Copper Sulphide after reaction

graphite ferric chloride. The reduction was carried out as described in Section 2.3.4. The morphology of the reduced compound was similar to that observed for graphite ferric chloride after reaction with nitrogen and hydrogen.

5.4.1 Morphology of the Reduced Graphite Ferric Chloride after Reaction.

Two main features were observed after reaction. The first feature, (Plate 44) was a number of aggregates distributed apparently throughout the graphite crystal. These regions were 100 nm in diameter and some displayed a star shaped contrast effect in bright field. Some small (15 nm diameter) bright discs were also present in this area associated with dark areas, as in the graphite ferric chloride after reaction (Section 5.2.4). The second feature, Plate 46, was a distorted moiré pattern in the form of irregular, curved lines. Aggregates were again present. The presence of the distorted moiré pattern was accompanied by streaking in the electron diffraction pattern.

5.4.2 Electron Diffraction of the Reduced Graphite Ferric Chloride after Reaction.

Areas containing the aggregates and small bright discs in a dark background material displayed a polycrystalline ring pattern superimposed on a graphite spot pattern as in Plate 45. The spacings measured are listed in Table 14 (Column 1). Some of the spacings correspond to $FeCl_2$. However, the 0.374, 0.188, 0.166, 0.145 (faint) and 0.123 nm spacings could not be identified easily. It is interesting to note that the 0.374, 0.188 and 0.123 nm spacings were in the ratios 1:2:3 and these spacings correspond well to ammonium chloride (111), (222) and (333) spacings (Table 14, Column 2).

The diffraction pattern from Plate 46 has a similar basic

TABLE 14

Electron Diffraction Results. Reduced Graphite $FeCl_3$ after reaction

Reduced Graphite Ferric Chloride After N_2/H_2 563K		NH_4 Cl (250°C) (ASTM-Index)		Reduced Graphite Ferric Chloride after But/H_2		Reduced Graphite Ferric Chloride +But/H_2 573K			$FeCl_3$ after But/H_2 573K	Gr $FeCl_2$ (Ohhashi and Tsujikawa 1974)		
		cubic		Average		Plates 52, 54						
d_{nm}	Assignment	d_{nm}	Index	d_{nm}	Assignment	d_{nm}	Assignment			d_{nm}	Assignment	Index
0.374Px		0.378	111	0.58Px	$FeCl_2/FeCl_3$	0.309arc	$FeCl_2$	100	0.508 $FeCl_2$	0.312	$FeCl_2$	100
0.307	$FeCl_2$ 100			0.38		0.254	$FeCl_2$	104				
				0.341		0.213	G	$10\bar{1}0$	0.303 $FeCl_2/FeCl_3$	0.213	G	$10\bar{1}0$
0.213	G $10\bar{1}0$			0.310	$FeCl_2/FeCl_3$					0.180	$FeCl_2$	110
				0.300	$FeCl_3$	0.181arc	$FeCl_2$	110	0.254 $FeCl_2$			
0.188Px		0.189	222			0.157-4arc	$FeCl_2$	200		0.156	$FeCl_2$	200
0.180Px	$FeCl_2$ 110			0.267	$FeCl_2$				0.178 $FeCl_2$	0.104	$FeCl_2$	300
0.166Px		0.163	400	0.212	G $10\bar{1}0$	0.213	G $1\bar{1}20$					
0.145Px	310	0.145f	420	0.208	$FeCl_3$	0.116arc	$FeCl_2$	300	0.170 $FeCl_2$	0.090	$FeCl_2$	220
0.123Px		0.124	333	0.180	$FeCl_2$							
0.123	G $11\bar{2}0$			0.175	$FeCl_3$	0.104arc	$FeCl_2$	300	0.111 $FeCl_2$	a_G parallel to a $FeCl_2$		
				0.170	$FeCl_2$							
				0.165	$FeCl_2$							
				0.155	$FeCl_2$							
				0.147	$FeCl_2/FeCl_3$							
				0.123	G $11\bar{2}0$							

G = Graphite

Plate 44

Reduced Graphite Ferric Chloride

after reaction with N_2/H_2 at 563K

containing aggregates in the graphite

x 100000

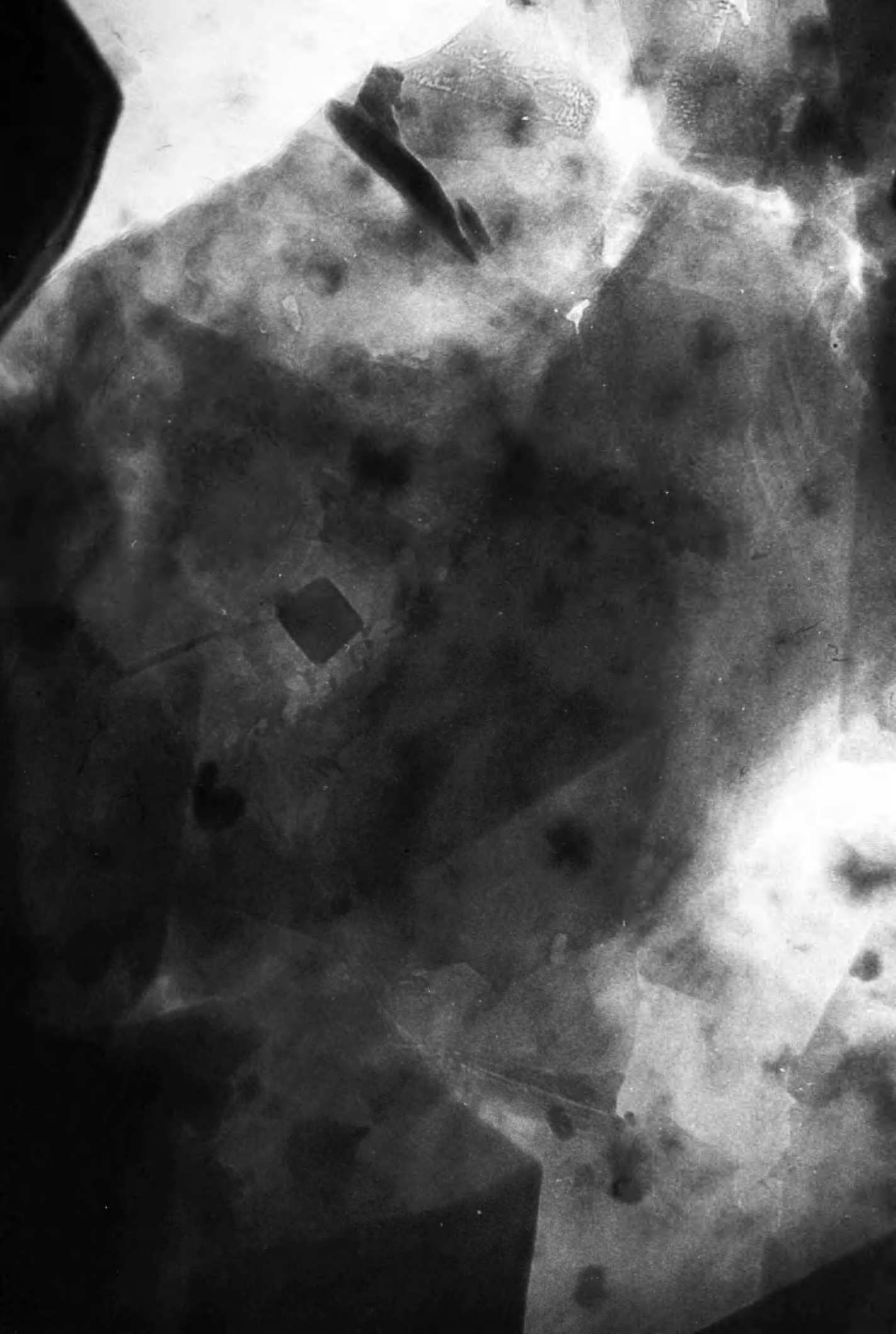

Plate 45

Selected Area Diffraction Pattern from

Reduced Graphite Ferric Chloride

containing aggregates after reaction

Plate 46

Reduced Graphite Ferric Chloride

after reaction with N_2/H_2 at 563K

containing aggregates and distorted moirés

x 98000

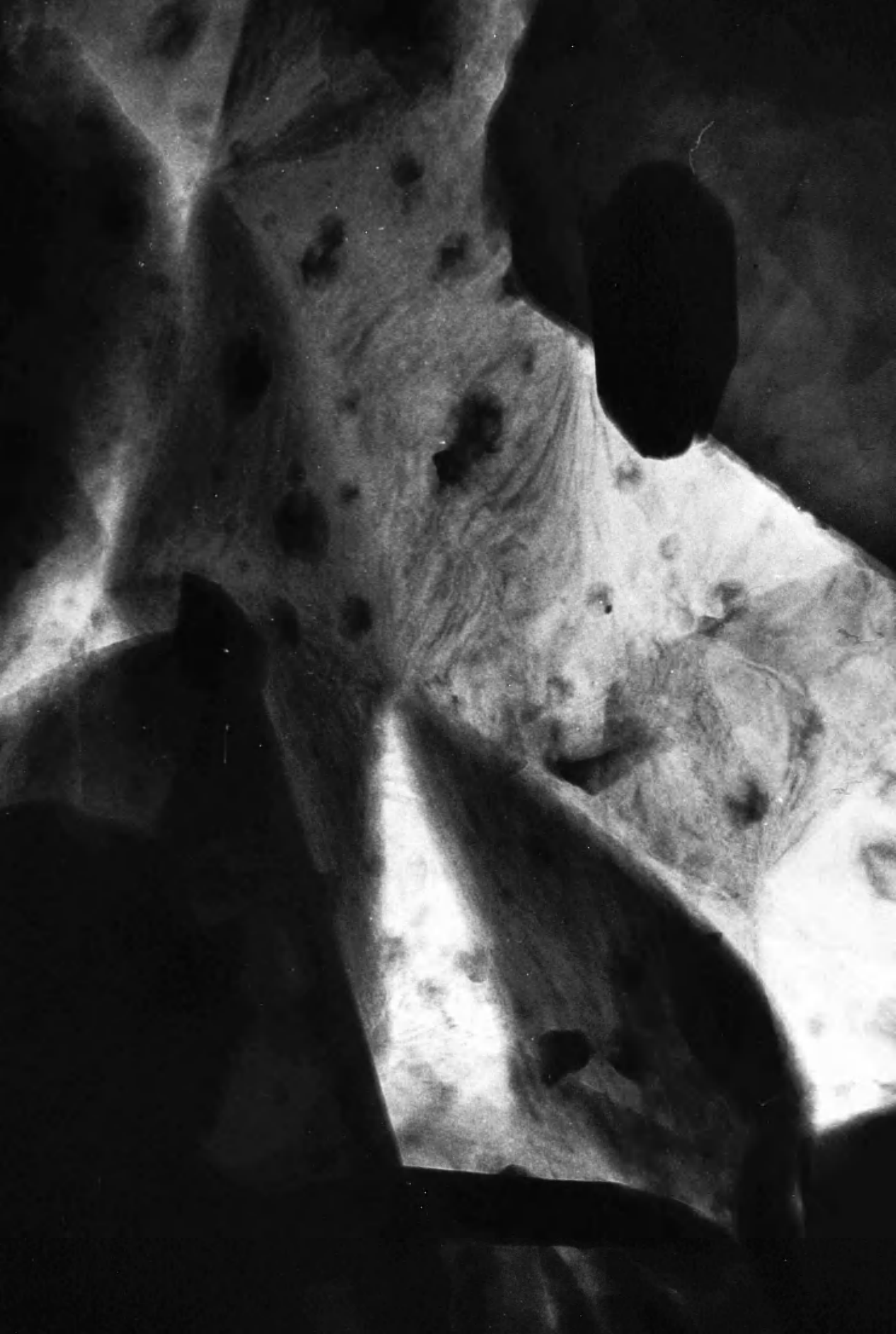

Plate 47

Selected Area Diffraction Pattern from

Reduced Graphite Ferric Chloride

containing aggregates and distorted moirés

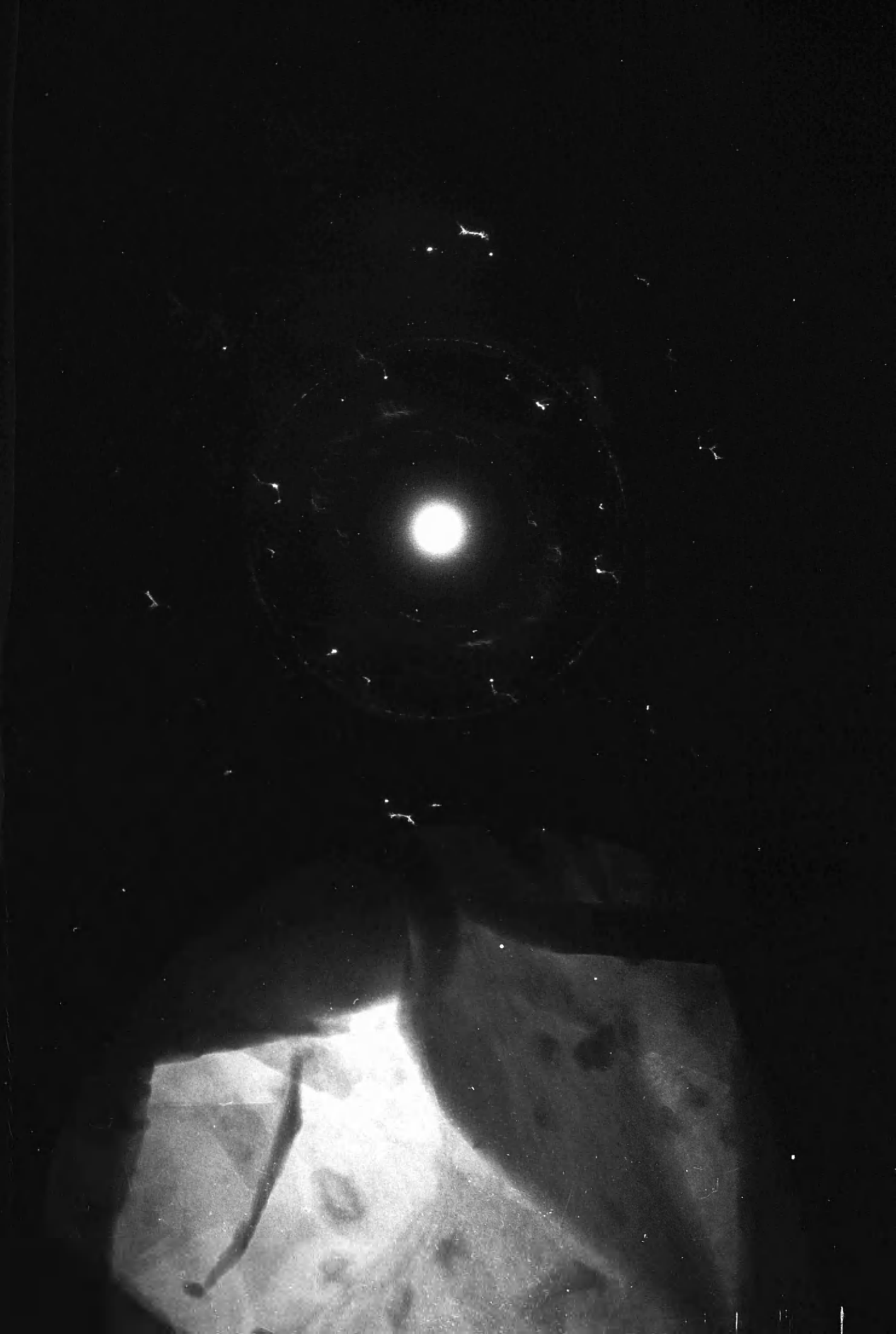

pattern to Plate 45 but with an unsymmetrical streaking effect (Plate 47) associated with one of the graphite crystals and the inner polycrystalline reflections. The size of the streaks increases with increasing g-vector in the graphite [110] direction.

Streaks in the diffraction pattern usually arise from changes in the shape of the reciprocal lattice points either from the shape of the crystal defects or lattice strain. Crystallographically oriented defects such as precipitates can give rise to streaks and the intensity distribution at a reciprocal lattice point is increased in the direction normal to the thin dimension of the particles. Elastic distortion of the matrix can also cause streaking and the main distinction between the two effects is that extension of the reciprocal lattice point due to strain is strongly dependent on the indices at that point, while crystal shape effects cause all points to be extended equally, including the origin.

In this case, as the streaking effect was unsymmetrical, no streaks were present in the transmitted spot, and some distortion of the lattice was evident from the moiré patterns observed in bright field, it is likely that lattice strain is contributing to the appearance of streaks. However, the Y shaped form of the streaks cannot be explained in this way and must arise from precipitate shape effects. The upright of the Y was always parallel to one of the graphite $\{10\bar{1}0\}$ planes and represents a crystallite plane parallel to this plane. On the evidence available, it is therefore suggested that some of the precipitates are in the form of small triangular pyramids with their {111} planes parallel to the c-direction of graphite (Fig 14). This structure could also explain the star shaped contrast effect in bright field assuming that it arose from absorption contrast.

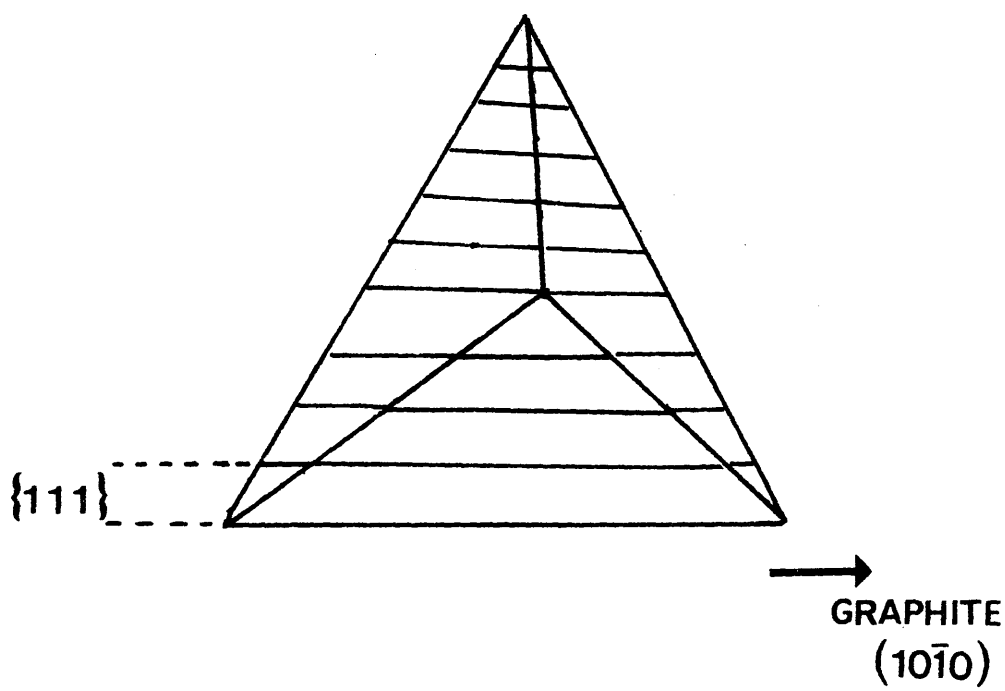

In plane view of precipitate

Figure 14. Proposed Structure of Precipitates formed after Reaction of N_2/H_2 over Reduced Graphite Ferric Chloride.

5.5 Reduced Graphite Ferric Chloride: Reaction with Butadiene and Hydrogen

5.5.1 Introduction

The reaction of hydrogen with butadiene was chosen in order to yield information on possible selectivity in the catalytic properties of graphite intercalation compounds. The reaction could proceed by isomerisation, partial or complete hydrogenation, partial decomposition or complete decomposition to carbon. The compound was examined in the electron microscope after reaction to determine any structural changes.

5.5.2 Morphology of Reduced Graphite Ferric Chloride after Reaction

Examination of the compound after reaction revealed that it was a mixture of materials consisting of graphite, the reduced graphite ferric chloride and a solid reaction product.

In addition to areas of rod-like inclusions (Plate 38, Section 5.2.4), the reduced graphite ferric chloride, after reaction, exhibited features which are shown in Plates 48 and 50. The main feature consisted of a dark area containing small ($\sim$10-20 nm) bright discs (Plate 48). This type of area was also observed in both the graphite ferric chloride and reduced compound after reaction with nitrogen and hydrogen.

A new triangular feature was also observed. The edges of the triangular feature were parallel to the graphite $[11\bar{2}0]$ direction and in some cases the central portion of the triangle contained a bright irregular area (Plate 50). Some of these features exhibited a star shaped contrast effect similar to that observed in the agglommerations in the reduced compound after reaction with nitrogen and hydrogen. Some of the triangular features appeared to overlap indicating that they were within the graphite lattice.

Plate 48

Reduced Graphite Ferric Chloride

after reaction with Butadiene and Hydrogen

at 573K exhibiting dark areas with small bright discs

x 138700

Plate 49

Selected Area Diffraction Pattern from

Reduced Graphite Ferric Chloride

after Reaction with Butadiene and Hydrogen

at 573K exhibiting dark areas and small bright discs

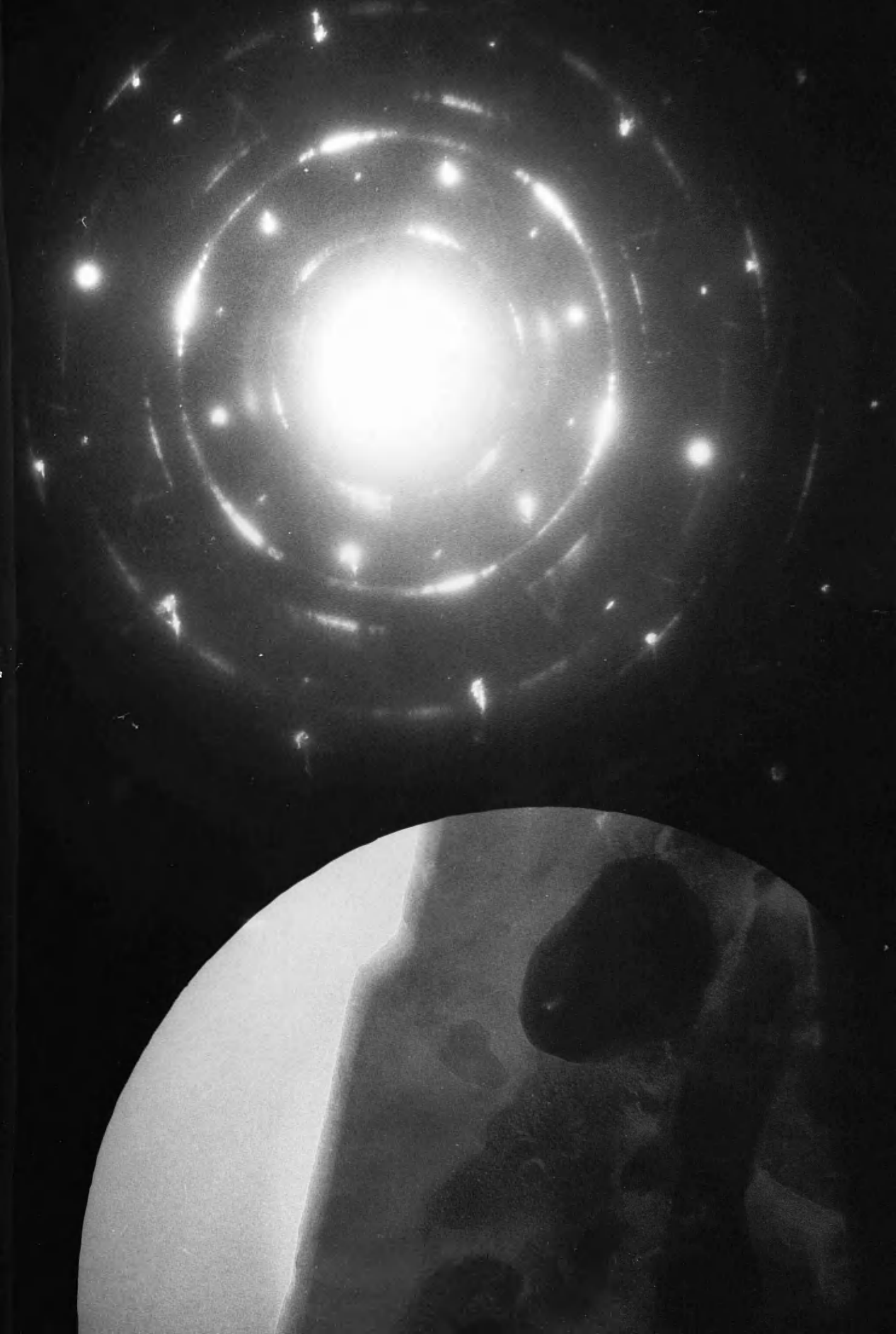

Plate 50

Reduced Graphite Ferric Chloride

exhibiting triangular features after reaction

with Butadiene and Hydrogen at 573K

x 102960

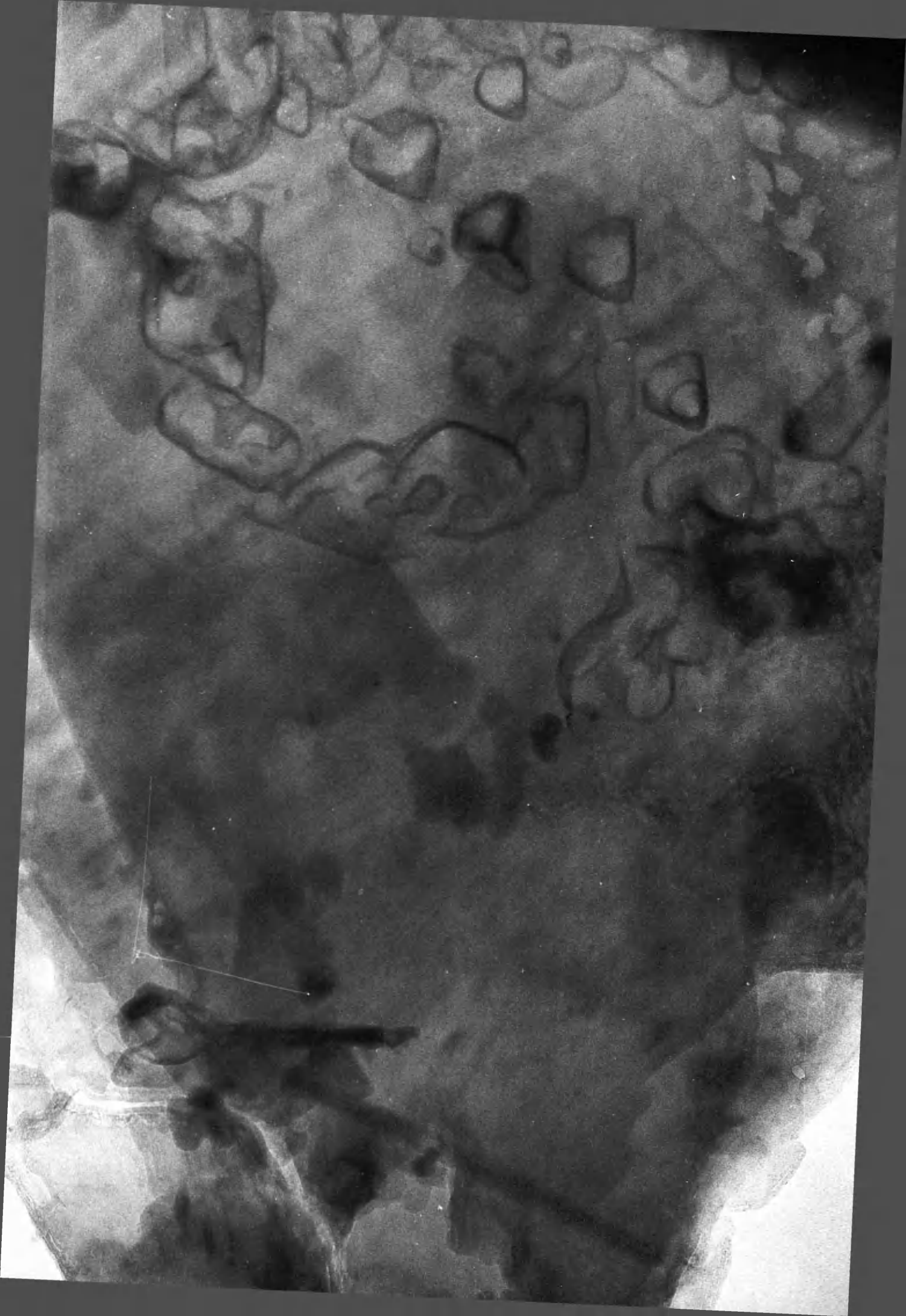

Plate 51

Selected Area Diffraction Pattern from

Reduced Graphite Ferric Chloride

exhibiting triangular features after reaction

with Butadiene and Hydrogen at 573K

5.5.3 Solid Reaction Product

The solid reaction product was almost electron transparent, with a random wavy appearance (Plate 52). The diffraction pattern from this material (Plate 53), consisted of diffuse rings similar to that observed for amorphous carbon.

A comparative experiment, performed with $FeCl_3$ only, produced a solid reaction product with a similar appearance and diffraction pattern. This suggests that $FeCl_2$ was the catalyst for the formation of the solid product. It is probable that this product is a butadiene polymer.

5.5.4 Electron Diffraction of Reduced Graphite Ferric Chloride After Reaction with Butadiene and Hydrogen

The electron diffraction results from the reduced graphite ferric chloride are shown in Table 14, columns 3 and 4. The spacings are compared with results from ferric chloride after reduction and reaction under the same conditions (column 5) and with spacings from graphite ferrous chloride (2nd stage)(Ohhashi and Tsujikawa 1974). It would appear that, after reaction, most of the iron is in the form of $FeCl_2$ with only a few incompletely reduced areas. Under the same conditions, pure $FeCl_3$ was completely reduced to $FeCl_2$.

Typical diffraction patterns, Plates 49 and 51, show a hexagonal pattern of areas superimposed on the single crystal graphite pattern. This pattern is similar to that observed for graphite ferric chloride after reaction with nitrogen and hydrogen which was identified as graphite ferrous chloride, in agreement with Ohhashi and Tsujikawa (1974). An extra arc was present at 0.254 nm in both patterns indicating that not all the ferrous chloride was oriented with the a-axis parallel to the graphite a-axis. The triangular features did not produce any extra reflections in the diffraction pattern.

Plate 52

Solid reaction product after

reaction of reduced Graphite Ferric Chloride with

Butadiene and Hydrogen

x 82000

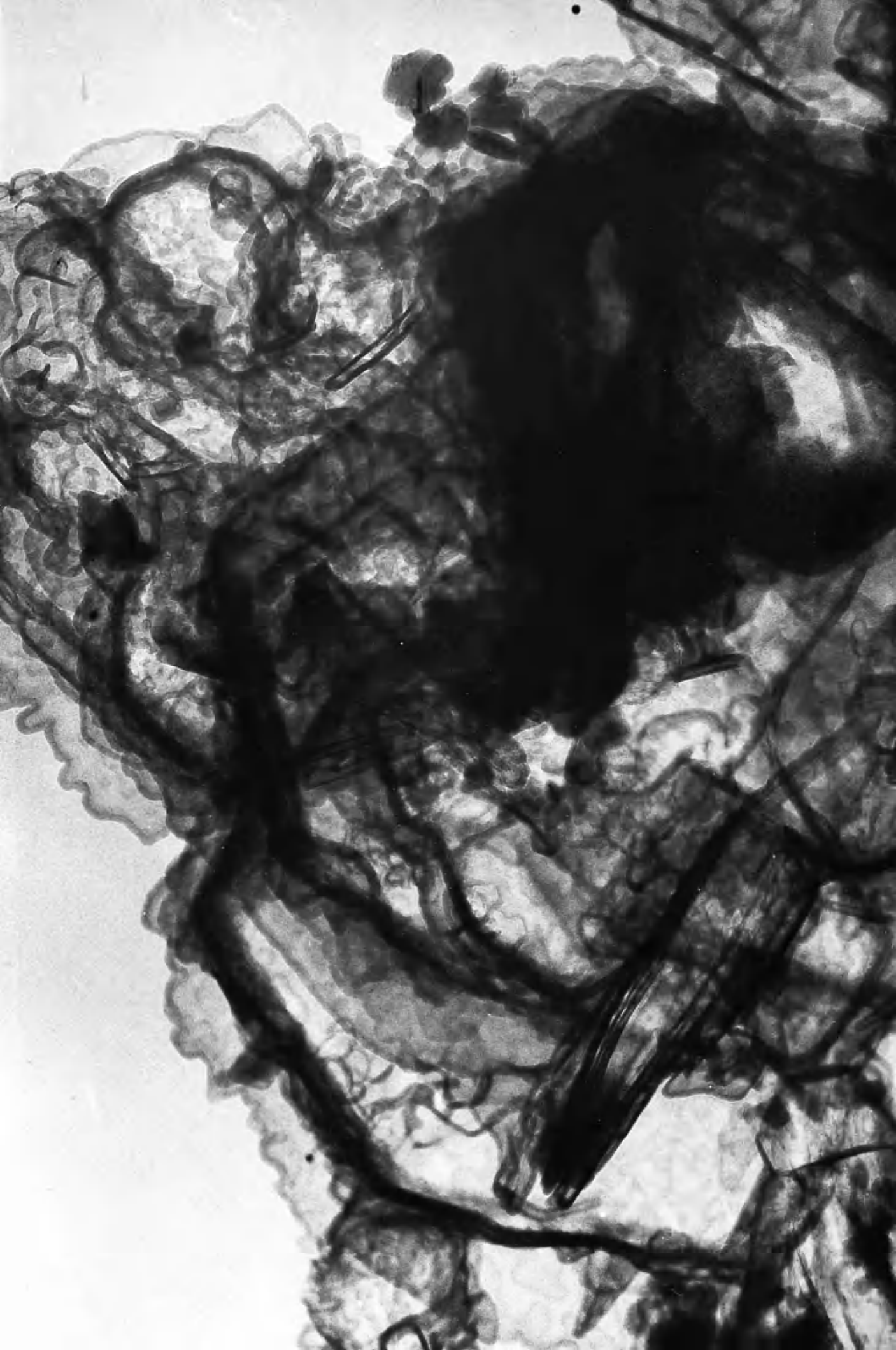

Plate 53

Diffraction pattern of solid reaction product

In addition, streaks are present in Plate 49 at 0.386, 0.136 and 0.117 nm indicating the presence of two sets of small cubic crystallites with their thin dimensions at 60^{o} to each other associated with the graphite. These crystallites could not be identified using the limited data available.

5.5.5 Catalytic Results for Reaction of Reduced Graphite $FeCl_3$ with Butadiene/Hydrogen

Reduced graphite ferric chloride, prepared as described in section 2.3.4, was allowed to react at 573K with a 25% butadiene, hydrogen mixture at one atmosphere for periods from 18 to 24 hours. (Table 5). Comparative reactions using reduced $FeCl_3$ and graphite were carried out under the same conditions.

From gas chromatography, the gaseous products of reaction of graphite ferrous chloride with butadiene and hydrogen, were HCl, butane, but-1-ene, and but-2-ene. The results were variable but the average conversion of butadiene was 20%. In one case, almost complete conversion to butane was obtained.

Reaction of the reduced $FeCl_3$ resulted in an average of 80% conversion of butadiene. The products of reaction were the same as those found for the graphite ferrous chloride compound. In the presence of graphite, no reaction of butadiene was observed.

In addition to the hydrogenation reaction, polymerisation of butadiene also occurred as indicated by the polymer observed by T.E.M. (section 5.5.3)

6. ACCEPTOR COMPLEXES OF GRAPHITE: DISCUSSION

6.1 Graphite Ferric Chloride

In this study, the graphite ferric chloride compound was a mixture of graphite and a material which exhibited morphological features similar to those observed for the potassium graphite compound. The main features, however, in this compound were bright discs in a dark background. Line moiré patterns and distorted or ring moirés were less common.

Interpretation of these features, using the potassium graphite morphology as a model, indicates that the dark areas correspond to fully intercalated areas and the bright discs correspond to unintercalated regions. These bright discs could arise either from $FeCl_3$ or Cl_2 vapour produced at the preparation temperature and trapped within the graphite, or as a result of dissociation of the $FeCl_3$ produced by the heating effect of the beam. This latter case has been observed in studies of the graphite ferric chloride residue compound (Heerschaap and Delavignette 1967).

Electron diffraction from these areas did not give the oriented graphite ferric chloride diffraction pattern observed by Cowley and Ibers (1956), although an oriented $FeCl_2$ pattern was observed on reduction (sections 5.2.4 and 5.4.2). The presence of the less ordered polycrystalline ring pattern with the $[001]$ $FeCl_2$ direction parallel to the graphite c-direction, and in some areas, of the simple graphite pattern, may indicate some liquefaction of the $FeCl_3$ as a result of electron beam heating. The diffraction results, however, confirm that the $FeCl_3$ layer stacking in the graphite c-direction is different to that in pure $FeCl_3$ (Cowley & Ibers 1956).

Using Hérold's model, (section 1.3.3), the regions of distorted moirés can be interpreted as regions of a higher stage graphite ferric chloride compound containing discrete regions of the intercalate. It is interesting to observe (Plate 31) that the area of distorted or ring moiré patterns is adjacent to a free graphite and a fully intercalated

area. This suggests that these areas are an intermediate formed during the phase segregation reported to occur on cooling (Cowley and Ibers 1956, Novikov et al 1970).

Line moirés are observed associated with the intercalation process and probably arise from relative rotation of the graphite lattice as a result of unpinning during intercalation. It is also possible that in some areas they may arise from the small relative rotation of overlapping ferric chloride layers in a similar manner to that reported for Graphite $MoCl_5$ (stage 4) (Syme Johnson 1967).

The boundary dislocations and dislocation loops of trapped intercalate, observed in the residue compound (Amelinckx and Delavignette 1967) were rarely observed in this study. This indicates that decomposition to the residue compound on exposure to the high vacuum conditions of the microscope had not occurred. The high resolution study of the concentrated graphite $FeCl_3$ (Thomas, et al 1976) showed that in the very small regions studied, removal of complete layers of $FeCl_3$ could take place in high vacuum in an ordered manner to form a mixture of first, second, fifth and sixth stages in close proximity in the graphite crystal.

Washing of the graphite ferric chloride with acid solution may remove ferric chloride layers from the compound. There is some controversy over the manner of this removal as the work of Brusset et al (1967) indicated that the removal of ferric chloride layers was random while the work of Hooley and Soniassy (1970) suggested that layer removal was ordered.

From this work, washing with acid produced folds in some thin graphite crystallites, possibly as a result of collapse of the graphite sheets on rapid and complete intercalate removal. This agrees with the work of Hooley and Soniassy (1970) who showed that thin

flakes are readily intercalated and decomposed. However, if only a few layers of ferric chloride are removed from the graphite, no observable contrast changes in the final image would be produced.

The morphology of the compound studied indicates that it is mainly a mixture of graphite and a first stage graphite ferric chloride compound with a small amount of lower stage compound. This agrees well with the analytical results (section 5.2.3) and the work of Cowley and Ibers (1956) and Novikov et al (1970).

6.2 Reaction of Graphite Ferric Chloride with Nitrogen and Hydrogen

In this study, the graphite ferric chloride compound did not liberate any gaseous ammonia after reaction with nitrogen and hydrogen. Reduction of the ferric chloride compound occurred with the evolution of HCl. Electron diffraction results showed that graphite ferrous chloride had been formed.

The graphite ferrous chloride pattern obtained indicated that the ferrous chloride layers were in two forms; oriented with respect to the graphite, and a less ordered arrangement with the [001] $FeCl_2$ direction parallel to the graphite c-direction. Assignment of the oriented pattern is not straightforward. According to Ohhashi and Tsujikawa (1974) this pattern arises from the second stage compound. However, in the present study, the initial preparation conditions and analysis indicates that the first stage graphite $FeCl_3$ compound is formed. However, the pattern observed can be explained if the diffraction pattern from the first and second stage compounds, are identical. This may be the case as the structures in the "stage" model for first and second stage intercalation compounds are similar. Alternatively, the reduction process, in which the iron inter-atom distance is decreased, produces discrete $FeCl_2$ regions within

the layer and ordering of these regions in the c-direction may produce the second stage compound. This process has been observed in the reaction of potassium graphite with CO (Daumas and Herold 1969, section 1.3.7) and the structure of the resulting compounds has been explained by the bent layer model (Daumas and Herold 1971).

The extra hexagonal spot pattern present in some areas could only arise as a result of double diffraction. This implies that the $FeCl_2$ system, compared to the $FeCl_3$ in the graphite ferric chloride, is more ordered in the c-direction.

It is therefore suggested that the areas giving rise to the oriented diffraction patterns could be produced by the reduction of the original fully intercalated graphite ferric chloride regions present before reaction. The more randomly oriented $FeCl_2$ compound could arise from a lower stage graphite ferric chloride compound.

The morphology of the ordered graphite ferrous chloride compound exhibited small rod-like inclusions which could be micro-crystallites within the lattice. In some areas these rods were in associations with bright discs and dark areas which may indicate incomplete reduction of the intercalated flake.

Small bright discs in the graphite, associated in some areas with a dark background matrix, were also visible in these areas. If the bright discs are an absorption effect, as found for potassium graphite, and represent gas bubbles within a matrix, then it is likely that the bright discs are bubbles of HCl gas formed on reduction of the ferric chloride. In support of this view, the bright discs are often present at the crystallite edges which would be expected as a result of reaction preferentially occurring at these sites. In addition, diffusion of the HCl bubbles to the crystallite edge from the centre of the matrix would be expected. These features are also

observed in the pre-reduced graphite ferric chloride after reaction with nitrogen and hydrogen and with butadiene and hydrogen.

In the less ordered graphite ferrous chloride compound, a few diffuse aggregates were present within the lattice. This less ordered compound was more common after reaction and some degradation of the fully intercalated material may have occurred under reaction conditions. The discrete regions of ferric chloride in the lower stage ferric chloride compound could form the diffuse aggregates observed on reduction.

Some decomposition of the compound appeared to take place with the extent of decomposition being a function of temperature. After reaction at 573K, elliptical dense areas with fresnel fringes were observed. These features, could arise from expulsion of ferric chloride or ferrous chloride from the graphite to form a wedge shaped drop. Massive expulsion of $FeCl_3$ was observed in bright field after heating to 673K after reaction. Further evidence of expulsion of $FeCl_3$ is given by the formation of the hydrate which could only be formed on exposure of the expelled $FeCl_3$ to air after reaction. The small bright discs in the dark background matrix may represent areas of expelled $FeCl_3$ which have subsequently been reduced.

From this study, the reduction of the fully intercalated graphite ferric chloride appears to take place within the graphite layer planes to form $FeCl_2$ layers within the graphite. The rod-like formations may indicate some microcrystallite aggregation in the layers. Reduction of the lower stage compounds, where descrete areas of $FeCl_3$ already exist, could result in some agglommeration of material within the lattice. The formation of many crystallites of $FeCl_2$ within the layers after reaction may be the final stage of the process of agglommeration and represent a dilute or residue compound.

6.3 Reaction of Graphite Ferrous Chloride

6.3.1 Synthesis of Ammonia

The electron diffraction results after reaction of the graphite ferrous chloride with nitrogen and hydrogen indicate that some compound formation had occurred within the lattice. The streak pattern and strain effects observed in some areas confirm this. Although there is insufficient data to identify the extra reflections observed in the electron diffraction patterns, the results indicate that NH_4Cl may have been formed.

As no compound formation was found in the unreduced compound, it is suggested that the reduction reaction prevented the dissociative adsorption of nitrogen. Partial elimination of this reaction by pre-reduction of the compound subsequently produced reaction sites where nitrogen adsorption could occur. Any HCl trapped within the graphite lattice or formed from previously unreduced graphite ferric chloride would react with any ammonia produced to form NH_4Cl.

Evidence has already been presented for the presence of trapped HCl (section 6.2). The reaction of nitrogen and hydrogen over reduced graphite ferrous chloride has been studied briefly by other workers (Ichikawa et al 1972d). No production of ammonia was reported.

6.3.2 Reaction with Butadiene and Hydrogen

From the catalytic results (section 5.5.5), polymerisation and hydrogenation of butadiene occurs over graphite ferrous chloride. Reaction over pre-reduced ferric chloride under the same conditions formed the polymer as the main reaction product in addition to hydrogenation products. It is therefore likely that the $FeCl_2$ is the catalyst for the polymerisation reaction.

The catalytic sites associated with this reaction could not

be determined unambiguously however. There is some evidence that reaction had taken place both on the surface and within the graphite ferrous chloride lattice.

The morphology of the compound after reaction indicated a large number of small (10nm) bright discs which were mainly associated with a dark background matrix. From the appearance of the compound after reduction (section 6.2) these areas may represent expelled $FeCl_3$ which was subsequently reduced to $FeCl_2$. Diffraction indicated that the $FeCl_2$ was oriented with respect to the graphite. It is likely that these areas of surface $FeCl_2$ act as a reaction site for polymerisation.

Another possible reaction site is within the graphite lattice. There is some evidence for this from the appearance of the oriented triangular features observed only after the butadiene/hydrogen reaction and which do not produce extra reflections in the diffraction pattern. (Plates 52 and 53). The contrast observed from these features could be diffraction or absorption contrast. Overlap of the features indicates that they are within the graphite layers. It is therefore possible that they are polymeric material and that reaction sites exist within the graphite layers.

The irreproducibility of results may be explained by the variation in amount of $FeCl_2$ on the surface of the graphite and extent of reaction within the graphite layers.

The hydrogenation reaction may occur on the sites for the polymerisation reaction. However, HCl was also found after reaction despite pre-reduction of the graphite ferric chloride. This indicates that either some $FeCl_3$ remained unreduced or further reduction of the $FeCl_2$ to finely divided iron had occurred. It is therefore possible that a small amount of finely divided iron on the surface of the graphite acts as the catalyst for the hydrogenation reaction.

From these studies it has been shown that reduction of the graphite ferric chloride compound with hydrogen allows retention of the layer structure of the compound and order with respect to the graphite lattice. The morphology of the graphite ferrous chloride, which is known to have no electronic interaction of the ferrous chloride with the conduction band (Hooley et al 1967, 1968, Novikov et al 1970) does not show any of the features associated with the true intercalation compounds. There is evidence that nitrogen, hydrogen and butadiene can diffuse into the graphite and react over ferrous chloride within the interplanar spaces.

6.4 Graphite Copper Sulphide

The electron diffraction results indicate that the graphite copper sulphide $CuS_{1.3}$, (Croft 1956c) has been reduced to graphite Cu_2S. There was no evidence of an orientation relationship between the graphite and Cu_2S, and the morphology of the compound indicated that regions of intercalate were present, typical of a high stage compound (section 4.1). The presence of folds suggest that some decomposition of the original compound has occurred in some areas. The particles which were within or on the surface of the graphite were a mixture of copper and sulphur. These elements could be present from the original preparation of the compound. The reaction of the graphite CuS with nitrogen and hydrogen to form H_2S and graphite Cu_2S is analogous to the reduction observed for the graphite ferric chloride.
[13]

7. GRAPHITE IRON: RESULTS

7.1 Electron Microscopy of Graphite Iron

The graphite iron, after preparation, had a layer of material coating the surface and was therefore cleaned by successive washings with THF, methanol and ethanol.

7.1.1 Morphology of Graphite Iron

The graphite iron compound was not homogeneous and, in addition to free graphite, two main types of area were observed; folded regions and regions of ring moiré patterns.

Examination of the compound in the electron microscope was difficult because many areas exfoliated abruptly as a result of the heating effect of the beam and produced areas containing many folds in an overlapping network throughout the graphite lattice (Plate 54). Particles 20-200 nm in diameter and a few bright discs were observed trapped within the folds.

The second type of area, which was stable in the electron beam, exhibited distorted or ring moiré patterns, and dot moirés. In addition, there was an unusual moiré pattern consisting of three straight parallel fringes with a spacing of ca. 20 nm (Plate 56). These fringes varied in length from 2μm to <0.1μm. Superimposed on these features was a ripple or bend contrast effect. The moiré patterns which were only visible on inspection of the photographic plate are typical of intercalated regions.

7.1.2 Effect of Solvents on Graphite Iron

The graphite iron was treated with a range of dilute and concentrated mineral acids, (HCl, H_2SO_4 and HNO_3), followed by a water wash. The effect of these treatments is shown in Plates 58 and 59.

Concentrated acid treatment produced large (40-700 nm diameter) mobile bright discs and a network of folds in the graphite

Plate 54

Graphite Iron after exfoliation in the electron beam

x 105000

Plate 55

Selected Area Diffraction Pattern from

exfoliated Graphite Iron

Plate 56

Area of Graphite Iron exhibiting distorted moiré patterns

x 131200

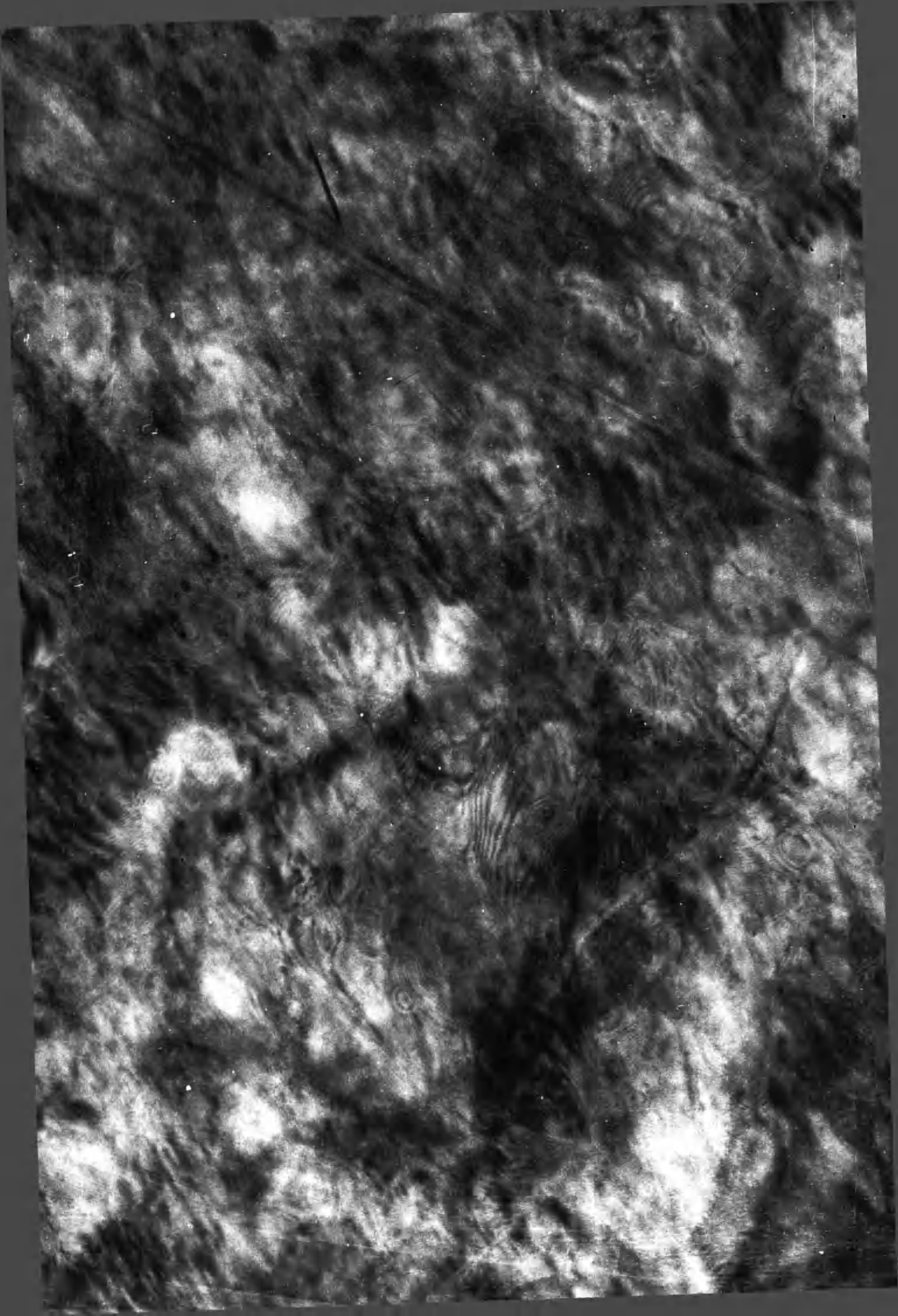

Plate 57

Selected Area Diffraction Pattern from

Graphite Iron exhibiting moiré patterns

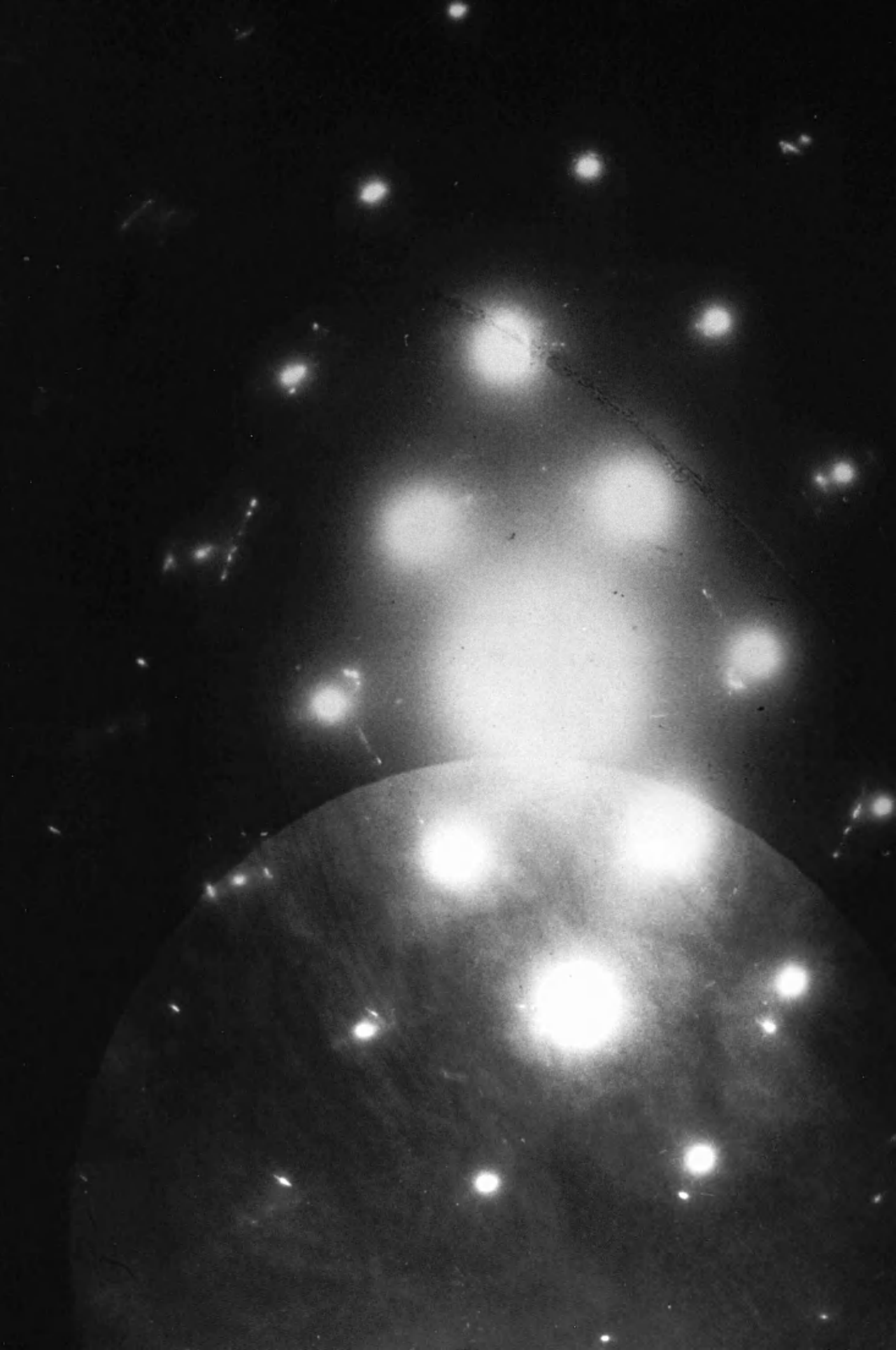

Plate 58

Graphite Iron after concentrated H_2SO_4 treatment

x 81900

lattice (Plate 58). Areas containing dense regular discs were also visible. These features are very similar to those reported for the graphite bisulphate compound (Carr 1965, 1970). No particles were observed after washing.

Dilute acid treatment followed by a water wash removed most of the extraneous material from the surface. Large mobile bright discs were observed in association with a network of folds in the graphite lattice (Plate 59). The large discs had a sharp inner edge surrounded by a diffuse darker outer zone. When the compound was dried at 353K the bright discs were no longer mobile.

7.1.3 Electron Diffraction of Graphite Iron

a) Areas exhibiting Interference Effects

The diffraction patterns associated with the areas which displayed distorted moiré patterns, were distorted from hexagonal symmetry (Plate 57). They were single crystal patterns with large variations in interplanar spacings, intensities of reflections and angular displacement. This distortion was also observed in the potassium graphite intercalated regions (Section 3.4.1.). The spacings found for graphite iron are listed in Table 15.

Some small arcs and diffuse reflections were also observed on a few patterns, but the pattern distortion produced uncertainties in the symmetry and value of the d-spacings derived from these reflections. The extra spacings listed have been approximately corrected for the distortion by multiplying by the ratio of the known d-spacing to the observed d-spacing for the associated graphite reflections. Extra reflections were also present which were probably double diffraction spots.

b) Folded Regions

Typical diffraction patterns from this type of area

Plate 59

Graphite Iron after dilute HCl treatment

x 89670

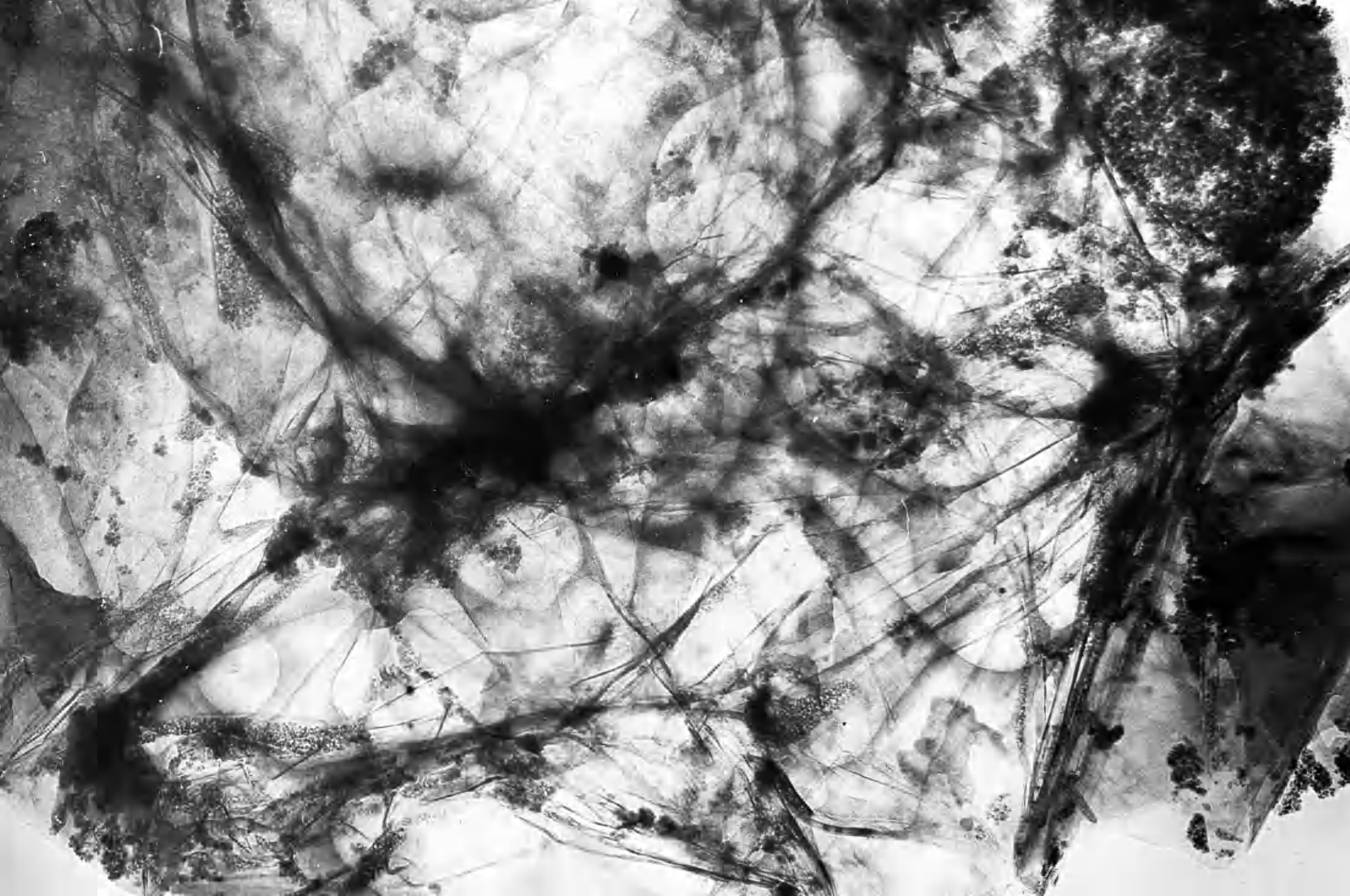

Plate 60

Selected Area Diffraction Pattern from

Graphite Iron after dilute acid wash

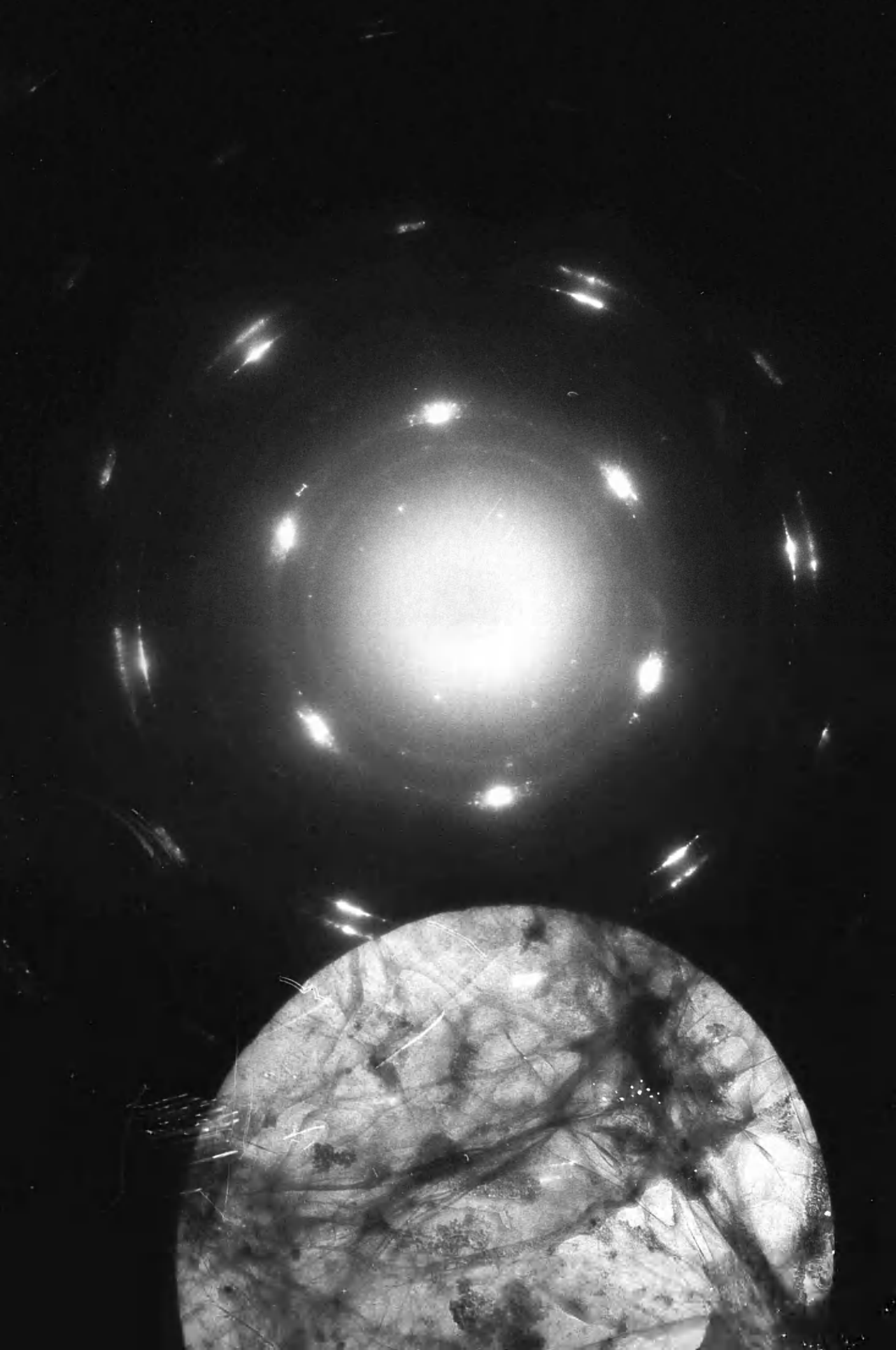

are shown in Plates 55 and 60. The graphite single crystal pattern has been replaced by a polycrystalline arc or ring pattern. The appearance of a ring pattern appeared to be associated with an increased number of folds in the lattice. The graphite $10\bar{1}1$ and $11\bar{2}2$ reflections were present and in the arc pattern the corresponding planes were parallel to the $\{10\bar{1}0\}$ and $\{11\bar{2}0\}$ graphite planes.

7.1.4 Electron Diffraction from Graphite Iron treated with acid.

The diffraction patterns from the graphite iron compound, treated with dilute and concentrated mineral acids, and washed with water, were similar to the folded regions of the graphite iron washed with THF, methanol, and ethanol. In addition to the polycrystalline pattern, graphite and polycrystalline material was present which was identified as $LiNO_3$ after the nitric acid wash, and LiCl after the hydrochloric acid wash (Table 16). Treatment with dilute or concentrated sulphuric acid removed LiCl and there was some evidence for the formation of $Fe_2O_3.H_2O$.

7.2 Powder X-ray Diffraction of Graphite Iron

Powder X-ray diffraction patterns of graphite iron were obtained before and after washing with THF, methanol and ethanol, and after nitric acid treatment to remove any surface iron. The spacings are listed in Table 17.

No high c-spacings were observed although a very broad diffuse halo was present at 0.4-0.48 nm. The main impurity observed in the unwashed graphite iron and the compound washed with organic solvents was LiCl. The nitric acid wash removed LiCl. Any αFe present would be masked by the graphite and LiCl reflections with the exception of the (200) αFe spacing. This spacing was not observed. The nitric acid treatment produced a series of spacings which were not identified

TABLE 15

Electron Diffraction of Graphite Iron

Intercalated		Exfoliated	
d_{nm}	Assignment	d_{nm}	Assignment
0.252-0.241	arc (corr)	0.295	LiCl
		0.277	
0.186-0.17	G $10\bar{1}0$	0.212	G $10\bar{1}0$
		0.202	G $10\bar{1}1$
0.132	arc (corr)	0.192	
		0.182	LiCl
0,115-0.111	G $11\bar{2}0$	0.123	G $11\bar{2}0$
		0.115	G $11\bar{2}2$
0.114	arc (corr)	0.105	G $20\bar{2}1$

TABLE 16

Electron Diffraction of Graphite Iron after washing in Concentrated Acid

HCl		HNO_3		H_2SO_4	
d_{nm}	Assignment	d_{nm}	Assignment	d_{nm}	Assignment
0,338	G 0001	0,342-0,335	G 0001	0.253	Fe_2O_3 H_2O
0.212	G $10\bar{1}0$	0.300		0.230	
0.206		0.253	$LiNO_3$	0.212	G $10\bar{1}0$
0.202	G$10\bar{1}0$/Fe	0.212	G $10\bar{1}0$	0.206	
0.190		0.202	G $10\bar{1}1$	0.202	G$10\bar{1}1$
0.182	LiCl	0.195	$LiNO_3$	0.195	Fe_2O_3 H_2O
0.123	G $11\bar{2}0$	0.176	$LiNO_3$	0.170	Fe_2O_3 H_2O
0.121		0.152	$LiNO_3$	0.159	
0.115	G $11\bar{2}2$	0.123	G $11\bar{2}0$	0.123	G $11\bar{2}0$
		0.115	G $11\bar{2}2$	0.116	G $11\bar{2}2$

TABLE 17

Graphite Iron: Powder X-ray Diffraction Results

Sample / Spacings	Graphite Fe Unwashed			Unground washed (THF. etc)			Graphite HNO_3 Wash		
	d_{nm}	Intensity	Assign ment	d_{nm}	Intensity	Assign ment	d_{nm}	Intensity	Assign ment
							0.459	s	
							0.418	m	
	0.335	vs(broad)	G	0.335	vs(broad)	G	0.335	vs(broad)	G
	0.334						0.310	w	
	0.295	s	LiC1	0.295	s	LiC1		w	
	0.277	w					0.282	s	
	0.267	w							
	0.256	s	LiC1	0.256	s	LiC1			
					vw		0.236	m(broad)	
				0.228	vw		0.233	m(broad)	
	0.212	m	G	0.212	m	G	0.212	s	G
	0.202	s	G/αFe	0.202	s	G/αFe	0.208	w	
							0.202	s	G/αFe
	0.181	m	LiC1/G	0.181	m	LiC1/G			
	0.168	s	G	0.167	s	G	0.167	vs	G
	0.154	m	LiC1/G	0.155	m	LiC1/G			
	0.148	2	LiC1	0.148	vw	LiC1			
	0.123	s	G	0.124	s	G_1	0.124	s	G
	0.117	w	LiC1/αFe	0.116	w	LiC1/αFe	0.117	m	LiC1/αFe
	0.115	m	G/LiC1	0.114	w	G/LiC1	0.112	w	G
	0.109	w		0.112	w	G			
	0.104	w	G	0.105	m	G	0.099	w	G
	0.099	m	G						

G = Graphite m = medium s = strong
vs = very strong w = weak

unambiguously. They could be assigned to biphenyl or to $Fe(NO_3)_3 9H_2O$.

The graphite 0002 line was very broad indicating the formation of small graphite crystallites. However, line broadening from powder diffraction lines is not a reliable estimate of crystallite size (Carr 1970). The only unassigned spacings in the unwashed graphite iron and the product washed with organic solvents were 0.277, 0.267 and 0.228nm. It is possible that these could correspond to 0004 reflections related to 0.55, 0.54 and 0.456 nm spacings corresponding to 0002 reflections similar to those reported by Novikov and Vol'pin (1971, 1975) (Table 18). The d-spacings of possible products are listed in Table 18 for comparison. No direct comparison of a stage I graphite ferric chloride compound reduced with lithium biphenyl is available.

7.3 HVEM of Graphite Iron

The graphite iron was examined using an AEI EM7 1 MeV electron microscope. The main features observed were folds in the graphite and a number of particles of material 20-600 nm in diameter. (Plate 61). No bright discs were observed. Stereomicroscopy at $\pm\frac{1}{2}^{o}$ or at $\pm 1^{o}$ showed that the folds and particles were dispersed throughout the graphite lattice. In addition, some material was observed which was in the form of narrow bands 50 nm wide with straight parallel sides extending for several hundred nm. In some cases, these exhibited extinction bands across the narrow dimension.

7.4 Optical Examination of Graphite Iron

The graphite iron flakes were examined in a Wild optical microscope. The maximum expansion of the graphite flake was observed at the edge of the flake (Plate 62). This expanded area was 15μm above the central part of the graphite flake.

TABLE 18

X-ray Data: Possible Products

LiCl		Gr $FeCl_3$ Stage II reduced by Lithium Biphenyl (Novikov et al 1971)		Gr $FeCl_2$ Stage I reduced by Lithium Biphenyl (Novikov et al 1971)		Gr HSO_4^- Residue Compound (Carr 1970)		Gr Fe Stage I (Novikov et al 1975)	
d_{nm}	Assignment	d_{nm}	Assignment	d_{nm}	Assignment	d_{nm}	Assignment	d_{nm}	Assignment
0.297	111	0.958	001	0.958	001			I_c =	0.58
0.257	200	0.466	002	0.466	002				
0.182	220	0.337	G	0.424					
0.155	311	0.298	LiCl	0.384		0.3352	G0002		
0.148	222	0.283		0.337	G				
0.128	400	0.253	LiCl	0.317	003	0.2123	$G10\bar{1}0$		
0.118	331	0.203	G αFe	0.298		0.2031	$G10\bar{1}0$		
0.115	420			0.283		0.1677	G0004		
0.105	422	0.123	G	0.256	LiCl				
0.099	511			0.203	G αFe				
01091	440			0.181	LiCl				
				0.155	LiCl				
				0.148	LiCl				
				0.128	LiCl				
				0.123	G				
				0.118	LiCl				
				0.115	LiCl				
				0.105	009				

Plate 61

Graphite Iron examined at 1 MeV

Exfoliated region containing particles and folds

x 76680

Plate 62

Optical Micrograph of Graphite Iron Flake

x 99

7.5 Chemical Composition

7.5.1 Thiocyanate Method

Graphite iron samples were analysed colorometrically as described in Section 2.3.6 and the results are listed in Table 19 (a). The iron content of the graphite iron determined by this method was found to be 10% of that calculated for a stage I compound. Treatment with concentrated acid removed some of the iron from the compound.

7.5.2 Gravimetric Method

The graphite iron was analysed by ashing as described in Section 2.3.6. The results, listed in Table 19 (b), show that the compound contained an amount of iron which was higher than that estimated by the solution method but lower than that calculated for a stage I compound (30.5% Cowley and Ibers 1956). The effect of the acid wash was to remove iron from the compound.

As the compound contained LiCl, THF and probably some biphenyl in addition to iron, an attempt was made to correct for the effect of these in the results. In addition to the iron oxide, a white powder was present after ashing the compound. This material was separated and weighed. In addition, the total amount of material evolved from the sample on heating was estimated to be 25% of the initial weight of the graphite iron, (see section 7.6.4). The results, corrected for the white powder and volatile material, indicate that either the compound is dilute or that some of the iron has been volatilised during the gravimetric determination.

7.6 Effect of Heat on Graphite Iron

7.6.1 Optical Examination

Heating the graphite iron caused violent expansion of the graphite flake (Plate 63). The compound increased in size and its appearance was characteristic of exfoliated graphite.

TABLE 19

Chemical Analysis of Graphite Iron

(a) Thiocyanate Method

Sample	% Fe
Graphite Iron THF ETOH MeOH washed	4.3
Graphite Iron washed with dil. HCl	3.8
Graphite Iron washed with Conc HCl	2.2

(b) Gravimetric Method

Sample	%Fe	Corrected results %Fe
Graphite Iron THF, ETOH, MeOH wash	14.8	20.1
Graphite Iron washed with dil. HCl	10.6	14.6
Graphite Iron washed with dil. HNO_3	9.8	13.7

Plate 63

Optical Micrograph of Graphite Iron heated

above 383K

x 660

7.6.2 Transmission Electron Microscopy

The graphite iron, after heating to 653K, exhibited folds in the graphite lattice. In addition, many particles, 20-200 nm in diameter, were also present (Plate 64). It was not possible to determine at this stage if the particles were within or on the surface of the graphite.

Some graphite iron was also heated in situ in the electron microscope. Agglomeration of particles in areas where no particulate material had been visible was observed, particularly in the range 573-673K. Above this temperature, the particles did not appear to increase in size but some in situ particle catalysed oxidation of graphite was observed above 873K in oxygen (Plate 66). The oxidation channels overlapped indicating that the iron particles were within the graphite lattice.

7.6.3 Electron diffraction of heated graphite iron

A typical electron diffraction pattern is shown in Plate 65. The pattern consists of a polycrystalline graphite pattern with extra reflections at 0.335, 0.204 and 0.114 nm similar to that observed from regions of exfoliated graphite. There is evidence of a cubic arc pattern at 0.204 nm superimposed on the graphite pattern and extra reflections are present at 0.206, 0.179 and 0.153 nm.

7.6.4 Gaseous Products

Graphite iron washed with THF, methanol, and ethanol was heated to 653K in RV4 using System II (Section 2.2.1). The products were collected and identified by gas infra-red analysis. At 383K, THF was evolved from the compound. Rapid evolution of THF occurred above 550K accompanied by the production of methane. The average weight loss after heating to 473K was 6% and at 653K was 26%.

Plate 64

Graphite Iron after heating to 653K

exhibiting particles and folds

x 968000

Plate 65

Selected Area Diffraction Pattern from

Graphite Iron after heating to 653K

Plate 66

Graphite Iron after in situ reaction

with O_2 for 48 minutes at 923K

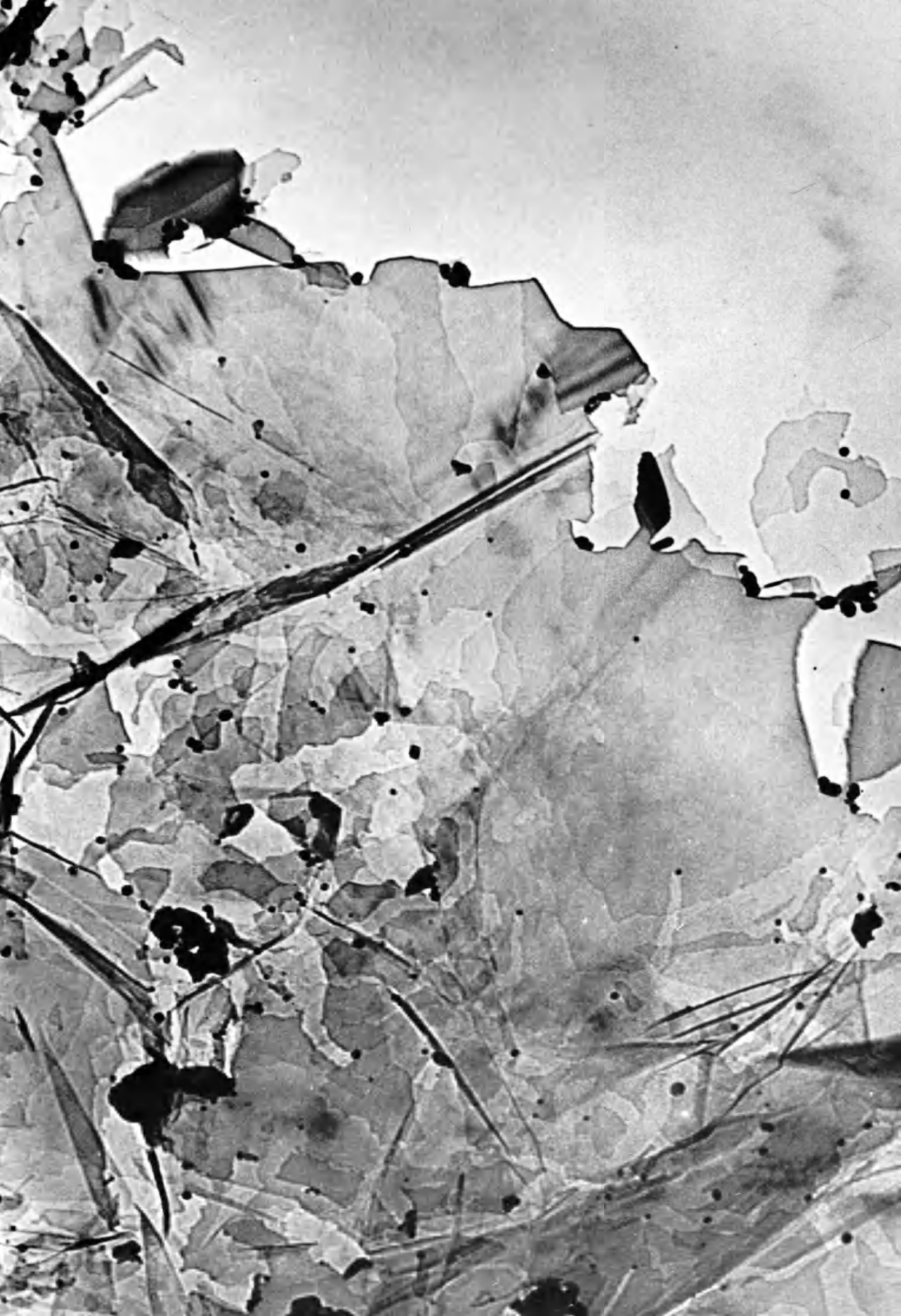

7.7 Reaction of Graphite Iron with Butadiene and Hydrogen

7.7.1 Variation in Graphite Iron Morphology with Reaction Temperature.

The graphite iron compound was cleaned with organic solvents and reacted with a 33% butadiene/hydrogen gas mixture at temperatures in the range 273 to 693K (Table 5). Product analysis (see Section 8.1) showed that the main reaction occurred in the temperature range 623-693K.

a) Morphology after reaction at 373K

A typical area of graphite iron after reaction at 373K is shown in Plate 67. The material had a very grainy appearance which could arise from the presence of many low contrast small bright discs. The graphite also contained a few very small (2-5 nm thick) folds. Electron opaque material exhibiting fresnel fringes on one edge was also observed. At this temperature the compound retains THF although some exfoliated areas were also found similar to that in plate 54. These areas contained many folds with a few large bright discs in addition to some particles (ca 100 nm diameter).

b) Morphology after reaction at 553K.

After reaction at 553K, not all the graphite iron had exfoliated, and some intercalated areas were observed (Plate 68) which exhibited distorted moiré fringes. Areas containing parallel sided, overlapping bands of material were also evident. The focus condition for these features indicated that they extended outwards in the graphite c-direction. Particulate material was also observed.

c) Morphology after reaction at 623K

After reaction at 623K, the graphite iron intercalation compound was completely decomposed. The main morphology observed was that of exfoliated graphite with large scale agglommeration of

Plate 67

Graphite Iron after reaction with Butadiene

and Hydrogen at 373K

x 121600

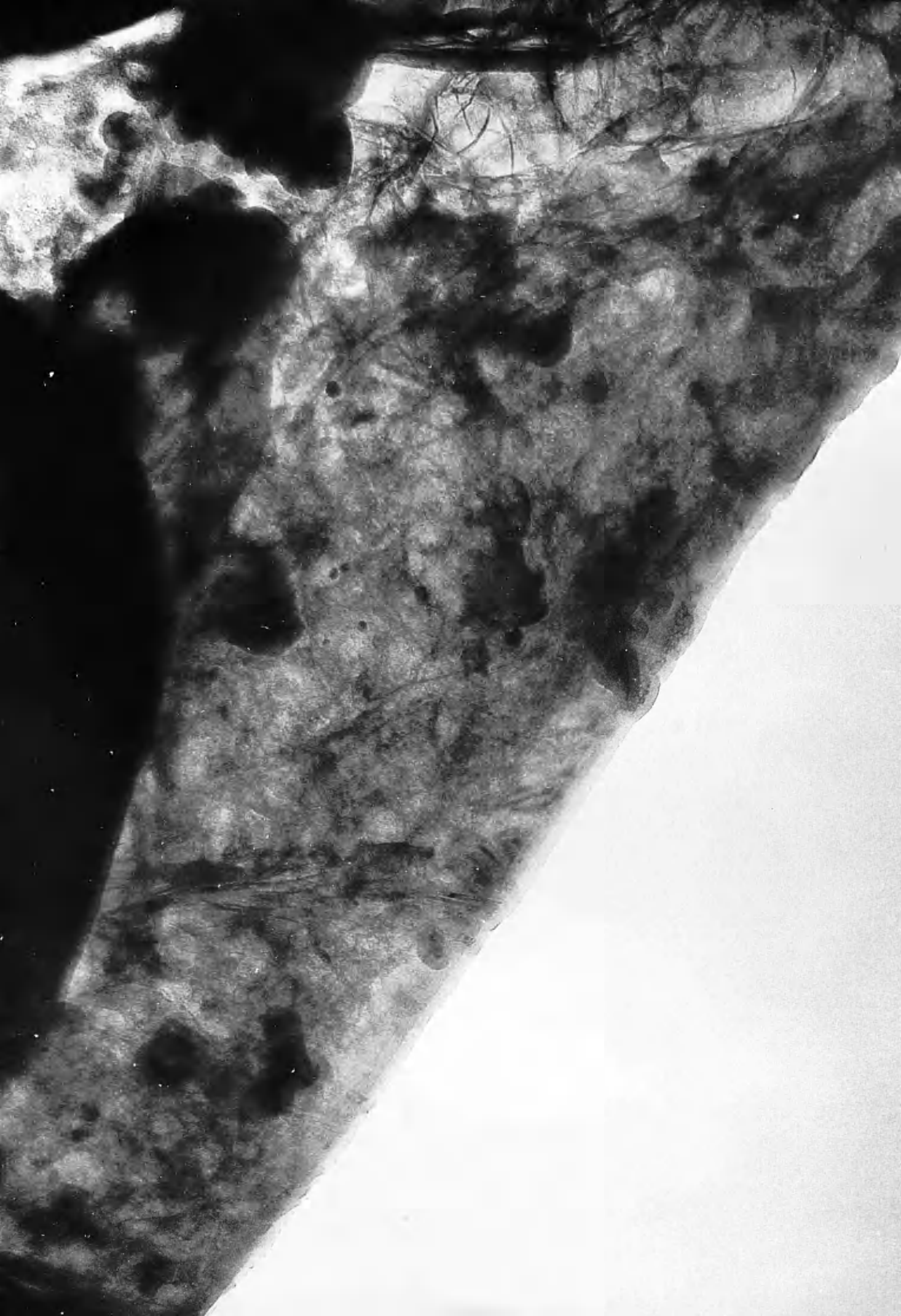

Plate 68

Graphite Iron after reaction with Butadiene

and Hydrogen at 553K

x 77000

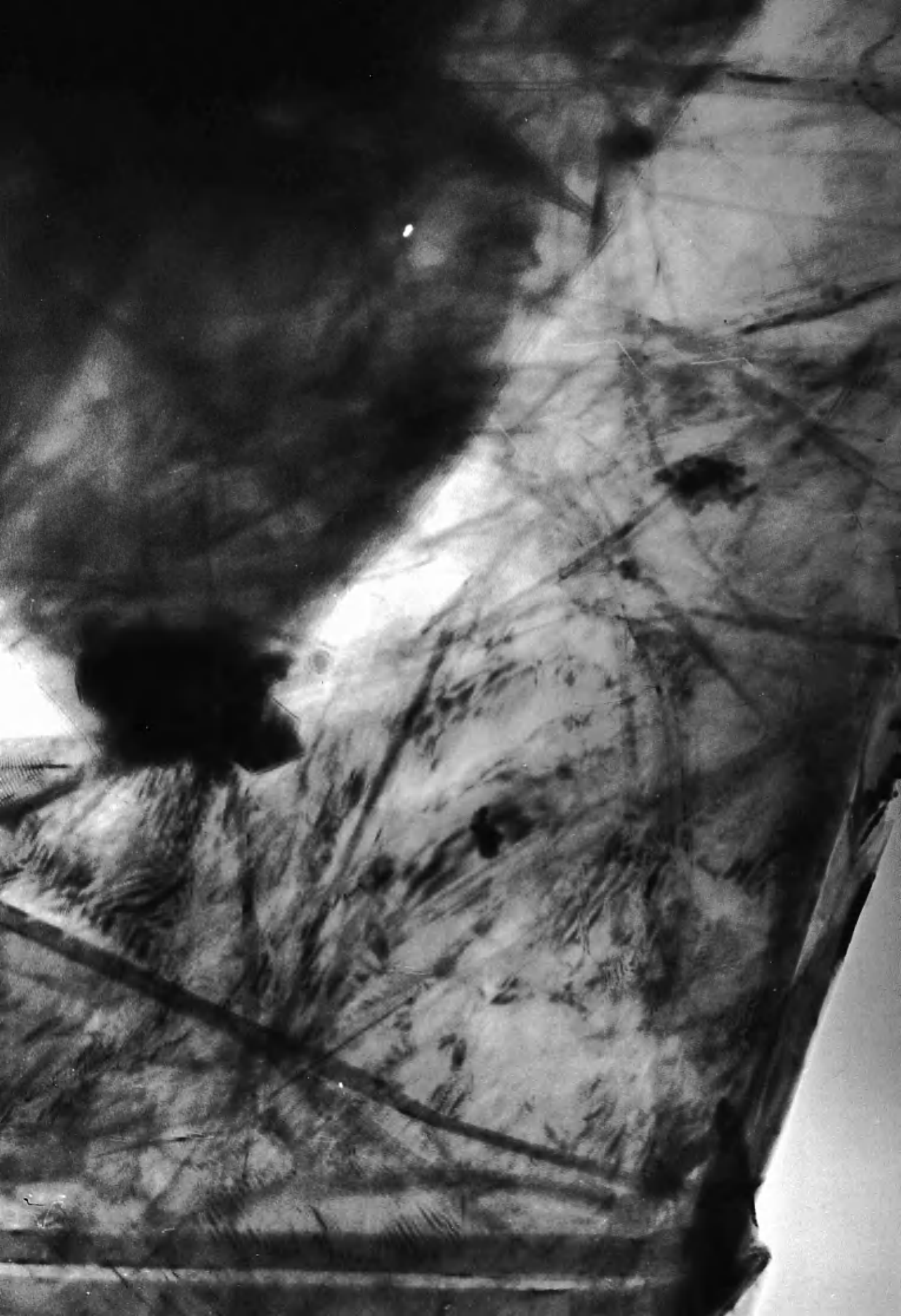

Plate 69

Selected Area Diffraction from Graphite

Iron after reaction with Butadiene and Hydrogen at 553K

particles within the graphite, on the surface, and at the edges of the graphite flakes (Plates 70, 71, 73). The particles were 20-200 nm in diameter and tended to be in clusters near folds in the lattice.

A solid reaction product was also observed, which had three different growth sites. This deposit appeared to have grown as amorphous 50-100 nm in diameter, whiskers either from a particle which remained on the graphite surface, (Type A, Plate 70), or from the graphite with a particle either enclosed or exposed at the tip of the growth, (Type B, Plate 71). Small loops of deposit were also observed growing on the graphite surface, (Type C, Plate 73), not associated with particles or folds in the lattice. Type B growth was the most common form observed.

In all cases, the folds present in the lattice were of two types; random kinked folds forming a network through the graphite and folds which either contained some electron dense material or exhibited extinction bands.

d) Morphology after reaction above 623K.

The morphology of the graphite iron after reaction at 643-693K was very similar to that observed after reaction at 623K. Types A, B and C growths are again observed. At 643K (Plate 74) small particles, which appeared to be less electron dense, but approximately the same size as the electron dense particles, were observed.

The type C deposit on the graphite surface was less common with increasing temperature, but at 663K, these growths were observed along the edge of a graphite flake, (Plate 75), forming a convoluted, wavy structure. This structure was very similar to the polymeric material observed after reaction of graphite ferrous chloride with butadiene and hydrogen under similar conditions (section 5.5.3).

7.7.2 Graphite Iron Morphology after Reaction with Butadiene.

The main difference in morphology of the graphite iron

Plate 70

Graphite Iron after reaction with Butadiene

and Hydrogen at 623K

showing Type A whisker growth and particles in the graphite

x 96000

Plate 71

Graphite Iron after reaction with Butadiene

and Hydrogen at 623K

showing the main type B whisker growth

x 72000

Plate 72

Selected Area Diffraction Pattern from

Graphite Iron after reaction with Butadiene

and Hydrogen at 623K (Type B)

Plate 73

Graphite Iron after reaction with Butadiene

and Hydrogen at 623K

showing Type C loop deposit

x 100000

Plate 74

Graphite Iron after reaction with Butadiene

and Hydrogen at 643K

with small thin particles

x 90800

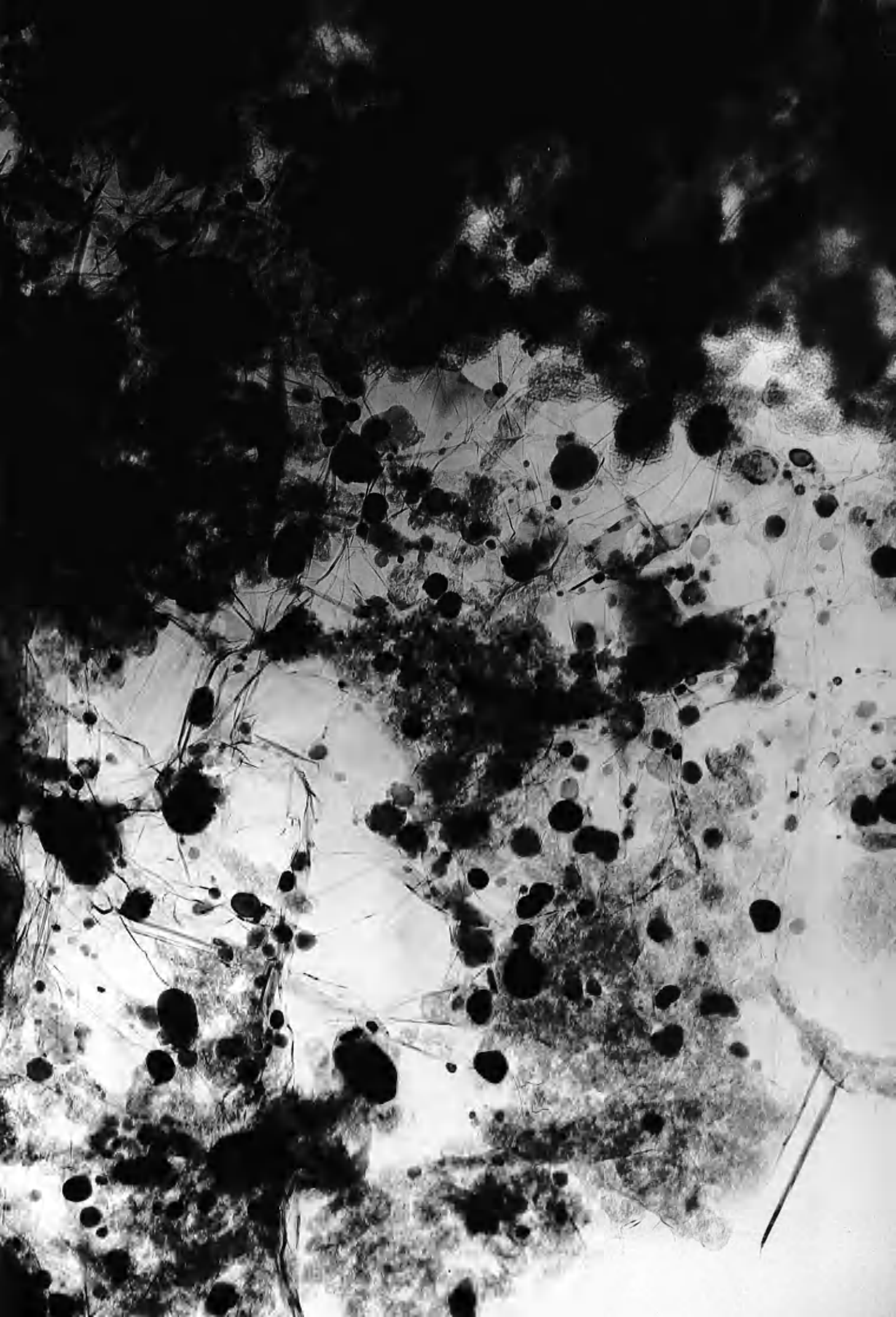

Plate 75

Graphite Iron after reaction with Butadiene

and Hydrogen at 663K

showing polymeric type material

x 194000

after reaction with butadiene alone at 623K, was that type B growth was less common. Mainly type A whisker growth, characterised by the particle remaining on the graphite surface, (Plate 76), and type C were observed.

The type C growth on the surface of the graphite appeared to be more common after reaction with butadiene alone. This material was in the form of angular loops 10-20 nm in diameter (Plate 78). As before, (section 7.7.1), the deposits were remote from the particles or folds in the graphite. The variation in focus condition for these growths indicated that either the surface of the graphite was very uneven or that some of the growths were within the lattice.

7.7.3 Graphite iron morphology after HNO_3 wash and reaction at 663K.

After reaction, it was observed that the graphite contained many electron dense particles on the surface or edges of the graphite flake (Plate 79), although no particulate material was observed before reaction. It is interesting to note that the solid reaction product deposit was in the form of a layer of material coating the particles. In some cases this covered only half the particle indicating that the particle was partly exposed on the surface of the graphite.

7.7.4 HVEM of Graphite Iron after reaction.

Examination of the graphite iron after reaction with butadiene and hydrogen at 673K by stereomicroscopy showed that a large number of particles and folds were present on the surface and distributed within the graphite (Plate 81). Electron diffraction (Plate 82) showed that some of the particles present were lithium chloride. Many diffuse reflections were also present which could

Plate 76

Graphite Iron after reaction with Butadiene alone at 623K showing Type A whisker growth

x 928000

Plate 77

Selected Area Diffraction Pattern from

Graphite Iron after reaction with Butadiene

alone at 623K (Type A)

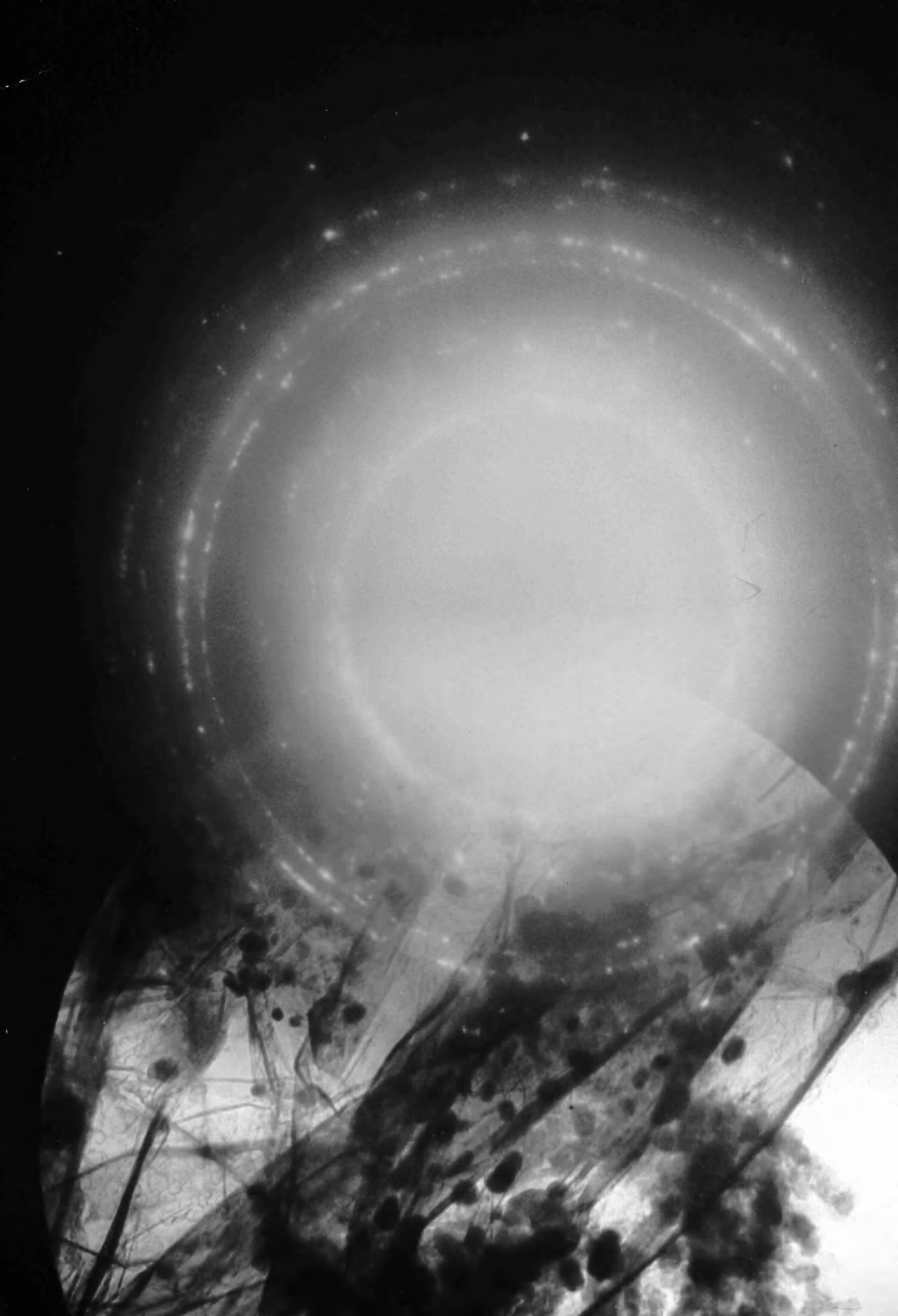

Plate 78

Graphite Iron after reaction with Butadiene

alone at 623K showing small loop deposit (Type C)

x 90000

Plate 79

Graphite Iron after HNO_3 wash

and reaction at 663K with Butadiene and Hydrogen

x 138600

Plate 80

Selected Area Diffraction Pattern from

Graphite Iron after HNO_3 wash

and reaction at 663K with Butadiene and Hydrogen

Plate 81

Graphite Iron after reaction with Butadiene

and Hydrogen at 673K examined at 1 MeV

x 73620

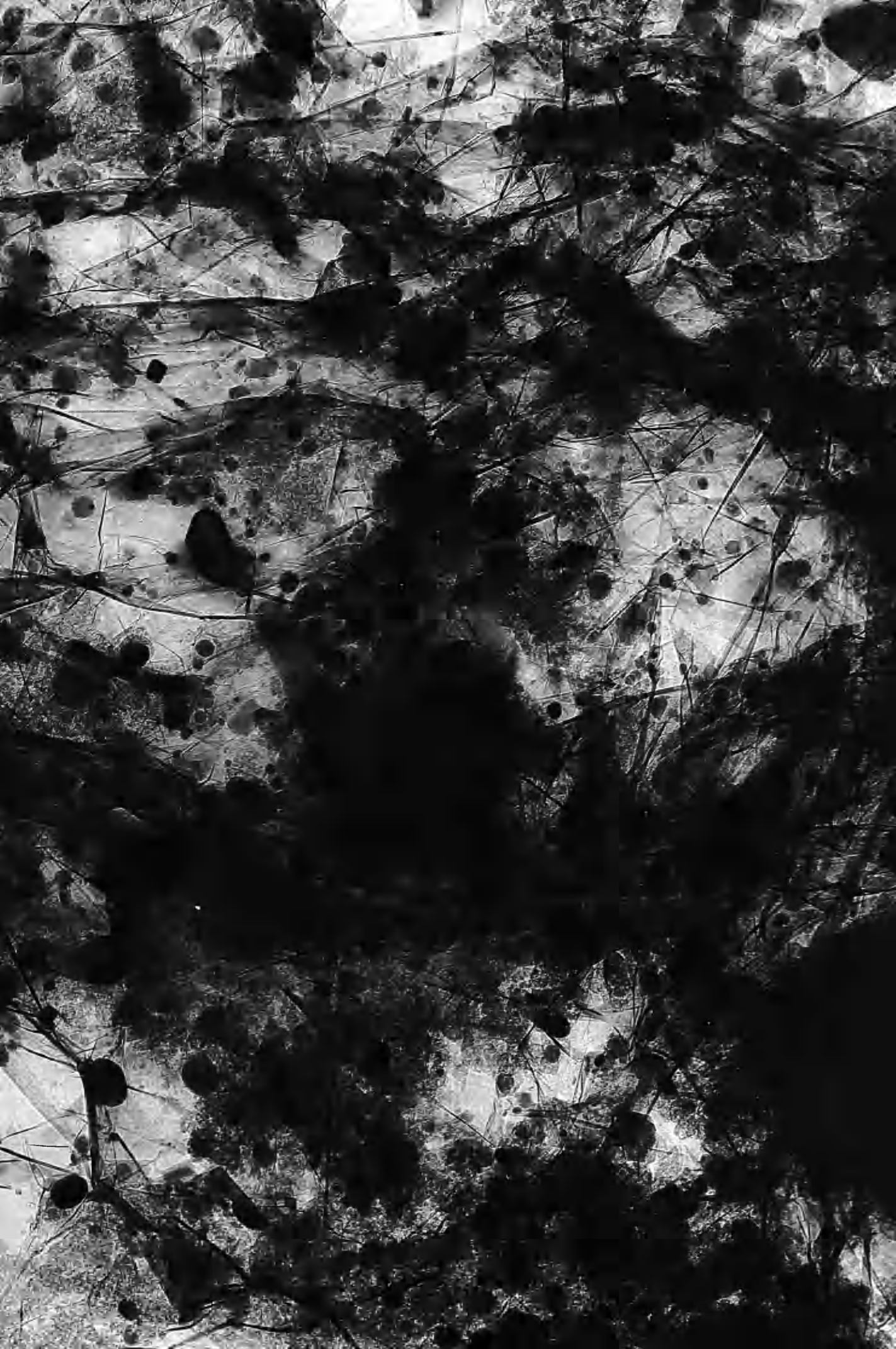

Plate 82

1 MeV Diffraction Pattern from Graphite Iron after reaction with Butadiene and Hydrogen at 673K

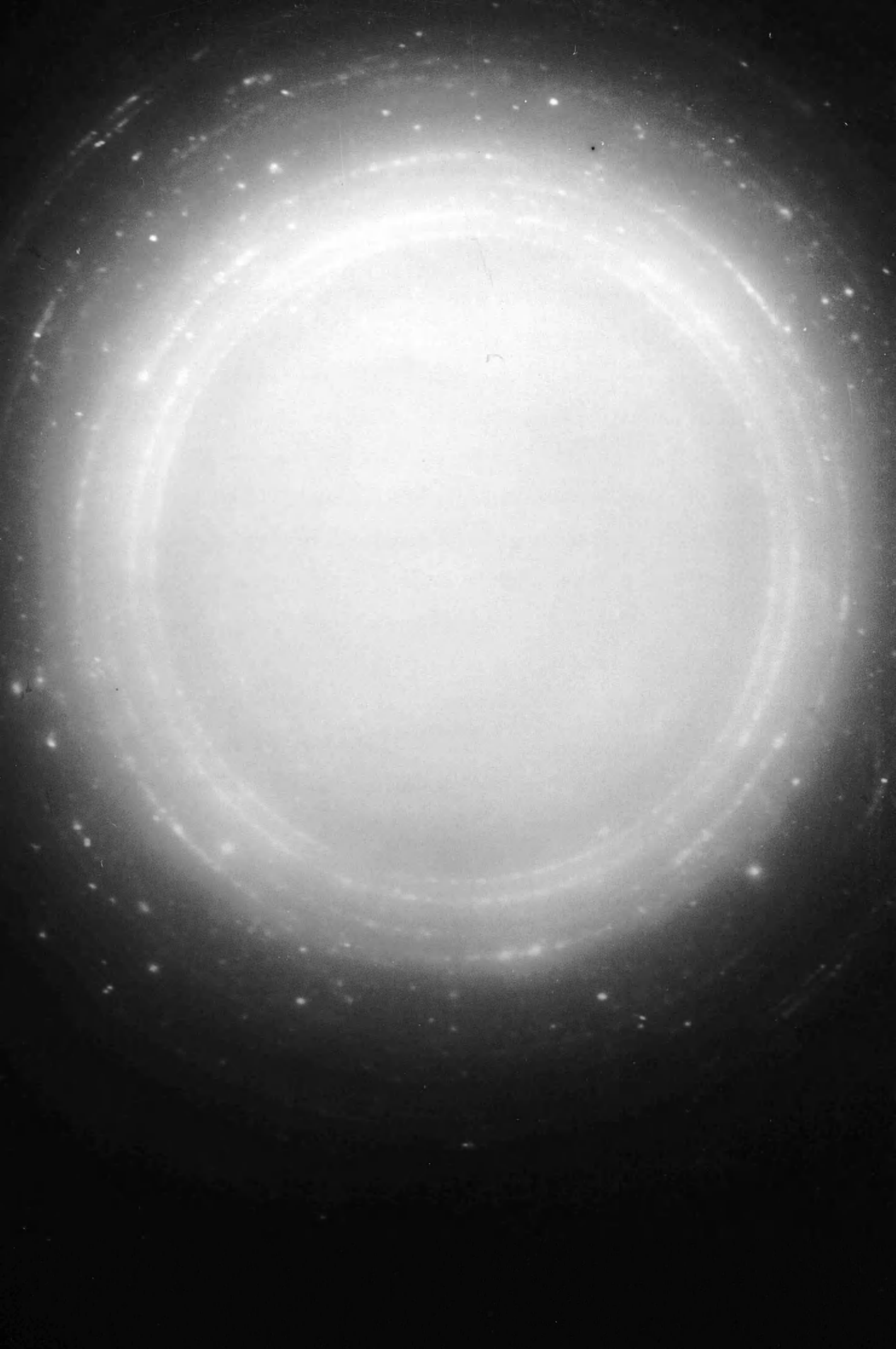

not be identified. However, a dark field micrograph, Plate 83, derived from the reflections in the range 0.213-0.203 nm showed that the particles associated with the solid reaction product and distributed through the graphite were contributing to these reflections.

7.8 Electron diffraction of Graphite Iron after Reaction

Two main types of electron diffraction patterns were found after reaction corresponding to regions exhibiting interference effects and exfoliated graphite (section 7.7.1).

The intercalated regions, which displayed distorted moiré fringes, present after reaction at temperatures up to 573K, had a distorted single crystal graphite pattern similar to that observed before reaction (Section 7.1.3, Plate 69). Some extra reflections were present which could be attributed to double diffraction effects, but no regular superlattice reflections were observed. The spacings observed are listed in table 20.

The exfoliated graphite regions, characterised by folds in the lattice, produced a graphite diffraction pattern identical to that observed before reaction consisting of arcs or rings and including the 0001, $10\bar{1}1$, and $11\bar{2}2$ reflections. The 0001 reflection was more common with increasing temperature. LiCl reflections were also present, usually as weak polycrystalline reflections. Areas containing particles and deposited material had a superimposed zone of diffuse scattered reflections in the range 0.21 to 0.14 nm. (Plates 72, 77 and 84). Table 20 lists the spacings observed after reaction at a range of temperatures for the graphite iron and deposited material.

7.8.1 Variation with Reaction Temperature

At temperatures <573K, some of the material giving rise to the extra polycrystalline rings (Table 20) was identified as LiCl. The presence of αFe particles was difficult to detect as a result

TABLE 20

Electron Diffraction Results: Graphite Iron after Reaction

Reaction Gas	Butadiene/Hydrogen														Butadiene	
Reaction Temperature	Intercalated Areas 573K		373K		573K		623K		643K		663K		693K		Gr Fe HNO_3 washed 668K		Deposit		623K	
	d_{nm}	Assignment	d_{nm}	Assignment	d_{nm}	Assignment	d_{nm}	Assignment	d_{nm}	Assignment	d_{nm}	Assignment	d_{nm}	Assignment	d_{nm}	Assignment	d_{nm}	Assignment	d_{nm}	Assignment
			0.343	G	0.346	G	0.337	G			0.345	G	0.343	G	0.258		0.345		0.343	G
			0.294Px	LiCl	0.304						0.337	G			0.251	Fe_3C				
	0.206		0.256Px	LiCl	0.292	LiCl							0.256	LiCl					0.286	
	0.158	G1010			0.255	LiCl	0.254	LiCl						Fe_3O_4						
			0.213	G	0.212	G	0.210	G	0.210	G	0.211	G	0.211	G	0.213	G	0.210		0.210	G
							0.206		0.207	Fe_3O_4/FeC_3	0.206		0.208	Fe_3O_4	0.203	Fe_3C	0.203		0.201	G
	0.127	G	0.203	G	0.202	G	0.195				0.202	G	0.204	G	0.189	Fe_3C				
		1120	0.181Px	LiCl			0.183	LiCl					0.181	LiCl					0.183	Fe_3C
	0.103						0.162		0.162	Fe_3O_4/FeC_3					0.154	Fe_3C			0.173	Fe_3C
			0.151Px	LiCl					0.153	Fe_3C			0.161	Fe_3O_4/FeC_3					0.162	Fe_3C
			0.147Px	LiCl			0.123	G	0.123	G	0.123	G	0.154	Fe_3C						
							0.114	G	0.116	G	0.115	G	0.123	G	0.124	G	0.123		0.123	G
			0.123	G	0.123	G	0.105	G	0.107				0.116	G	0.119		0.116		0.116	G
			0.115	G	0.116	G									0.101					

G = Graphite
Px = polycrystalline pattern

Plate 83

Dark Field of Graphite Iron after reaction with Butadiene and Hydrogen at 673K using ring reflections at 0.213 - 0.203 nm

x 11664

Plate 84

Selected Area Diffraction Pattern from

Graphite Area containing particles and deposited material

formed on Graphite Iron after reaction with Butadiene

and Hydrogen at 663K

of interference with the graphite ($10\bar{1}1$) spacing and the αFe (110) spacing. No αFe 200 reflections were observed.

Above 573K, diffraction spacings were found which could not be explained as LiCl but could be assigned to Fe_3C or Fe_3O_4. The spacings observed after reaction in the range 623-693K were very similar (Table 20).

7.8.2 Deposited Material

The type A,B and C deposited material and the polymeric material, (Plate 75) were all associated with either particles or the graphite matrix or both. Electron diffraction of these materials was therefore usually complicated by the background matrix pattern. Plate 85 is the diffraction pattern from some type A whisker growth which had become detached from the matrix. This showed faint diffuse rings with spacings of 0.34, 0.21 and 0.123 nm corresponding to an amorphous carbon pattern.

No diffraction pattern was obtained from the looped material deposited on the graphite surface or the polymeric material.

Diffraction patterns from whisker growth with particles at the tip (Type B) shown in Plates 72&84 had extra reflections which were associated with the 0.21 nm carbon ring and could be assigned to αFe or Fe_3C.

7.8.3 Graphite iron washed with HNO_3 after reaction

Selected area electron diffraction of areas of the compound containing particles after reaction produced a polycrystalline pattern similar to that observed for the exfoliated graphite. In Plate 80, there is some streaking in the pattern, indicating that the crystallites are thin. The extra spacings observed could be assigned to a carbide, Fe_3C (Table 20).

Plate 85

Selected Area Diffraction Pattern from

Type A whisker growth

7.9 X-ray Diffraction of Graphite Iron after Reaction

Powder X-ray diffraction studies were carried out on graphite iron and graphite iron washed with HNO_3, after reaction with butadiene and hydrogen. The results are listed in table 21 and are compared with graphite iron after reaction and treatment with boiling HCl.

The results show that LiCl persisted throughout the reaction and subsequent treatment. The extra spacings observed in graphite iron after reaction could be attributed to αFe and Fe_3O_4. As the reaction was carried out under reducing conditions the oxide must have been formed in air after removal of the compound from the reaction system. It is also possible that there may be a contribution from Fe_3C.

The results from the graphite iron compound washed with HNO_3 prior to reaction show that αFe and LiCl are present after reaction. The αFe and LiCl spacings were weak, indicating that only a small amount of these phases were present probably as a result of removal of most of this material by acid treatment. The remaining spacings could not be identified.

Treatment with HCl resulted in loss of αFe spacings from the diffraction pattern.

The graphite reflections were broad in every case, indicating the formation of small graphite crystallites.

7.10 Analysis of Graphite Iron after Reaction

Samples of graphite iron reacted at a maximum temperature of 673K were analysed by the thiocyanate method. The results are listed in table 22. The graphite iron after reaction had a range of iron content within the limits shown. These values for the graphite iron are close to the calculated iron content for a first stage compound

TABLE 21

Powder X-ray Diffraction Results: Graphite Iron After Reaction

Graphite Iron After reaction at 693K			Graphite Iron washed with HNO_3 after reaction at 673K			Graphite iron after reaction at 693K washed with HCl		
d_{nm}	Intensity	Assign ment	d_{nm}	Intensity	Assign ment	d_{nm}	Intensity	Assign ment
0.340-0.333	vs(broad)	G	0.340-0.332	vs	G	0.3352	vs	G
						0.3300	s	
0.3106	w		0.3071	vw		0.3272	vs	FeOOH
0.2964	s	LiCl/Fe_3O_4	0.3036	vw		0.3017	vw	
0.2830	w							
0.2720	w							
0.2560	s	LiCl	0.2561	w	LiCl	0.2565	w	LiCl/FeOOH
0.2518	vw	Fe_3C/Fe_3O_4	0.2482	vw				
0.2429	w	Fe_3O_4	0.2416	w	Fe_3O_4			
0.2218	w		0.2271	m				
0.2120	s	G	0.2120	m	G	0.2122	m	G
0.2025	s	G/αFe	0.2080	m		0.2085	w	
0.1830	s	LiCl	0.2024	m	G/αFe	0.2023	s	G
0.1675	s	G	0.1901	w		0.1832	m	LiCl
0.1545	m	G/LiCl	0.1862	w		0.1671	s	G
0.1480	m	LiCl/Fe_3O_4	0.1812	w	LiCl	0.1631	w	
0.1438	w	αFe	0.1672	s	G	0.1550	w	LiCl
0.1291	vw	Fe_3O_4	0.1540	w	LiCl			
0.1237	m	G	0.1483	w	LiCl			
0.1184	w	LiCl	0.1432	vw	αFe			
0.1161	w	αFe	0.1237	m	G	0.1235	m	G
0.1153	w(broad)	G/LiCl	0.1163	w	αFe	0.1162	m	G
0.1127	w	G	0.1153	m	G/LiCl	0.1153	m	G
0.1053	m	G	0.1124	w	G	0.1127	w	G
0.0996	w	G	0.0995	w	G	0.0993	w	G

vs = very strong s = strong w = weak vw = very weak G = Graphite

Table 22

Analysis of Graphite Iron After Reaction

Sample	% Fe
Graphite Iron after reaction	24.2 - 30.8%
Graphite iron washed with dilute HCl then reacted	14 - 17.8%
Graphite Iron HNO_3 after reaction	9.7% - 13%

(Cowley and Ibers 1956).

The iron content of the compound washed with acid was lower than that found for the compound washed with organic solvents.

Comparison of these results with those found before reaction (Table 19(a), section 7.5.1) indicates that the iron is now in a form which is readily dissolved in acid and can therefore be detected by this method.

8. REACTION OF GRAPHITE IRON WITH BUTADIENE AND HYDROGEN: RESULTS

The activity of the graphite iron compound for the hydrogenation of butadiene was examined over the temperature range 313 - 673K. 0.15 g of the graphite iron compound was allowed to react in a static system with a 33% butadiene/hydrogen gas mixture at a total pressure of 750 torr (measured at room temperature) for 22 hours (Section 2.4.6, Table 5). Figure 15 shows the distribution of the products in the gas mixture after reaction. The percentages of product have been corrected for any THF contribution.

8.1 Product Distribution

The activity of the graphite iron was temperature dependent and can be broadly classified into three temperature regimes. Negligible activity for any reaction was observed in the range 313 - 373K. From 373 - 573K, a maximum of 20% conversion of butadiene to a mixture, shown by gas chromatography to consist of but-1-ene and cis and trans but-2-ene, occurred. Minor amounts of propane, ethane, and butane, were also present. It is interesting to note that the onset of this reaction coincided with the change in catalyst morphology as a result of exfoliation on evolution of THF (section 7.6).

The major reaction occurred in the range 573 - 673K with decomposition of butadiene to methane. Butene was present up to 593K and trace amounts of butane were produced at all temperatures. Bright field transmission electron microscopy of the catalyst showed that the decomposition of butadiene was accompanied by large scale carbon deposition (section 7.7).

8.2 Comparison of Other Heterogeneous Systems with Graphite Iron

The reactions observed on the graphite iron compound could have been the result of catalytic action by the compound,

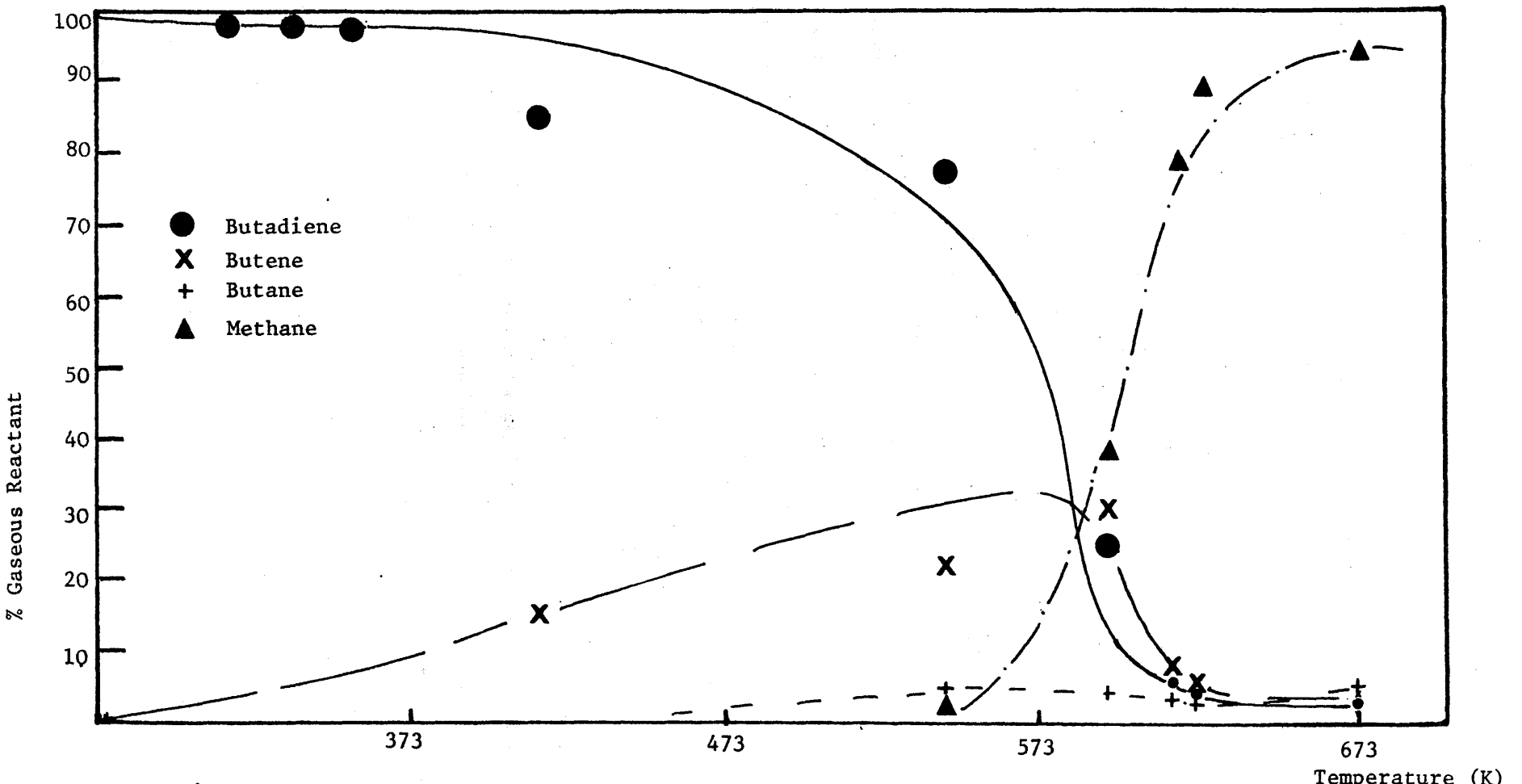

Figure 15. Reaction of Butadiene and Hydrogen over Graphite Iron.

by the graphite surface, by iron particles, or even by the expanded graphite layers. Therefore, a similar set of test conditions were set up for graphite, graphite bisulphate intercalation compound, iron powder and graphite iron washed with nitric acid, to remove any surface iron, to try to establish which properties of the graphite iron were responsible for the behaviour observed. The reaction of butadiene, and the butane, methane and ethane production for each system are shown in Figures 16 - 19.

8.2.1. Iron Powder

The iron powder used in this reaction had an average particle diameter of 1μm compared to the 20-200 nm diameter iron particles observed in graphite iron. Assuming that the average particle diameter in graphite iron was 100 nm and that all the iron was on the surface of the graphite, the expected surface area would be twice that for an equivalent weight of iron powder. In order to compensate for this effect, the weight of iron powder used was twice that of graphite iron.

In the temperature range 313 - 373K, the iron exhibited no catalytic behaviour, in common with graphite iron and the other systems studied.

Above 373K, the iron was very active for the hydrogenation of butadiene with almost complete conversion of the butadiene to a mixture of butenes, (Figure 17). This agrees well with the behaviour observed by Bond et al (1964).

Further reaction occurred in the range 573 to 673K and there was a major change in the reaction products, with the formation of ethane and methane. Ethane, however, was not a major product after reaction of graphite iron. A comparison of methane and ethane production for each catalyst is shown in figures 18 and 19. At

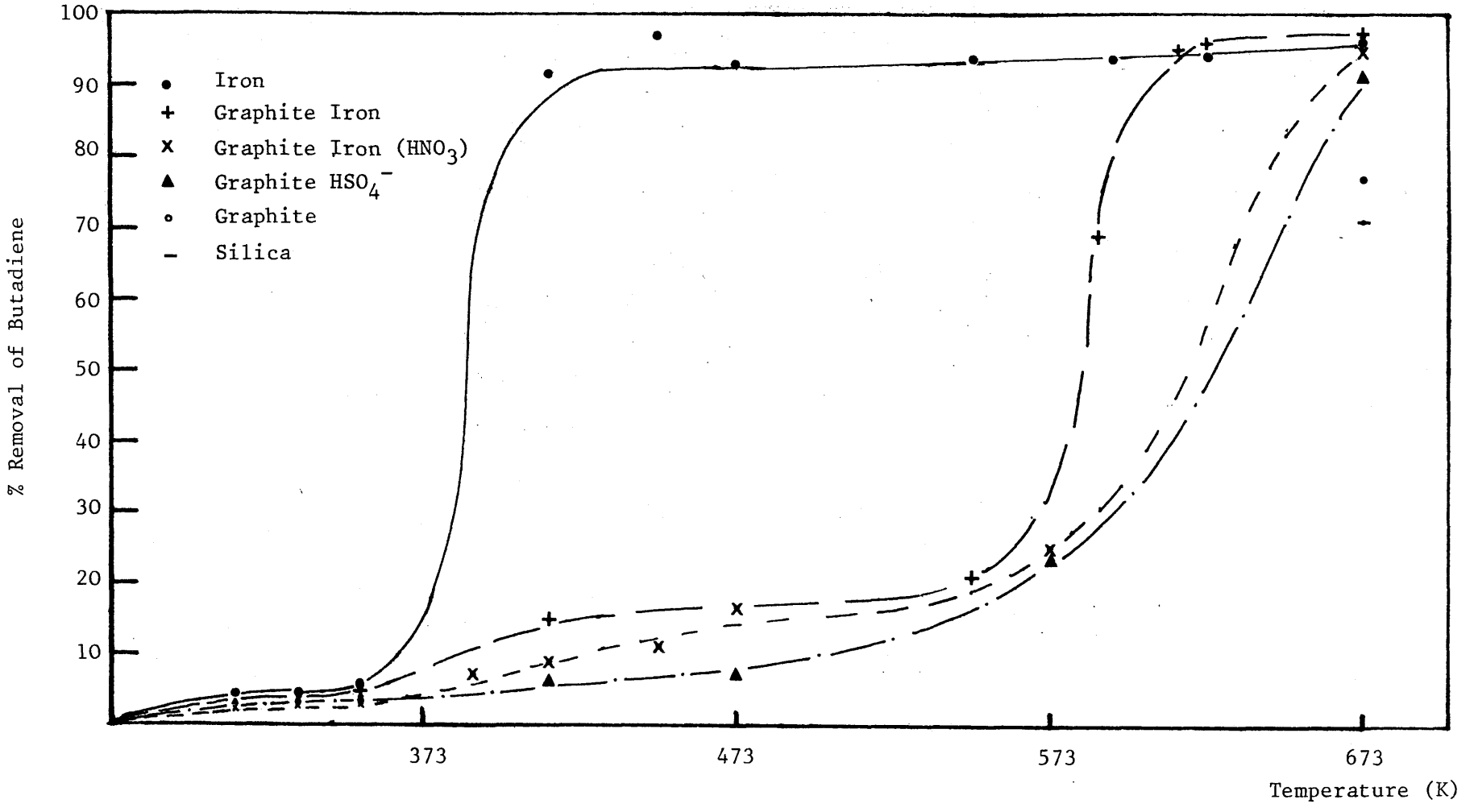

FIGURE 16: Reaction of Butadiene and Hydrogen with a range of Catalysts

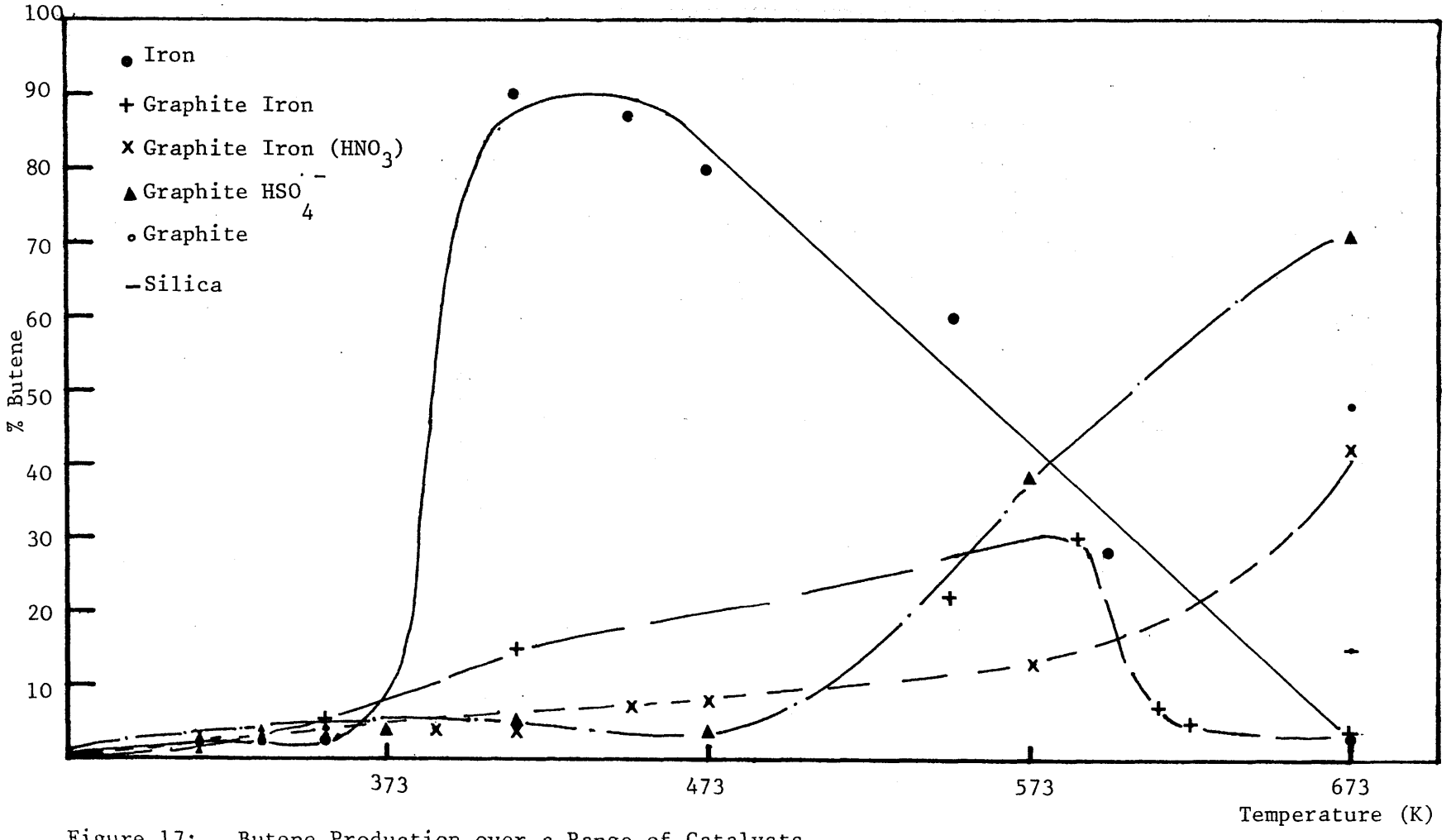

Figure 17: Butene Production over a Range of Catalysts

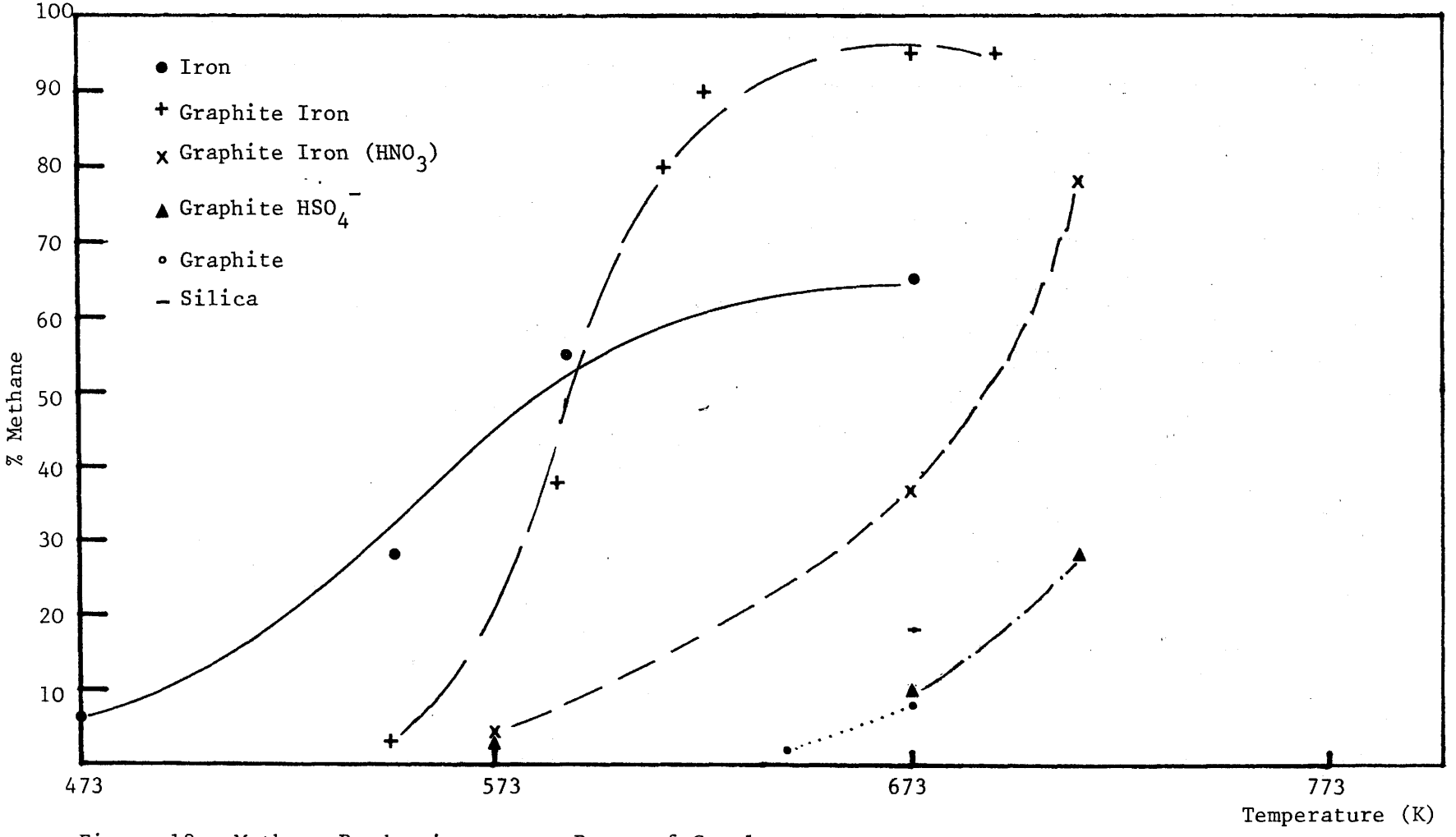

Figure 18: Methane Production over a Range of Catalysts

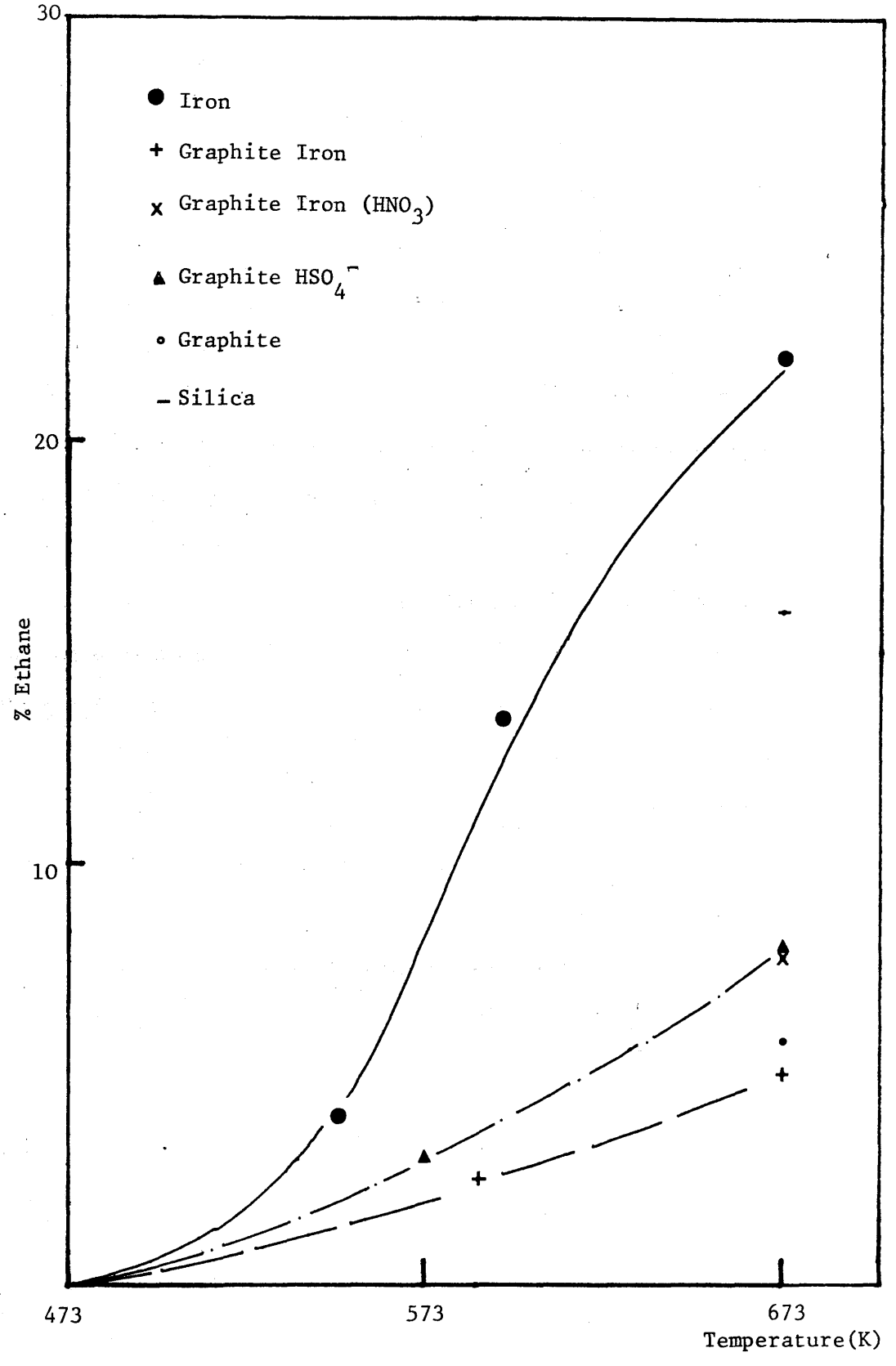

Figure 19: Ethane Production over a Range of Catalysts

673K benzene was also formed.

8.2.2 Graphite iron washed with dilute HNO_3

Treatment of graphite iron with dilute HNO_3 removes surface iron and part of the iron within the graphite, (Section 7.5). The treated compound exhibited less activity than graphite iron for hydrogenation in the range 373 - 573K (Figure 17), and above 573K, less activity for methane production (Figure 18), although both systems exhibited similar trends. Minor products of reaction above 573K were ethane and butane.

8.2.3 Homogeneous Reaction

In the higher temperature range, 573 - 673K, homogeneous reaction becomes important and therefore reaction of butadiene and hydrogen in the silica tube alone and with graphite was studied briefly at 673K. The principal products after reaction in the silica tube were butene, ethane, and methane, indicating that hydrogenation of butadiene to butene and the cracking of butadiene to methane and ethane were the main reactions. Propane and butane were minor constituents of the gas mixture after reaction.

These results are not in agreement with those from the graphite system. In this case the major reaction product was butene, with only minor amounts of methane and ethane, indicating that hydrogenation of butadiene is the main reaction over graphite (Figures 16-19).

8.2.4 Graphite Bisulphate

The compound was prepared according to the method described by Carr (1965), and was used after being washed with water and vacuum dried for 6 hours. Subsequent heating of the graphite bisulphate to 473K caused decomposition of the retained HNO_3 and H_2SO_4 acids and evolution of $NO + SO_2$.

The behaviour of the graphite bisulphate, (Figures 16-19) was very similar to that observed over graphite alone. In the range 473 - 673K, the main reaction was the hydrogenation of butadiene to butene. However, the conversion to butene was higher over graphite bisulphate and could be the result of increased surface area. At 573K, the activity of graphite bisulphate for the hydrogenation reaction was similar to that of graphite iron, but the methane production reaction was not significant below 673K (Figure 18).

8.3 Reaction of Graphite Iron with Butadiene and Hydrogen in the Range 623-703K

From the results in section 8.1, it was observed that the main activity of graphite iron occurred at temperatures above 573K. The reaction of butadiene and hydrogen was therefore studied in detail at 623, 643, 663, and 703K.

8.3.1 Gaseous Product Distribution with Time

Figures 20-22 are typical graphs of the gaseous product distribution after reaction at 623, 643 and 703K. Reaction at 663K was similar to that at 643K. In order to relate the conversion of butadiene to the products, the C_1 fragment percentage was divided by 4, and the percentage of high molecular weight product, which corresponded to a dimer, was multiplied by two. The main products of the reaction common to all temperatures were methane and butene. Additionally, at 623K butane was found and at 703K only, a high molecular weight product was observed.

The reaction occurred in three stages. The first stage, corresponding approximately to a one hour reaction time, was the production of methane. From one to two hours reaction in the range 623-663K, hydrogenation of the remaining butadiene to butene was the main reaction. The nature of the third stage of reaction,

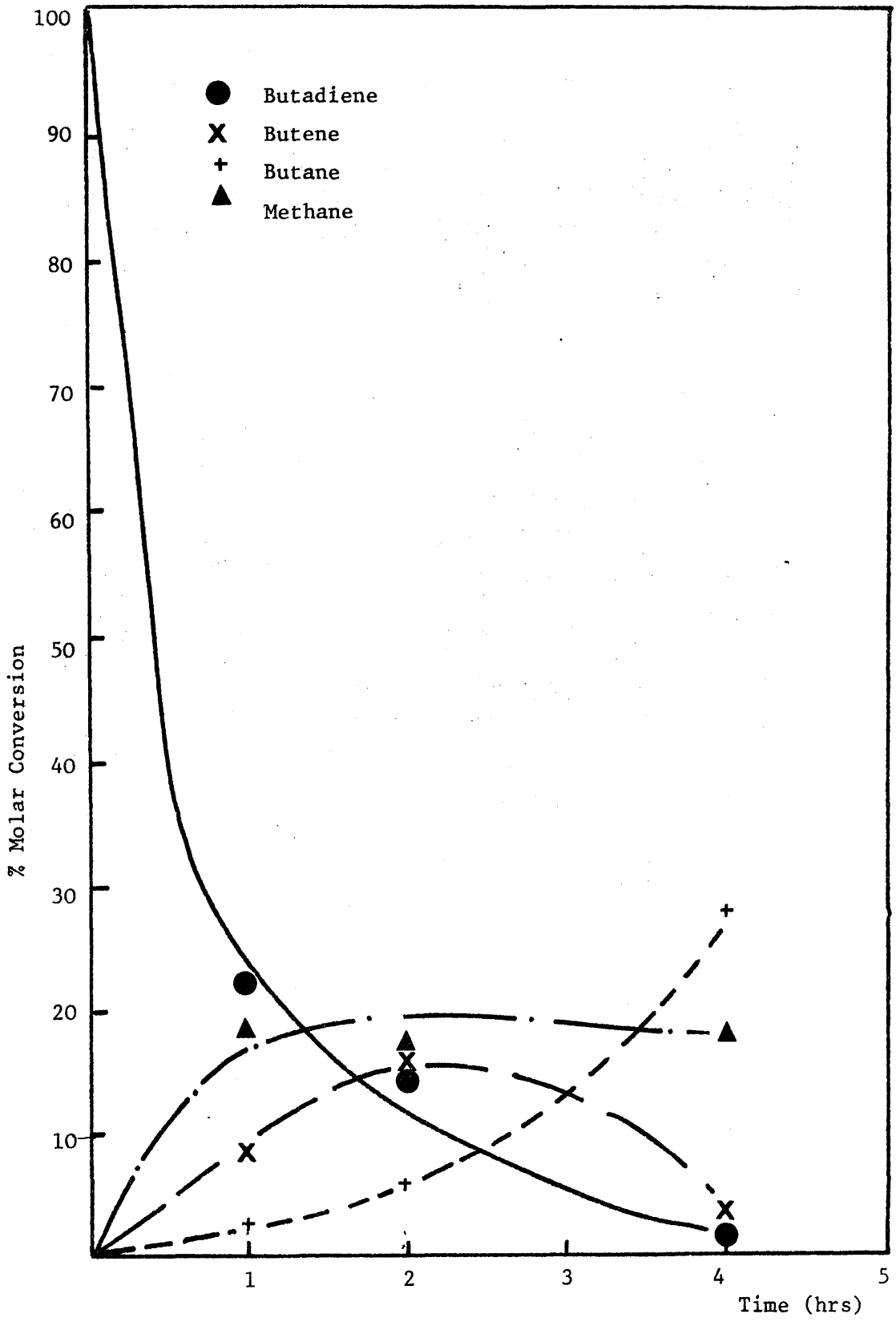

Figure 20. Gaseous Product Distribution after Reaction of Butadiene and Hydrogen over Graphite Iron at 623K.

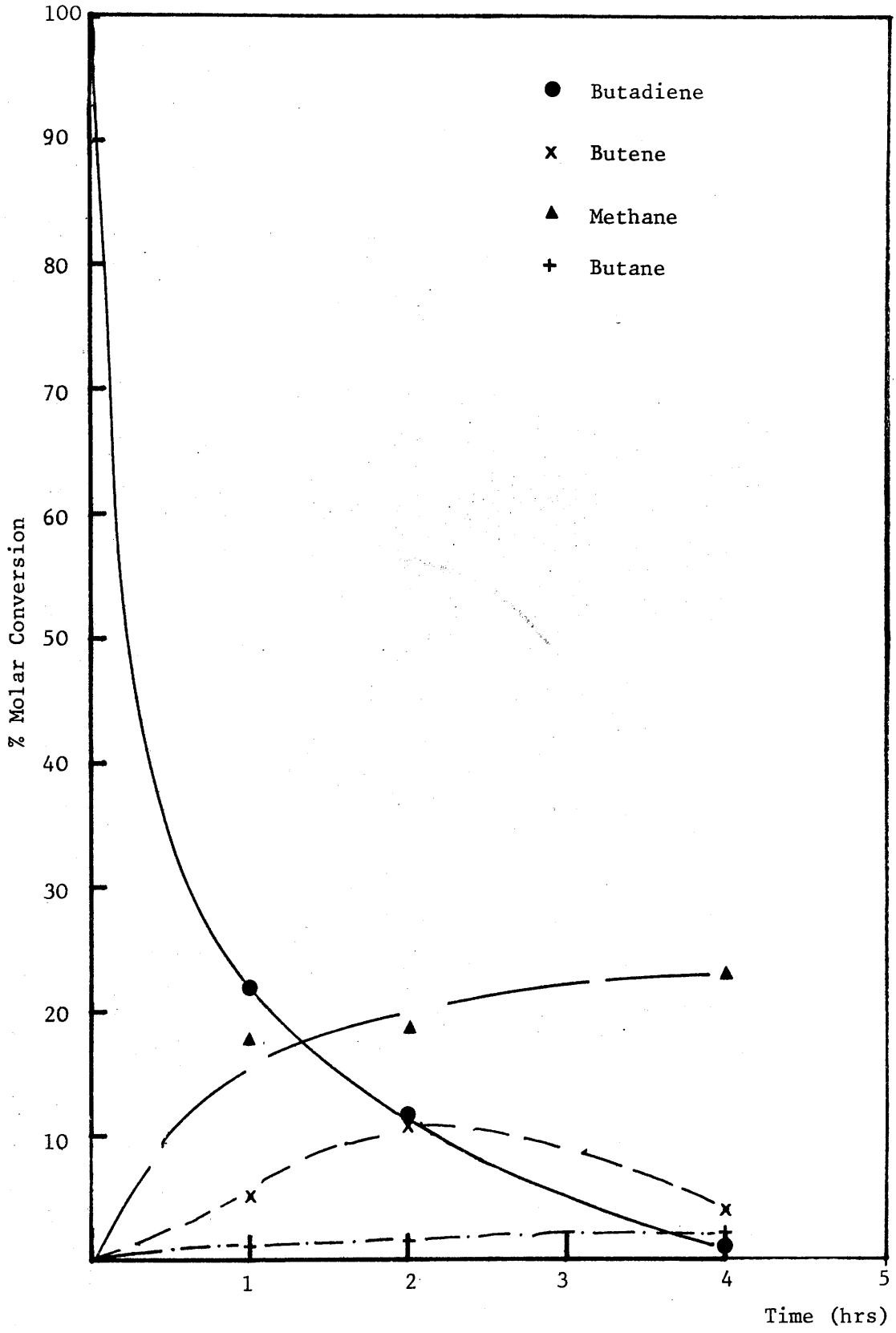

Figure 21: Gaseous Product Distribution after reaction of Butadiene and Hydrogen over Graphite Iron at 643K.

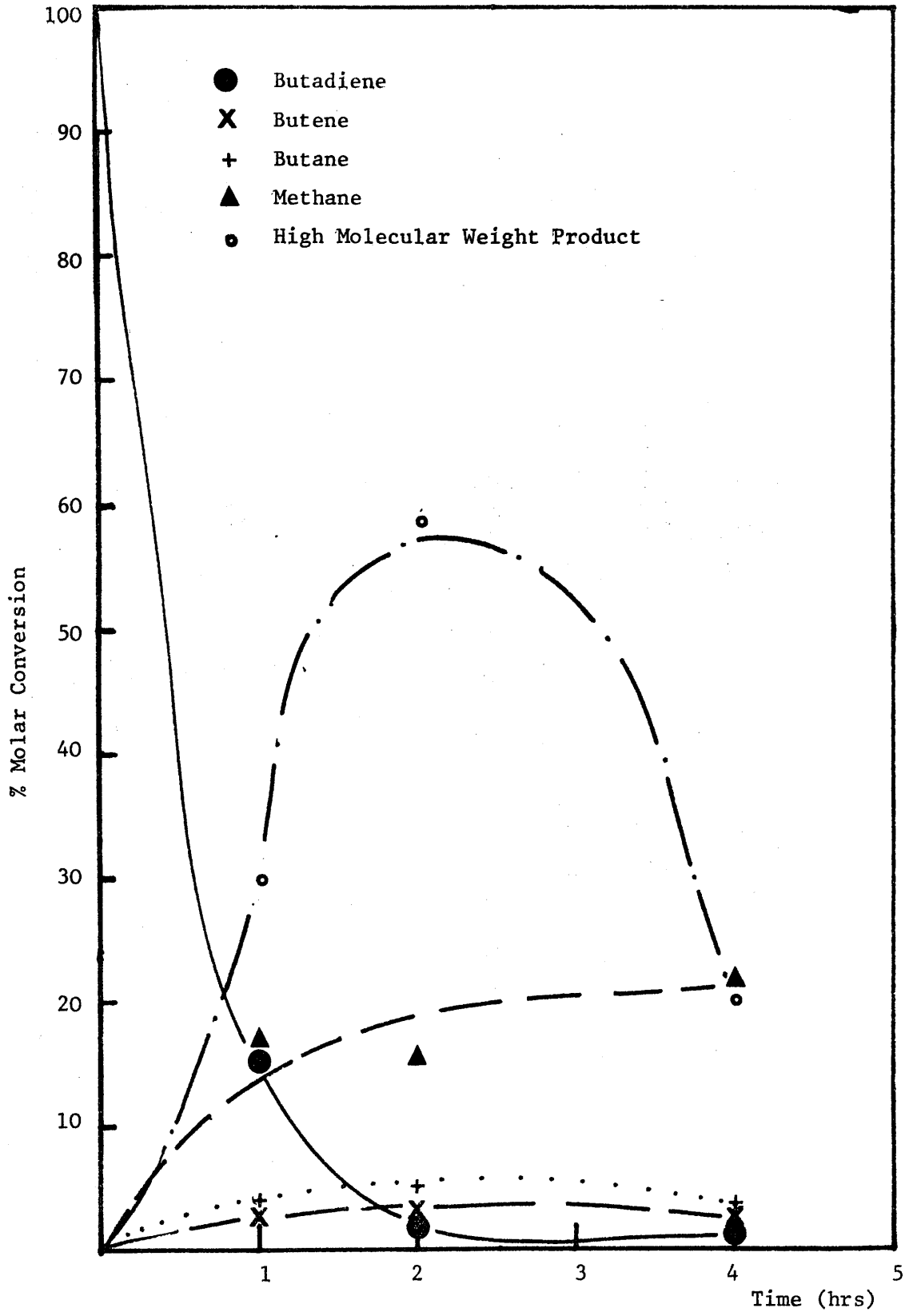

Figure 22. Gaseous Product Distribution after Reaction of Butadiene and Hydrogen over Graphite Iron at 703K.

which occurred at times > 2 hours depended on temperature.

8.3.2 Gaseous Product Distribution with Temperature

In the first stage methane production, an almost constant average conversion of 75% butadiene was observed at each temperature. Above 623K, in the second and third stages of reaction, there was a further increase in methane formation to form approx 90% of the gaseous products of reaction.

The hydrogenation of butadiene to butene was not significant in the first stage of reaction at each temperature. However, in the range 623-643K the conversion to butene increased with time in the second stage of the reaction. Above 643K, the hydrogenation products were present in only minor amounts indicating that further reaction had occurred. At 703K, a different product distribution was found in the second stage of the reaction with the formation of a high molecular weight product.

At 623K (Figure 20), butane was the major product in the third stage of the reaction, and there was a corresponding decrease in butene concentration, the methane level remaining constant. At higher temperatures, butane was present in small quantities. At 643 and 663K, the third stage of the reaction was characterised by a conversion of butene to methane, while at 703K, an increase in methane production was accompanied by a fall in the amount of high molecular weight product.

8.3.3 High Molecular Weight Product

This product was present after reaction at 703K. From the mass spectrum of the reaction products the main peak for this product occurred at 108m/e. and the cracking pattern was as follows.

$m/_e$	108	73	43	30
Relative Intensity	10	20	100	10

It is possible that this material could correspond to a butadiene dimer.

8.3.4 Carbon Deposition

From Figures 20-22, the results show that the gaseous products of the reaction do not account for all the reaction products and it was shown in section 7.7, that carbon had been deposited on the graphite iron surface. The mass balance for the reaction was calculated to quantify the amount of carbon deposited.

At the start of reaction, the butadiene and hydrogen concentrations were known. After reaction, the gaseous products were condensed out at 77K and analysed by mass spectroscopy. However, as the final pressure after condensation was high, in the order of 50-100 torr, it is unlikely that all the products of reaction were collected. In addition, at 77K, methane has a partial pressure of 10 torr. The uncondensed gas was therefore assumed to be a mixture of hydrogen and 10 torr of methane. A typical set of mass balance results at 643K are given below.

1 hr	$4C + 10H \rightarrow 2.0C + 9.8H$	8.1
2 hr	$4C + 10H \rightarrow 1.8C + 9.7H$	8.2
4 hr	$4C + 10H \rightarrow 1.3C + 10H$	8.3

$(C_4H_6 + 2H_2 \equiv 4C + 10H)$

It can be seen that the mass balance results of the gaseous products account for all the hydrogen in the system. The deficiency in carbon increased with time from 50-68%.

The variation of carbon deposition with temperature for the first stage of the reaction (1 hr), is presented below

Temperature (K)	% Carbon Deposited
623	47.5
643	50
663	70
703	30

The results show that for an almost constant butadiene conversion (Figures 20-22), section 8.3.2, there is an increase in carbon deposition at a temperature of 663K. At 703K, the amount of carbon depositied decreased, probably as a result of the dimerization reaction.

8.4 Reaction of Butadiene with Graphite Iron

The reaction of butadiene alone over graphite iron was examined briefly. The reaction products after 18 hours reaction at 620K are given below and compared to those found after reaction with a butadiene, hydrogen mixture.

Reaction Gas	% Products					
	CH_4	C_2H_6	C_3H_8	C_4H_6	C_4H_8	C_4H_{10}
Butadiene	63	2	10	7.5	3.5	14
Butadiene/Hydrogen	90	-	-	2	3	3

In reaction with butadiene, it appears that the rate of methane production over graphite iron was lower than that observed in the presence of hydrogen. The other main products C_3H_8, C_4H_8 and C_4H_{10}, must be the result of reaction with hydrogen generated by the carbon deposition reaction. The hydrogenation fragments C_2H_6 and C_3H_8 were observed only after reaction with butadiene alone.

From mass balance consideration, the overall reaction of butadiene is

$$100C_4H_6 \rightleftarrows 63CH_4 + 2C_2H_6 + 10C_3H_8 + 7.5C_4H_6 + 3.5C_4H_8 + 14C_4H_{10} + 203C + 45H \qquad 8.4$$

Therefore, approximately half of the available carbon is deposited

during the reaction and most of the hydrogen is accounted for in the hydrocarbon products of the reaction. The small hydrogen deficit could be attributed to the polymerisation reaction.

8.5 Reaction Rates

From the product distributions presented in section 8.3, it can be seen that the reaction of butadiene and hydrogen over graphite iron was complex with at least three reactions occurring simultaneously; carbon deposition, cracking of butadiene and butene to methane, and the hydrogenation of butadiene. As a result, the orders and rates of reaction cannot usefully be interpreted.

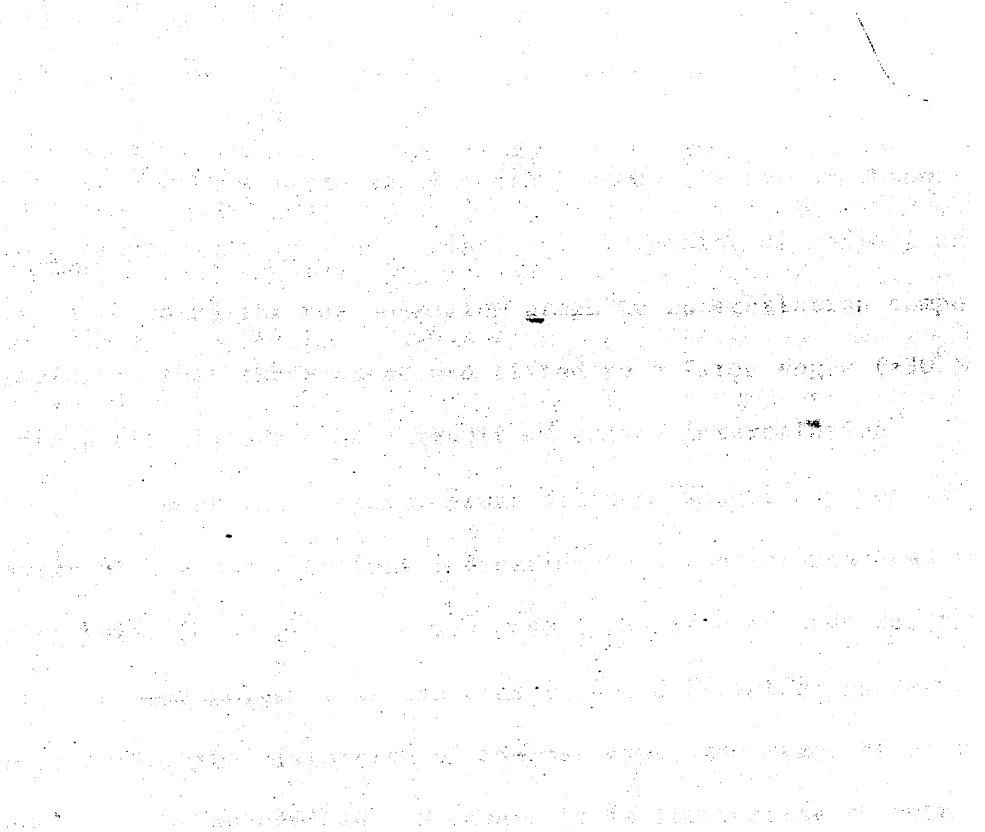

9. GRAPHITE IRON: DISCUSSION

9.1 Structure of Graphite Iron

The two main morphologies observed for the graphite iron compound, folded regions and regions of ring moiré patterns, can be ascribed to different graphite iron structures.

9.1.1 Form I

Areas exhibiting distorted or ring moiré patterns are extensive (>500 nm in diameter), and are similar to those associated with intercalation in potassium graphite and graphite copper sulphide. It is therefore likely that these patterns represent intercalated iron areas. The ring moiré patterns, from the arguments outlined in section 4.1, indicate that the intercalated areas are in the form of discrete islands.

The selected area diffraction patterns from these areas are distorted with a large angular displacement, apparent change in interplanar spacing, and variation in intensity of reflections. This was also found for the potassium graphite intercalation compound and indicates that these areas are tilted to a large angle (>30^{o}) or are internally distorted as a result of uneven intercalation.

Most intercalated areas did not exhibit any regular array of extra reflections indicating that the intercalated iron is disordered. However, in a few cases, the iron is ordered, giving rise to some polycrystalline arcs in the diffraction pattern. As a result of the distortion of the patterns, the symmetry of the arcs could not be determined. However, it is interesting to note that streaks with spacings close to the corrected spacings for the arcs (Section 7.1.3 and Table 15), were also present in the graphite ferrous chloride compound after reaction with butadiene and hydrogen (Section

5.5.4). These streaks have cubic symmetry. One possible arrangement of iron atoms within the graphite c-plane which would give this pattern with the observed spacings is shown in Figure 23(a).

This structure involves a cubic arrangement of iron with an a-spacing of 0.386nm. The spacings and angular displacements found from the electron diffraction patterns are given in Table 23 and compared to those calculated from this structure. The calculated and observed values are in reasonable agreement. The exact d values are dependent on the accuracy of the a-spacing which has a large uncertainty as it was obtained from a streak pattern.

The actual graphite interplanar distance in the intercalated iron is unknown, but assuming that there is an interaction with the conduction band electrons of the graphite a possible c-spacing is 0.466 nm (Novikov et al 1971, 1975a). (Figure 23(b)).

Such a structure could be formed easily by the reduction process and would involve only a minor amount of rearrangement from $FeCl_2$ where the iron interatomic distance is 0.361 nm. X-ray powder diffraction evidence is inconclusive. In addition, any reflections arising from this structure would be expected to be weak as most of the intercalated iron appears to be disordered. However, a weak halo at 0.466 nm was observed in agreement with the early work of Novikov et al (1971), and the extra spacing at 0.277 nm may represent the 110 reflection produced by the ordered structure.

Figure 23(b) represents a Stage I compound. The presence of a 0.466 nm halo therefore could indicate that Form I consists not only of islands of stage II and higher compounds as discussed for potassium graphite (section 4.1), but also stage I graphite iron with some of the intercalated iron in an ordered structure.

Table 23

Possible Interplanar Spacings for Intercalated Iron

Graphite Iron	Graphite $FeCl_2$ after Reaction of Butadiene and Hydrogen		Calculated Spacings from Fig. 23	
d_{nm}	d_{nm}	ϕ	d_{nm}	hkl
	0.386(A)		0.386	100
0.25 - 0.24			0.272	110
0.132	0.136(B)	45^{o} to A	0.136	220
0.114	0.117	ca 20^{o} to B	0.122	130

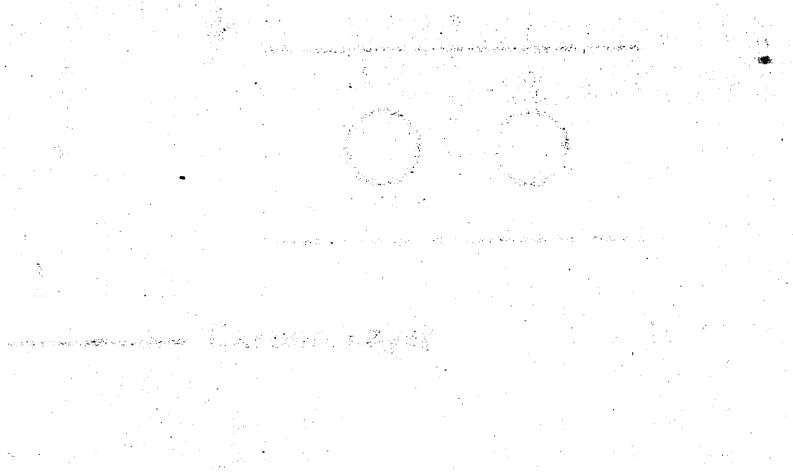

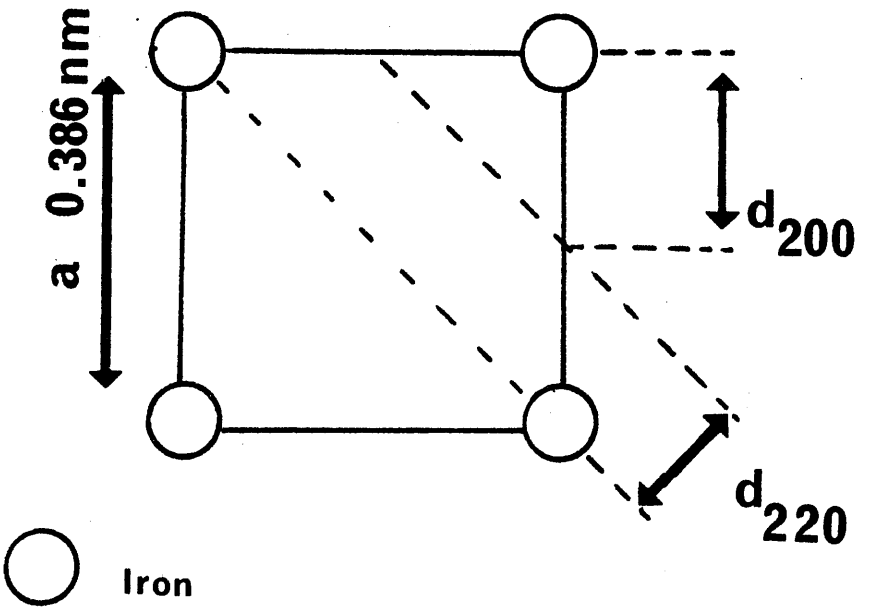

(a) Simple cubic in-plane arrangement of iron.

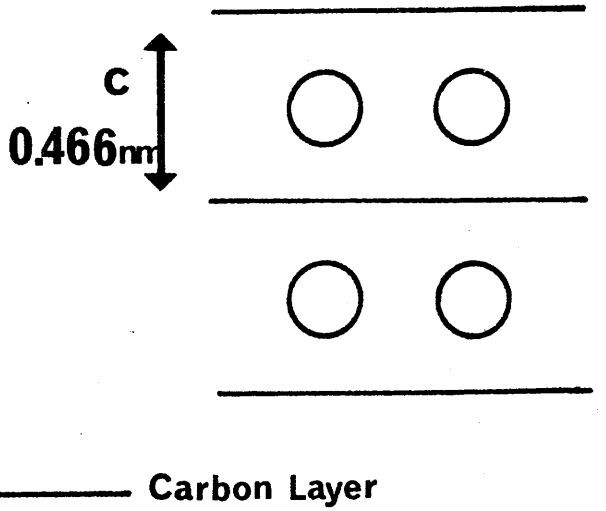

(b) Stacking arrangement for iron

Figure 23. Possible Structure for Intercalated Iron in Graphite Iron.

In addition to the ring moiré patterns, some minor features were also found. The unusual line moiré fringes, which were not observed in the other intercalation compounds studied, are similar to displacement fringes and could result from the presence of a regular thin particle at an angle to the graphite surface. Alternatively, they may result from orientation contrast produced at a boundary. However, these fringes traverse intercalated areas and therefore do not delineate an intercalation boundary. A possible explanation is that the moirés represent a thin magnetite dendrite within the layer planes, and may be the precursors of the parallel sided overlapping bands of material found after reaction (Section 7.7.1).

The series of fringes forming a ripple effect over these areas are not always present and could be assigned to bend contours.

9.1.2 Form II

The graphite iron compound also contained areas of intercalated THF. This THF is released violently on heating to produce exfoliated graphite with many folds in the lattice, giving rise to the extra graphite reflections observed in the electron diffraction pattern.

The small particles associated with this structure are dispersed throughout the graphite lattice and are more common in the thicker regions of the specimen. Electron diffraction (Table 15), showed that some of these particles are LiCl. The presence of αFe could not be shown either from the electron diffraction or X-ray diffraction results.

However, $FeCl_2$ crystallites were observed in the graphite ferric chloride compound before reduction (section 5.2.1), and the compound contains a high concentration of iron. It is likely therefore that some of the particles are iron. The particles are within the graphite lattice and are formed originally from the reduction of

intercalated layers. There is no evidence of strain in the surrounding matrix and therefore the particles are probably layers of iron sandwiched between graphite layers. In addition, the contrast associated with the particles indicates that they are composed of several iron layers stacked in the c-direction. This stacking arrangement is different to the αFe form.

Assuming that the stacking is Stage I with a Van der Waals interaction between the iron and graphite, the iron-iron c-spacing would be 0.58 nm (Novikov et al 1971, 1975a). However, in the present study, the 0.58nm reflection was not observed. It is therefore suggested that the iron crystallites in form II do not have an ordered stacking sequence in the c-direction.

From the areas studied at 1MeV and 100 KV it appears that Form II is the major form of the iron.

It is possible, however, that some of the iron is in neither Form I, nor Form II, but is finely dispersed through the lattice.

The moessbauer spectra from the graphite iron stage I compound reduced by lithium biphenyl (Novikov et al 1971, 1975a), was interpreted as indicating the presence of three main forms of iron. These are, a paramagnetic form arising from a graphite metal π complex, iron clusters which could result from monatomic layers of iron, and superparamagnetic clusters of α iron.

It is therefore suggested that the areas containing iron in Form I correspond to the graphite metal π complex and Form I is the true iron intercalation compound. The particles of iron within the graphite lattice, Form II, could correspond to the iron monolayer sandwich structure. It is probable that some of the particles are on the surface or at graphite flake edges which could allow formation

of a normal αFe structure. These small particles could act as the superparamagnetic clusters of αFe.

It was shown (Table 19a) by analysis after the acid wash, that approximately 2% of the total iron is accessible to the acid solvent. If this iron is mainly surface iron, the contribution of the superparamagnetic part of the diffraction pattern should be 2%. This low relative proportion and their small size would account for the absence of αFe spacings in this study and that of Vol'pin et al (1971, 1975a).

9.1.3 Acid Treatment

Bright discs, produced by treatment of the graphite iron compound with dilute and concentrated mineral acids, were similar to those observed in graphite bisulphate (Carr 1970). In potassium graphite, bright discs have been shown to be an absorption effect (Halpin 1971) and by analogy with potassium graphite (section 4.1), it is probable that these discs are gas bubbles in intercalated acid. The darker areas surrounding some of the bright discs could be explained by some recrystallisation of dissolved solute. This is supported by electron diffraction results which showed that the acid interacted with the LiCl to form $LiNO_3$ in the HNO_3 case and some iron oxide was formed with H_2SO_4 treatment.

Reaction of previously intercalated graphite in this reaction is much faster than ordinary graphite which required exposure to 30/70 HNO_3/H_2SO_4 mixture for 30 mins (Carr 1970). Such enhanced activity to re-intercalation of a previously intercalated graphite has been observed in the graphite ferric chloride - nitromethane system (Hooley 1972).

Further evidence of penetration of the graphite lattice by acid is given by the analysis results, Table 22, which show that

concentrated acid treatment removed up to 50% of the total iron present within the bulk graphite. No particles were observed after acid treatment.

9.1.4 Decomposition of Graphite Iron

Heating the graphite iron compound above 383K caused exfoliation of the graphite with the evolution of THF. This agrees with the work of Vol'pin et al (1971). The decomposition of the intercalated areas occurs above 573K with agglomeration of particles throughout the graphite lattice and expulsion to the surface and crystallite edges. The nucleation of these particles increases with increasing temperature above 573K.

These particles could not be identified unambiguously from the electron diffraction patterns which showed the presence of Fe_3C or Fe_3O_4 after reaction (Sections 7,6.3 and 7.8). However, the HVEM dark field observations indicate that the particles produce strong reflections in the 0.2 nm range and powder x-ray diffraction results confirm the presence of αF e and Fe_3O_4 which could only be formed from the original αFe. α iron was also observed after heating in hydrogen at 873K (Novikov 1971).

The formation of αFe particles within the lattice is possible after heating as the exfoliated graphite contains voids as a result of uneven expansion of the graphite. Therefore in some areas, the agglommeration of iron may no longer be constrained by the graphite c-planes.

The expulsion of most of the iron from the lattice is confirmed by the analysis results, Table 22, using the thiocyanate solution method. This indicated that, after heating, most of the iron is accessible to dissolution by acid.

This nucleation and expulsion of iron from the graphite lattice

is directly related to the catalytic behaviour observed.

9.2 Catalytic Action of Graphite Iron

From the catalytic results, section 8.1, it was shown that there are two temperature dependent reaction regimes; hydrogenation of butadiene (383-573K), and methane production associated with a solid reaction product (>573K).

9.2.1 Hydrogenation of 1,3 Butadiene

The hydrogenation of 1,3 butadiene has been studied over all Group VIII metals supported on alumina (Webb 1963, Meyer and Burwell 1963, Phillipson and Wells 1962, and Bond et al 1965. The reaction over iron has been studied at 471K (Bond 1964 Phillipson and Wells 1962) but no reaction rates are available.

The reaction is considered to occur by a two stage process. In the first stage, butene is the major product and in the second stage olefin hydrogenation and isomerization takes place. Over iron, the rate constant of the second stage is faster than the first stage (Bond 1964). However, butadiene is strongly adsorbed in this reaction, blocking catalytic sites, and second stage hydrogenation does not usually occur until the butadiene is completely reacted.

In the present study, significant reaction occurs over iron in the range 393-573K with conversion to the alkene. The reaction over graphite iron and graphite iron treated with HNO_3 to remove surface iron, is similar and is less than for iron under the same conditions. No reaction occurred over graphite bisulphate in this temperature range indicating that homogeneous reaction and reaction over a high surface area graphite is negligible. It is obvious therefore that reaction has occurred over graphite iron by diffusion and reaction within the layer planes with the reaction rate determined by gas access to the layers. Reaction occurred to butene and minor amounts

of butane in a similar manner to reaction over iron.

9.2.2 Carbon Deposition

From the morphology of the compound after reaction at 623-703K, deposition of the solid reaction product occurs mainly on the agglomerated iron particles. Electron diffraction indicated that the solid product was amorphous carbon. Evidence for carbon formation is also given by the observed carbon deficiency on the gas phase products (section 8.3.4). No carbon deposition was observed on particles within the graphite.

Most studies of carbon deposition reactions over metals to form carbon filaments from unsaturated hydrocarbons have been carried out at high temperatures. Typical temperatures for the production of carbon filaments from 1,3 butadiene are 998K (over cobalt) (Baker et al 1975) and 973K over nickel (Baird et al 1974). A comparative study of the pyrolysis of butadiene using nickel foils in the range 593 to >653K (Baird 1977 a, b) did not produce filamentary carbon.

In the present work, filamentary carbon formation from butadiene pyrolysis was studied in the range 623-703K. The filaments exhibited mainly an amorphous structure. This agrees with the observations of Baird et al (1974) after reaction at 973K over nickel foil. Only a few filaments were observed with the separate filament wall structure reported by Baker et al (1975).

In addition, in the present study the carbon filaments were of two types (A and B). Type A growth occurs with the metal particle remaining on the surface and Type B growth with the metal particle at the filament tip. The particular growth type dominant in a particular reaction appears to be dependent on the presence of hydrogen. This is demonstrated in the reaction of butadiene alone,

where mainly type A whisker growth was observed. Type B growth predominated in reaction with butadiene and hydrogen.

The role of hydrogen in carbon deposition from acetylene over nickel foils at 673-873K has been investigated (Bernardo and Lobo 1975), and the results indicated that hydrogen effects the stability of the metal particles or other phases involved so that the area for reaction is altered. In the present study, the variation in growth morphology suggests that hydrogen has altered the stability of the metal substrate, possibly by continuous reduction of the surface.

The activity of graphite iron for carbon deposition and methane production is higher than that of iron under the same reaction conditions. The gaseous product distributions for iron and graphite iron are dissimilar, indicating that different reaction mechanisms are involved.

It is interesting that over graphite and graphite bisulphate, hydrogenation of butadiene to butene is the preferred reaction. This confirms that the activity of the graphite iron compound for deposition reactions is associated with the metal particles on the graphite.

9.2.3 Polymerisation Reaction

In addition to the carbon deposition reaction polymerisation of butadiene also occurs. The loop deposit (Type C) forms a convoluted structure similar to the polymerised material observed after reaction over graphite ferrous chloride. An amorphous carbon containing deposit has also been observed on decomposition of C_2H_2 over nickel on silica at 850K and was ascribed to a C_2H_2 polymer (Baker et al 1972).

In the present study, the growth site for the polymer appeared to be the graphite surface remote from folds or particles.

In addition, the extent of polymerisation increased in the absence of hydrogen.

The rate of the homogeneous dimerization of 1,3 butadiene in the range 446-660K has been determined (Kistiakowsky and Ransom 1939) and could account for the amount of dimer found in the present study.

9.3 Reaction Mechanism

From the results in section 8.3 for the reaction of 1,3 butadiene and hydrogen over graphite iron in the range 623-703K, three reaction stages have been identified. A detailed mechanism can be proposed for the first stage of reaction in which the main products are carbon and methane with only trace amounts of C_2 or C_3 species.

The adsorption of butadiene usually involves the formation of a strongly adsorbed species.

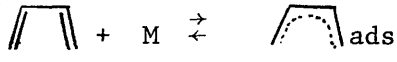

9.1

Partial hydrogenation and isomerisation can then occur to form but-1-ene or but-2-ene.

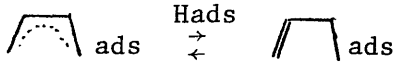

9.2

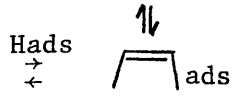

9.3

But-2-ene may be hydrogenated to butane or desorbed.

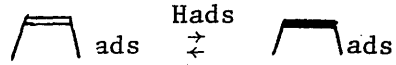

9.4

9.5

In a similar manner, but-1-ene may be hydrogenated or desorbed.

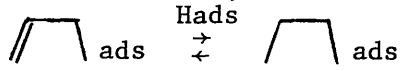

9.6

9.7

The adsorbed butane from reactions 9.4 and 9.6 may also be desorbed.

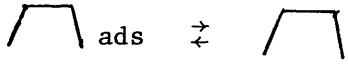

9.8

In but-1-ene, however, the c_3-c_4 bond (gas phase) is weaker than a normal c-c bond (Egger and Cocks 1973), and bond rupture could occur to form an adsorbed propenyl radical and a methyl radical which can be readily hydrogenated to methane.

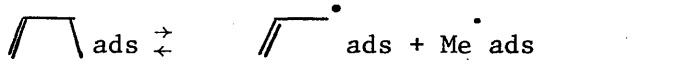

9.9

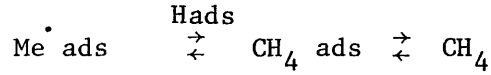

9.10

The propenyl radical, formed by reaction 9.9, can form adsorbed propene, 9.11, which can be hydrogenated, 9.12, or desorbed, 9.13. In addition, the propenyl radical can be pyrolysed to carbon and adsorbed hydrogen.

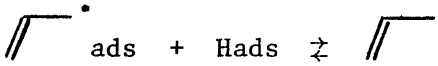

9.11

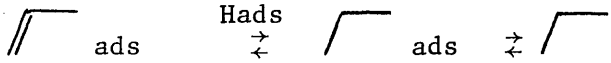

9.12

9.13

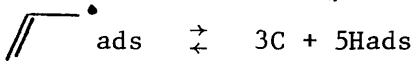

9.14

If reactions 9.4 - 9.7 are slower than reaction 9.9, this mechanism accounts for the small amount of butene and butane observed after reaction. Similarly, the absence of c_3 and c_2 species is explained if reactions 9.11-9.13 are slower than reaction 9.14.

The overall equation for the first stage of reaction is therefore

$$C_4H_6 \rightleftarrows CH_4 + 3C + 2H \qquad 9.15$$

The ratio of deposited carbon to CH_4 would therefore be 3:1, as found after reaction at 623 and 643K (Figs. 20 and 21). Above 643K the C:CH_4 ratio is 2:1, probably indicating that a secondary direct cracking reaction to carbon with no methane by-product is occurring.

In the decomposition of butadiene, as no hydrogen is present initially reaction 9.2 cannot occur. The butadiene must therefore crack to produce carbon and adsorbed hydrogen. One possible direct

cracking route is via a diacetylene intermediate

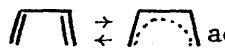

$$\text{ads} \rightleftarrows 4\text{Hads} + \equiv - \equiv \text{ads} \qquad 9.16$$

$$\equiv - \equiv \text{ads} \rightleftarrows 4\text{C} + 2\text{Hads} \qquad 9.17$$

The adsorbed hydrogen produced in this reaction may then be used as proposed in reactions 9.2 - 9.14. However, from section 8.4, the overall reaction after 18 hours involves the hydrogenation of butadiene to butene and butane, and the formation of c_2 and c_3 species, in addition to cracking to carbon and hydrogen (equation 8.4).

The butene and butane observed may be formed by reactions 9.2 - 9.8. The propane could be accounted for by reactions 9.9-9.12 and ethane could be formed by the dimerization of methyl radicals formed in reaction 9.9 which is favoured by low Hads concentrations.

$$\dot{C}H_3 \text{ ads} + \dot{C}H_3 \text{ ads} \equiv CH_3 - CH_3 \text{ ads} \rightleftarrows CH_3 - CH_3 \qquad 9.18$$

If propenyl radicals are the source of carbon and also of propane, the ratio of propenyl: methyl for the reaction is 1.1:1 thus indicating that as in the hydrogen, butadiene case, the formation of adsorbed butenyl and its subsequent fission to methyl and propenyl is the major reaction route.

No hydrogenation reactions to propane or butane occurred in the presence of excess hydrogen and the cracking rates were faster. It is therefore suggested that the cracking reactions 9.9 and 9.14 could be promoted by hydrogen, possibly by affecting the catalytic sites for reaction. This effect has been reported for but-1-ene over nickel at 773K (Bernardo and Lobo 1975).

The second and third stages of reaction of butadiene and hydrogen over graphite iron are temperature dependent (section 8 3.2). The second stage, in general, involves hydrogenation rather than cracking reactions and can be described by equations 9.1-9.3.
At high temperatures, 703K, dimerization also occurs. The onset of

the hydrogenation reaction in the second stage may indicate that most of the reaction sites for carbon deposition from adsorbed butene have been deactivated. Other sites for butadiene adsorption may still be present at which butene desorption is favoured over cracking or hydrogenation.

In the third reaction stage, when butadiene is no longer present to provide a source of butene, removal of butene by a slow hydrogenation reaction at low temperatures and by a slow cracking reaction at higher temperatures, can be observed.

10. INTERCALATION COMPOUNDS : CONCLUSIONS

10.1 Structural Features

Both donor and acceptor intercalation compounds of graphite exhibit similar morphologies when examined by transmission electron microscopy.

The features observed depend on the physical properties of the intercalate and the stage of the compound.

Stage I complexes of graphite ferric chloride and potassium graphite have completely filled interlayer spaces and are identified as areas of dark matrix (Sections 4.1 and 6.1). The bright discs observed associated with these areas are the result of an absorption effect (Halpin and Jenkins 1971) and arise probably from vapourisation of the intercalate phase under preparative conditions.

Large scale interference effects, in particular distorted moiré patterns, are observed in concentrated compounds of potassium graphite, graphite copper sulphide and graphite iron and are similar to those observed in graphite bisulphate (Carr 1965, 1970). Electron diffraction of these areas indicates that they are distorted. It has therefore been proposed (Section 4.1), that the observed contrast is interface contrast, and that these areas contain islands of stage II and higher intercalation compounds formed according to Hêrold's Bent Layer Model (Section 1.3.3). These islands can vary in size and, from the observed overlap of islands, there may be some disorder in the c-direction. It is also possible that islands of stage I compound are also formed particularly in the case of graphite iron.

It is possible therefore that the concept of a stage model on the macro scale is unrealistic.

It is interesting to note that the colour of the intercalation compounds has not been explained to date. One explanation which could

account for the colour and also the moiré effects observed is the formation of "electron bubbles" as in the potassium/liquid ammonia system where the free electron orients the surrounding matrix to form a cavity. Some features common to the K/liquid NH_3 and K/graphite systems are listed below.

Property		K/Liquid NH_3	K/Graphite
colour	conc.	gold	gold
	dil.	blue	blue
magnetic properties		paramagnetic	paramagnetic
charge carriers		n-type	n-type
Electrical properties specific resistance	(ohm cm.)	2×10^{-4}	7×10^{-6}

Calculations (B.C. Webster personal communication 1971) estimated the energy of such an electron bubble in potassium graphite to be 0.5 - 1 ev. Preliminary experiments using phase sensitive optical techniques and E.S.R. at 77K failed to produce evidence for electron bubbles. However, trapping of charge carriers at intercrystalline junctions and thermal effects may have masked the signals.

Similar studies using well parallelised potassium graphite at very low temperatures (5K) would provide a realistic test for this model.

A mechanism for the reduction of graphite ferric chloride to graphite ferrous chloride and to graphite iron can be proposed to explain the agglomeration of material observed in these compounds.

When the graphite ferrous chloride compound is formed from the Stage I graphite ferric chloride, the iron-iron interatomic distance decreases from 0.606 nm to 0.361 nm. This process will produce gaps

within the intercalate layer and some aggregation does occur. In addition, as there is no interaction with the graphite conduction band in graphite ferrous chloride the metal atoms are free to interact normally as in a bulk crystal. The aggregation process can therefore lead to crystallites interleaved within the graphite layers which resemble stage I or higher type in their stacking order in the c-direction but do not form a complex with graphite. Formation of the graphite iron can involve either a further decrease in the iron-iron a-distance to 0.286 nm, as in bulk iron, and the consequent interaction of the iron atoms to form crystallites, or can involve minor rearrangement of the ferrous chloride iron distribution resulting in discrete islands of stage I or higher intercalation compound. Moessbauer studies, (Novikov et al 1975a) indicate that THF found associated with the areas of crystallites is not the result of an iron-THF interaction. In a true graphite iron complex, THF could not be accommodated by the c-distance of 0.466 nm. The THF, therefore, occupies the residual space within the c-plane formed during the progressive aggregation of iron on reduction.

Bright discs observed in graphite intercalation compounds signify areas which contain vapour phase material which may be introduced during preparation or reaction. For example, in the graphite bisulphate residue compound (Carr 1965, 1970) they may be explained as bubbles of sulphuric acid or water vapour trapped in a liquid phase within the lattice. The THF retained within the graphite iron compound is rarely observed in the form of bright discs (Plate 67) as the heating effect of the beam causes exfoliation of the graphite. The bright discs are also observed after reaction of graphite ferric chloride with N_2/H_2 which produces bubbles of trapped HCl.

10.2 Reaction of Intercalation Compounds

None of the intercalation compounds exhibited any marked catalytic activity for the reactions studied. In the potassium graphite, graphite ferric chloride and graphite copper sulphide interactions with N_2/H_2, chemical and morphological changes occurred. Potassium graphite appears to have a low catalytic activity for ammonia synthesis because the compound is destroyed by reaction with the primary product to form KNH_2. This reaction possibly occurs via a ternary intermediate formed within the graphite layers. The graphite ferric chloride and graphite copper sulphide are destroyed by reduction of the intercalate within the graphite layers to form a mixture of graphite and the reduced metal salt.

However the graphite ferric chloride reduced compound, graphite ferrous chloride, may have some activity for ammonia synthesis as precipitates were found within the graphite after reaction (Section 5.4.1) which were provisionally identified as NH_4Cl. The activity of the graphite ferrous chloride for the polymerisation of butadiene appears to be similar to that of free ferrous chloride which may be expected as it is not a true intercalation compound. In addition, there is some diffraction evidence that a small amount of iron may also be formed under reaction conditions which would be active for the hydrogenation of butadiene. It is not clear from the results, in this case, whether the major reaction occurs on the surface or within the graphite compound. However the reaction of H_2 and CO over pre-reduced graphite ferric chloride (Hooley et al 1977) indicates that the main reaction site is $FeCl_2$ on the graphite surface.

Reaction of gases within the layer planes is contrary to the conclusion of Hooley et al (1977) that modified chemical or catalytic

activity of metal salt intercalated graphite is not the result of diffusion between the layer planes. These workers studied only one reaction, the Fischer Tropsch synthesis, over graphite ferric chloride and examination of their substrate would probably have revealed that a reduction reaction had also occurred within the graphite layers.

In the reaction of butadiene and hydrogen over graphite iron, the activity for the hydrogenation reaction was low compared to free iron and could be attributed to reaction within the graphite layers in common with the other systems studied. However the major catalytic activity is towards carbon deposition and is observed only on complete decomposition of the graphite iron.

Filamentary growth on iron is unusual at the low temperatures studied and the activity of the iron particles in graphite iron for this reaction may be useful for further mechanistic studies on carbon deposition.

From this study of intercalation compounds, very little catalytic activity can be ascribed to true intercalation compounds. It is possible that catalytic properties claimed for other intercalation systems may also be the result of decomposition of the compound.

Further insights on this topic may be obtained by the use of modern electron optical techniques. More detailed analysis of the structural features observed in this work may be carried out using a high precision goniometer stage. In addition, for the graphite iron compound, final identification of the particulates observed before and after reaction may be achieved by the micro diffraction and micro X-ray analysis techniques available in STEM instruments. Auger analysis would also be useful in identification of the actual

chemical state of the species involved in reactions.

These techniques together with the methods described in this thesis could also be applied to other graphite metal compounds, and in particular to study the structure of the potassium graphite iron compound which is claimed to be active for ammonia synthesis (Vol'pin et al 1975c, 1977).

REFERENCES

Agar, A., 1960 , Brit. J. Appl. Phys., 11, 504.

Alderson, R.H. and Halliday, J.S., 1965, "Techniques for Electron Microscopy" Ed. Kay, 478.

Amelinckx, S., 1963, "The interaction of radiation with solids", 68.

Amelinckx, S. and Delavignette, P., 1960a, Phil. Mag., 5, 533.

Amelinckx, S. and Delavignette, P., 1960b, Nature, 185, 603.

Amelinckx, S. and Delavignette, P., 1960c, Phys. Rev. Lett., 5, 50.

Amelinckx, S. and Delavignette, P., 1961, "Direct Observation of Imperfections in Crystals" Proc. Tech. Conf., 295.

Amelinckx, S. and Delavignette, P., 1963, "Electron Microscopy and Strength of Crystals", Interscience, 441.

Andrews, K.W., Dyson, D.J. and Keown, S.R., 1967, "Interpretation of Electron Diffraction Patterns", London.

Bach, B., 1971, C.R. Acad. Sci. Ser.B., 273, 666-9.

Bach, B. and Ubbelohde, A.R., 1971, J. Chem. Soc. A., 3669½

Bach, B., Evans, E.L., Thomas, J.M. and Barber, M., 1971, Chem. Phys. Lett., 10(5),547.

Bacon, G.E., 1950, Acta. Cryst., 3, 137.

Bacon, G.E., 1951, Acta. Cryst., 4, 558.

Bacon, G.E., 1952, Acta. Cryst., 5, 392.

Bacon, G.E.,1958, AERE Report M/R 2702.

Bacon, R. and Sprague, R., 1961a, "Direct Observation of Imperfections in Crystals", Proc. Tech. Conf., 357, Interscience.

Bacon, R. and Sprague, R., 1961b, Proc. Fifth Carbon Conference, 466.

Baird, T., Fryer, J.R. and Grant, B., 1974, Carbon, 12, 591-602.

Baird, T., 1977a, "Reactivity of Solids", Proc. of 8th Int. Symp., 143.

Baird, T., 1977b,"Developments in Electron Microscopy and Analysis", 219-222.

Baker, C., Gillin, L.M. and Kelly, A., 1965, 2nd Ind. Carbon and

Graphite Conf. London.

Baker, R.T.K., Barber, M.A., Harris, P.S., Feates, F.S. and Waite, R.J., 1972, J. Catal., 26, 51-62.

Baker, R.T.K., Gadsby, G.R. and Terry, S., 1975, Carbon, 13, 245-6.

Barker, J.A. and Croft, R.C. 1953, Austral. J. Chem., 6, 302.

Bassett, G.A., Pashley, D.W. and Menter, J.W., 1957, Nature, 179, 752.

Bassett, G.A., Menter, J.W. and Pashley, D.W., 1958, Proc. Roy. Soc. A., 246, 345.

Beguin, F. and Setton, R., 1976, J. Chem. Soc. Chem. Commun., 15, 611.

Bernal, J.D., 1924, Proc. Roy. Soc. A,106 749.

Bernardo, C.A. and Lobo, L.S., 1975, J. Catal., 37, 267-278.

Boeck, A., and Rudorff, W., 1973, Z. anorg. Allg. Chem., 397, 179-86.

Boehm, H.P. and Hofmann, U., 1955, Z. anorg. Allg. Chem., 278, 58.

Boersma, M.A.M., 1974, Cat. Rev. Sci. Eng., 10(2), 243-280.

Bollman, W., 1960, Phil. Mag. 5, 621.

Bollman, W., 1961a, Proc. 5th Conf. Carbon, Phil. II, 303.

Bollman, W., 1961b, Proc. Eur. Reg. Conf. Electron Microscopy, Delft., 330.

Bollman, W., 1961c, Proc. Int. Conf. Properties of Reactor Materials, 132.

Bollman, W., 1962, Phil. Mag., 7, 1513.

Bond, G.C., Webb, G., Wells, P.B. and Winterbottom, J.M., 1965, J. Chem. Soc., 3218.

Bond, G.C. and Wells, P.B., 1964, Advances in Catalysis, 15, 92.

Bonifiglioni, G. and Majoni, A., 1964, J. Appl. Physics, 35, (3), 683-5.

Brusset, H. and Martin-Lefèvre, C., 1967, Bull. Soc. Chim. Fr., 9, 3348.

Carr, K.E., 1965, Thesis, University of Glasgow, Glasgow.

Carr, K.E., 1970, Carbon, 8, 155-166.

Colin, M., Hérold, A., Daumas, N., Diebold, R. and Saehr, D., 1967, Ch m. Soc. Spec. Publ. 22, 309-16.

Colin, M. and Hérold, A., 1971, Bull. Soc. Chim. Fr., 6, 1982.

Cosslett, V.E., 1970, Inst. Elect. Eng., 117, 1489.

Coulson, C.A., 1947, Nature, 159, 265.

Coulson, C.A. and Taylor, E., 1952, Proc. Phys. Soc. A., 65, 815.

Cowley, J.M. and Ibers, J.A., 1956, Acta. Cryst., 9, 421.

Cracknell, A.P., 1969, Adv. Phys., 18(70), 681-818.

Croft, R.C., 1952, J. Appl. Chem. 2, 557.

Croft, R.C., 1956a, Austral, J. Chem., 9, 184.

Croft, R.C., 1956b, Austral, J. Chem., 9, 206-211.

Croft, R.C., 1956c, Austral, J. Chem., 9, 201.

Croft, R.C., 1960, Quarterly Reviews, 14, 1.

Daumas, N. and Hérold, A., 1969, Compt. rend., 268c, 373.

Daumas, N. and Hérold, A., 1971, Bull. Soc. Chim. Fr., 5, 1598-1604.

Dawson, I.M. and Follett, M.A.C., 1959, Proc. Roy. Soc. A., 253, 390.

Debye, P. and Scherrer, P., 1917, Phys. Z., 18, 291.

Delavignette, P. and Amelinckx, S., 1960, Phil. Mag., 5, 729.

Delavignette, P. and Amelinckx, S., 1961, Proc. Eur Reg. Conf. Electron Microscopy. Delft, 404.

Derleth, H. and Fischer, H., 1972, Ger. Offen. Pat. no. 2041167.

Diebold, R. and Hérold, A., 1961, Compt. rend., 252C, 1328.

Diebold, R. and Hérold, A., 1963, Bull. Soc. Chim. France, 578.

Dowell, W.C.T., Farrant, J.L. and Rees, A.L.G., 1954, Proc. Int. Conf. Electron Microscopy, London, 279.

Dowell, W.C.T., Farrant, J.L. and Rees, A.L.G., 1958, 4th Int. Conf. Electron Microscopy, Berlin, 367.

Dresselhaus, M.S., Dresselhaus, G. and Fischer, J.E., 1977, Phys. Rev. B., 15(6), 3180.

Dzurus, M.L., and Hennig, G.R., 1957, J. Chem. Phys., 27, 275.

Ebert, L.B., 1976, Annu. Rev. Mater. Sci., 6, 181-211.

Eeles, W.T. and Turnbull, J.A., 1963, Nature, 198, 877.

Eeles, W.T. and Turnbull, J.A., 1965, Proc. Roy. Soc. A., 283, 179.

Egger, K.W. and Cocks, A.T., 1973, Helv. Chim. Acta., 56(5), 1537-52.

Eisch, J.J. , 1963, J. Org. Chem., 28, 707.

Evans, E.L. and Thomas, J.M., 1975, J. Solid State Chem., 14, 99-111.

Ewald, P.P., 1914, Sitzungsber. Munch. Akad., 4, 7.

Finch, G.I. and Wilman, H., 1936, Proc. Roy. Soc. A., 155, 345.

Fisher, R.M., Szirmae, A., McLear, J.H., 1970, Anal. Chem., 42, 362R.

Franklin, R.E., 1951, Acta. Cryst., 4, 253.

Fredenhagen, K. and Cadenbach, G., 1926, Z.anorg. Chem., 158, 249.

Fredenhagen, K. and Suck, H., 1929, Z. anorg. Chem., 178, 353.

Freeman, A.G., 1968, J. Chem. Soc. Chem. Commun., 193.

Freeman, A.G., 1974, 4th Ind. Carbon and Graphite Conf., 97.

Frenzel, A., 1933, Dissertation (Tech. Hochschule Berlin).

Friedel, J., 1964, "Dislocations".

Fryer, J.R., 1968, Siemens Review XXXV, 13.

Fryer, J.R., 1974, 8th Int. Cong. Electron Microscopy, Canberra, I, 680.

Gevers, R., 1963, "The Interaction of Radiation with Solids", 471.

Ginderow, M.D. and Setton, M.R., 1968, Compt. rend., 266C, 1515.

Golé, J. and Stein, C., 1968, J. Polymer Sci. Part C., 16, 3779-88.

Golé, J., Quang Tho Pham, Essel, A., 1973, J. Polymer. Sci. Polym. Chem., 11(8), 1851-8.

Gross, R., 1962, Thesis, University of Nancy.

Haering, R.R. and Mrozowski, S., 1960, Prog. Semicond., 5, 273.

Haijitink, G.J., de Boer, E., Van der Meij, P.J. and Weijland, W.P., 1956, Rec. Trav. Chim., 75, 487.

Haine, M.E. and Mulvey, T., 1954, J. Sci. Instr., 31, 326.

Halpin, M.K. and Jenkins, G.M., 1971, 3rd Conf. Ind. Carbons and Graphite, 53.

Halpin, M.K., 1972, Thesis, University College of Swansea, Swansea.

Hambling, J.K. and Anderson, G.W., 1963, Chem. Abs., 58, 586g.

Hashimoto, H., 1962, Metal Physics, 8, 100.

Heerschap, M., Delavignette, P. and Amelinckx, S., 1964, Carbon, 1, 235-243.

Heerschap, M. and Delavignette, P., 1967, Carbon, 5, 383-4.

Heidenreich, R.D., 1964, "Fundamentals of Transmission Electron Microscopy" John Wiley.

Hennig, G.R., 1951, J. Chem. Phys., 19, 922.

Hennig, G.R., 1952, J. Chem. Phys., 20, 1438.

Hennig, G.R., 1956, Proc. 1st and 2nd Conf. on Carbon, Buffalo, USA, 103.

Hennig, G.R. and Dzurus, M.L., 1957, J. Chem. Phys., 27, 275.

Hennig, G.R., 1959, Progr. Inorg. Chem., 1, 125.

Hennig, G.R., 1960, Proc. 4th Conf. on Carbons, 221.

Hennig, G.R., 1965, J. Chem. Phys., 43, 1201.

Hennig, G.R. and McLelland, J.D., 1955, J. Chem. Phys., 23, 1431.

Hérold, A., 1951, C.R. Acad. Sci. Paris, 232, 1484.

Hérold, A., 1955, Bull. Soc. Chim. France, 999.

Hérold, A. and Saehr, D., 1965, Bull. Soc. Chim. Fr., 3130.

Hérold, A. and Carton, B., 1972, Bull. Soc. Chim. France, 4, 1337.

Hérold, A. and Daumas, N., 1971, Bull. Soc. Chim, Fr., 5, 1598-1604.

Hillier, J., 1954, Nat. Bur. Stand. Circ., 527, 413.

Hirsch, P.B., Horne, R.W. and Whelan, M.J., 1956, Phil. Mag., 1, 677.

Hirsch, P.B., Howie, A., Nicholson, R.B., Pashley, D.W., Whelan, M.J., 1965 "Electron Microscopy of Thin Crystals".

Hohlwein, D., Grigutsch, F.D. and Knappwost, A., 1969, Z. Phys. Chem., 65, 322-5.

Hohlwein, D., Readman, P.W., Chamberod, A., Coey, J.H.D., 1974, Phys. Stat. Solid., 64, 305.

Hohlwein, D. and Metz, W., 1974, Z. Kristallogr., 139, 279-96.

Hohlwein, D. and Metz, W., 1975, Carbon, 13(1), 84-6.

Hooley, J.G. and Bartlett, M.W., 1967, Carbon, 5, 417.

Hooley, J.G., Bartlett, M.W., Liengme, B.V. and Sams, J.R., 1967, Phys. Lett., 25A, 127.

Hooley, J.G., Bartlett, M.W., Liengme, B.V. and Sams, J.R., 1968, Carbon, 6, 681.

Hooley, J.G. and Soniassy, R.N., 1970, Carbon, 8, 191-196.

Hooley, J.G., 1972, Carbon, 10, 155-163.

Hooley, J.G., 1973b, Carbon, 11, 225-236.

Hooley, J.G., 1973a, Bienn, Conf. Carbon, Abstr. Prog. 11th, 193-4.

Hooley, J.G., Parkash, S. and Chakrabartty, S.K., 1977, Carbon, 15, 307-310.

Howie, H., 1961, "Direct Observation of Imperfections in Crystals" Proc. Tech. Conf. 269, Interscience.

Howie, H. and Whelan, M.J., 1961, Proc. Eur. Conf. Electron Microscopy, Delft., 194.

Ichikawa, M., Soma, M., Onishi, T. and Tamaru, K., 1967, J. Catal., 9, 418.

Ichikawa, M., Sudo, M., Soma, M., Onischi, T. and Tamaru, K., 1969a, J. Amer. Chem. Soc., 91(6), 1538-9.

Ichikawa, M., Sudo, M., Soma, M., Onishi, T. and Tamaru, K., 1969b, J. Phys. Chem., 73, 1174.

Ichikawa, M., 1970, Ger. Offen. 2114769, C.A. 76, 156271u.

Ichikawa, M., Inoue, Y. and Tamaru, K., 1972a, J. Chem. Soc. Chem. Commun., 16, 928-9.

Ichikawa, M., Noguchi, T. and Tamaru, K., 1972b, J. Polymer Sci. B., 10(8), 615-7.

Ichikawa, M., Kawase, K. and Tamaru, K., 1972c, J. Chem. Soc. Chem. Commun. 3, 177.

Ichikawa, M., Kondo, T. and Kawase, K., 1972d, J. Chem. Soc. Chem. Commun. 3, 176.

Ichikawa, M., Naito, S., Kawase, K., Kondo, T. and Tamaru, K., 1972e, Ger. Offen. Pat. no. 2149161.

Izui, K. and Fujita, F.E., 1963, J. Phys. Soc. Japan, 18, 467.

Jadhao, V.G., Singru, R.M., Joshi, G.M., Pisharody, K.P.R. and Rao, C.N.R., 1974, Z. Phys, Chem., 92, 139-47.

Jensen, K.A., Nygaard, B., Clisson, G. and Nielsen, P.H., 1965, Acta. Chem. Scand., 19, 768.

Juza, R. and Schmeckenberger, A., 1957, Z. Anorg. Chem. 292, 46.

Juza, R., Leuble, H. and Heinlein, L., 1949, Z. Anorg. Chem., 258, 105.

Karimov, Yu.S., Vol'pin, M.E., Zvarykina, A.V. and Noukov, Yu.N., 1971, Fiz. Tverd Tela., 13, 28.

Kay, D.H., 1965, "Techniques for Electron Microscopy".

Kistiakowsky, G.B. and Ransom, W.W., 1939, J. Chem. Phys., 7, 725.

Klotz, H. and Schneider, A., 1962, Naturwiss, 49, 448.

Knappwost, A., 1966, Ger. Offen. 1,223,350, C.A. 16567.

Knappwost, A. and Metz, W., 1969, Z. Phys. Chem., 64, 178.

Knappwost, A. and Grigutsch, F.D., 1969, Nature, A, 24(4), 601-6.

Knoll, M. and Ruska, E., 1932, Z. Phys. 78, 318.

Korshak, V.V., Vol'pin, M.E., Gribova, I.A., Krasnov, A.P., Novikov, Yu.N. and Kamenskii, I.V., 1973, Plast. Massy., 1, 20.

Lagrange, P., Métrot, A. and Hérold, A., 1974, C.R. Acad. Sci. Ser. C., 278, 701.

Lagrange, P., Portmann, M.H. and Hérold, A., 1976, C.R. Acad. Sci. Ser. C., 283, 557.

Laidler, D. and Taylor, A., 1940, Nature, 146, 130.

Lalancette, J.M., Rollin, G. and Dumas, P., 1972, Can. J. Chem, 50, 3058.

Lalancette, J.M. and Roussel, R., 1976a, Can. J. Chem., 54, 2110.

Lalancette, J.M., Roy, L., Lafontaine, J., 1976b, Can. J. Chem., 54(15), 2505-8.

Le Poole, J.B., 1947, Philips tech. Rdsch., 9, 33.

Lipson, H. and Stokes, A.R., 1942a, Nature, 149, 328.

Lipson, H. and Stokes, A.R., 1942b, Proc. Roy. Soc. A., 181, 101.

Lukesh, J.S., 1950, Phys. Rev., 80, 226.

Lukesh, J.S., 1951a, J. Chem. Phys., 19, 384.

Lukesh, J.S., 1951b, J. Chem. Phys., 19, 1203.

Maire, J. and Mering, J., 1959, Proc. 3rd Conf. on Carbon, 337.

Mashinskii, V.I., Postnikov, V.A., Novikov, Yu.N., Lapidus, A.L., Vol'pin, M.E. and Eidus, Ya.T., 1976, Izv. Akad. Nauk. SSSR, Ser. Khim., 9, 2018.

Matayuma, E., 1962, Nature, 193, 61.

McDonnell, F.R.M., Pink, R.C. Ubbelohde, A.R., 1951, J. Chem. Soc. 191.

McClure, J.W., 1959, Proc. 3rd Carbon Conf. Buffalo, 179.

Merrick, H.F., 1963, Thesis, University of Cambridge.

Meyer, .E.F. and Burwell, R.L., 1963, J. Amer. Chem. Soc., 85, 2881.

Mitsuishi, T., Nagasaki, H., Uyeda, R., 1951, Proc. Imp. Acad. Japan, 27, 86.

Montet, A., Perlow, O., Campbell, O., Hennig, G.R. and Boyle, , 1968, Carbon, 6, 228.

Nixon, D.E. and Parry, G.S., 1967, Nature, 216, 5118.

Nixon, D.E. and Parry, G.S., 1968, Brit. J. Appl. Phys., 1, 291.

Nominé, N. and Bonnetain, L., 1967, C.R. Acad. Sci. Paris Ser. C., 264c, 2086.

Nominê, N. and Bonnetain, L., 1968, C.R. Acad. Sci. Paris Ser. C., 266(12), 867-8.

Novikov, Yu.N. and Vol'pin, M.E., 1971, Usp. Khim., 40(9), 1568-92.

Novikov, Yu,N., Kazakov, M.E., Zvarykina, A.V., Astakhova, I.S. and Vol'pin, M.E., 1971, Zh. Strukt. Khimii., 12, 3, 486-495.

Novikov, Yu.N., Vol'pin, M.E., Prusakov, .VE., Stukan, R.A., Goldanskii, V.I., Semion, V.A. and Struchkov, Yu.T., 1970, Zh. Strukt. Khimii, 11, 6, 1039-47.

Novikov, Yu.N., Slinkin, A.A., Pribytkova, N.A., Leznover, L.I., Rubinstein,, A.M. and Vol'pin, M.E., 1973, Kinet. Katal, 14, 3, 633.

Novikov, Yu.N., Vol'pin, M.E., Lapkina, N.D., Kasatochkin, V.J., Struchkov, Yu.T., Kazakov, M.E., Stukan, R.A., Povitskij, V.A., Karimov, Yu.S. and Zvarykina, A.V., 1975 a, J. Amer. Chem. Soc., 97, 3366.

Novikov, Yu.N., Postnikov, V.A., Nefed'ev, A.V. and Vol'pin, M.E., 1975b, Izv. Akad. Nauk. SSSR. Sei. Khim., 10, 2381.

Ohhashi, K. and Tsujikawa, I., 1974, J. Phys. Soc. Japan, 37(1), 63-70.

Ottmers, D.M. and Rase, H.F., 1966, Ind. Eng. Chem., 58, 8, Fundamentals 5, 3, 302.

Panenotov, I. and Rashkov, I., 1972, J. Polym. Sci., 10(4), 1267-70.

Parry, G.S. and Nixon, D.E., 1968, Brit. J. Appl. Phys., 1, 291.

Parrod, J. and Beinert, G., 1961, J. Polymer. Sci., 53, 99.

Paul, D.E., Lipkin, D.E. and Weissman, S.E., 1956, J. Amer. Chem. Soc., 78, 116.

Phillips, R., 1960, Brit. J. Appl. Phys., 11, 504.

Phillipson, J.J. and Wells, P.B., 1962, unpublished work.

Podall, H.E. and Foster, N.E., 1958, J. Org. Chem., 23, 82 and 401.

Rashkov, I., Merle, F., Mai, C., Golé, J. and Panayotov, I., 1976, C.R. Hebd. Seances Acad. Sci. Ser. C., 283(8), 339.

Read, W.T., 1953, "Dislocations in Crystals".

Recke, W.D., 1961, Optik, 18. 278.

Riley, H.L., 1945a, Fuel, 24, 8.

Riley, H.L., 1945b, Fuel, 24, 43.

Rodewald, P.G., 1976, U.S. Pat. No. 3976714.

Rose, M., Naceache, C. and Golé, J., 1967, Compt. Rend. 266, 421.

Rudoff, W. and Hofmann, U., 1938, Zeit. Anorg. Allgem. Chem., 238, 1.

Rudorff, W. and Schulz, E., 1940, Z. Anorgan. Chem., 245, 121.

Rudorff, W., and Rudorff, G., 1947a, Z. Anorg. Allgem. Chem., 253, 281.

Rudorff, W. and Rudorff, G., 1947b, Chem. Ber., 80, 417.

Rudorff, W. and Schulz, E., 1954a, Angew. Chem., 66, 305.

Rudorff, W. and Schulz, E., 1954b, Z. Anorg. Chem., 277, 156.

Rudorff, W., Schulz, E. and Rubisch, D., 1955, Z. anorg. Chem., 282, 232.

Rudorff, W., and Landel, A., 1958, Z. Anorg. Allgem. Chem., 293, 327.

Rudorff, W., 1959, Angew. Chem., 71, 487.

Ruff, O. and Brettschneider, O., 1934, Z. Anorg. Allgem. Chem., 217, 1.

Saehr, D. and Hérold, A., 1960a, Compt. rend., 250, 545.

Saehr, D. and Hérold, A., 1960b, Bull. Soc. Chim. France, 1039.

Saehr, D. and Hérold, A., 1965, Bull. Soc. Chim. France, 3130.

Salzano, F.J. and Aronson, S., 1965a, J. Chem. Phys., 43, 149.

Salzano, F.J. and Aronson, S., 1965b, J. Chem. Phys., 42, 1323.

Salzano, F.J. and Aronson, S., 1966a, J. Chem. Phys., 45, 2221.

Salzano, F.J. and Aronson, S., 1966b, J. Chem. Phys., 45, 4551.

Salzano, F.J. and Aronson, S., 1967, J. Chem. Phys., 47(8), 2978.

Schafhaeutl, P., 1841, J. Prakt. Chem., 21, 155.

Schleede, A. and Wellmann, M., 1932, Z. Phys. Chem. B18, 4.

Schmidhammer, L. and Gabler, W., 1972, Ger. Offen. 2023455 CA. 76, 45708x.

Scott, H.D., Walker, J.F. and Hansely, V.L., 1934, J. Amer. Chem. Soc., 58, 2442.

Slinkin, A.A., Novikov, Yu.N., Pribytkova, N.A., Leznover, L.I., Rubinstein, A.M. and Vol'pin, M.E., 1973, Kinet. Katal., 14, 3, 633.

Slonczewski, J.C. and Weiss, P.R., 1958, Phys. Rev., 109, 272.

Snell, F.D. and Snell, C.T., 1954, "Colorimetric Methods of Analysis", II, 814.

Stein, C., Poulenard, J., Bonnetain, L. and Golé, J., 1965, C.R. Acad. Sci. Paris, 260, 4503.

Stein, C., Bonnetain, L. and Golé, J., 1966, Bull. Soc. Chim. France, 3155.

Stein, C., 1967, Compt. rend., 264C, 16.

Syme-Johnson, A.W., 1967, Acta. Cryst., 23, 770.

Tamaru, K., 1970, Catalysis Reviews, 4, 161.

Thomas, J.M., Millward, R.G., Davies, N.C. and Evans, E.L., 1976, J. Chem. Soc. Dalton, 23, 2443-5.

Thiele, H., 1932, Z. Anorg. Allg. Chem., 207, 304.

Tominaga, T., Sakai, T. and Kimura, T., 1974, Chem. Lett., 8, 853-8.

Touzain, P. and Armand, M., 1976, Carbon '76 Int. Conf. 154-7.

Tricker, M.J., Evans, E.L., Cadman, P. and Davies, N.C., 1974, Carbon, 12, 499-502.

Ubbelohde, A.R., McDonnell, F.R.M. and Pink, R.C., 1951, J. Chem. Soc. 191.

Ubbelohde, A.R., 1957, Nature, 180, 380.

Ubbelohde, A.R., Blackman, L.C.F., Mathews, J.F., 1959, Nature, 183, 454-6.

Ubbelohde, A.R. and Lewis, F.A., 1960, Graphite and its Crystal Compounds. O.U.P.

Ubbelohde, A.R., 1961, J. Chem. Phys., 58, 107.

Ubbelohde, A.R. and Murray, J.J., 1969a, Proc. Roy. Soc. A, 312, 371

Ubbelohde, A.R., 1969b, Proc. Roy. Soc. A, 309, 327.

Ubbelohde, A.R., 1969c, Carbon, 7, 523.

Ubbelohde, A.R., 1971a, Proc. Roy. Soc. A, 321, 445-460.

Ubbelohde, A.R., 1971b, Nature, 232 (5305), 43-4.

Vogel, A.I., 1961, "Quantitative Inorganic Analysis", 785.

Vol'pin, M.E., Novikov, Yu.N., Prusakov, V.E., Stukan, R.A., Goldanskii, V.I., Semion, V.A. and Struchkov, Yu.T., 1970a, Zh. Strukt. Khimii, 11, 6, 1039-1047.

Vol'pin, M.E., Struchkov, Yu.S., Novikov, Yu.N. and Semion, V.A., 1970b, Izv. Akad. Nauk. SSSR. Ser. Khim., 2608.

Vol'pin, M.E., Novikov, Yu.N., Kasakov, M.E., Zvarykina, A.V. and Astakhova, I.S., 1971, Zh. Strukt. Khimii, 12, 3, 486-495.

Vol'pin, M.E., Novikov, Yu.N., Lapkina, N.D., Kasatochkin, V.J., Struchkov, Yu.T., Kazakov, M.E., Stukan, R.A., Povitskij, V.A., Karimov, Yu.S. and Zvarykina, A.V., 1975a, J. Amer. Chem. Soc., 97, 3366.

Vol'pin, M.E., Novikov, Yu.N., Postnikov, V.A. and Nefed'ev, A.V., 1975b, Izv. Akad. Nauk. SSSR. Ser. Khim., 10, 2381.

Vol'pin, M.E., Postnikov, V.A., Dmitrienko, L.M., Ivanova, R.F., Dobrolyabova, N.L., Golubova, M.A., Gapeeva, G.I., Novikov, Yu.N. and Shur, V.B., 1975c, Izv. Akad. Nauk. SSSR. Ser. Khem. 2642.

Vol'pin, M.E., Novikov, Yu.N., Postnikov, V.A., Shur, V.B., Bayerl, B., Kaden, L., Warren, M., Dmitrienko, L.M., Stukan, R.A. and Nefed'ev, A.V., 1977, Z. anorg. allg. Chem., 428, 321.

Wallace, P.R., 1947, Phys. Rev., 71, 622.

Watanabe, K., Soma, M., Onishi, T. and Tamaru, K., 1971, Nature, Phys. Sci., 233, 160.

Watanabe, K., Soma, M., Onishi, T. and Tamaru, K., 1972, J. Chem. Soc. Chem. Commun., 2, 39-40.

Watanabe, K., Kondow, T., Soma, M., Omishi, T. and Tamaru, K., 1973, Proc. Roy. Soc. London. A., 333, 51-67.

Webb , G., 1963, Thesis, University of Hull, Hull.

Whelan, M.J. and Hirsch, P.B., 1957, Phil. Mag., 2, 1121 and 1303.

Whelan, M.J. and Howie, A., 1960, Proc. Eur. Reg. Conf. on Electron, University, Delft, 1, 194.

Williamson, G.K., 1961, "Prop. of Reactor Materials", 144.

Williamson, G.K. and Baker, C., 1958, Proc. Roy. Soc. A., 249, 114.

Williamson, G.K. and Baker, C., 1960, Proc. Eur. Reg. Conf. Electron Microscopy, Delft, 326.

Williamson, G.K. and Baker, C., 1961, Proc. 5th Conf. Carbon II, 521.